From excitation-contraction coupling to gene expression: Roles of RYR1 and $Ca_v1.1$ in myogenesis

Inaugural-Dissertation

zur

Erlangung des Doktorgrades

der Mathematisch-Naturwissenschaftlichen Fakultät

der Universität zu Köln

vorgelegt von

Dilyana Filipova

aus Gabrovo

Köln, 2018

Bericherstatter:	Prof. Dr. Niels Gehring
	Prof. Dr. Stefan Herzig
Tag der mündlichen Prüfung:	20. 07. 2018

“It’s still magic even if you know how it’s done.”

Terry Pratchett

Table of Contents

Table of Figures

Table of Tables

Abbreviations*

#	Number
°C	Degree celsius
°t	Temperature
4-CmC	4-chloro-m-cresol
Å	Angstrom
a.k.a.	Also known as
AA	Amino acid
ACh	Acetylcholine
AChR	Acetylcholine receptor
Actb	Beta-actin
ADP	Adenosine diphosphate
AGCC	Genechip® Command Console
APE1	Apurinic/apyrimidinic endonuclease 1
Apoe	Apolipoprotein E
aRNA	Amplified RNA
ATP	Adenosine triphosphate
ATP	Adenosine triphosphate
bHLH	Basic helix-loop-helix
BMP	Bone morphogenic protein
Bmp4	bone morphogenic protein
bp	Base pair
BSA	Bovine serum albumin
Ca^{2+}	Calcium
cADPR	Cyclic ADP ribose
CaM	Calmodulin
CamKII	Calmodulin kinase II
Cav1.1	The pore-forming subunit of DHPR
cDNA	Copy DNA
cDNA	Copy DNA
CIRC	Calcium-induced calcium release
CMMC	Center for Molecular Medicine Cologne
CREB	Camp response element-binding protein
cRNA	Complimentary RNA
cryoEM	Electron cryomicroscopy
Ct	Threshold cycle
Cytb	Cytochrome B
DEG	Differentially regulated gene
DHPR	1,4-dihydropyridine receptor
DM	Dermomyotome
DML	Dorsomedial lip
DNA	Deoxyribonucleic acid
dNTP	Deoxyribonucleotide triphosphate
ds	Double-stranded
e.g.	For example
E14.5	Embryonic day 14.5
E18.5	Embryonic day 18.5
ECC	Excitation-contraction coupling
ECM	Extracellular matrix
ERK1/2	Extracellular signal-regulated kinases 1 and 2
EtOH	Ethanol
FC	Fold change
FDR	False discovery rate
FKBP12	12-kda FK506-binding protein
Fwd	Forward
Gapdh	Glyceraldehyde 3-phosphate dehydrogenase
GO	Gene ontology
GO BP	Gene ontology biological process
GO CC	Gene ontology cellular component
GPCR	G-protein-coupled receptor
h	Hour(s)
H_2O	Water
H_2O_2	Hydrogen peroxide
Hh	Hedgehog
HPP-1	Hypokalemic periodic paralysis
IVT	*In vitro* transcription
JNK	Jun N-terminal kinase
kb	Kilobase
kDa	Kilodalton
KEGG	Kyoto Encyclopedia of Genes and Genomes
KO	Knockout
lncRNAs	Long non-coding RNAs
Lpl	Lipoprotein lipase
MA	Microarray
MAPK	Mitogen-activated protein kinase
MH	Malignant hypertermia
min	Minute
miRNA	Micro RNA
ml	Milliliter
MRF	Myogenic regulatory factor
Mrf4	Myogenic regulatory factor 4
mTOR	Mammalian target of rapamycin
MY	Myotome
Myf5/6	Myogenic factor 5/6
MyHC	Myosin heavy chain
MyoD	Myogenic determination factor 1
Myog	Myogenin
NA	Not available
Na^{+}	Sodium
nAChR	Nicotinic acetylcholine receptor
NC	Notochord
NMJ	Neuromuscular junction
NO	Nitric oxide
NT	Neural tube
nt	Nucleotide
NTP	Ribonucleotide triphosphate
№	Number

Pax3/7	Paired-homeobox transcription factor 3/7	SCs	Satellite cells
PC	Principal component	SE	Surface ectoderm
PCA	Principal component analysis	Shh	Sonic hedgehog
PCR	Polymerase chain reaction	Shh	Sonic hedgehog
PKCϴ	Protein kinase C theta	Six1/4	Sine oculis-related homeobox transcription factor 1/4
PP1	Protein phosphatase 1	SPRY	SplA kinase ryanodine receptor domain
PP2A	Protein phosphatase 2A	SR	Sarcoplasmic reticulum
PPAR	Peroxisome proliferator-activated receptor	ss	Single-stranded
qRT-PCR	Quantitative real-time PCR	Stac3	SH3 and cysteine rich domain 3
Rev	Reverse	Suppl.	Supplementary
RMA	Robust multiarray analysis	TAC	Transcriptome analysis console
RNA	Ribonicleic acid	TdT	Terminal deoxynucleotidyl transferase
ROS	Reactive oxygen species	TF	Transcription factor
Rplp0	Ribosomal protein, large, P0	TGF	Transforming growth factor
rpm	Revolutions per minute	Tm	Melting temperature
Runx1	Runt-related transcription factor 1	Uba52	Ubiquitin A-52 residue ribosomal protein fusion product 1
RYR1	Type 1 ryanodine receptor	UDG	Uracil-DNA glycosylase
S.E.M.	Standard error of the mean	VLL	Ventrolateral lip
S.E.M.	Standard error of the mean	Wnt	Wingless-related integration site
S1000A1	S100 calcium-binding protein A1	WP	Wiki pathways
SC	Sclerotome		

*The abbreviations of genes used less than 3 times are explained directly in the text.

Zusammenfassung

Als Hauptfunktion der differenzierten Skelettmuskulatur gilt die Kontraktion, welche den Lebewesen die aktive Bewegung ermöglicht. Die Kontraktion spielt jedoch auch eine wichtige Rolle in der Myogenese und ist daher unerlässlich für die korrekte Ausbildung und Organisation des muskuloskeletalen Systems. Auf molekularer Ebene erfordert die Initiierung der Skelettmuskelkontraktion das Zusammenspiel zweier mechanisch gekoppelter Ca^{2+} Kanäle, der Hauptuntereinheit des 1,4-Dihydropyridin-Rezeptors ($Ca_v1.1$) und des Typ 1 Ryanodin-Rezeptors (RYR1), im Rahmen der sogenannten elektromechanischen Kopplung (ECC). Obwohl mehrere funktionelle und strukturelle Studien im Laufe letzten Jahrzehnten ein tieferes Verständnis der Rolle von $Ca_v1.1$ und RYR1 beim ECC ermöglicht haben, bleibt die genaue Rolle, die sie bei der Regulation der Genexpression während der Muskelentwicklung spielen unklar.

Die vorliegende Arbeit untersucht die morphologischen und globalen Veränderungen im Transkriptom der Extremitätenmuskulatur von RYR1- und $Ca_v1.1$-defizienten ($RYR1^{-/-}$ und $Cav1.1^{-/-}$) Mäusen zu Beginn (E14.5) und am Ende (E18.5) der sekundären Myogenese. In beiden Modellen sind bereits zum Zeitpunkt E14.5 erste Veränderungen der Muskelstruktur feststellbar. In diesem Stadium wird in $Ca_v1.1^{-/-}$ Skelettmuskeln auch eine erhöhte Apoptoserate beobachtet. Microarray-Analysen zeigen diskrete Veränderungen des Transkriptoms beider Mutanten zum Zeitpunkt E14.5, mit einer Herunterregulation von Genen, die hauptsächlich mit Innervation und Neuronenentwicklung in $RYR1^{-/-}$- und mit Muskelkontraktion in $Ca_v1.1^{-/-}$-Skelettmuskeln assoziiert sind. Zum Zeitpunkt E18.5 weist sowohl die $RYR1^{-/-}$- als auch die $Ca_v1.1^{-/-}$-Skelettmuskulatur schwerere strukturelle Anomalien, Fibrose sowie Anzeichen einer Entwicklungsverzögerung auf. Dieses späte Stadium ist durch einen hohen Überlappungsgrad der identifizierten differentiell exprimierten Gene (DEGs) zwischen $RYR1^{-/-}$ und $Ca_v1.1^{-/-}$ gekennzeichnet: Beide Mutanten zeigen eine fehlerhafte Regulation zahlreicher Gene, die am Aufbau der kontraktilen Maschinerie beteiligt sind, Veränderungen in der Expression von Transkripten globaler Signalwege sowie von multiplen microRNAs. Mutantenspezifische Transkriptomveränderungen zu E18.5 deuten auf Veränderungen in der Zusammensetzung der extrazellulären Matrix in $RYR1^{-/-}$-Muskeln und im Lipidstoffwechsel in $Ca_v1.1^{-/-}$-Muskeln hin. Zudem beeinträchtigt das Fehlen von RYR1 im Muskel das normale Verhältnis von $Ca_v1.1$ Spleißvarianten zum Zeitpunkt E14.5 sowie den Gesamt-Expressionslevel von $Ca_v1.1$ mRNA zum Zeitpunkt E18.5.

Zusammenfassend heben die Ergebnisse dieser Arbeit die Bedeutung von $Ca_v1.1$ und RYR1 für die korrekte Durchführung des Genexpressionsprogramms während der sekundären Myogenese in Skelettmuskeln der Maus hervor. Darüber hinaus ergeben sich Einblicke in die Synergie, aber auch in die spezifischen Rollen der beiden Ca^{2+}-Kanäle während der Skelettmuskelentwicklung.

Abstract

The main function of differentiated skeletal muscle is contraction, allowing for movement. However, contraction also has important developmental roles and thus is indispensable for proper muscle formation and organization. On a molecular level, the initiation of skeletal muscle contraction relies on the interplay of two mechanically coupled Ca^{2+} channels - the principal subunit of the 1,4-dihydropyridine receptor ($Ca_v1.1$) and the type 1 ryanodine receptor (RYR1), the key event in the process of excitation-contraction coupling (ECC). While multiple functional and structural studies over the last decades have led to a deeper understanding of the roles of $Ca_v1.1$ and RYR1 in ECC, their specific involvement in muscle development and in gene expression remains obscure.

The present work analyzes the morphological and global transcriptomic changes occurring in limb skeletal muscle from RYR1- and $Ca_v1.1$-deficient ($RYR1^{-/-}$ and $Ca_v1.1^{-/-}$, respectively) mice at the beginning (E14.5) and at the end (E18.5) of secondary myogenesis. In both models initial muscle structure alterations are already observable E14.5. At this stage, increased apoptosis is observed only in $Ca_v1.1^{-/-}$ limb skeletal muscle. Microarray analyses reveal discrete transcriptomic changes in both mutants at E14.5, with downregulation of genes primarily associated with innervation and neuron development in $RYR1^{-/-}$, and with muscle contraction in $Ca_v1.1^{-/-}$ skeletal muscle. At E18.5, both $RYR1^{-/-}$ and $Ca_v1.1^{-/-}$ skeletal muscles are characterized by more severe structural malformation, fibrosis, and signs of developmental retardation. At this stage a high number of the detected differentially expressed genes (DEGs) overlap i $RYR1^{-/-}$ and $Ca_v1.1^{-/-}$. Both mutants display a failure to upregulate the expression of many genes involved in the buildup of the contractile machinery and exhibit changes in the expression of global signaling pathways and multiple microRNAs. Mutant-specific transcriptomic changes point to changes in the composition of the extracellular matrix in $RYR1^{-/-}$ muscle and in the lipid metabolism in $Ca_v1.1^{-/-}$ muscle. Finally, the absence of RYR1 in $RYR1^{-/-}$ mice alters the ratio of $Ca_v1.1$ splice variants at E14.5, and the total $Ca_v1.1$ mRNA levels at E18.5.

Taken together, the results of this work highlight the importance of $Ca_v1.1$ and RYR1 for the proper execution of the developmental gene expression program during secondary myogenesis in mouse limb skeletal muscle. Furthermore, it provides insights into mutual but also specific roles of each Ca^{2+} channel during skeletal muscle development.

1 Introduction

1.1 The skeletal muscle organ

In humans skeletal muscle is the largest organ by mass, accounting for approximately 40% of the total body weight, 50-75% of all body proteins and up to 50% of the entire protein turnover (Frontera & Ochala, 2015; Janssen, Heymsfield, Wang, & Ross, 2000). Together with the cardiac muscle, the skeletal muscle is composed of striated muscle tissue, named after its characteristic pattern of alternating light and dark regions, when observed under a microscope. Out of the three muscle tissue types – skeletal, cardiac and smooth – the skeletal muscle is the only one that is under a conscious, voluntary control (Klinke, 2005). Skeletal muscle is a part of the musculoskeletal system that also includes bones, cartilage, tendons, connective tissue, blood vessels and nerves (Deries & Thorsteinsdottir, 2016). As a part of the musculoskeletal system different groups of skeletal muscles are involved in the execution of various movements, mimics and maintenance of postures and breathing. From a metabolic point of view, skeletal muscle is one of the major organs participating in energy metabolism, glucose uptake and storage and is an essential reservoir for carbohydrates and amino acids (Wolfe, 2006).

The skeletal muscle organ is described by a high degree of complexity and plasticity in both structural and functional aspect. Therefore, substantial changes in skeletal muscle mass and composition can be caused by exercise, diet and other physiological conditions, as well as by various diseases and ageing (Hoppeler, 2016).

1.1.2 Skeletal muscle structure

Muscle, connective and nervous tissue, as well as parts of the circulatory system are all entangled in the buildup of the skeletal muscle organ and contribute to its elaborate characteristics and functions. In healthy adults the predominant part of the organ consists of muscle tissue, although adipose tissue can also constitute a substantial part, especially in some pathological conditions (Frontera & Ochala, 2015; Javan et al., 2013). Depending on the developmental stage, species and (patho-)physiological condition, the skeletal muscle tissue comprises various cell types of the myogenic lineage (Buckingham et al., 2003). Fully developed muscle tissue is mostly composed of long, cylindrical,

multinucleated cells called muscle fibers or myofibers (Lang, Thews, & Schmidt, 2000). The muscle fibers are terminally differentiated post-mitotic cells with a diameter between 10 and 100 μm and a length up to several cm that are situated in parallel relative to each other in bundles called fascicles (Fig. 1) (Lang et al., 2000). Branches of motor-neurons' axons form complex chemical synapses with each myofiber, called neuromuscular junctions (NMJs). Three layers of connective tissue contribute to the myofiber organization in skeletal muscle – epimysium, covering the whole outer surface of a muscle; perimysium – covering each of the fascicles; and endomysium – covering each of the muscle fibers. (Fig. 1) (Lang et al., 2000). Furthermore, a mesh of extracellular matrix, called basal lamina, lies between the endomysium and the fiber membrane – the sarcolemma, ensheathing multiple quiescent muscle stem cells – satellite cells (SCs) – located along the periphery of each fiber. These are quiescent mononucleated muscle stem cells that are activated upon muscle injury or disease and differentiate into mature myofibers.

Each muscle fiber contains hundreds of myofibrils – rod-shaped structures, composed of parallel thick and thin myofilaments that contain the muscle active contractile proteins (Huxley & Hanson, 1954), as well as of titin filaments, responsible for passive force development and elasticity (Linke & Kruger, 2010). Microscopically, the myofilaments in the myofibrils are arranged in regularly alternating darker and lighter regions, aligned across the myofibrils and myofibers, giving rise to the typical striation pattern of skeletal muscle (Huxley, 1961). The microscopically denser (darker) regions constitute the anisotropic bands – A-bands, and the less dense (lighter) regions – the isotropic bands – I-bands (Fig. 1). The A-bands are divided in half by a lighter H-zone, and in the middle of the I-bands darker, narrower regions – the Z-discs – mark the borders of the smallest morphological units of striated muscle – the sarcomeres (Fig. 1) (Huxley, 1961). Thin filaments are directly attached to the Z-discs and protrude in the I- and A-bands but at rest do not reach the center of the sarcomere, forming the less dense H-zone, whereas thick filaments occupy only the A-band regions and are indirectly attached to the Z-discs via titin filaments. At rest, the length of each sarcomere from one Z-disc to another is approximately 2.2 to 2.4 μm. When contraction is initiated, cross-bridges are formed between the thick and the thin myofilaments, causing the thin filaments to slide towards the M-line, leading to a disappearance of the H-zone and a shortening of the I-bands and consequently – of the sarcomere to approximately 2.0 μm (Klinke, 2005). Thus, the simultaneous shortening of the sarcomeres along the myofibrils of a muscle fiber leads to the shortening of the whole fiber and consequently – of the whole muscle.

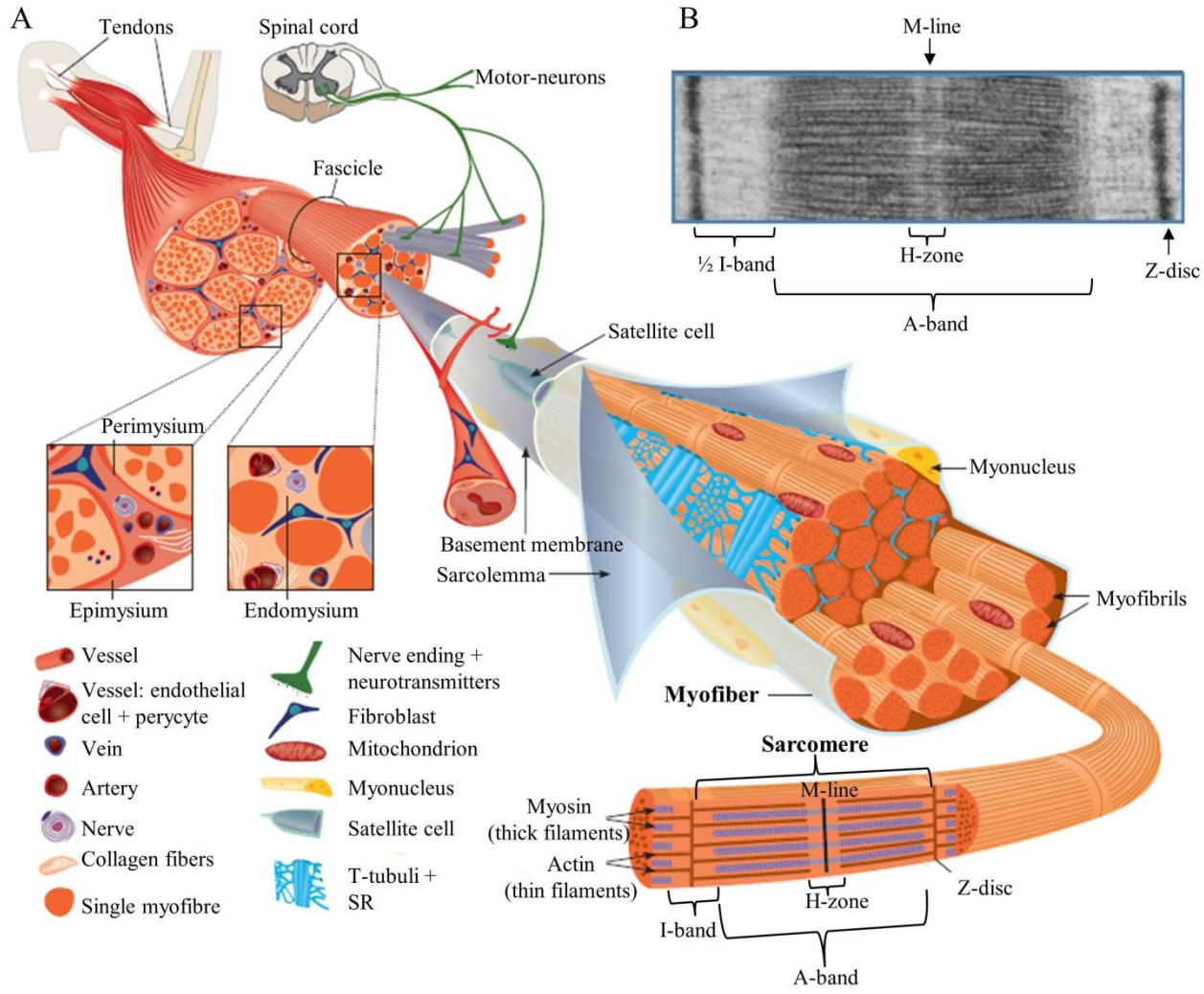

Fig. 1: Skeletal muscle and associated structures.
(A) A scheme of the skeletal muscle structure, showing the hierarchical organization of skeletal muscle starting from the whole organ down to the intracellular architecture of individual muscle fibers. Deep tubular invaginations of the sarcolemma called the T-tubuli form an intracellular network with the terminal cisternae of the myofibers' endoplasmic reticulum – the sarcoplasmic reticulum (SR). Most of the intracellular space of the myofibers is taken up by numerous myofibrils, consisting of thick (myosin) and thin (actin) myofilaments that are perfectly aligned and build up the skeletal muscle's contractile machinery. The smallest functional units of this machinery are the sarcomeres. Each sarcomere contains a microscopically denser A-band, thick filaments and two halves of a brighter I-band, containing the thin filaments. In the middle of the A-band is a narrow lighter region – the H-zone, and in the middle of it there is a denser line – the M-line, anchoring the thick and thin filaments. Two darker vertical regions – the Z-discs – mark the borders of each sarcomere. Beside the myofibrils, the myofibers possess a high mitochondrial content due to the muscle's high energy demands. Other organs like blood vessels (veins and arteries) and cell types like nerves and fibroblast contribute to the functions and structure of skeletal muscle. **(B)** An electron micrograph of a sarcomere. Modified from (Lang et al., 2000) and (Tajbakhsh, 2009).

1.1.3 Proteins of the contractile machinery

Multiple diverse proteins are involved in the sarcomeric structure and regulate skeletal muscle contractile properties (Fig. 2). The main two proteins in the execution of muscle contraction and in

the composition of the thick and thin myofilaments are myosin and actin, respectively (Huxley, 1961).

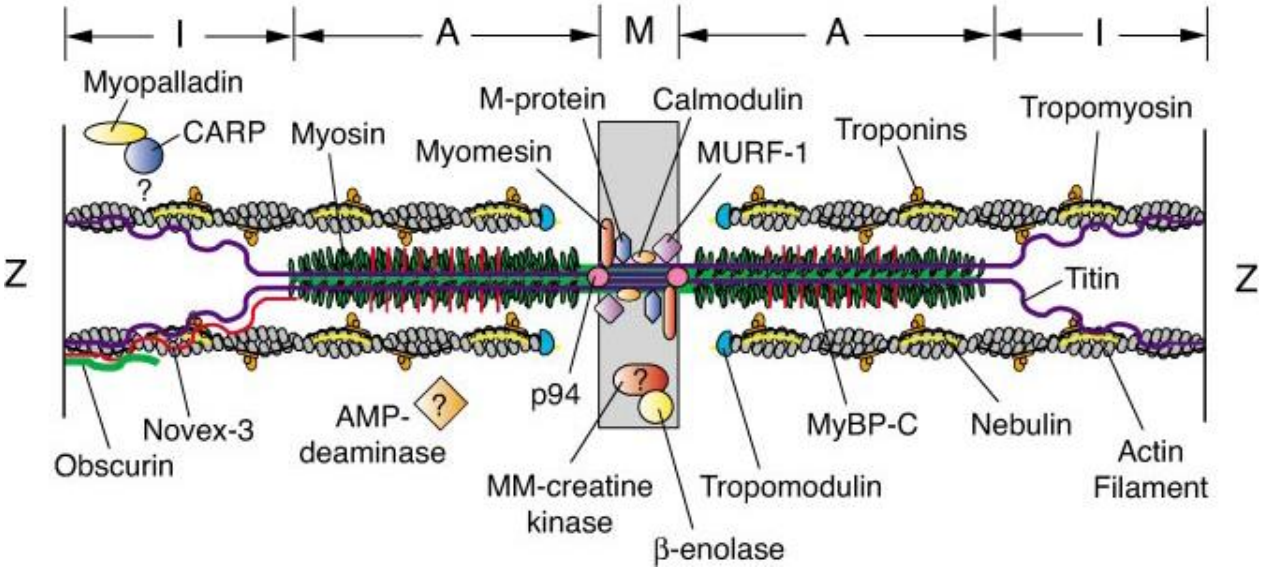

Fig. 2: A molecular model of the sarcomeric structure between two Z-discs.
The I-band, A-band and M-line regions are schematically represented. Multiple diverse proteins bind to and contribute for the functions of the myofilaments. Components whose binding sites are unknown are shown with question marks. Abbreviations stand for: CARP, cardiac ankyrin repeat protein; MM-creatin kinase, M-line creatin kinase; MyBP-C, myosin binding protein C; MURF-1, muscle-specific ring-finger 1. Modified from (Clark, McElhinny, Beckerle, & Gregorio, 2002).

Approximately 300 myosin molecules polymerize to form the thick myosin filaments (Fig. 2). Each myosin protein is composed of two heavy chains (MyHCs) and four light chains – 2 regulatory and 2 essential light chains. Each MyHC is composed of an α-helical domain, called a "tail" and a globular domain, called a "head" (Klinke, 2005). The two MyHC tails are coiled around each other and are connected to the myosin heads via an elastic transition, called a "hinge" or "neck". The myosin heads distal ends contain catalytical domains that are able to bind actin and hydrolyze adenosine triphosphate (ATP). The two regulatory and essential myosin light chains bind to the hinges and the proximal ends of the myosin heads and together with the hinges act as molecular levers, facilitating the cross-bridges between the myosin heads and the actin filaments. Each half of the myosin filaments is bound to 3 – 6 titin molecules that bind the free myosin filaments termini and form elastic filaments, anchored at the Z-discs. Throughout the A-bands the titin filaments align with the myosin filaments, whereas in the I-bands the titin filaments continue freely and in these regions they exhibit substantial stretch capabilities (Klinke, 2005).

Actin is the most abundant protein in striated muscle and is found either in a monomeric state (G-actin), or as a homopolymer, forming long actin filaments (F-actin) (Pollard, 1990). In mammals six actin isoforms exist and are usually characterized by their isoelectric points as α, β and γ actin, where α actin isoforms are specific for skeletal and cardiac muscle (Clark et al., 2002). Around 400 globular G-actin monomers polymerize into filamentous F-actin to form the actin filaments (Fig. 2). The actin filaments have a double helical structure with 2x7 actin monomers in each turn (Klinke, 2005). Muscle contraction is initiated in the cross-bridge cycle that involves several steps, including actin binding to the myosin heads, that in turn release ADP and inorganic phosphate, P_i, generating a power stroke, pulling the actin filaments towards the M-line and resulting in sarcomere shortening (Huxley, 2000). Binding of ATP to the myosin heads allows their detachment from the actin filaments, and its hydrolysis to ADP and P_i by the myosin ATPase returns the myosin heads to their pre-stroke ("cocked") position, thus closing the cross-bridge cycle. Regulatory proteins like the filamentous tropomyosin and the globular troponin complex bind to actin filaments' double helical grooves at regular intervals and are vital for proper regulation of contraction (Klinke, 2005). Each tropomyosin protein is associated with a troponin complex, composed of three subunits – troponin T (tropomyosin-associated troponin), troponin I (inhibitory troponin) and troponin C (Ca^{2+}-binding troponin). When the intracellular calcium $[Ca^{2+}]_i$ concentration in the muscle fibers is lower than 10^{-7} mol/L tropomyosin sterically obstructs the myosin binding sites on the actin filaments. However, when the Ca^{2+} concentration rises above this level, Ca^{2+} binds to the troponin C proteins, which act as Ca^{2+} sensors, and induce rearrangement in the troponin complex and the tropomyosin associated with it (Klinke, 2005). Thus, actin's myosin binding sites become exposed to build cross bridges with myosin and facilitate muscle contraction.

Titin, the biggest known mammalian protein (3,000 to 3,700 kDa) makes up the main part of the third type of myofilaments – the titin filaments (Fig. 2). In contrast to actin and myosin, titin does not actively contribute to muscle contraction but is vital for passive force and dynamic stiffness development (Bartoo, Linke, & Pollack, 1997). Moreover, the titin filaments integrate multiple signaling cascades, as various signaling proteins and molecules bind to the titin filaments (Kruger & Kotter, 2016; Linke & Kruger, 2010).Titin filaments' NH_2-termini are anchored at the Z-discs and stretch through the I- and A-bands up to the M-line (Linke & Kruger, 2010). In the I-bands the titin filaments possess flexible domains that act as a molecular spring. In the A-Bands they bind to the myosin filaments.

A fourth filament system, consisting of the giant protein nebulin, is also involved in the sarcomeric structure and functions (Fig. 2). More specifically, nebulin binds to the thin filaments and determines their length by influencing the minimum length of actin polymerization (Ottenheijm & Granzier, 2010). Nebulin also maintains myofibrillar alignment by regulating desmin localization, a key protein linking adjacent Z-disc (Shah et al., 2002). Additionally, nebulin affects muscle contractility by regulating the cross-bridge cycling kinetics and Ca^{2+}-sensitivity of force generation (Bang et al., 2009; Chandra et al., 2009).

The Z-discs, marking the lateral boundaries of the sarcomeres and acting as an anchoring point for the myofilaments discussed above, are multiprotein complexes consisting largely of a backbone made of antiparallel α-actinin homodimers (Frank, Kuhn, Katus, & Frey, 2006). Various additional structure and signaling proteins like desmin, the muscle lim protein (MLP), and telethonin take part in the buildup and functions of the Z-discs (Fig. 3) (Clark et al., 2002). Peripheral Z-disc proteins bind to proteins from the muscle fiber plasma membrane – the sarcolemma – and form complex structures, linking the sarcomeres and the sarcolemma called "costameres" (Ervasti, 2003). Since the Z-discs anchor the myofilaments and together with the costameres facilitates the link between the sarcolemma and the muscle's contractile machinery, they play a central role in mechanosensing and mechanotransduction (Frank et al., 2006).

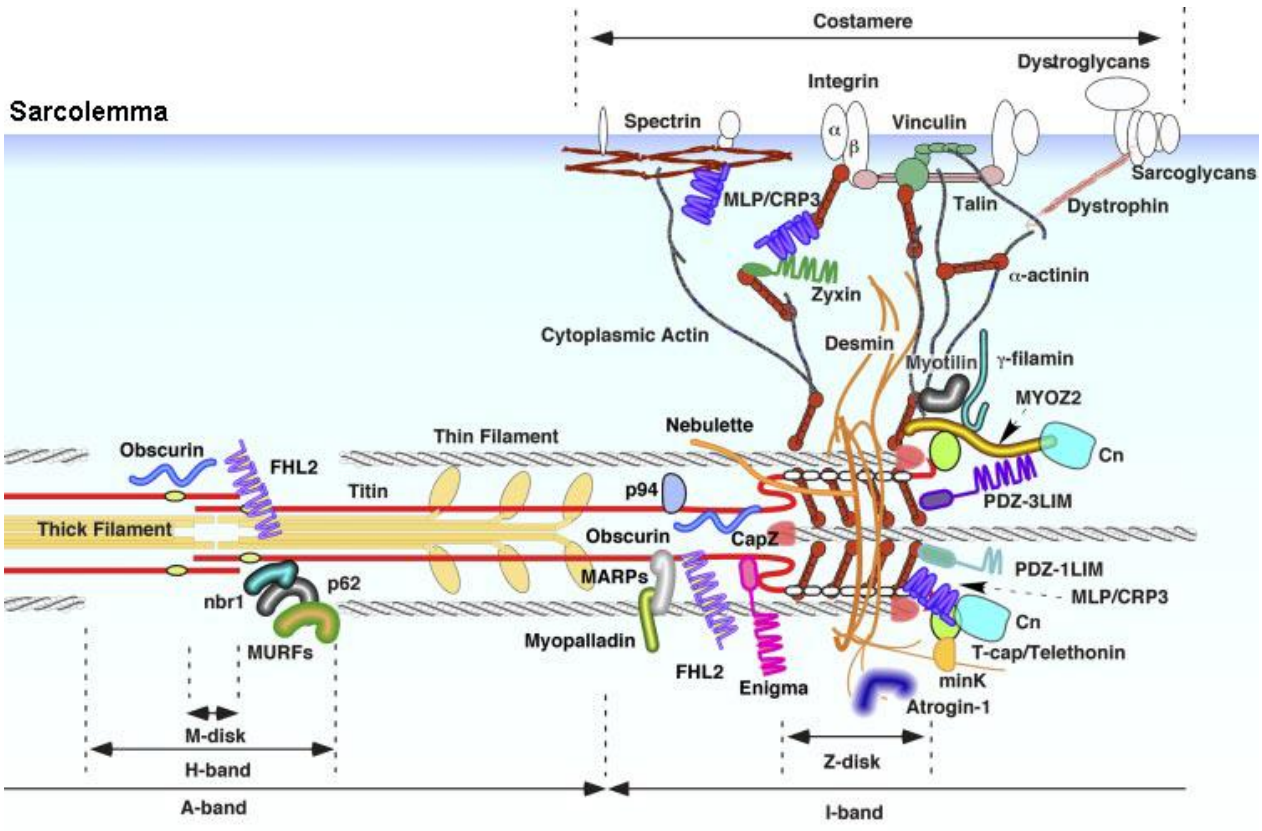

Fig. 3: Z-disc and costamere structure.
The scheme represents the multitude of proteins and molecules that have been identified as components of the Z-discs and costameres. Abbreviations stand for: MYOZ2, myozenin 2 (carsarin 1); Cn, calcineurin; PDZ-3LIM, one-PDZ and three-LIM domain protein; PDZ-1LIM, one-PDZ and one-LIM domain protein; MLP/CRP3, muscle-specific LIM protein/cysteine-rich protein 3; FHL2, four-and-a-half LIM protein 2; MAPRs, muscle ankyrin repeat proteins; MURFs, muscle-specific ring-finger proteins; nbr1, neighbor of Brca1 gene 1; mink, misshapen-like kinase 1. Modified from (Hoshijima, 2006).

1.1.4 Skeletal muscle architecture, metabolism and fiber type

The contractile properties of the different skeletal muscles are determined by a variety of factors like muscle architecture, metabolism and by the types of fibers (Lieber & Friden, 2000; Schiaffino & Reggiani, 2011). Structural differences like muscle and fiber length, as well as the physiological cross-sectional area and the angle of the fibers relative to the axis of force generation (pennation angle) contribute to the specific mechanical properties of different skeletal muscles (Lieber & Friden, 2000). Furthermore, the composition and the mechanical properties of the sarcolemma and the extracellular matrix (ECM) also influence skeletal muscle's contractile functions directly (Campbell & Stull, 2003; Gillies & Lieber, 2011).

The energy demands of skeletal muscle can drastically fluctuate dependent on its activity and the frequency and strength of contraction. During exercise skeletal muscle can consume more than 100-fold more energy than during rest, requiring rapid metabolic adaptations (Sahlin, Tonkonogi, & Soderlund, 1998). Moreover, skeletal muscle is a primary site for glucose uptake and acts as a reservoir for carbohydrates, amino acids and proteins that can be distributed to other parts of the body under stress conditions or illness (Argiles, Campos, Lopez-Pedrosa, Rueda, & Rodriguez-Manas, 2016). Skeletal muscle fibers use ATP as their primary energy source and therefore utilize both anaerobic and aerobic pathways in order to avoid ATP depletion (Sahlin et al., 1998). Anaerobic pathways used for ATP generation – mostly phosphocreatine degradation and glycogen breakdown – are more common during short high-intensity physical activity (Westerblad, Bruton, & Katz, 2010). Aerobic metabolism, on the other hand, dominates during long submaximal exercise, and consists mostly of β-oxidation of fatty acids or degradation of carbohydrates via the citric acid cycle (Westerblad et al., 2010). Hence, a substantial part of the skeletal muscle fibers' volume is taken up by mitochondria, where the aerobic ATP production takes place (Lundby & Jacobs, 2016).

The skeletal muscle fibers are not homogenous in terms of their contractile and metabolic properties, but can be divided into several fiber types. Several criteria have been used for fiber classification into different types and their results are not always in agreement with one another (Scott, Stevens, & Binder-Macleod, 2001). Initially myofibers were divided into "red", "white" or "intermediate" based on their color; and into "fast-twitch" or "slow-twitch" based on their contractile kinetics (Barnard, Edgerton, Furukawa, & Peter, 1971). Later, in accordance with their energy metabolism, myofibers were classified into "slow oxidative", "fast oxidative, glycolytic" and "fast glycolytic" (Barnard et al., 1971; Greising, Gransee, Mantilla, & Sieck, 2012; Schiaffino & Reggiani, 2011). On the basis of the pH lability of actomyosin ATPase staining, myofibers can be also classified as type I, IIa, IIb and IIx (Greising et al., 2012). Each of the latter fiber types has also been found to express a specific isoform of MyHC, specifically $MyHC_{slow}$, $MyHC_{2A}$, $MyHC_{2B}$ and $MyHC_{2X}$ in the type I, IIa, IIb and IIx fibers, respectively (Schiaffino & Reggiani, 2011). Some muscles composed of type IIb fibers have also been shown to co-express $MyHC_{2B}$ and $MyHC_{2X}$ (Greising et al., 2012). Additionally, two developmental MyHC isoforms have been identified – embryonic $MyHC_{emb}$ and neonatal $MyHC_{neo}$, which predominate during embryonic and early postnatal development (Agbulut, Noirez, Beaumont, & Butler-Browne, 2003; Greising et al., 2012).

1.2 Skeletal muscle development

1.2.1 Myogenesis – definition and models

Myogenesis – the generation of muscle tissue – is a complex multistep process that has been a subject of intensive studies (Asfour, Allouh, & Said, 2018; Bentzinger, Wang, & Rudnicki, 2012; Edgeworth, 1899; Read, Takeda, & Kirkaldy-Willis, 1971). Generally one can discriminate between developmental and regenerative myogenesis – the first one begins in the embryonic development and describes the *de novo* formation of skeletal muscle, whereas the second one occurs upon muscle injury or atrophy and serves for the production of new muscle fibers in place of the damaged ones. Very similar processes take place in both types of myogenesis; however there are also some specific distinctions (Tajbakhsh, 2009). Failure in the proper execution of either type of myogenesis can cause a wide range of diseases like myopathies, rhabdomyosarcoma and cachexia; as well as severe developmental disorders like the Duchenne and Becker muscular dystrophies (Emery, 2002).

Multiple *in vitro* and *in vivo* models are being utilized in the physiological and pathophysiological studies of skeletal myogenesis, each having advantages and disadvantages (Abmayr & Pavlath, 2012; Chal & Pourquie, 2017). Diverse *in vitro* models spanning from classical muscle cell lines like C2C12 through pluripotent stem cells (PSCs)-derived cell lines to modern lab-on-a-chip models are rapidly improving and constitute homogenous systems allowing easy handling, quick results and personalized patient-specific analysis (Agrawal, Aung, & Varghese, 2017; Burattini et al., 2004; Chal & Pourquie, 2017). Nevertheless, up to now they have not been able to reproduce the full structural and functional complexity of the entire skeletal muscle organ and lack vital components of the skeletal muscle microenvironment like fiber innervation, the crosstalk with the ECM and with other organs, all contributing to proper muscle development (Fredette & Landmesser, 1991; Nassari, Duprez, & Fournier-Thibault, 2017). The *in vivo* models for myogenesis comprise versatile vertebrate and invertebrate model organisms (Abmayr & Pavlath, 2012; Kim, Jin, Duan, & Chen, 2015; Sparrow, Hughes, & Segalat, 2008). While each of them has a set of advantages and drawbacks, the *in vivo* models pose a more physiological and accurate representation of myogenesis and can be better related to the myogenic events in humans. The main limitations of using *in vivo* myogenic models are that they are often more costly, harder to generate and to handle, the experiments require more time, the observed myogenic events might differ from those in humans and there are significant ethical concerns and limitations (Hartung, 2008). A lot of the fundamental work

elucidating the mechanisms of myogenesis has been performed on chick embryos (Allen & Pepe, 1965; McLennan, 1983; Read et al., 1971; Shellswell, 1977). *Caenorhabditis elegans*, *Drosophila melanogaster* and zebrafish have also proven themselves as valuable models for the examination of different aspects of muscle development (Abmayr & Pavlath, 2012; Armant, Gourain, Etard, & Strahle, 2016; Fox et al., 2007; Sparrow et al., 2008; Te & Reggiani, 2002). However, in the last several decades the mouse has emerged as probably the most frequently used *in vivo* model for myogenesis in (patho)physiological research (Durbeej & Campbell, 2002; Tondeleir, Vandamme, Vandekerckhove, Ampe, & Lambrechts, 2009). As a mammalian model, it has the advantages that it closely resembles the myogenic events in the human, has a high degree of genetic similarity to humans and can be easily genetically manipulated (Kablar & Rudnicki, 2000). Despite the differences that inevitably arise when comparing different species and the disadvantages of *in vivo* models discussed above, the mouse is one of the most advantageous and exploited model for skeletal myogenesis (Abmayr & Pavlath, 2012; Kablar & Rudnicki, 2000; Tajbakhsh, 2009; Watson, Riordan, Pryce, & Schweitzer, 2009).

1.2.2 Myogenesis in the mouse

In mice skeletal muscle development begins *in utero* and continues 2-3 weeks after birth (Fig. 4). The prenatal period begins between the 8^{th} and 9^{th} embryonic day (E8.5 – E9) and lasts approximately until E18.5 or until birth (Tajbakhsh, 2009). It involves a number of events and different muscle precursor and progenitor cells, normally described by the presence and expression of specific myogenic markers, which undergo several successive differentiation steps before reaching maturity (Bryson-Richardson & Currie, 2008). The prenatal myogenesis can roughly be divided into three main developmental stages that partially overlap – somitogenesis, primary and secondary myogenesis.

Around E4.5 the primary tissue types – trophectoderm, epiblast and primitive endoderm are established (Arnold & Robertson, 2009). Subsequently, around E6.0 under the influence of regional differences in gene expression they form the tree germ layers of the prepatterned embryo – the ectoderm, mesoderm and endoderm (Arnold & Robertson, 2009). In respect to the midline of the embryo the mesoderm is separated into tree anatomical layers – the paraxial, intermediate and lateral mesoderm (Bentzinger et al., 2012).

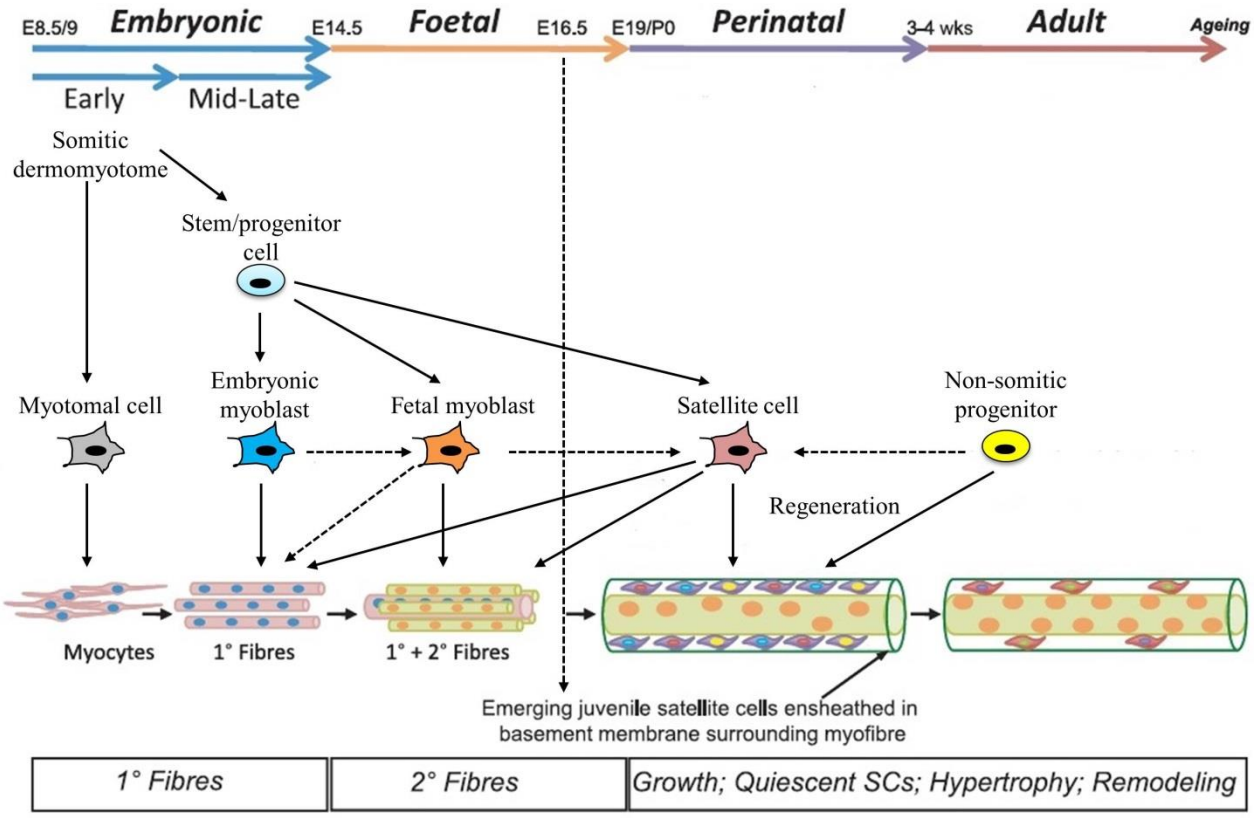

Fig. 4: Mouse myogenesis timeline.
In the mouse the first myogenic events take place at E8.5/E9 when the somites are formed, giving rise to myotomal cells which subsequently differentiate into the first myocytes. The somatic dermomyotome also releases stem/progenitor cells which further differentiate into embryonic and fetal myoblasts and satellite cells (SCs) –quiescent myogenic cells, important for postnatal muscle regeneration. From the mid-late stages (E10.5-E12.5) to the end of embryonic development at E14.5, primary (1°) fibers are formed from the embryonic myoblasts via several steps of differentiation. The myogenic events up to E14.5 constitute the primary myogenesis. From E14.5 until birth (around E18.5 to E20.5) the fetal development in the mice coincides with a second wave of myogenic events called secondary myogenesis, in which fetal myoblasts develop into secondary (2°) fibers. The first SCs arise approximately 2 days prior birth (E16.5) and contribute to the muscle growth, maturation and hypertrophy from the perinatal period into adulthood. Some non-somitic progenitor cells are also implicated in the adult muscle regeneration. Modified from (Tajbakhsh, 2009) and (Biressi, Molinaro, & Cossu, 2007a).

Around E8.5 oscillations of gene expression and gradients of morphopgene concentration leads to pair-wise concentration of the paraxial mesoderm left and right of the neural tube into transitory spherical epithelial structures called somites that develop in the direction from the head to the tail (Fig. 5) (Kablar & Rudnicki, 2000). All skeletal muscles except the superficial neck muscles develop from the somites (Deries & Thorsteinsdottir, 2016). A polarity within the somites is then established and they develop dorso-ventral compartments. The ventral compartments gives rise to the mesenchymal sclerotome which later develops into cartilage and bones, and the dorsal part of the somites forms the dermomyotome (Bentzinger et al., 2012). All skeletal muscles with the exception of some muscles of the head in mice and other vertebrates arise from cells of the dermomyotome.

Multiple signaling molecules and pathways are involved in the formation of the dermomyotome and the subsequent muscle development (Fig. 5) (Bentzinger et al., 2012). As the embryo develops, terminally differentiated, mononucleated cells emerge from the dorsomedial and ventrolateral lips of the dermomyotome and form the primary myotome (Bentzinger et al., 2012; Biressi et al., 2007a). This process involves muscle progenitor cells (MPCs) translocating from the dermomyotome to a ventrically-located domain, followed by MPC elongation so that at the end the cells span the entire somite length along the cranio-caudal axis of the embryo (Biressi et al., 2007a). A population of satellite cells that remain until adulthood are also formed (Gros, Manceau, Thome, & Marcelle, 2005). The epaxial part of the dermomyotome gives rise to the dorsal muscles and its hypaxial part to the trunk and limb muscles (Bentzinger et al., 2012).

Only a small fraction of cells are terminally differentiated during the formation of the primary myotome. The somatic dermomyotome produces $Pax3^{+}/Pax7^{+}$ double positive MPCs that differentiate into embryonic and fetal myoblasts and satellite cells, that will later differentiate into primary, secondary and adult muscle fibers (Fig. 4) (Biressi et al., 2007a). From approximately E10.5 to E14.5 an intensive myogenic phase called primary myogenesis takes place (Biressi et al., 2007a). Several differentiation steps occur simultaneously at this stage: Early on, around E11 embryonic myoblasts invade the myotome and most probably fuse with the myotomal myocyes. At the same time embryonic myoblasts migrate to the limb buds and fuse into multinucleated primary (1°) fibers. A small number of myotubes participate in the composition of the skeletal muscles during primary myogenesis (Biressi et al., 2007a).

From E14.5 until birth (E18.5 to E20.5), coinciding with the fetal development in the mouse, another wave of myogenic events takes place – the secondary myogenesis (Tajbakhsh, 2009). During secondary myogenesis fetal myoblasts fuse and differentiate into secondary (2°) fibers that initially form in the vicinity of the zones of innervation, initiating the neuromuscular junctions (NMJs) formation (Duxson, Usson, & Harris, 1989; Tajbakhsh, 2009). Additionally, at the end of secondary myogenesis, around E16.5, the first juvenile satellite cells emerge and are ensheathed under a basal lamina (Tajbakhsh, 2009). The skeletal muscles grow substantially and the first spontaneous movements can be detected around at E14.5 (Kodama & Sekiguchi, 1984). It has been shown that embryonic and fetal myoblasts – the MPCs generating the 1° and 2° fibers, respectively, have distinct global expression profiles (Biressi et al., 2007b).

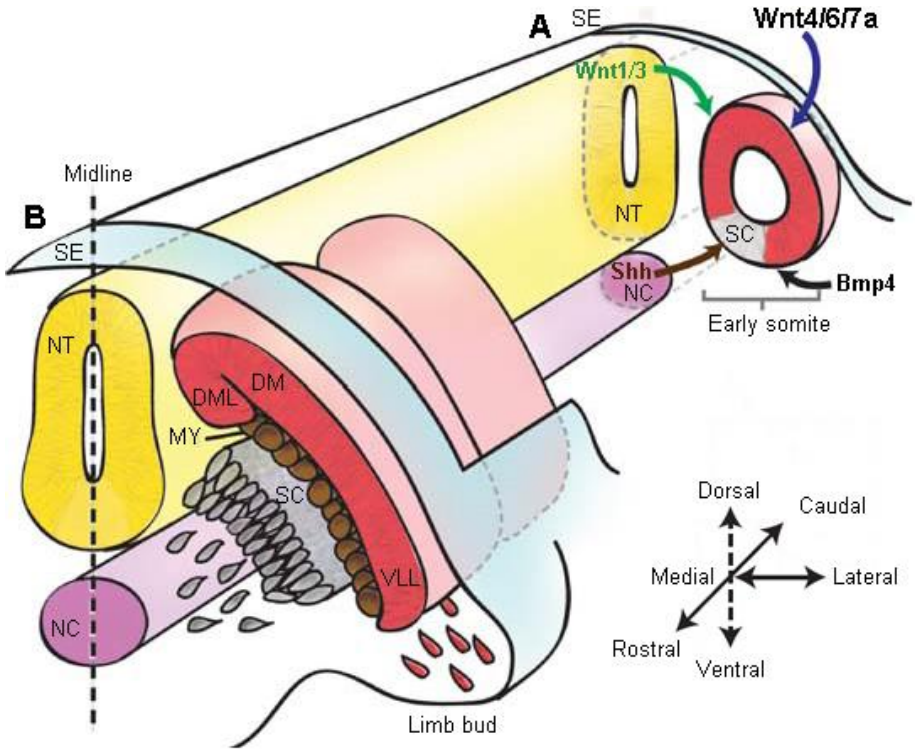

Fig. 5: Somitogenesis.
The early **(A)** and late **(B)** stages of somitogenesis are schematically represented. **(A)** In the early somite the development of the sclerotome (SC) and dermomyotome (DM) is initiated via morphogens and signaling molecules secreted from different parts of the embryo. On the one hand the bone morphogenic proteins (BMPs) from the lateral plate of the somite maintain the undifferentiated state of the somites. On the other hand, the dorsal neural tube (NT) and the surface ectoderm (SE) secrete Wnts, which together with the Sonic hedgehog (Shh) signaling factor, secreted from the neural tube floor plate and the notochord (NC), promote the formation of the sclerotome. **(B)** In the later stages of somite development, muscle progenitor cells (MPCs) leave the dorsomedial (DML) and ventrolateral (VLL) lips of the dermomyotome and differentiate into the myotome (MY). Limb bud formation is initiated by Pax3-positive ($Pax3^{+}$) MPCs that delaminate and migrate from the ventrolateral lips of the dermomyotome. Modified from (Bentzinger et al., 2012).

Consequently, the 1°and 2° fibers differ in their expression of MyHC isoforms – 1° express embryonic, phenotypically slow MyHC, whereas 2° fibers express neonatal, phenotypically fast MyHC (Biressi et al., 2007a). Other muscle-specific genes like muscle creatine kinase, β-enolase and protein kinase C theta (PKCϴ) are also differentially regulated in 1° and 2° muscle fibers (Biressi et al., 2007a). Thus, the primary myogenesis lays the pattern of the developing skeletal muscle, whereas the secondary myogenesis is the period for growth and differentiation. Further postnatal muscle growth and maturation is achieved primarily via the consecutive fusion of neonatal fibers with each other and with satellite cells (Biressi et al., 2007a; Tajbakhsh, 2009).

1.2.3 Signaling cascades during myogenesis

Each step of the myogenic program is executed under the strict control of a plethora of interconnected signaling pathways and cascades. Due to their versatile nature, different groups of muscles emerge under the control of specific regulatory networks (Tajbakhsh, 2009). The following sections will focus mainly on the regulatory mechanisms throughout prenatal limb myogenesis.

1.2.3.1 Myogenic regulatory factors (MRFs)

The myogenic regulatory (MRFs) are a group of transcription factors (TFs) that induce, control and maintain the myogenic fate of MPCs and muscle cells at each stage of their differentiation pre- and postnatally (Asfour et al., 2018). The first identified MRF – the myogenic determination factor 1 (MyoD) was described for its properties that upon activation it induces myogenic transformation of a fibroblast cell line (Davis, Weintraub, & Lassar, 1987). Since then another three TFs have been identified having similar properties – myogenic factor 5 (Myf5), myogenin (MyoG) and myogenic regulatory factor 4 (Mrf4, a.k.a. Myf6 and herculin) (Braun, Buschhausen-Denker, Bober, Tannich, & Arnold, 1989; Rhodes & Konieczny, 1989; Wright, Sassoon, & Lin, 1989).These four classical MRFs share three very similar structure domains, listed from the N- to the C-terminus of the proteins: a cysteine/histidine domain, a basic helix-loop-helix (bHLH) domain, and a serine/threonine-rich domain (Asfour et al., 2018). The bHLH domain is the most important one for the activation of a cellular myogenic program, as it can bind a DNA sequence, known as E-box, present in the promoters and enhancers of downstream muscle-specific genes and activate their expression (Berkes & Tapscott, 2005). Prior to DNA binding MRFs form homo-, or more frequently heterodimers with other bHLH proteins, often with the class of E2A proteins which are ubiquitously expressed (Massari & Murre, 2000). The expression levels and activity of the MRFs are controlled via multiple signaling networks and TFs like the myocyte enhancer factor 2 (MEF-2) family. Furthermore, some MRFs can enhance their own expression (MyoD and MyoG) or direct that of other MRFs (Asfour et al., 2018). The MRFs have partly overlapping and redundant myogenic functions. For example, knock out mouse models for Myf5 or MyoD have a normal skeletal muscle phenotype other than a short delay in the embryonic myogenesis in the Myf5 knockout (KO), whereas double Myf5:MyoD null mutants are completely devoid of muscles and myogenin (Braun, Rudnicki, Arnold, & Jaenisch, 1992; Rudnicki, Braun, Hinuma, & Jaenisch, 1992; Rudnicki et al., 1993). Therefore, Myf5 and MyoD exhibit a functional redundancy and at least one of them is

necessary for normal myogenesis. Conversely, homozygous MyoG KO mice have a severe reduction of skeletal muscle and a prevalence of undifferentiated myoblasts, although they have normal levels of MyoD (Hasty et al., 1993). This data shows that Myf5 and MyoD are important for myoblast specification early in the embryonic development, whereas MyoG acts downstream and is essential for late muscle development and differentiation. Mrf4 KO mice have higher MyoG levels and a phenotypically normal skeletal muscle but Mrf4:MyoD double KOs display a severe muscle deficiency similar as the MyoG null mice (Rawls et al., 1998). This indicates that Mrf4 represses MyoG expression and that there is some redundancy in the Mrf4 and MyoD roles for muscle differentiation.

Four other TFs have proven to be indispensable for early commitment to the myogenic program and induction of the initial myogenic events (Bentzinger et al., 2012). These are the paired-homeobox transcription factors 3 and 7 (Pax3/7) and the Sine oculis-related homeobox TFs 1 and 4 (Six1/4), which due to their contribution to the myogenic program can also be viewed as MRFs (Bentzinger et al., 2012). In all vertebrates at least one of the Pax3 and Pax7 TFs is conserved (Noll, 1993). Dermomyotomal cells and all MPCs express Pax3 and Pax7, however long-range migrating MPCs that form the initial limb musculature only express Pax3 (Bentzinger et al., 2012). Loss-of-function Pax3 mouse mutants do not form the hypaxial domain of the somite, resulting in loss of limb and diaphragm muscles, although they develop some epaxial-derived muscles (Bentzinger et al., 2012; Bober, Franz, Arnold, Gruss, & Tremblay, 1994). Pax3 acts upstream of MyoD and Pax3:Myf5:Mrf4 triple KOs mouse do not form any skeletal muscles and lack MyoD expression (Bentzinger et al., 2012). Pax7 KO mice did not exhibit abnormalities in embryonic muscle development but showed a requirement for Pax7 for satellite cell specification (Seale et al., 2000). Pax3 and Pax7 also exhibit some functional redundancy, since the Pax3:Pax7 mouse double mutant has a more severe phenotype than the Pax3 mutant alone, characterized by an almost complete failure in the embryonic myogenesis and a development only of the primary myotome (Relaix, Rocancourt, Mansouri, & Buckingham, 2005). Experiments with conditional deletions of either $Pax3^{+}$ or $Pax7^{+}$ cell populations have shown that Pax3 ablation is embryonically lethal, whereas loss of Pax7 leads to impairment of later myogenic stages, leading to smaller muscles with fewer myofibers at birth (Bentzinger et al., 2012; Hutcheson, Zhao, Merrell, Haldar, & Kardon, 2009; Seale et al., 2000). Thus, the $Pax3^{+}$ cells are characterized as founder MPCs that set the template for myogenesis in the limbs, whereas $Pax7^{+}$

cells contribute at a later stage to the secondary fiber formation and satellite cells specification (Bentzinger et al., 2012).

The Six1 and Six4 TFs act upstream of Pax3 and are crucial for the specification and commitment of the MPCs to the myogenic lineage (Fig. 6) (Bentzinger et al., 2012). Six1 and Six4 bind the eyes-absent homologs Eya1 and Eya2 that act as transcriptional cofactors and translocate to the nucleus, where they induce the transcription of downstream MRFs like Pax3, MyoD, MyoG and Mrf4 (Grifone et al., 2005). While Six4 KO mice do not exhibit significant developmental changes, Six1 KO neonates die at birth and show severe developmental abnormalities of multiple organs, including skeletal muscle (Laclef et al., 2003; Ozaki et al., 2001). Moreover, double KOs mice for Six1:Six4 or Eya1:Eya3 fail to upregulate Pax3 expression and hence do not develop limb and hepaxial trunk musculature (Grifone et al., 2007; Grifone et al., 2005). These results demonstrate that there is some redundancy in the functions of the TFs Six1 and Six4, as well as in these of their cofactors Eya1 and Eya2. The hepaxial (but not the epaxial) dermomyotome has active enhancer binding regions for both Six TFs and Pax3 in the Myf5 gene, indicating that the Six TFs and Pax3 drive Myf5 transcription in these muscles (Bentzinger et al., 2012).

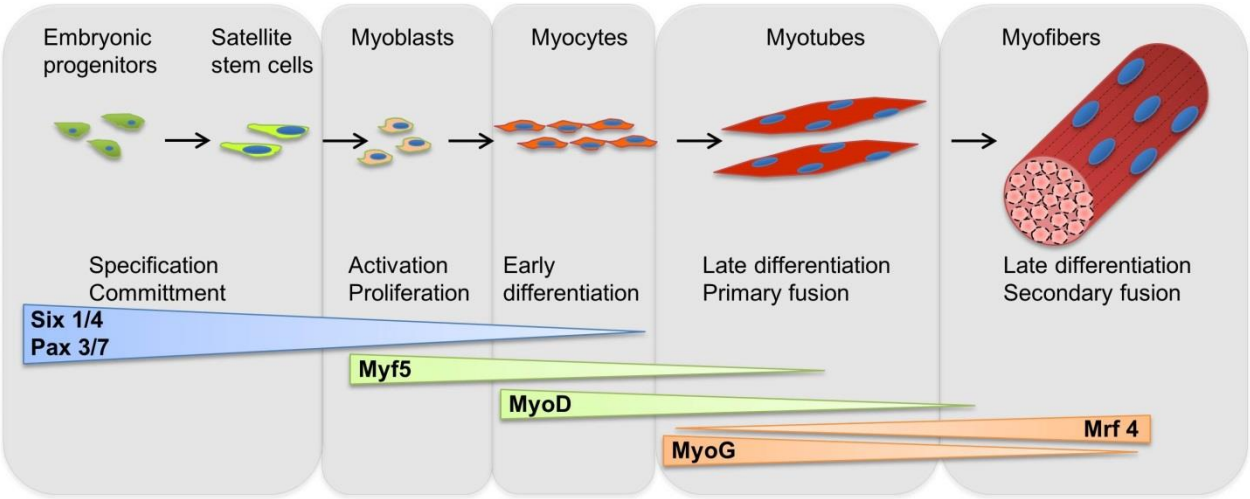

Fig. 6: MRFs hierarchy during myogenesis.
The expression and activation patterns of the MRF genes directs the proper transition of the myogenic stages and differentiation events in the MPCs. Six1/4 and Pax3/7 regulate the early embryonic progenitor cell specification; Myf5 and MyoD commit cells to the myogenic program; and MyoG and Mrf4 guide myocyte and myotubes fusion required for terminal differentiation. Modified from (Bentzinger et al., 2012).

Because of the strict spatiotemporal expression and activity of the MRFs in different populations of cells from the myogenic lineage, the presence of specific MRFs is also used as a marker for these cell populations and the corresponding developmental stages (Fig. 6).

1.2.3.2. Morphogens and signaling pathways involved in myogenesis

As mentioned above many major signaling pathways are involved in muscle development. One of them is the Wnt signaling pathway that comprises a canonical Wnt/β-catenin pathway, and several non-canonical Wnt pathways the main two of which are the Wnt/jun N-terminal kinase (JNK) pathway; and the Wnt/calcium pathway (Rao & Kuhl, 2010). The mechanism of action of all pathways involves secreted glycoproteins – the Wnts – that bind to receptors of the Frizzled (Fzd) family located on the plasma membrane that in turn often activate G-protein coupled receptors (GPCRs) and trigger various downstream cellular responses (Rao & Kuhl, 2010). The Wnt pathways control not only myogenesis but also the development of many other organs and structures, as well as bone development and limb patterning (Church & Francis-West, 2002). Multiple Wnts and their respective Fzd receptors regulate the expression of the MRFs and, as mentioned above (Fig. 5), induce the specification of MPCs in the somites (Bentzinger et al., 2012). For example, Wnt1 and Wnt3 secreted from the neural tube upregulate Pax3 and Myf5, whereas Wnt6 and Wnt7a positively regulate the expression of MyoD (Bentzinger et al., 2012). Wnts are also important for cell migration, morphology, terminal muscle differentiation and muscle fiber specification (Church & Francis-West, 2002). It has been demonstrated that in the mouse limb development the canonical β-catenin pathway is necessary for fetal myoblast specification and therefore, for secondary myogenesis and fiber type predetermination (Hutcheson et al., 2009).

Another signaling pathway that positively regulates early myogenic specification is the Hedgehog (Hh) signaling pathway, with the Sonic hedgehog (Shh) secreted protein being indispensable for myogenesis (Bentzinger et al., 2012). The notochord and neural tube secrete Shh that – like the Wnts – binds to receptors on the plasma membrane and triggers a downstream cascade, leading to an upregulation of the expression of group of TFs called GLI (Tickle & Towers, 2017). Together with certain Wnts, they induce the expression of Myf5 and MyoD, thus promoting MPCs to myogenic commitment and differentiation (Borello et al., 2006; Munsterberg, Kitajewski, Bumcrot, McMahon, & Lassar, 1995; Voronova et al., 2013). KO mice lacking Shh die perinatally and exhibit severe developmental abnormalities, including the absence of limb formation (Chiang et al., 1996).

Contrary to the positive effects of the Wnt and the Shh pathways for myogenic specification and differentiation, a subclass of the transforming growth factor beta (TGF-β), the bone morphogenic proteins (BMPs), inhibit certain MRFs and thus – the myogenic progression (Gaarenstroom & Hill, 2014). BMPs exert their functions in the somites through SMAD TFs promoting Pax3 expression, while inhibiting the expression of Myf5 and MyoD (Gaarenstroom & Hill, 2014). Wnts and Shh increase the secretion of Noggin that binds and inactivates BMPs and thus induces MyoD expression (Reshef, Maroto, & Lassar, 1998). In this way BMPs ensure the accumulation of MPCs prior the onset of muscle differentiation (Ono et al., 2011). The signals from the Wnt and BMP pathways are integrated in the periodic activity of the Notch signaling pathway, which similarly to the BMPs suppresses myogenic progression and prevents premature differentiation of MPCs (Hofmann et al., 2004; Kuroda et al., 1999). Furthermore, proper Notch signaling is imperative for the generation of satellite cells during fetal development (Vasyutina, Lenhard, & Birchmeier, 2007).

The mitogen-activated protein kinase (MAPK) pathway – a cascade of several consecutive phosphorylation steps, each activating a downstream kinase – is one of the most robust cellular signaling networks (Pearson et al., 2001). It includes three major signaling pathways: the extracellular signal-regulated kinases 1 and 2 (ERK1/2) pathway; the c-Jun N-terminal kinase (JNK) pathway; and the p38 pathway – all of which are implicated in the regulation of myogenesis (Jones, Fedorov, Rosenthal, & Olwin, 2001; Perdiguero et al., 2007; Xie et al., 2018). All three MAPK branches involve multiple steps and molecular interaction during the signal transmission. In short, the p38 pathway is a positive and the JNK pathway is a negative regulator of myogenic differentiation, whereas the ERK1/2 pathway has dual functions (Jones et al., 2001; Li & Johnson, 2006; Lluis, Perdiguero, Nebreda, & Munoz-Canoves, 2006; Xie et al., 2018; Yang et al., 2006).

The phosphoinositide 3-kinase (PI3K), the protein kinase B (Akt) and mammalian target of rapamycin (mTOR) form another global signaling pathway – the PI3K/Akt/mTOR pathway that positively regulates muscle differentiation and hypertrophy (Ge & Chen, 2012). In particular, mTOR stimulates primary and secondary fusion involved in the formation of nascent myotubes and myofibers, respectively (Ge & Chen, 2012).

As evident from the examples above, the regulation of skeletal myogenesis involves multiple signaling pathways that often overlap and interact with each other (their function is summarized in Table 1). Furthermore, the development of the limbs and their muscles is not only controlled by the

mere presence or absence of a particular signal but is fine-tuned by concentration gradients of FGFs, Wnts and other morphogens (Bentzinger et al., 2012). In addition, signals in the form of morphogens and mechanical stimuli from non-muscle cells and tissues like fibroblasts, nerves, blood vessels, bones and tendons, as well as the ECM, contribute to myogenesis and their own development is in turn regulated by muscle-derived factors and muscle contraction (Deries & Thorsteinsdottir, 2016).

In the last decade micro RNAs (miRNAs) – small non-coding RNAs with a length of approximately 22 nucleotides (nts), designated as Mir# or miR#, whrere # is the miRNA number – have gained a growing attention due to their versatile regulatory roles in virtually all cellular processes, including development and differentiation (Bartel, 2004). The majority of miRNAs act as posttranscriptional repressors and have multiple mRNA targets which they bind complementary, preventing their expression and reducing their molecular stability (Bartel, 2004). Many miRNAs have been implicated in skeletal myogenesis and their number grows as high-throughput analysis methods become more accessible (Castel et al., 2018). A group of 3 muscle-specific miRNA families – Mir206, Mir1 and Mir133 – the last two of which contain more than one family members, are called MyoMirs due to their intense regulation of every step of skeletal muscle development (Table 1) (Luo, Nie, & Zhang, 2013). While Mir206 and Mir1 promote muscle differentiation and exit from the cell cycle, Mir133 inhibits differentiation and promotes myoblast proliferation (Chen et al., 2006; Luo et al., 2013). The MyoMirs are regulated and in turn regulate the expression of the MRFs and contribute to the elaborate myogenic regulatory network (Horak, Novak, & Bienertova-Vasku, 2016).

Table 1: Summary of the functions of diverse signaling pathways in myogenesis

Signaling pathway / molecules	Functions in myogenesis
Wnt pathway	↑ MPCs specification in the somites ↑Myf5, MyoD expression • Regulates cell migration, morphology, terminal muscle differentiation and muscle fiber specification
Shh pathway	↑Myf5, MyoD expression ↑ myogenic commitment ↑ muscle differentiation
BMP pathway	↑ MPCs proliferation ↓ muscle differentiation
Notch pathway	↑ MPCs proliferation ↑ satellite cells formation ↓ muscle differentiation
MAPK pathway	• p38 pathway: ↑ muscle differentiation • JNK pathway: ↓ muscle differentiation • ERK1/2 pathway: ↑ myoblast proliferaton and fusion ↓ muscle growth
PI3K/Akt/mTOR pathway	↑ primary and secondary fusion

Signaling pathway / molecules	Functions in myogenesis
	↑ differentiation and hypertrophy
miRNAs	• Mir1 and Mir 206: ↑ muscle differentiation • Mir133: ↑ myoblast proliferation ↓ muscle differentiation • other miRNAs – versatile roles in myogenesis

1.2.3.3. Ca^{2+} and mechanotransduction in skeletal muscle development

A further level of complexity in skeletal muscle is added by the signaling events elicited by Ca^{2+} and mechanotransduction in the major function of this organ – the muscle contraction. Calcium is a potent second messenger that is involved in virtually all cellular processes and signaling pathways in all organs and tissues (Clapham, 2007). It has important functions in both developmental and regenerative myogenesis, influencing each myogenic stage including cell cycle transition, MPCs proliferation, MRF expression and terminal differentiation (Benavides Damm & Egli, 2014; Hauser, Saarikettu, & Grundstrom, 2008). Next to its roles in other signaling cascades, in skeletal muscle Ca^{2+} homeostasis and dynamics is vital for contraction, as described above (Klinke, 2005). Upon contraction initiation the $[Ca^{2+}]_i$ can rise up to a 100-fold in comparison to its concentration at rest (resting $[Ca^{2+}]_i$) and thus, significantly influences a number of Ca^{2+}-sensitive regulatory proteins and pathways (Gehlert, Bloch, & Suhr, 2015). The mechanical stress derived from muscle contraction itself triggers an intricate downstream network of mechanotransduction responses that largely overlap, regulate and amplify the Ca^{2+}-mediated signaling events. Thus, the interplay between rises of $[Ca^{2+}]_i$ and the resulting mechanotransduction signaling is pivotal for normal myogenesis and is a part of probably the most researched process in skeletal muscle – the excitation-contraction coupling (Benavides Damm & Egli, 2014; Gehlert et al., 2015).

1.3 Excitation-contraction coupling (ECC)

The term excitation-contraction coupling (ECC) describes the translation of the electrical signals transmitted from the motor neurons into the mechanical response of muscle contraction (Sandow, 1952). At specific pre-patterned regions at the surface of each myofibers, called motor endplates, the projections of the motor neuron axons form chemical synapses – the neuromuscular junctions (NMJs) (Hescheler, 2008). Thus, NMJs are the foci of muscle innervation and their proper development is under a strict control of a complex three-way communication between the muscle, the

motor neurons and presynaptic Schwann cells (Darabid, Perez-Gonzalez, & Robitaille, 2014). Each myofiber is innervated by one of the axonal terminals of a motor neuron and the sum of all fibers innervated by the same motor neuron (including the motor neuron itself) constitutes a motor unit (Buchthal & Schmalbruch, 1980). The number of motor units and their fiber type determines the mechanical properties of the individual muscles and muscle groups (Buchthal & Schmalbruch, 1980).

In myofibers ECC is achieved by a rapid transient rise in $[Ca^{2+}]_i$ in response to electrical stimulation, leading to Ca^{2+} binding to the TnC of the troponin complex and a subsequent contraction initiation (Klinke, 2005). Contrary to cardiac muscle contraction that requires Ca^{2+} flow into the cell from the extracellular space, the skeletal muscle contraction relies solely on Ca^{2+} released into the cytoplasm from the sarcoplasmic reticulum (SR) – the main internal Ca^{2+} storage in skeletal muscle (Armstrong, Bezanilla, & Horowicz, 1972; Lamb, 2000).

In the NMJs ECC begins as an action potential (AP) reaches a nerve terminal and causes exocytosis of the neurotransmitter acetylcholine (ACh) from the neuron's presynaptic membrane into the synaptic cleft (Sine, 2012). ACh then binds to nicotinic ACh receptors (nAChRs) that are densely clustered on the muscle's postsynaptic membrane (Sine, 2012). This leads to a local membrane depolarization that activates juxtaposed voltage-gated sodium (Na^+) channels that produce an inward Na^+ current, resulting in a further membrane depolarization and transmission of the AP along the sarcolemma (Catterall, 1988; Flucher & Daniels, 1989). As the AP propagates, it leads to depolarization of deep vertical invaginations of the sarcolemma – a tubular membrane network called the T-tubuli. The T-tubuli are located in a close proximity to the terminal cisternae of the SR, forming specific junctional structures known as triads that consist of a T-tubule surrounded by two SR terminal cisternae (Fig. 7) (Fahrenbach, 1965). Precisely the triadic junctions, also called "junctional feet", are the point of signal transmission translating the depolarization of the sarcolemma into a Ca^{2+} efflux from the SR (Dulhunty, 2006). In the context of ECC, this signal transmission is facilitated by the interplay of two Ca^{2+} channels: the 1,4-dihydropyridine receptor (DHPR), located on the T-tubular membrane and acting as a voltage sensor; and the type 1 ryanodine receptor (RYR1), located on the SR membrane and forming the SR Ca^{2+} release unit (Rios & Brum, 1987; Takeshima et al., 1994). Although not demonstrated directly, a model of direct mechanical coupling between DHPR and RYR1 is supported by an accumulating body of evidence and is widely accepted as the basis of skeletal type ECC (Adams, Tanabe, Mikami, Numa, & Beam, 1990; Block, Imagawa,

Campbell, & Franzini-Armstrong, 1988; Rios & Brum, 1987; Takekura, Bennett, Tanabe, Beam, & Franzini-Armstrong, 1994; Tanabe, Beam, Powell, & Numa, 1988).

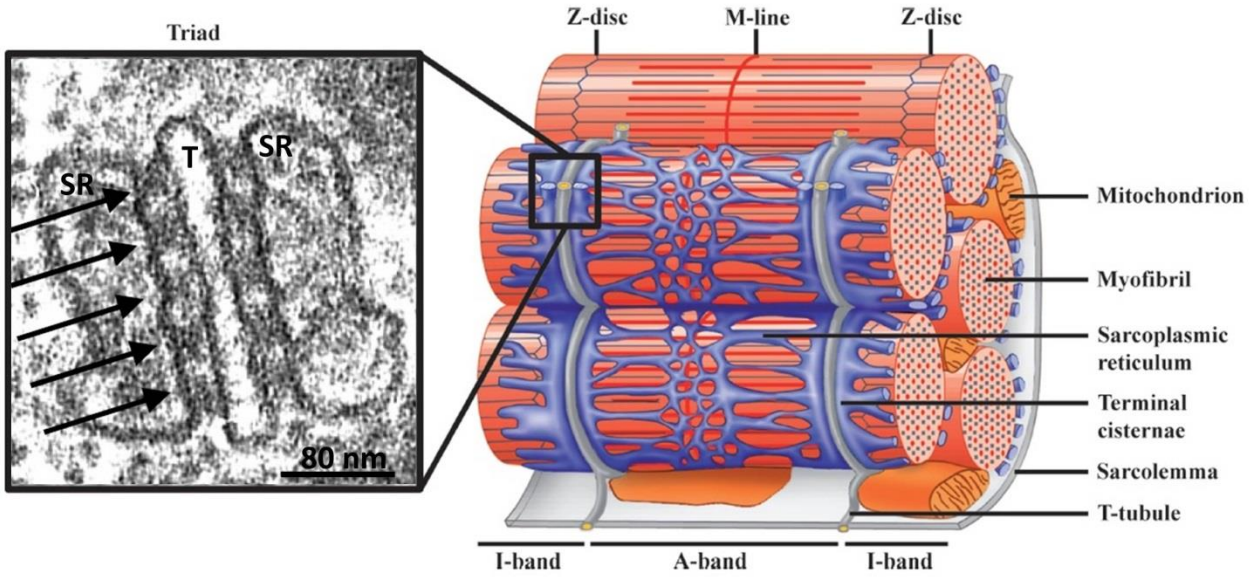

Fig. 7: Triad structure.
Left: An electron micrograph of a triad in a frog skeletal muscle, consisting of a centrally located T-tubule (T), flanked by two terminal cisternae of the SR. The electron dense regions indicated by the arrows are the junctional feet between the T-tubules and the terminal SR cisternae. Modified from (Dulhunty, 2006). **Right:** A schematic representation of a skeletal myofibers internal structure highlighting the T-tubuli – SR network and its position in relation to the myofibrils and the sarcomeric regions. Modified from (Al-Qusairi & Laporte, 2011).

1.3.1 DHPR: structure and functions of the $Ca_v1.1$ principal subunit

DHPR belongs to the family of L-type Ca^{2+} channels, owing their name to their sensitivity to 1,4-dihydropyridines (Reuter, Porzig, Kokubun, & Prodhom, 1985). Unlike the L-type Ca^{2+} channels in other tissues, the skeletal DHPR is characterized by a slow activation and even slower inactivation (Bannister & Beam, 2013). DHPR is a heterotetrameric channel, consisting of one principal subunit – $Ca_v1.1$ (also called α_{1S}) – that spans the T-tubular membrane and acts as a voltage sensor; and three auxiliary subunits – β_{1a}, $\alpha_2\delta$-1 and γ_1 (Fig. 8A) (Catterall, 2000). $Ca_v1.1$, encoded by the gene *Cacna1s*, forms the channel pore and transduces the AP signal to the Ca^{2+} release unit, RYR1, therefore $Ca_v1.1$ is often used instead of DHPR as a description of the whole channel (Bannister & Beam, 2013; Wu et al., 2016). The auxiliary subunits modulate the localization and electrophysiological properties of $Ca_v1.1$-mediated Ca^{2+} currents and have a different degree of importance for ECC. The intracellular cytosolic subunit β_{1a} is necessary for proper targeting, expression and gating of $Ca_v1.1$, and is implicated in the interaction between $Ca_v1.1$ and RYR1 in the

course of ECC (Gregg et al., 1996; Lacerda et al., 1991; Rebbeck et al., 2011). The γ_1 subunit is a transmembrane protein that negatively regulates $Ca_v1.1$ conductance, as well as voltage-dependent Ca^{2+} entry and Ca^{2+} release (Freise et al., 2000; Ursu, Schuhmeier, Freichel, Flockerzi, & Melzer, 2004).

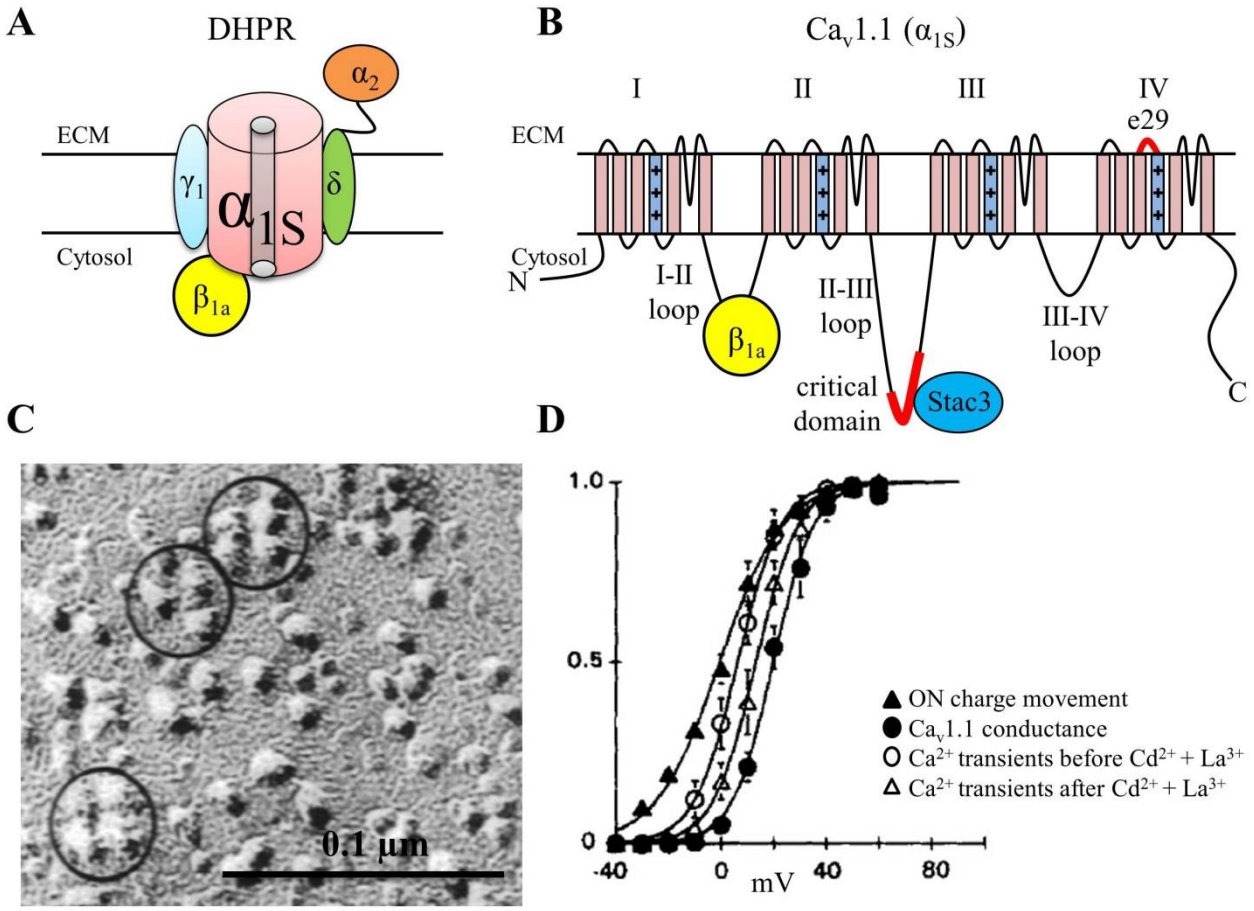

Fig. 8: Structure and properties of DHPR
(A) DHPR is a heterotetramer consisting of one principal subunit – $Ca_v1.1$ – and three auxiliary subunits – β_{1a}, $\alpha_2\delta$-1 and γ_1. $Ca_v1.1$ forms the channel pore (shown as gray cylinder in the middle of $Ca_v1.1$), carries the voltage sensor for membrane depolarization, and activates RYR1 during ECC. Modified from (Obermair, Tuluc, & Flucher, 2008). **(B)** Schematic structure of $Ca_v1.1$, consisting of four homologous repeats (I - IV) connected via cytoplasmic linkers called loops. Each of the four repeats comprises of six transmembrane α-helices, with the fourth α-helix carrying a sequence of basic AAs – the voltage sensor (shown as blue cylinders with three pluses). The I-II loop binds the β_{1a} subunit and promotes the channel trafficking to the T-tubular membrane. The II-III loop is believed to be a crucial element in the postulated mechanical coupling to RYR1, which it activates upon membrane depolarization and thus has a pivotal role in ECC. Pivotal for this coupling is the so called "critical domain" (shown in red) in the middle of the II-III loop that binds Stac3 – a protein that is also necessary for the signal transmission to RYR1. The $Ca_v1.1$ repeat IV carries exon 29 (e29, shown in red) that undergoes developmentally regulated alternative splicing and alters $Ca_v1.1$'s conductance properties. Both the N- and C-terminus are cytoplasmic. Modified from (Bannister & Beam, 2013) and (Polster, Nelson, Papadopoulos, Olson, & Beam, 2018a). **(C)** A scanning electron photograph of a freeze-fracture through the surface membrane of myotubes, showing groups of $Ca_v1.1$ tetrads (exemplified in circles). Modified from (Takekura et al., 1994). **(D)** Comparison of the voltage dependence of charge movements (black triangles), $Ca_v1.1$ Ca^{2+} currents (black circles) and Ca^{2+} transients before and after Ca^{2+} current inhibition by Cd^{2+} and La^{3+} (hollow circles and hollow triangles,

respectively). The graph demonstrates that contraction initiating Ca^{2+} transients precede $Ca_v1.1$ Ca^{2+} currents and are not impeded by their inhibition. Modified by (Garcia, Tanabe, & Beam, 1994).

The $\alpha_2\delta$-1 subunit consists of the α_2 extracellular peptide and the δ single-pass membrane peptide, linked via disulfide bonds. This is the only DHPR subunit that is significantly expressed also in tissues other than skeletal muscle (Bannister & Beam, 2013; Obermair et al., 2008). Its main known functions in skeletal muscle are to slow DHPR's activation kinetics and to facilitate Ca^{2+} transients during prolonged membrane depolarization (Gach et al., 2008; Obermair et al., 2005). While $Ca_v1.1$ and $\beta1_a$ are essential for ECC and organism survival, the loss of $\alpha_2\delta$-1 or γ_1 does not have significant effects on ECC (Bannister & Beam, 2013; Obermair et al., 2008). $Ca_v1.1$ is a central player in ECC. It senses membrane depolarization and induces opening of RYR1, thus facilitating Ca^{2+} release and consequently muscle contraction (Beam & Bannister, 2010; Rios & Brum, 1987). The primary structure of $Ca_v1.1$ was originally obtained for rabbit skeletal muscle and the rabbit $Ca_v1.1$ isoform is still utilized in many experiments (Fig. 8B) (Martinez-Ortiz & Cardozo, 2018; Tanabe et al., 1987; Wu et al., 2016). It consists of four homologous repeats (I, II, III and IV), each containing six α-helices (termed S1 to S6) that span the sarcolemma (Bannister & Beam, 2013; Catterall, 1995). The fourth α-helix (S4) of each repeat carries a region of equally spaced basic amino acids (AAs) that gate the opening and closing of $Ca_v1.1$ (Bezanilla, 2000). At rest, the sarcolemma is in a hyperpolarized state, having a membrane potential on the inner side of approximately –80 mV in comparison with the outer side (MacIntosh, Holash, & Renaud, 2012). During ECC initiation the AP depolarizes the membrane to approximately +30 mV, leading to a topological reorientation of the positively charged AAs in the S4 segments, recorded as a gating current (a.k.a. charge movements) and causing downstream conformational rearrangements and a subsequent Ca^{2+} release from the SR (Bezanilla, 2000). Therefore, the S4 segments of $Ca_v1.1$ (and in a broader sense, the whole $Ca_v1.1$) constitute the voltage sensors during ECC (Bannister & Beam, 2013; Beam, Knudson, & Powell, 1986; Rios & Brum, 1987).

The four homologous $Ca_v1.1$ repeats are connected via three cytoplasmic linkers, called loops, carrying the names of the repeats they are attached to – the I-II, II-III and III-IV loops (Fig. 8B). The I-II loop has a binding site for the β1a subunit and is necessary for the proper $Ca_v1.1$ targeting to the T-tubular membrane (Bannister & Beam, 2013). The II-III loop has been the subject of extensive studies since initial experiments suggested an immediate role in RYR1 activation upon ECC initiation (el-Hayek, Antoniu, Wang, Hamilton, & Ikemoto, 1995; Grabner, Dirksen, Suda, & Beam, 1999; Tanabe, Beam, Adams, Niidome, & Numa, 1990). Especially important for this interaction is a

45 AAs region in the middle of the II-III loop, termed the "critical domain", that determines the specific properties of skeletal type in contrast to cardiac type ECC (Nakai, Tanabe, Konno, Adams, & Beam, 1998). It has been recently demonstrated that the SH3 and cysteine rich domain 3 (Stac3), a protein that is also necessary for skeletal ECC, binds to the critical domain and most likely participates in the $Ca_v1.1$-to-RYR1 signal transmission (Polster et al., 2018a).

Scanning electron microscopy of myotubes freeze fractures suggests that $Ca_v1.1$ molecules are ordered in arrays of membrane particles in groups of four (tetrads, Fig. 8C) (Takekura et al., 1994). $Ca_v1.1$ KO myotubes lack tetrad formation and ectopic expression of $Ca_v1.1$ restores junctional tetrads (Takekura et al., 1994).

A combination of electrophysiological approaches and fluorescence microscopy have demonstrated that in cultured myotubes charge movements in response to electrical stimulation precede Ca^{2+} transients that in turn appear prior $Ca_v1.1$ Ca^{2+} conductance (Fig. 8D) (Garcia et al., 1994). This comes to show that the L-type Ca^{2+} current from $Ca_v1.1$ is not required for contraction-related Ca^{2+} transients, which is one of the major differences between skeletal and cardiac type ECC. Furthermore, next to the "orthograde" signal transduction from $Ca_v1.1$ to RYR1 in ECC initiation, a second "retrograde" signaling from RYR1 to $Ca_v1.1$ augments $Ca_v1.1$ Ca^{2+} conductance and the kinetics of current traces (Nakai et al., 1996). In RYR1-null myotubes only very low amplitude of L-type currents are observed that could be rescued by RYR1 expression (Nakai et al., 1996). Since the L-type Ca^{2+} currents are not necessary for ECC, their physiological function has been a subject of a vigorous discussion. While some propose that Ca^{2+} currents from $Ca_v1.1$ may help replenish internal Ca^{2+} store during prolonged activity, others have demonstrated that ablation of these currents do not affect muscle performance (Bannister & Beam, 2013; Dayal et al., 2017). Interestingly, during embryonic and early fetal development, an alternatively spliced $Ca_v1.1$ isoform lacking exon 29 ($\Delta 29$ $Ca_v1.1$) is being highly expressed in murine skeletal muscle and its expression diminishes with the developmental progression (Tuluc et al., 2009). Unlike the adult full length $Ca_v1.1$, the $\Delta 29$ $Ca_v1.1$ conducts strong Ca^{2+} currents and activates at a lower voltage (Tuluc et al., 2009). The $\Delta 29$ $Ca_v1.1$ has been implicated in the regulation of muscle nAChR prepatterning and seems to play an important role for the correct innervation of the developing skeletal muscle (Flucher & Tuluc, 2011).

$Ca_v1.1$ acts as a voltage sensor not only for RYR1 during ECC, but it also mediates the depolarization-induced activation of 1,4,5-trisphosphate (IP3) receptors (IP3Rs) (Araya et al., 2003).

IP3Rs are Ca^{2+} channels located on the SR that, unlike RYR1, produce slow Ca^{2+} transients that do not trigger muscle contraction. The IP3R-mediated Ca^{2+} transients are involved in the regulation of the expression of multiple genes and since IP3Rs are also activated by membrane depolarization, their regulatory activity has been described as "excitation-transcription coupling" (Arias-Calderon et al., 2016; Juretic, Urzua, Munroe, Jaimovich, & Riveros, 2007).

1.3.2 RYR1: structure and functions

The three types of ryanodine receptors in mammals – RYR1, RYR2 and RYR3 – are intracellular Ca^{2+} release channels, located on the SR or the endoplasmic reticulum (ER) membrane (Flucher et al., 1993). RYRs are the largest known ion channels and owe their name to their susceptibility to ryanodine – a plant-derived alkaloid that interacts with open RYRs and at low concentrations ($\leq$70 µM) locks the receptors in a semi-conducive state, whereas at high concentrations ($\geq$200 µM) inhibits their conductance (Buck, Zimanyi, Abramson, & Pessah, 1992). RYR1 is expressed in skeletal muscle and is located on the SR membrane, where it acts as the Ca^{2+} release unit for ECC (Inui, Saito, & Fleischer, 1987; Marks et al., 1989). RYR2 is expressed primarily in cardiac muscle and has similar functions in cardiac-type ECC. The main difference to RYR1 is that unlike RYR1, RYR2 is activated by extracellular Ca^{2+} entering the cardiac cells via cardiac DHPR ($Ca_v1.2$) in a process called Ca^{2+}-induced Ca^{2+} release (CICR) (Lamb, 2000; Van Petegem, 2012). The third subtype, RYR3, was originally discovered in the brain but is also transiently expressed in many other tissues, including in some skeletal muscles (Conti, Gorza, & Sorrentino, 1996; Nakashima et al., 1997; Protasi et al., 2000). Although RYR3 does not directly participate in ECC, it is involved in muscle development and assists RYR1-mediated CICR in neonatal skeletal muscle (Bertocchini et al., 1997; Yang et al., 2001).

The RYR1 Ca^{2+} channel is a giant homotetramer with a staggering molecular weight of approximately 2.2 mega Da (Takeshima et al., 1989). Each RYR1 subunit consists of around 5000 AAs, more than 80% of which form a large N-terminal cytoplasmic region, containing multiple functional domains, and the rest ~ 500 AAs, a C-terminal transmembrane domain that forms the channel pore (Du, Sandhu, Khanna, Guo, & MacLennan, 2002; Efremov, Leitner, Aebersold, & Raunser, 2014; Yan et al., 2014; Zalk et al., 2014) (Fig. 9A). Although only separate RYR1 domains have been successfully crystalized, the development of super resolution microscopy techniques and in particular of electron cryomicroscopy (cryoEM) in the last four years has led to near-atomic

models of RYR1 structure (Efremov et al., 2014; Yan et al., 2014; Zalk et al., 2014). These models have shown that multiple long range allosteric interactions as distant as 200 Å away from the channel pore can influence its conductance state (Van Petegem, 2015). Nevertheless, higher resolution models are needed for more precise detection of the exact points of interaction between $Ca_v1.1$ and RYR1.

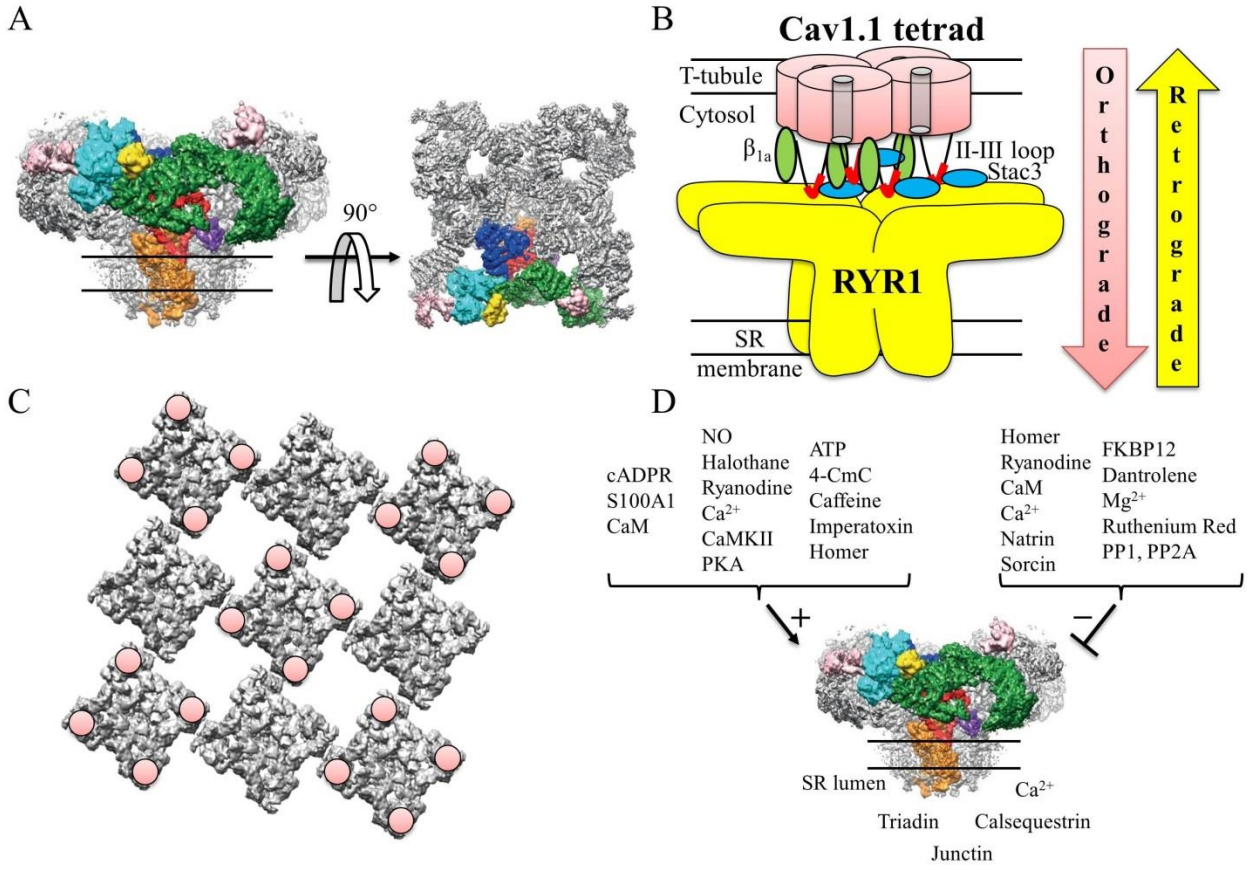

Fig. 9: Structure and properties of RYR1
(A) A pseudoatomic model of RYR1 at a 4.8 Å resolution obtained from cryoEM data displays RYR1 in view from the plane of the SR membrane (black lines, left) and from the cytosol (right). The colors designate different structural domains found within one protomer. Modified from (Zalk et al., 2014). **(B)** The scheme exemplifies the direct mechanical coupling between a $Ca_v1.1$ tetrad on the T-tubular membrane and an opposing a RYR1 channel on the SR membrane. Activation of channel conductance is transmitted from $Ca_v1.1$ to RYR1 via orthograde signaling and from RYR1 to $Ca_v1.1$ via retrograde signaling. Modified from (Dulhunty, 2006). **(C)** A RYR1 2D checkerboard pattern model shows the interactions between individual RYR1s (gray squares) and between RYR1s and $Ca_v1.1$s (pink dots). Each second RYR1 is coupled to a $Ca_v1.1$ tetrad. Upon activation via orthograde signals the RYR1s that are coupled to $Ca_v1.1$ activate the neighboring RYR1s via a proposed allosteric coupled gating mechanism. Modified from (Van Petegem, 2015) and (Yin, D'Cruz, & Lai, 2008). **(D)** The scheme shows a partial overview of proteins, small molecules and ions known to positively (+) or negatively (-) modulate RYR1 conductance. Some modulators (Ca^{2+}, CaM) have a dual action in this respect, dependent on their concentration or complex formation. Abbreviations stand for: cADPR, cyclic ADP ribose; S100A1, S100 calcium-binding protein A1; CaM, calmudulin; NO, nitric oxide; CamKII, calmodulin kinase II; ATP, adenosine triphosphate; 4-CmC, 4-chloro-m-cresol; FKBP12, 12-kDa FK506-binding protein; PP1, protein phosphatase 1; PP2A, protein phosphatase 2A. Modified from (Zalk et al., 2014) and (Van Petegem, 2015).

As described above, RYR1 and $Ca_v1.1$ are involved in an intricate bi-directional communication, composed of an orthograde signaling from $Ca_v1.1$ to RYR1, and a retrograde signaling from RYR1 to $Ca_v1.1$ so that each channel modulates the activity of the other one (Nakai et al., 1996) (Fig. 9B). In addition to RYR1 activation, $Ca_v1.1$ also stabilizes RYR1 at rest and reduces RYR1 passive Ca^{2+} leak (Eltit et al., 2011). The retrograde signaling from RYR1 enables the slow L-type Ca^{2+} currents through $Ca_v1.1$, which are greatly reduced in RYR1 null mutant cells (Avila & Dirksen, 2000; Nakai et al., 1996). Moreover, the absence of RYR1 leads to an impairment of tetradic formation (Takekura, Nishi, Noda, Takeshima, & Franziniarmstrong, 1995). Several domains on the cytoplasmic part of RYR1 seem to be involved in the interaction with $Ca_v1.1$ and β_{1a} (Van Petegem, 2015). Especially important for ECC and tetrad formation is the divergent region 2, located between two SPRY (SplA kinase ryanodine receptor domain) domains (Perez, Mukherjee, & Allen, 2003; Sheridan et al., 2006). We have recently shown that a protein containing the first 4300 AAs of the rabbit RYR1 that is entirely cytosolic (termed RYR1 soluble foot or $RYR1_{1:4300}$) is targeted to the triadic junctions, co-localizes with $Ca_v1.1$ and restores retrograde signaling (Polster et al., 2018b). Hence, the most important determinants for the $Ca_v1.1$-RYR1 bidirectional communication from the RYR1 side are most likely contained entirely in the cytoplasmic RYR1 region.

RYR1 channels can form highly ordered 2D crystalline arrays in which the corners of each channel face those of another four RYR1s, forming a checkerboard-resembling pattern (Fig. 9C) (Yin & Lai, 2000). Each of the four RYR1 subunits interacts with one of the four $Ca_v1.1$ molecules in a tetrad (Fig. 9C). However, only every second RYR1 interacts with $Ca_v1.1$s (Yin et al., 2008). The orthograde signals from $Ca_v1.1$ are transmitted to the rest of the RYR1 very likely via allosteric interactions with their $Ca_v1.1$-bound neighbors – the postulated phenomenon of coupled gating (Marx, Ondrias, & Marks, 1998).

In addition to $Ca_v1.1$, a large number of other proteins, peptides, ions and other molecules bind to and modulate RYR1, contributing to the complexity of this channel's regulation (Fig. 9D) (Dias & Vogel, 2009; Van Petegem, 2015). An important RYR1 activator is the 12-kDa FK506-binding protein (FKBP12) – a small protein that binds each RYR1 subunit and stabilizes RYR1's closed state (Van Petegem, 2015). Some modulators can have dual roles, such as cytosolic Ca^{2+} that activates RYR1 at lower concentrations and inactivates it at higher concentrations. SR luminar Ca^{2+} and the Ca^{2+}-buffering protein calsequestrin together with other luminar proteins like triadin and junctin also modulate RYR1 conductance (Wei, Gallant, Dulhunty, & Beard, 2009). Similarly, calmodulin (CaM)

– an EF-hand-containing protein with a high affinity for Ca^{2+} – directly binds to RYR1 and dependent on the cytosolic Ca^{2+} concentration activates or inhibits it (Tripathy, Xu, Mann, & Meissner, 1995). Furthermore, RYR1's conductance is affected by a variety of post-translational modifications like oxidation, phosphorylation, palmitoylation and S-nitrosylation (Witherspoon & Meilleur, 2016). This intricate multimolecular fine-tuning underlines the importance of the correct ECC signal transmission and proper RYR1-mediated Ca^{2+} release.

1.3.3 $Ca_v1.1$ and RYR1: diseases and animal models

Due to the large size of the of $Ca_v1.1$ and RYR1, the multitude of their interactions with other proteins and molecules, and the potent outcome of their functions – Ca^{2+} release and muscle contraction – disturbances in their action or regulation have been linked to diverse diseases. Around 75% of the cases of hypokalemic periodic paralysis type 1 (HPP-1) – a disease characterized by periods of muscle weakness and paralysis – are caused by mutations in $Ca_v1.1$ (Striessnig, Bolz, & Koschak, 2010). Mutations in RYR1 are the leading cause of malignant hyperthermia (MH) – a life-threatening pharmacogenetic disorder triggered by certain anesthetics and characterized by a hypermetabolic state, fever and rhabdomyolysis (Mathews & Moore, 2004). Mutations in $Ca_v1.1$ have also been linked to MH. In addition, various mutations in both channels have been liked to congenital myopathies like central core disease, multiminicore disease and CACNA1S congenital myopathy (Jungbluth et al., 2018; Mathews & Moore, 2004; Schartner et al., 2017). Manifestation of these diseases often starts in early age and progresses with development. Therefore, information about the full spectrum of the roles of $Ca_v1.1$ and RYR1 in muscle development is urgently needed.

Different *in vitro* and *in vivo* models have been utilized in the analysis of $Ca_v1.1$ and RYR1 properties (Chelu et al., 2005; Dayal et al., 2017; Powell, Petherbridge, & Flucher, 1996; Zvaritch et al., 2007). Two mouse models – the $Ca_v1.1$ null *dysgenic* and the RYR1 null *dyspedic* mice – have proven to be invaluable for the examination of the structural and functional properties of these channels in the context of ECC (Buck, Nguyen, Pessah, & Allen, 1997; Chaudhari, 1992; Pai, 1965b; Takeshima et al., 1994). Both models have very similar phenotypes. Namely, the heterozygous mice ($RYR1^{+/-}$ and $Ca_v1.1^{+/-}$) are phenotypically undistinguishable from their wild type (WT, $^{+/+}$) littermates and exhibit no changes in their lifespan, fertility and ECC. On the contrary, the skeletal muscle of homozygous *dyspedic* and *dysgenic* mice (for clarity referred to as $RYR1^{-/-}$ and $Ca_v1.1^{-/-}$ in the following text) cannot support ECC, thus they are paralyzed and die at birth from asphyxia. In

addition, both RYR1$^{-/-}$ and $Ca_v1.1^{-/-}$ mice appear smaller than their WT and heterozygous littermates, possess a characteristic spinal curvature, small limbs and enlarged necks (Fig. 10). Skeletal muscle from RYR1$^{-/-}$ and $Ca_v1.1^{-/-}$ neonates bears features of structural and developmental impairment (Pai, 1965b; Takeshima et al., 1994). Still, the full range of the alterations caused by the absence of RYR1 or $Ca_v1.1$ throughout the development of the skeletal muscle remains unknown.

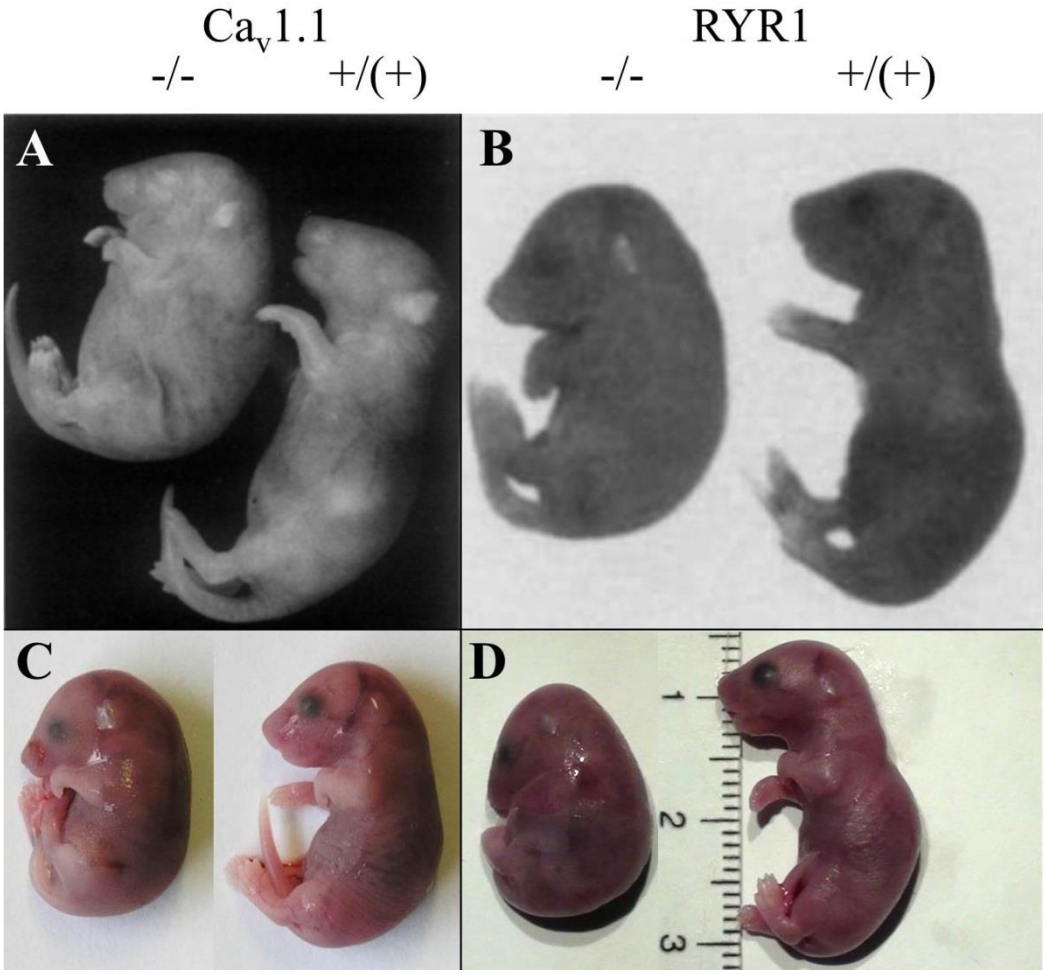

Fig. 10: Cav1.1 and RYR1 null mice.
Photographs show comparisons of homozygous ($^{-/-}$), and "normal" (+/(+), heterozygous or WT) $Ca_v1.1$ **(A, C)** and RYR1 **(B, D)** new born littermates. Compared to their respective $^{+/-}$ or $^{+/+}$ littermates, homozygous $Ca_v1.1^{-/-}$ and RYR1$^{-/-}$ neonates are smaller, have smaller limbs and a marked spinal curvature. **(A, B)** Photographs are modified from the original publication describing the mouse models for the first time (Pai, 1965a) and (Takeshima et al., 1994); **(C, D)** Photographs of typical neonates used in the present work. Note that the RYR1$^{-/-}$ mice used in this work carry the mutation causing loss of RYR1 on a slightly different position (RYR1 exon 10) than in (B, RYR1 exon 2) (Buck et al., 1997).

1.4 Aims

This work aims to examine the global gene expression changes caused by the absence of RYR1 or $Ca_v1.1$ throughout skeletal muscle development, utilizing limb skeletal muscle as a model. More precisely, two major aims are addressed:

I. The first part of this work aims to determine how the absence of RYR1 affects the skeletal muscle transcriptome at E18.5 – the end of fetal development. Specifically, the limb muscle histology and the transcriptomic profiles of $RYR1^{-/-}$ and $RYR1^{+/-}$ E18.5 littermates are compared. The expression changes of muscle's structure proteins and developmental markers are evaluated and the differential regulation of impacted signaling pathways is analyzed.

II. The second part of this work aims to compare the changes caused by the absence of either RYR1 or $Ca_v1.1$ in the beginning (E14.5) and the end (E18.5) of secondary myogenesis. At each time point, the histological and transcriptomic profiles of WT ($^{+/+}$), heterozygous ($^{+/-}$) and homozygous ($^{-/-}$) RYR1 and $Ca_v1.1$ limb skeletal muscles are compared. The differences and similarities in the structural and expression changes between the RYR1 and $Ca_v1.1$ lines are analyzed in respect to the developmental time point – E14.5 or E18.5 and in respect to the developmental dynamics of these changes from E14.5 to E18.5.

2 Materials and Methods

2.1 Materials

2.1.1 Instruments and Reagents

Instruments and Reagents	Supplier / Source
Antibodies	
Anti-mouse activated caspase-3 , rabbit (clone C92-605)	BD Biosciences
Anti-rabbit, goat, biotinylated	Vector Laboratories
Chemicals	
2-methylbutane (C_5H_{12})	Merk
3,3`-Diaminobenzidine tetrahydrochloride hydrate (DAB)	Sigma Aldrich
6X DNA Loading Dye	Thermo Fisher
Acetone	Carl Roth
Bovine serum albumin (BSA)	Sigma
Chloroform ($CHCl_3$)	Merk
CutSmart Buffer, 10x	NEB
D-Glucose	Merk
Dimethyl sulfoxide (DMSO)	Sigma Aldrich
dNTP (Deoxynucleotide) solution mix [10 mM]	Thermo Fisher
DreamTaq Green PCR Buffer (2x)	Thermo Fisher
Eosin G-solution	Carl Roth
Ethanol DAB 96%	Merck
Ethylenediaminetetraacetic acid (EDTA)	Fluka
Glacial acetic acid	Merk
Hematoxylin solution modified acc. To Gill II	Merk
HEPES	Sigma Aldrich
Hidrogen peroxide (H_2O_2)	Merk
LE Agarose	Biozym

Instruments and Reagents	Supplier / Source
Normal Goat Serum	Vector Laboratories
Phosphate buffered saline (PBS), solution	Biochrom
Phosphate-buffered saline (PBS) tablets	Thermo Fisher
Potassium chloride (KCl)	Fluka
RNAlater	Qiagen
Sodium chloride (NaCl)	Carl Roth
Sodium hydroxide (NaOH)	Riedel-de Haën
Tissue-Tek® O.C.T. Compound	Sakura® Finetek
Tris base	Sigma Aldrich
Trizma-HCl	Sigma Aldrich
Water, nuclease free	Promega
Xylene	Carl Roth
Enzymes	
DreamTaq® DNA Polymerase	Thermo Fisher
EarI	Fermentas
Equipment and Instrumentation	
AxioCam MRc camera	Zeiss
Axiophot Zeiss microscope	Zeiss
Benchtop Centrifuge 5415 D	Eppendorf
CM3050 S Leica cryostat	Leica
Consort E122 Powersupply	Consort
GeneChip® Fluidics Station-450	Affymetrix / Thermo Fisher
GeneChip® Hybridization Oven-645	Affymetrix / Thermo Fisher
GeneChip® Scanner-3000-7G	Affymetrix / Thermo Fisher
Gel documentation system, version 3.28.16.01.2009	INTAS
KL 1500 electronic Halogen cold light source	Schott
Lab-Line Titer Plate Shaker	Thermo Fisher

Instruments and Reagents	Supplier / Source
Magnetic Stand for 96-well plates	Ambion
Mastercycler® Gradient thermal cycler	Eppendorf
Micro forceps	Aesculap
Micro scissors	Aesculap
MicroAmp® Fast 96-Well Reaction Plates (0.1 mL)	Applied Biosystems
MicroAmp™ Optical Adhesive Film	Applied Biosystems
MoGene 2.0 ST arrays, format 100	Affymetrix / Thermo Fisher
Mouse Genome 430 2.0 arrays	Affymetrix / Thermo Fisher
NanoDrop; 1000 Spectrophotometer	Thermo Fischer
Olympus Fluoview1000 system	Olympus
Pestles, steel	neoLab
StepOne™ Plus Real-Time PCR System	Applied Biosystems
Wild Heerbrugg M3 stereomicrpscope	Leica
Kits	
AMV First Strand cDNA Synthesis Ki	NEB
GeneChip® 3′ IVT Express Kit	Affymetrix / Thermo Fisher
GeneChip® Hybridization, Wash, and Stain (HWS) Kit	Affymetrix / Thermo Fisher
GeneChip® WT PLUS Reagent Kit	Affymetrix / Thermo Fisher
GoTaq® qPCR Master Mix kit	Promega
Maxwell® 16 LEV simplyRNA Tissue Kit	Promega
QuantiTect® Reverse Transcription Kit	Qiagen
Vectastain® Elite® ABC-HRP Kit	Vector Laboratories
Markers	
DNA Ladder 100 bp, 1kb	Thermo Fisher
RiboRuler High Range RNA Ladder	Thermo Fisher

Instruments and Reagents	Supplier / Source
Software	
ClustVis online tool	https://biit.cs.ut.ee/clustvis/
CorelDRAW X5	Corel Corporation
Database for Annotation, Visualization and Integrated Discovery (DAVID)	https://david.ncifcrf.gov/
Enrichr online enrichment tool	http://amp.pharm.mssm.edu/Enrichr/
Expression Console™ Software 1.4	Affymetrix / Thermo Fisher
Fluoview, FV10-ASW 2.1 Viewer	Olympus
GeneChip® Command Console (AGCC)	Affymetrix / Thermo Fisher
GeneChip® Operating Software (GCOS)	Affymetrix / Thermo Fisher
GraphPad Prism 4.00	GraphPad
LIMMA-package	(Smyth, 2004)
OligoPerfect™ Designer	Thermo Fisher
Primer-BLAST	NCBI
R-package	(Irizarry, 2003)
StepOne Software v2.3	Applied Biosystems
Transcriptome Analysis Console 3.0	Affymetrix / Thermo Fisher
ZEN Imaging Software	Zeiss

2.1.2 Primers

All forward (Fwd) and reverse (Rev) primers (Table 2) were dissolved in Tris-EDTA buffer (TE, 10 mM Tris, 1 mM EDTA, pH 7.5) to 100 mM stock solutions and 10 mM working solutions. All primers were supplied by Sigma Aldrich.

Table 2. Primers sequences and amplicon size used for PCR and qRT-PCR analyses.

Gene	Primers (5' to 3')	Amplicon (bp)
Primers used in genotyping PCR analyses		
Ryr1 (WT allele)	Fwd: GGACTGGCAAGAGGACCGGAGC Rev: GGAAGCCAGGGCTGCAGGTGAGC	419
Ryr1 ($^{-/-}$ allele)	Fwd: GGACTGGCAAGAGGACCGGAGC Rev: CCTGAAGAACGAGATCAGCAGCCTCTGTCCC	300
Cacna1s	Fwd: GCTTTGCAGATGTTCGGGAAGATCGCCATGG Rev: GCAGCTTTCCACTCAGGAGGGATCCAGTGT	271
Primers used PCR analyses of Cav1.1 full length and Δ29 splice variants		
Cacna1s Exons 28-32	Fwd: TCCTAATCGTCATCGGCAGC Rev: TTTATCTGCGTCCCGTCCAC	343 / 286

Gene	Primers (5' to 3')	Amplicon (bp)
Primers used in qRT-PCR analyses		
Abra	Fwd: GCCCCCAAAACTCTGTCTCC Rev: GACAACCGTTCTGGTCACCT	111
Actb	Fwd: GCCTCACTGTCCACCTTCCA Rev: AAAACGCAGCTCAGTAACAGTC	115
Ankrd1	Fwd: CCTGCGAGGCTGATCTCAAT Rev: CGCACCGAAGGTCATCAAGA	110
Bai3	Fwd: AGTATGGAGGAAGGCCCTGT Rev: GTGGCTCCATGAACTCCATT	107
Cacna1s exons 10-11	Fwd: GCCACTCTGGTTGACCCATT Rev: GGACATGAAGTACTGGCGCA	115
Cdh3	Fwd: CAACGAAGCCCCTGTGTTTG Rev: CTCCTTGTCTGGGTCCTGTG	109
Col19a1	Fwd: TTGGATTGCCAGGAGAACAT Rev: CAGCATCACCCTTCAGACCT	114
Creb5	Fwd: AGGGAGTTGAAGGCTACTGGA Rev: TCTGCAGCTCCGACCTATCT	107
Cytb	Fwd: CCATTCTACGCTCAATCCCCA Rev: AGGCTTCGTTGCTTTGAGGT	109
Derl3	Fwd: ATGCTCTTCGTGTTCCGCTA Rev: GCAGAGTCATAAGAACACCACC	109
Eda2r	Fwd: AGAGGATGGATTTGATCTGTTGTTG Rev: AAGGCAGTTGTCACGCTCTC	106
Flcn	Fwd: GCTGGGATTACCGAACTGAG Rev: AGGCGATCTGTCGTAACACC	110
Fn1	Fwd: GGTTCGGGAAGAGGTTGTGA Rev: ATGGCGTAATGGGAAACCGT	105
c-Fos	Fwd: AGTCAAGGCCTGGTCTGTGT Rev: TCCAGCACCAGGTTAATTCC	100
Gapdh	Fwd: AGTGTTTCCTCGTCCCGTAG Rev: TGATGGCAACAATCTCCACT	119
Hbb-y	Fwd: TTGGCTAGTCACTTCGGCAAT Rev: AGGGCTCAGTGGTACTTGTG	107
Hdac4	Fwd: CCAATGCCAATGCTGTCCAC Rev: TGCGCCTCAATCAGAGAGTG	112
Irx2	Fwd: GTCTACACGTCGACTCGCTC Rev: ACACTCTGAGCCTGATTCGC	107
Jun	Fwd: GAAAAGTAGCCCCCAACCTC Rev: ACAGGGGACACAGCTTTCAC	106
Klf4	Fwd: TACCCCTACACTGAGTCCCG Rev: GGAAAGGAGGGTAGTTGGGC	110
Mcpt4	Fwd: GTGGGCAGTCCCAGAAAGAA Rev: GCATCTCCGCGTCCATAAGA	107
Mlip	Fwd: AAGCATGAACCAGGAAGCTCA Rev: CTGGACCCTCTCTTGTTTGCT	114
Mrf4	Fwd: GCAGAGGGCTCTCCTTTGTA Rev: AACGTGTTCCTCTCCACTGC	105
Mybpc2	Fwd: ACACTGAACATCCGCCGAC Rev: TGTGGCACTCGGACATCCA	113
Myf5	Fwd: GAAGGTCAACCAAGCTTTCG Rev: GCTCTCAATGTAGCGGATGG	109
Myl2	Fwd: AAAGAGGCTCCAGGTCCAAT Rev: CACCTTGAATGCGTTGAGAA	105
Mylpf	Fwd: ATAACCCCAGAAGAACTGCTCC	108

Gene	Primers (5' to 3')	Amplicon (bp)
	Rev: TTCTCTTGGCCTTCTTGGGTG	
MyoD	Fwd: GGCTACGACACCGCCTACTA Rev: GTGGAGATGCGCTCCACTAT	110
MyoG	Fwd: CTGCACTCCCTTACGTCCAT Rev: CCCAGCCTGACAGACAATCT	103
Nefl	Fwd: TTCAGGATCTATGGCAATGTGA Rev: TCCCATGAGGTTGCACATGAA	115
Nell1	Fwd: ATCAGAGGAAGGCGTTTGGG Rev: AGCACGGAGACTCAACAACC	111
Pax3	Fwd: AAACCCAAGCAGGTGACAAC Rev: AGACAGCGTCCTTGAGCAAT	115
Pax7	Fwd: ATTACCTGGCCAAAAACGTG Rev: AGTAGGCTTGTCCCGTTTCC	105
Rplp0	Fwd: GATTCGGGATATGCTGTTGG Rev: TCGGGTCCTAGACCAGTGTT	108
Six1	Fwd: CCTGGGGCAAAATGATGTAT Rev: CAAAGCATGAGCAAGCCAAC	112
Six4	Fwd: GGCCAGAGGTTGTTGTTTGT Rev: GGCAGCCAAGCTGTGTAAGT	109
Sox10	Fwd: TACCTTTGCCTTGCACCCTT Rev: AAAGGGGCAGCGATGTGTTA	111
Trib1	Fwd: TAACAAACTCCCCCTTGCTG Rev: CAACGCAGAACAGTCATGGT	105
Trpm3	Fwd: AAGGCTTTGACTTTCTGTCATCTG Rev: TTCAACAGTGGGTCCAATAGCA	105
Uba52	Fwd: ATTGAGCCATCCCTTCGTCAG Rev: CTTCTTCTTGCGGCAGTTGAC	111
Ucp1	Fwd: GGAGGTGTGGCAGTGTTCAT Rev: AAGCATTGTAGGTCCCCGTG	112

2.2 Methods

All procedures were performed as described in (Filipova et al., 2016) and (Filipova et al., 2018).

2.2.1 Ethics statement

All animal experiments were carried out in accordance with the guidelines of the European Commission (Directive 2010/63/EU) and of the German animal welfare act (TierSchG). The mice were housed in the Animal Facility of the Center for Molecular Medicine Cologne (CMMC), a part of the Medical Faculty of the University of Cologne according to the European Union Recommendation 2007/526/EG. All experimental protocols and procedures were approved by the local governmental authorities (Landesamt für Natur, Umwelt und Verbraucherschutz, North Rhine-Westphalia, license № AZ84-02.05.20.13.080 and 84-02.04.2015.A054). Effort was taken to minimize animal suffering.

2.2.2 Animal procedures and skeletal muscle preparation

All mice (the RYR1$^{+/-}$ *dyspedic* (ry1$_{42}$) and the Ca$_v$1.1$^{+/-}$ *dysgenic* mouse (*mdg*) lines) were from the C57BL/6J background (Buck et al., 1997; Pai, 1965b). Heterozygous RYR1$^{+/-}$ or Ca$_v$1.1$^{+/-}$ male and female mice were subjected to timed mating with the duration of 31 hours (pairing was only among lines: either RYR1$^{+/-}$ x RYR1$^{+/-}$ or Ca$_v$1.1$^{+/-}$ x Ca$_v$1.1$^{+/-}$). The pregnant females of each line were sacrificed either at day 14.5 and or at day 18.5 post coitum by cervical dislocation; the fetuses were rapidly sacrificed by decapitation and used immediately for skeletal muscle preparation. Each fetus was handled separately (Filipova et al., 2018; Filipova et al., 2016).

2.2.2.1 Morphological analyses

Comparison of the overall morphology, body shape and size of littermates from different genotypes, was carried out after taking whole-body photographs of animal fetuses (n = 3) at E14.5 and E18.5 of each of the following genotypes: RYR1$^{+/+}$ (WT), RYR1$^{+/-}$, RYR1$^{-/-}$; Ca$_v$1.1$^{+/+}$ (WT), Ca$_v$1.1$^{+/-}$, and Ca$_v$1.1$^{-/-}$. Representative photographs from each group are shown (Figs. 13 and 22).

2.2.2.2 Skeletal muscle preparation

The fetuses were kept on ice during skeletal muscle sample collection. The skin from the front and hind limbs was removed with the help of micro forceps and micro scissors. The limb skeletal muscle of each fetus was dissected and pooled for each animal in RNAlater on ice. Subsequently the samples were centrifuged for 10 min at 16,000 x g, the RNAlater was then removed and the samples were immediately frozen in liquid nitrogen and stored at -80 °C until use.

The fetuses were genotyped via PCR as described below. For the analysis of E18.5 RYR1$^{-/-}$ vs. RYR1$^{+/-}$ (3.1 Results part I) the limb skeletal muscle samples either from two heterozygous RYR1$^{+/-}$ and two homozygous RYR1$^{-/-}$ littermates from two litters were used (n = 4 biological replicates = 4 animals for each group). For the analysis of both RYR1$^{-/-}$ and Ca$_v$1.1$^{-/-}$ at E14.5 and E18.5 (3.2 Results part II) from each litter the limb skeletal muscle samples from one WT, one heterozygous (either RYR1$^{+/-}$ or Ca$_v$1.1$^{+/-}$) and one homozygous (either RYR1$^{-/-}$ or Ca$_v$1.1$^{-/-}$) mutant littermate were used in the subsequent analyses (n = 3 biological replicates = 3 animals for each group).

2.2.2.3 Genotyping

A small terminal segment from the tail of each fetus was lysed in 100 µl lysis buffer (25 mM NaOH, 0.1 mM EDTA) at 95 °C for 30 minutes, followed by an addition of 100 µl ice-cold neutralization buffer (40 mM Trizma-HCl) on ice. One µl of each sample was used as a template for genotyping PCRs using the DreamTaq Polymerase as per manufacturer's instructions (Table 3). For genotyping the RYR1 line *(Ryr1* gene*)* the WT (+) allele and the mutant (-) allele were amplified in separate PCR reactions with the primers from Table 2. For genotyping the $Ca_v1.1$ line (*Cacna1s* gene), the genomic *Cacna1s* locus carrying the mutation – a single nucleotide deletion (Chaudhari, 1992), was amplified via PCR with the primers indicated in Table 2. The resulting PCR products were subsequently subjected to a restriction analyses via *Ear*I. *Ear*I digests only the PCR product from the WT *$Ca_v1.1$* allele but not the mutant allele. PCR products and *Ear*I digestions were analyzed via runs on 2% agarose gels.

Table 3. Genotyping PCR reactions composition and PCR program.

PCR reactions		**PCR program RYR1**			**PCR program $Ca_v1.1$**		
18.25 µl	H_2O	1 x	94 °C	5 min	1 x	95 °C	2 min
2.50 µl	10x DreamTaq Green Buffer	30x	94 °C	40 sec	35x	95 °C	30 sec
0.50 µl	10 mM dNTPs		72 °C	30 sec		60 °C	45 sec
1.25 µl	10 µM Fwd primer		72 °C	30 sec		72 °C	50 sec
1.25 µl	10 µM Rev primer	1 x	72 °C	5 min	1 x	72 °C	7 min
0.25 µl	DreamTaq Polymerase	Hold	4 °C		Hold	4 °C	
1.00 µl	Tissue lysate						

2.2.3 Histological analysis and immunohistochemistry

The preparation and analysis of histological cross-sections, stainings and immunohistochemical reactions were performed with the kind assistance of PD Dr. Anna Brunn and Mariana Carstov from the group of Prof. Dr. Martina Deckert from the Department of Neuropathology at the University Hospital of Cologne.

2.2.3.1 Preparation of cryosections

Immediately after the fetuses have been sacrificed, the lower limbs were vertically positioned on cardboard slices coated with Tissue-Tek® O.C.T. Compound and additional Tissue-Tek® was applied to cover the limbs. The cardboard slices with the limbs were snap-frozen in dry ice – 2-methylbutane mixture at approximately -79 °C for at least 10 minutes (min.). The limbs were stored at -80 °C until further use. Limb transverse sections with a thickness of 10 µm were produced

on a CM3050 S Leica cryostat with a chamber temperature of -20 °C and transferred on microscope slides. The sections were stored -80 °C until further use.

2.2.3.2 Fixation

The sections were fixed via incubation in acetone for 10 min, followed by incubation in chloroform for 7 min. Subsequently the fixed sections were allowed to dry out for 15 min. All procedures were performed at room temperature.

2.2.3.3 Hematoxylin and eosin (H&E) staining

The microscope slides with the fixed histological sections were stained with H&E according to Table 4 and subsequently sealed with microscope cover slips. All procedures were performed at room temperature.

Table 4. H&E staining protocol.

Procedure	Reagent (Cat. #, Source)	Incubation
1) Hematoxylin staining	Hematoxylin solution modified acc. To Gill II	3 min.
2) Wash	Tap H_2O	5 min.
3) Eosin staining	Eosin G-solution, 0.5 %	3 min.
4) Rinse	Distilled H_2O (d H_2O)	~ 10 sec.
5) Dehydration	50 % EtOH	~ 30 sec.
	70 % EtOH	~ 30 sec.
	90 % EtOH	~ 30 sec.
	100 % EtOH	2 x 5 min.
	Xylene	2 x 5 min.

2.2.3.4 Immunohistochemical stainings of activated caspase-3

The microscope slides with the fixed histological sections were stained for activated caspase-3 according to Table 5 and subsequently sealed with microscope cover slips. All procedures were performed at room temperature.

Table 5. Activated caspase-3 staining protocol.

Procedure	Reagent (Cat. #, Source)	Incubation
1) Blocking	5 % BSA + 5 % Normal Goat Serum	20 min.
2) Primary antibody	Monoclonal rabbit anti-mouse activated caspase-3 (clone C92-605; BD Biosciences, Heidelberg, Germany), diluted 1:500 in PBS	60 min
3) Washing	PBS	10 min.
4) Secondary antibody	5 µl Biotinylated Goat anti-rabbit (Cat. # BA-1000, Vector Laboratories, Burlingame, CA, USA) + 15 µl 5 % Normal Goat Serum per 1 ml PBS	
5) Wash	PBS	10 min.
6) Avidin-Biotin complex formation	Vectastain® Elite® ABC-HRP Kit: 10 µl Reagent A + 10 µl Reagent B + 1 ml PBS	30 min.

Procedure	Reagent (Cat. #, Source)	Incubation
7) Washing	PBS	10 min.
8) Visualization	1.4 mM 3,3`-Diaminobenzidine tetrahydrochloride hydrate (DAB) + 0.07 % H_2O_2	10 min.
9) Wash	dH_2O	10 min.
10) Hematoxylin staining	Same as in Table 4, steps 1), 2) and 5)	

2.2.3.5 Microscopy

The histological and immunohistological stainings were analyzed under an Axiophot Zeiss microscope and photographed with an AxioCam MRc camera. Scale bars were calculated via the ZEN Imaging Software.

2.2.4 RNA extraction

Total RNA from frozen skeletal muscle tissue was extracted with the *Maxwell 16 LEV simplyRNA Tissue Kit* using a Maxwell 16 instrument according to the manufacturer's instructions. Briefly, prior RNA extraction a 1-Thioglycerol/Homogenization Solution mixture was prepared (20 µl of 1-Thioglycerol per 1 ml of Homogenization Solution, 200 µl mixture per sample) and lyophilized DNAze I was dissolved in 275 µl of nuclease-free H_2O + 5 µl of Blue Dye. For each sample One Maxwell® 16 LEV Cartridge (MCE) was positioned on a Maxwell® 16 LEV Cartridge Rack and a LEV Plunger was positioned in well #8 of each cartridge. Labelled 0.5 ml elution tubes containing 50 µl of nuclease-free H_2O each were positioned in front of each MCE.

Samples were transported in liquid nitrogen. 200 µl of ice-cold 1-Thioglycerol/Homogenization Solution mixture was added to each sample on ice and the samples were rapidly homogenized mechanically via a steel micropestle. 200 µl of Lysis Buffer was added to each homogenate, subsequently the samples were vortexed for 15 sec. The total amount of each sample (~ 400 µl) was transferred to well #1 of a MCE. 5 µl of DNase I were pipetted to well #4 of each MCE. The Maxwell® 16 LEV Cartridge Rack carrying the MCEs with the samples was inserted into a Maxwell 16 instrument and the "simplyRNA" protocol was utilized for RNA extraction.

One µl of each sample was used for measurement of the RNA concentration via a NanoDrop 1000 Spectrophotometer. RNA samples were diluted to a concentration of 100 ng/µl and 250 or 500 ng of each RNA sample were analyzed via runs on 2% agarose gels next to 2 µl of RiboRuler High Range RNA Ladder.

2.2.5 cDNA synthesis

Reverse transcription reactions of total RNA were performed for cDNA synthesis via the *AMV First Strand cDNA Synthesis Kit* as per manufacturer's instructions and as described in (Filipova et al., 2016); or via the *QuantiTect® Reverse Transcription Kit* as per manufacturer's instructions and as described in (Filipova et al., 2018). Below is a brief description of both protocols.

AMV First Strand cDNA Synthesis Kit. 100 ng total RNA from each sample were used in each reaction. 2 µl of 50 µM $d(T)_{23}$ VN primer and nuclease-free H_2O to a final volume of 8 µl were added to each sample. The samples were incubated at 70 °C for 5 minutes and placed on ice. 10 µl of AMV Reaction Mix and 2 µl of AMV Enzyme Mix were added to each sample. The samples were incubated at 42 °C for one hour, followed by an inactivation at 80 °C for 5 minutes. Samples were then put on ice and diluted with nuclease-free H_2O to a final volume of 50 µl. All cDNA samples were stored at -20 °C.

QuantiTect® Reverse Transcription Kit. One µg (10 µl of 100 ng/µl) total RNA was used for cDNA synthesis. Genomic DNA elimination reactions were prepared according to Table 6 and incubated at 42 °C for 2 minutes. Subsequently, reverse transcription reactions (Table 6) were prepared and incubated at 42 °C for 30 minutes, followed by an inactivation at 95 °C for 3 minutes. All cDNA samples were diluted to a final volume of 1 ml and stored at -20 °C.

Table 6. QuantiTect® Reverse Transcription reactions setup.

Component	Volume
Genomic DNA elimination	
gDNA Wipeout Buffer, 7x	2 µl
Total RNA (100 ng/µl)	10 µl
nuclease-free H_2O	2 µl
Total volume	14 µl
Reverse-transcription	
Quantiscript Reverse Transcriptase	1 µl
Quantiscript RT Buffer, 5x	4 µl
RT Primer Mix	1 µl
Entire genomic DNA elimination reaction	14 µl
Total volume	20 µl

2.2.6 Quantitative real-time PCR (qRT-PCR)

Quantitative real-time PCRs (qRT-PCRs) were used for determination of the relative gene expression changes of selected genes of interest. All primers (Table 2) were designed using the OligoPerfect™ Designer (Thermo Fisher) or Primer-BLAST (Ye et al., 2012) with a melting temperature (Tm) range

of 58 °C – 60 °C , an optimal length of 20 bases and an amplicon between 100 and 120 bp, and were purchased from Sigma Aldrich. The qRT-PCR reaction mixtures were mixed in 0.1 ml MicroAmp Fast 96-well Reaction Plates. The *GoTaq® qPCR Master Mix* kit was used for preparation of the reaction mixtures according to the manufacturer's instructions in a final volume of 20 µl per reaction. cDNAs were diluted 1:10 with nuclease-free H_2O and 4 µl of the dilutions were used as a reaction template in the qRT-PCR reactions (Table 7). qRT-PCRs were performed in a StepOnePlus™ real-time thermal cycler. Technical triplicates of each sample were assayed in one run (40 cycles) composed of three stages: 1. Activation at 95°C for 10 min, 2. Denaturation at 95°C for 15 s and annealing/extension at 60°C for 1 min for each cycle, 3. Melt curve at 95°C for 15 s, 60°C for 1 min and 95°C for 15 s.

Table 7. qRT-PCR reactions composition.

Component	Volume
GoTaq® qPCR Master Mix, 2X	10 µl
CXR Reference Dye	0.2 µl
10 µM Fwd primer	2 µl
10 µM Rev primer	2 µl
cDNA (diluted 1:10)	4 µl
nuclease-free H_2O	1.8 µl
Total volume	20 µl

qRT-PCR data were analyzed using relative quantification and the Ct method (Ct is the threshold cycle) as described previously (Yuan, Reed, Chen, & Stewart, 2006), with the reference genes *Gapdh* or *Cytb* genes as the endogenous control (described in the Results and Discussion parts). For each biological sample and analyzed gene an average Ct value was calculated from the values of the technical triplicates. The level of gene expression was calculated by subtracting the averaged Ct values for endogenous control from those of the gene of interest, resulting in a ΔCt value, as in equation (1). The relative expression was calculated as the difference (ΔΔCt) between the ΔCt of the test sample (e.g. $RYR1^{-/-}$ or $Ca_v1.1^{-/-}$) minus that of the control sample (e.g. WT) as in equation (2). The relative expression of genes of interest were calculated as a fold change (FC) relative to the expression of the same genes in the control sample and expressed as $2^{-\Delta\Delta Ct}$, as shown in equation (3). Equations for calculation of the relative gene expression level in qRT-PCR experiments:

(1) $\Delta Ct = Ct_{\text{Target}} - Ct_{\text{Reference}}$

(2) $\Delta\Delta Ct = \Delta Ct_{\text{Test sample}} - \Delta Ct_{\text{Control sample}}$

(3) $FC_{\text{Target gene in test sample}} = 2^{-\Delta\Delta Ct}$

2.2.7 Analysis of $Ca_v1.1$ full length and Δ29 splice variants

The relative amount of $Ca_v1.1$ transcripts containing or lacking exon 29, i.e. $Ca_v1.1$ full length and Δ29, respectively, was determined within each sample by PCRs using the cDNA produced from 10 ng of total RNA from each sample as a template. The region between $Ca_v1.1$ exons 28 and 32 was amplified using the primers indicated in Table 2. PCRs were performed using the DreamTaq Polymerase according to the manufacturer's protocol and as indicated in Table 8. The PCR program consisted of an initial DNA denaturing step at 95°C for 3 minutes, followed by 35 cycles of 95°C for 30 seconds, 55°C for 30 seconds and 72°C for 1 minute; with a subsequent 5 minute elongation step at 72°C and a final holding step at 4°C. Full length $Ca_v1.1$ transcripts containing exon 29 produced a 343 bp PCR product, while those lacking exon29, $Ca_v1.1$ Δ29, resulted in a smaller product, 286 bp. The two PCR products were separated electrophoretically on 2 % agarose gels and the bands were digitized via the INTAS documentation system. Band intensities were quantified with the image analysis module implemented in the FluoView1000 software. In the process of band intensity quantification, background correction was performed locally for each lane. Subsequently, the intensity integral of each band was calculated by summing the intensity values of all pixels belonging to that band. The sum of the two intensity integrals was regarded as 100%, so that the fractional intensity (in %) of each band, with or without exon 29, could be calculated

Table 8. PCR reactions composition of the Cav1.1 Δ29 analysis.

Component	Volume
H_2O	14.25 µl
10x DreamTaq Green Buffer	2.50 µl
10 mM dNTPs	0.50 µl
10 µM Fwd primer	1.25 µl
10 µM Rev primer	1.25 µl
DreamTaq	0.25 µl
cDNA	5.00 µl
Total volume	25.00 µl

2.2.8 Microarrays

All microarray (MA) reagents, kits and instruments were purchased from Affymetrix (Thermo Fisher) or from the suppliers recommended in the respective Affymetrix manuals. The first MA analysis, examining the global transcriptomic changes in E18.5 $RYR1^{-/-}$ vs. $RYR1^{+/-}$ limb skeletal muscle, was performed with Mouse Genome 430 2.0 array chips and the *GeneChip® 3' IVT* (*in vitro* transcription) *Express Kit*. The second MA analysis, examining the gene expression profiles of E14.5 and E18.5 WT ($^{+/+}$), heterozygous ($^{+/-}$) and homozygous ($^{-/-}$) mutant RYR1 and $Ca_v1.1$ limb skeletal

muscle was performed with MoGene 2.0 ST array chips and the *GeneChip® WT PLUS Reagent Kit*. All procedures were carried out according to the manufacturer's recommendations. In both analyses sample hybridization to the array chips, as well as arrays wash and stain procedures were performed via *the GeneChip® Hybridization, Wash, and Stain (HWS) Kit* according to the manufacturer's instructions. All array chips were scanned in a Gene-Chip Scanner-3000-7G instrument. Detailed manuals about experimental procedures, kits specifications and instrument operations are freely available at the manufacturer's web site, http://www.thermofisher.com/. Below is a brief description of the main experimental procedures of each of the performed MA analysis. Technical handling of array chips was performed with the kind assistance of Margit Henry and Tamara Rotshteyn from the Gene Expression Affymetrix Facility at the Center for Molecular Medicine Cologne (CMMC).

2.2.8.1 MA analysis of E18.5 RYR1$^{-/-}$ vs. RYR1$^{+/-}$ limb skeletal muscle

An overview of the main steps and incubation times in the MA analysis of E18.5 RYR1$^{-/-}$ vs. RYR1$^{+/-}$ limb skeletal muscle is shown in Fig. 11. All thermal incubation steps were performed via a thermal cycler except if otherwise indicated.

All procedures were performed with components of the *GeneChip® 3' IVT Express Kit* as described in (Filipova et al., 2016) and according to the kit user manual. Briefly, 100 ng of total RNA from each biological replicate (limb skeletal muscles from 4 RYR1$^{-/-}$ and 4 RYR1$^{+/-}$ E18.5 fetuses) were used in the initial first-strand single-stranded (ss)-cDNA synthesis reaction. On ice, 2 µl of 1:5.000.000 diluted Poly-A RNA controls, serving as internal positive controls, were mixed with each RNA sample and nuclease-free H_2O was added to each sample to a final volume of 5 µl. For the first-strand cDNA synthesis procedure 5 µl of First-Strand Master Mix was added to each sample, followed by incubation at 42 °C for 2 hours. Next, the second-strand cDNA synthesis step was performed by adding 20 µl of Second-Strand Master Mix to each sample on ice. Samples were incubated at 16 °C for 1 hour, followed by 65 °C for 10 minutes. *In vitro* transcription (IVT) of the double-stranded (ds)-cDNA, yielding amplified RNA (aRNA) and aRNA biotin labeling was performed by adding 30 µl of IVT Master Mix to each ds-cDNA sample, followed by an incubation at 40 °C for 16 hours.

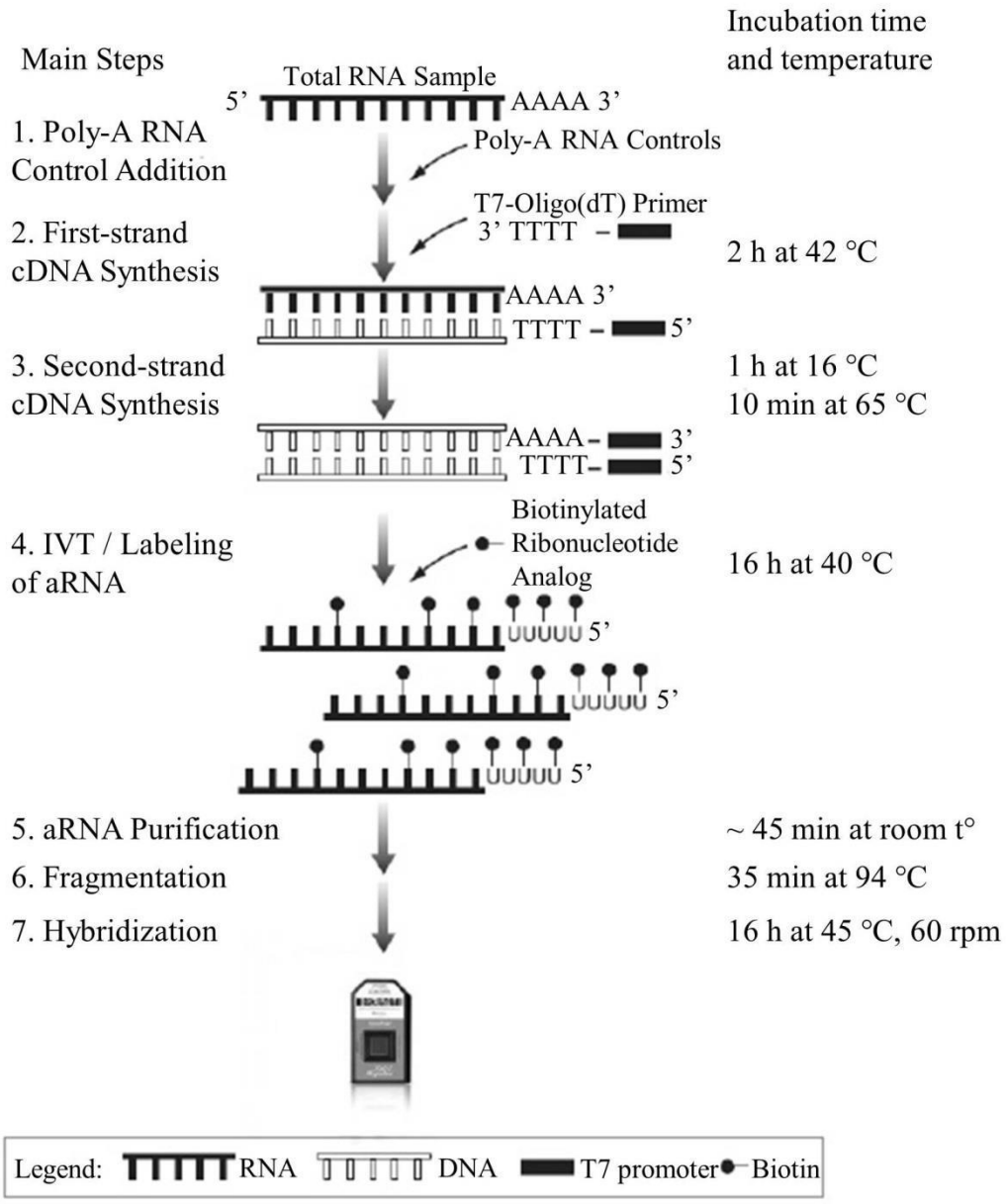

Fig. 11: A schematic workflow of the E18.5 RYR1$^{-/-}$ vs. RYR$^{+/-}$ MAs.
The scheme depicts the main experimental steps and incubation conditions in MAs preparation, starting with total RNA samples up to hybridization to Mouse Genome 430 2.0 array chips. The *GeneChip® 3' IVT Express Kit* was used in all experiments up to the hybridization step. Master mixes containing all reagents except the RNA-derived sample were used in all steps to assure equal handling and conditions of all samples. Modified from the *GeneChip® 3' IVT Express Kit User Manual* (Thermo Fisher).

In the following aRNA purification reaction unbound ribonucleotide triphosphates (NTPs), salts, enzymes and inorganic phosphate are removed. Purification of aRNA is achieved by the addition of 60 µl of aRNA Binding Mix (containing 10 µl of RNA binding beads) to each aRNA sample in a 96-well U-Bottom Plate, followed by the addition of 120 µl of 100% ethanol to each sample and gently shaking of the U-Bottom Plate at a plate shaker for 2 minutes. The U-Bottom Plate was then

transferred on a magnetic stand for 5 minutes to capture the aRNA-bound magnetic beads. The beads were then washed two times with 100µl of aRNA Wash Solution and again captured via a magnetic stand. The purified aRNAs was eluted in 50 µl of preheated (60 °C) aRNA Elution Solution and kept on ice or stored at -80 °C. Next, the aRNAs concentrations were measured via a NanoDrop spectrophotometer. 15 µg of each biotin-aRNA was fragmented via an addition of 8 µl of 5x Array Fragmentation Buffer and nuclease-free H_2O up to 40 µl total volume per reaction. The fragmentation was induced by an incubation at 94 °C fo 35 minutes. Samples were placed on ice or stored at -20 °C.

The following steps were performed via the *GeneChip® Hybridization, Wash and Stain Kit (HWS)*. 12.5 µg of each biotin-labeled aRNA sample were added to the Hybridization Cocktail (Table 9, left). The Hybridization Cocktail was heated at 99 °C for 5 minutes and at 45 °C for 5 minutes. 200 µl of Pre-Hybridization Mix was added to each of the Mouse Genome 430 2.0 array chips and the chips were incubated at 45 °C for 10 minutes in a GeneChip® Hybridization Oven-645 with rotation. The Pre-Hybridization Mix was extracted from the array chips and replaced by 200 µl of Hybridization Cocktail. The sample hybridization to the array chips was done at 45 °C with rotation at 60 rpm for 16 hours in a GeneChip® Hybridization Oven-645.

Table 9. Hybridization Cocktail for a single probe array.

Mouse Genome 430 2.0 arrays		**MoGene 2.0 ST arrays**	
Components	Amount	Components	Amount
Fragmented and labelled aRNA	12.5 µg (33.3 µl)	Fragmented and labelled ss-DNA	3.5 µg (41 µl)
Control Oligonucleotide B2 (3 nM)	4.2 µl	Control Oligonucleotide B2 (3 nM)	2.5 µl
20x Hybridization Controls (bioB, bioC, bioD, cre)	12.5 µl	20x Hybridization Controls (bioB, bioC, bioD, cre)	7.5 µl
2x Hybridization Mix	125 µl	2x Hybridization Mix	75 µl
DMSO	25 µl	DMSO	10.5 µl
Nuclease-free H_2O	50 µl	Nuclease-free H_2O	13.5 µl
Total volume	250 µl	Total volume	150 µl

After hybridization a project containing all necessary sample and experimental information was defined in a GeneChip® Command Console (AGCC) project. Each of the Mouse Genome 430 2.0 array chips were washed and stained with 600 µl of Stain Cocktail I, 600 µl of Stain Cocktail II and 800 µl of Array Holding Buffer from the *HSW* kit on a GeneChip® Fluidics Station-450. Subsequently, the array chips were scanned in an Affymetrix GeneChip® Scanner-3000-7G. Washing, staining and scanning was performed as described in the GeneChip® Expression Analysis Technical Manual (Thermo Fisher). Affymetrix GCOS software was used for the generation of .dat

and .cel files. Microarray data are available in the ArrayExpress database (www.ebi.ac.uk/arrayexpress) under the accession number E-MTAB-3608.

2.2.8.2 MA analysis of E14.5 and E18.5 of $^{+/+}$, $^{+/-}$ and $^{-/-}$ RYR1 and $Ca_v1.1$ limb skeletal muscle

An overview of the main steps and incubation times in the MA analysis of E14.5 and E18.5 WT ($^{+/+}$), heterozygous ($^{+/-}$) and homozygous ($^{-/-}$) mutant RYR1 and $Ca_v1.1$ limb skeletal muscle is shown in Fig. 12. All thermal incubation steps were performed via a thermal cycler except if otherwise indicated.

All procedures were performed with components of the *GeneChip® WT PLUS Reagent Kit* as described in (Filipova et al., 2018) and according to the kit user manual (Fig. 12).

In brief, from each sample 250 ng total RNA were used for first-strand cDNA synthesis. 5 µl of First-Strand Master Mix were added to each sample that has been previously mixed with Poly-A RNA controls as per the *GeneChip® WT PLUS Reagent Kit User Manual* instructions. The reactions were incubated at 25 °C for 1 h, then at 42 °C for 1 h and then at 4 °C for at least 2 minutes. Next, second-strand cDNA synthesis and RNA degradation by RNase H were simultaneously performed by addition of 20 µl of Second-Strand Master Mix to each sample and an incubation at 16 °C for 1 h, then at 65 °C for 10 minutes and then at 4 °C for at least 2 minutes. Next, the ds-cDNAs were used as template for *in vitro* transcription (IVT) reactions via the T7 RNA polymerase, resulting in complimentary RNAs (cRNAs). For this purpose 30 µl of IVT Master Mix were added to each sample, followed by incubation at 40 °C for 16 h, then at 4 °C until further use. Next, the cRNAs were purified from enzymes, salts, unbound NTPs and inorganic phosphates by adding 100 µl of Purification Beads to each cRNA sample in a 96-well U-bottom plate. The cRNA-bound Purification Beads were captured on a magnetic stand and washed 3 times with 200 µl of 80% ethanol. The cRNAs were eluted in 27 µl of preheated (65 °C) nuclease-free H_2O. The cRNAs concentrations were measured via a NanoDrop spectrophotometer. Next, 15 µg of each cRNA sample were used for a 2^{nd}-cycle ss-cDNA synthesis by adding 4 µl of 2^{nd}-Cycle Primers, containing the unnatural dUTP, to each cRNA sample and incubating the samples at 70 °C for 5 minutes, then at 25 °C for 5 minutes and then at 4 °C for 2 minutes.

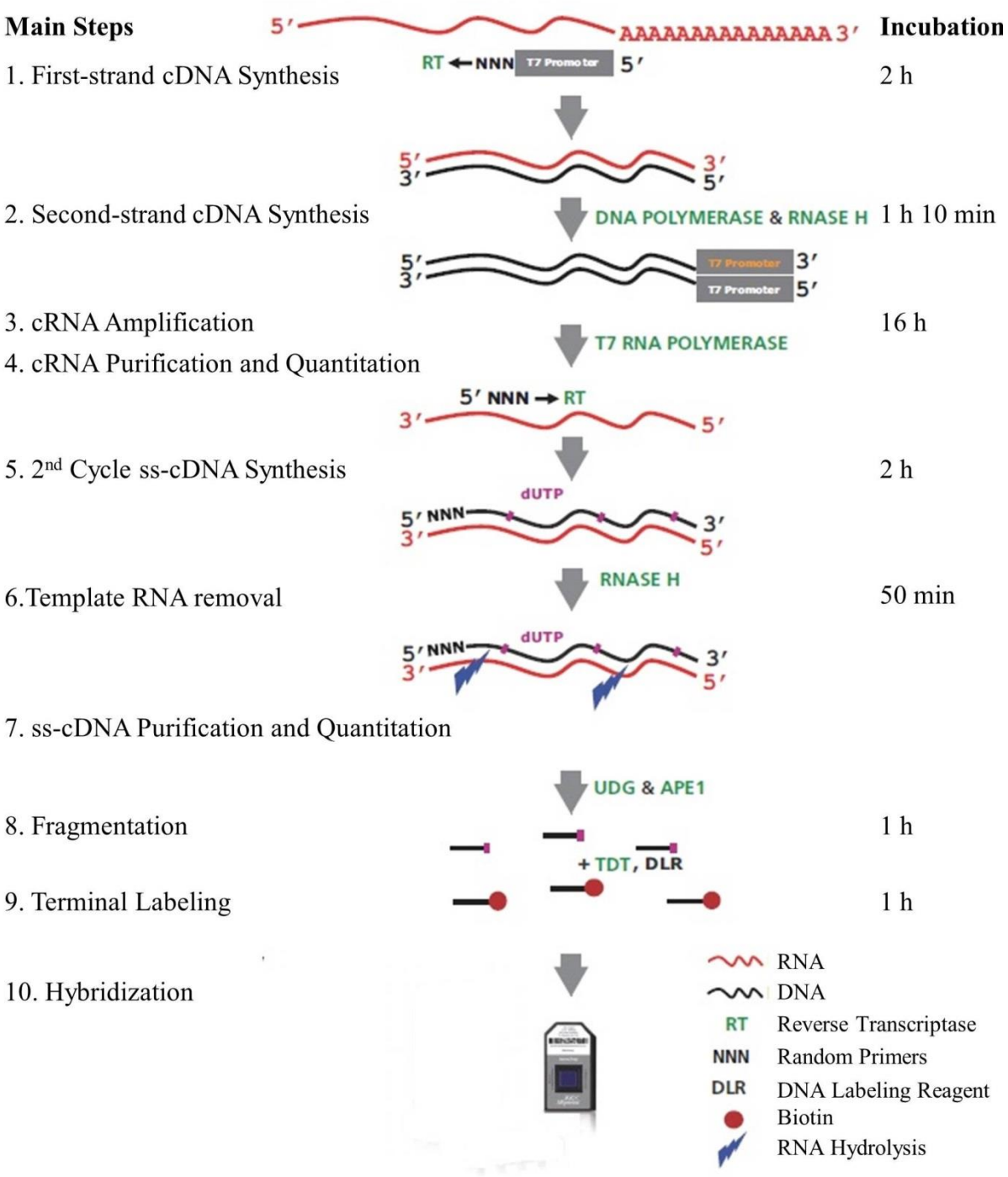

Fig. 12: A schematic workflow of the E14.5 and E18.5 $^{+/+}$, $^{+/-}$ and $^{-/-}$- RYR1and Cav1.1 MAs.
The scheme depicts the main experimental steps and incubation conditions in MAs preparation, starting with total RNA samples up to hybridization to MoGene 2.0 ST array chips. The *GeneChip® WT PLUS Reagent Kit* was used in all experiments up to the hybridization step. Master mixes containing all reagents except the RNA-derived sample were used in all steps to assure equal handling and conditions of all samples. Modified from the *GeneChip® WT PLUS Reagent Kit* User Manual (Thermo Fisher).

Then, 12 µl of 2nd-cycle ss-cDNA Master Mix were added to each sample on ice and the reactions were incubated at 25 °C for 10 minutes, then at 42 °C for 90 minutes, then at 70 °C for 10 minutes and then at 4 °C for at least 2 minutes. The cRNA templates were then hydrolyzed by an addition of 4 µl of RNase H to each sample and incubation at 37 °C for 45 minutes, then at 95 °C for 5 minutes and then at 4 °C for 2 minutes. Next, 11 µl of nuclease-free H_2O were added to each sample, bringing the total volume of the reactions to 55 µl. The 2nd-cycle ss-cDNAs were than purified via 100 µl of Purification Beads per sample, 1 x washing with 150 µl of 100% ethanol and 3 x washing with 200 µl of 80% ethanol as described above. The purified ss-cDNAs were eluted in 30 µl of preheated (65 °C) nuclease-free H_2O and their concentration was measured on a NanoDrop spectrophotometer. Next, 5.5 µg of each ss-cDNA sample were fragmented via a Fragmentation Master Mix containing uracil-DNA glycosylase (UDG) and apurinic/apyrimidinic endonuclease 1 (APE1) that introduce breaks at the dUTP residues. To each ss-cDNA sample 16.8 µl of the Fragmentation Master Mix were added and the reactions were incubated at 37 °C for 1 h, then at 93 °C for 2 minutes and at 4 °C for at least 2 minutes. 45 µl of the fragmented ss-cDNAs were terminally labeled with biotin via 15 µl of Labeling Master Mix, containing terminal deoxynucleotidyl transferase (TdT). The reactions were incubated at 37 °C for 1 h, then at 70 °C for 10 minutes and at 4 °C for at least 2 minutes. Samples were placed on ice or stored at -20 °C.

The following steps were performed via the *GeneChip® Hybridization, Wash and Stain Kit (HWS)*, similar to the procedures described above (in 2.2.8.1). 3.5 µg of each fragmented and labeled ss-DNA were used in the preparation of the Hybridization Cocktail (Table 9, right) and treated as described above. 130 µl of each Hybridization Cocktail were pipetted into MoGene 2.0 ST array chips (1 sample per array chip). Hybridization, wash, stain and scanning procedures were performed as described above (in 2.2.8.1). Microarray data are available in the ArrayExpress database (www.ebi.ac.uk/arrayexpress) under the accession number E-MTAB-5755.

2.2.9 Statistical analyses

All statistical analyses are performed as described in (Filipova et al., 2016) and (Filipova et al., 2018). In all analyses * indicates a P-value < 0.05; ** indicates a P-value < 0.01; *** indicates a P-value < 0.001.

2.2.9.1 Statistical analysis of qRT-PCR data

The relative expression values presented as a FC ($2^{-\Delta\Delta Ct}$) for each biological sample from all qRT-PCRs were analyzed in GraphPad Prism version 4.00 (GraphPad Software, La Jolla California USA, www.graphpad.com). Unpaired t-test analyses were done when comparing the relative expression levels of one test group versus one control and one-way ANOVA followed by Bonferroni's multiple comparisons test was performed when comparing multiple groups. Relative quantification values are presented as FCs plus/minus the standard error of the mean (S.E.M.) relative to the control group, which was normalized to an expression rate of 1.

2.2.9.2 Statistical analysis of $Ca_v1.1$ full length and Δ29 PCR data

The $Ca_v1.1$ full length and Δ29 band intensity values (as % of total intensity) were analyzed in GraphPad Prism version 4.00 (GraphPad Software, La Jolla California USA, www.graphpad.com). Unpaired t-test analyses were performed comparing the intensity of the $Ca_v1.1$ full length and Δ29 band in each biological sample.

2.2.9.3 Statistical analysis of the Mouse Genome 430 2.0 Microarrays

Robust Multiarray Analysis (RMA) was used for background correction, summarization and normalization (Bolstad, Irizarry, Astrand, & Speed, 2003). The quantile normalization method was implemented to normalize the raw dataset executable with R-package (Irizarry, 2003), carried out at the probe feature level. The differentially expressed genes were described by a linear model implementing R and the LIMMA packages (Smyth, 2004). Differentially regulated genes were determined based on cut-off values of 5% error rate ($P<0.05$), calculated by Moderated t- statistics according to Benjamini and Hochberg (Multiple Testing Correction). Additionally, to identify significantly expressed genes between the control and dysp sample groups, the degree of change with the threshold value $\geq \pm 1.5$ was used. Principal component (PC) analysis was performed using the Stats package in R using the prcomp function. The "x" attribute of the prcomp object was used to generate 2 dimensional scatter plots. Bioinformatical analyses in R were performed with the kind assistance of Dr. John A. Gaspar from the group of Prof. Dr. Agapios Sachinidis from the Institute for Neurophysiology at the University Hospital of Cologne.

2.2.9.4 Statistical analysis of the MoGene 2.0 ST Microarrays

The .cel files obtained by the microarray analyses were subjected to background correction, summarization and normalization by Robust Multiarray Analysis (RMA) and used for generation of .chp summarization files via the Expression Console™ Software 1.4 (Affymetrix / Thermo Fisher), and subsequently were used to produce a three dimensional PCA plot. The .chp files were used for gene level differential expression quantification, accompanied by One-Way Between-Subject ANOVA statistical analysis via the Transcriptome Analysis Console 3.0 (Affymetrix). Transcripts having a P-value ≤ 0.05 and a linear FC $\geq \pm 2$ for comparison of E18.5 vs. E14.5 sample groups, or a FC $\geq \pm 1.5$ for E14.5 vs. E14.5 and E18.5 vs. E18.5 sample groups, were considered as differentially expressed genes (DEGs). Volcano plots were generated using the Transcriptome Analysis Console 3.0 (Affymetrix / Thermo Fisher).

2.2.10 Enrichment Analyses

Gene enrichment analyses for DEGs identified upon the comparisons of different groups were performed with the databases *Gene Ontology for Biological Process* (GO BP, versions 2015 and 2017) and *Cellular Component* (GO CC, versions 2015 and 2017), *Kyoto Encyclopedia of Genes and Genomes* (KEGG, version 2015), *Reactome* (version 2015), *Panther* (version 2015) as well as with *Wiki Pathways* (WP, version 2016) using the *Enrichr* online enrichment tool (Chen et al., 2013). A P-value ranking was applied to all enrichment analyses.

The *David GO* (version 6.7) and *MGI GO* (version 2015) databases (Huang da, Sherman, & Lempicki, 2009; Smith et al., 2014), as well as manual data mining were additionally applied to identify DEGs directly connected to skeletal muscle.

2.2.11 Heatmaps and hierarchical clustering

Heatmaps and hierarchical clustering analyses were performed via the *ClustVis* online tool (Metsalu & Vilo, 2015) using unit variance row scaling. Hierarchical average linkage clustering measuring the average Euclidean distance was applied for both rows and columns.

3 Results

3.1 Part I: Analysis of fetal skeletal muscle lacking RYR1 at E18.5

The first objective of this work was to analyze how the absence of RYR1 affects fetal limb skeletal muscle morphology in general, and to detect the accompanying changes in global gene expression of this organ, in particular. To address these questions, I compared the gross body shape, limb skeletal muscle histology, and transcriptomic profiles of homozygous $RYR1^{-/-}$ and heterozygous $RYR1^{+/-}$ (control) littermates at E18.5, as reported in (Filipova et al., 2016). The heterozygous $RYR1^{+/-}$ animals were used as controls instead of WTs since they have been reported to show no phenotypic changes in respect to viability, fertility, muscle structure and performance (Buck et al., 1997). Moreover, by using the $RYR1^{+/-}$ animals as controls the transcriptomic analysis results remain unaffected by possible genetic compensatory mechanisms, arising from the presence of a single functional copy of the *Ryr1* gene, which would not play a role in the formation of the $RYR1^{-/-}$ phenotype. The main findings of this part of the results were reported in (Filipova et al., 2016).

3.1.1 Absence of RYR1 leads to an impairment of gross body morphology and limb skeletal muscle histology

In accordance to earlier studies (Buck et al., 1997; Takeshima et al., 1994), E18.5 $RYR1^{-/-}$ fetuses already displayed severe abnormalities when compared to their control $RYR1^{+/-}$ littermates (Fig. 13). An analysis of fetuses obtained from three different female mice at E18.5 revealed that the $RYR1^{-/-}$ mice exhibited an overall smaller body size, thinner limbs, enlarged necks and a typical spinal curvature. These changes indicated that the overall developmental program is severely affected in the $RYR1^{-/-}$ fetuses.

In order to gain a more detailed view on how skeletal muscle morphology is affected by the absence of RYR1, histological cross-sections of the distal hind limbs of control ($RYR1^{+/-}$) and $RYR^{-/-}$ littermates at E18.5 were prepared and analyzed. 10 µm thick cryo cross-sections were stained with H&E and the limb skeletal muscle structure was examined under a bright-field microscope at three different magnifications – 50-fold, 200-fold and 400-fold (Fig. 14).

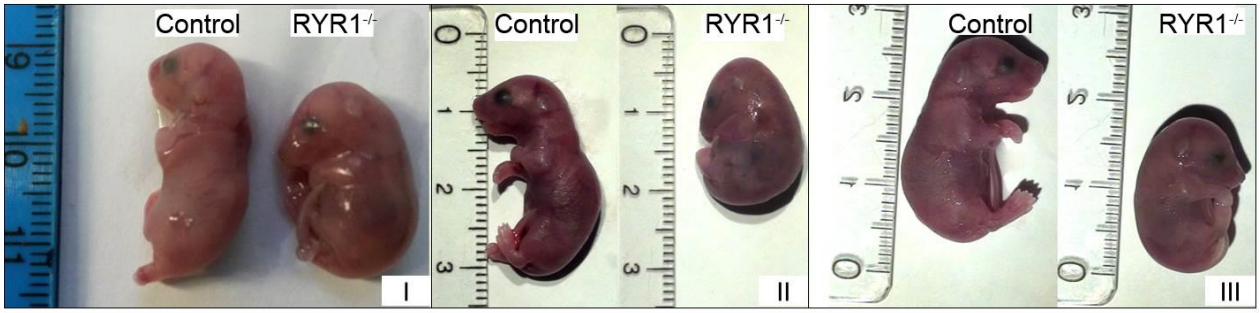

Fig. 13: Gross fetal morphology at E18.5.
Photographic representations of heterozygous RYR1$^{+/-}$ controls **(left)** and homozygous RYR1$^{-/-}$ **(right)** littermates at day E18.5 from three different litters (I, II and III). Modified from (Filipova et al., 2016).

The control limb skeletal muscle exhibited a normal, advanced degree of development with clearly visible fascicles, covered by a fascia (Fig. 14A left, and middle), consisting of terminally differentiated fetal fibers with peripherally located nuclei (Fig. 14A right). The RYR1$^{-/-}$ limb skeletal muscle, on the other hand, was characterized by disorganization (Fig. 14B). In these muscles no fascia could be observed, fascicles were almost entirely missing, with only small groups of cells visible (Fig. 14B left, middle). The predominant cell type in the RYR1$^{-/-}$ muscles were myotubes with only a few disorganized, immature fibers (Fig. 14A right).

These evident changes in the limb skeletal muscles of E18.5 RYR1$^{-/-}$ animals, compared to their control littermates, strongly hint at a developmental retardation in these animals. At E18.5 – at the end of prenatal development in the mouse – the formation of the limb skeletal muscle is almost complete (Tajbakhsh, 2009). Therefore, the impaired development of the RYR1$^{-/-}$ limb skeletal muscle may be caused by an active pause of the myogenic program at an earlier stage or by reactive processes of degeneration and elimination of muscle fibers, or by a combination of both.

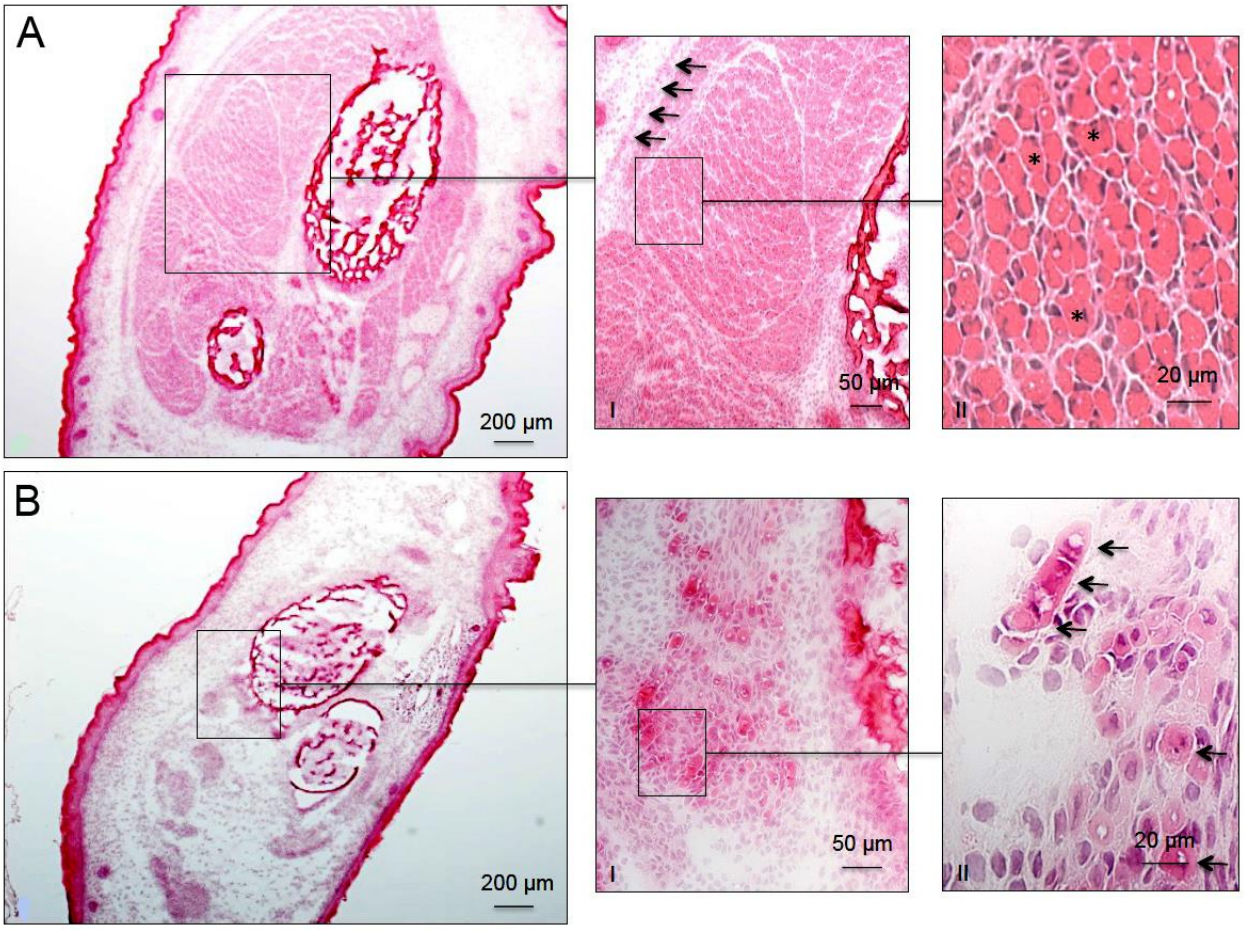

Fig. 14: E18.5 limb muscle histology.
Histological cross sections of distal hind limbs of E18.5 control **(A)** and RYR1$^{-/-}$ **(B)** littermates. **(A)** A well-developed internal muscular organization with structured fascicles, covered by a fascia (arrows) and consisting predominantly of terminally differentiated myofibers (*) were observed in the control animals. **(B)** In contrast, the RYR1$^{-/-}$ skeletal muscle was not well structured, fascia and fascicles were missing and only individual immature fibers with centrally-located nuclei were present (arrows). **(A & B)** H&E staining; original magnification x 50 (left panels), × 200 (insets I, middle); × 400 (insets II, right). Micrographs were taken by PD Dr. Anna Brunn. Modified from (Filipova et al., 2016).

3.1.2 Transcriptomic analysis of RYR1$^{-/-}$ skeletal muscle reveals multiple differentially regulated genes (DEGs)

One of the main aims of this study was to elucidate in detail the whole spectrum of transcriptomic changes occurring in RYR1$^{-/-}$ limb skeletal muscles at E18.5 that may be connected to the formation of the specific muscle phenotype described above. In order to address this question, the skeletal muscles of the fore- and hind limbs of 4 RYR1$^{-/-}$ and 4 control RYR1$^{+/-}$ littermates (n = 4 biological replicates per group) at E18.5 from 2 litters were dissected and pooled for each animal. The samples from all animals were handled separately and used for RNA extraction. The quality and

concentrations of the resulting RNAs were analyzed (Fig. 15) and subjected to microarray analyses (MAs, Fig. 16) (Filipova et al., 2016).

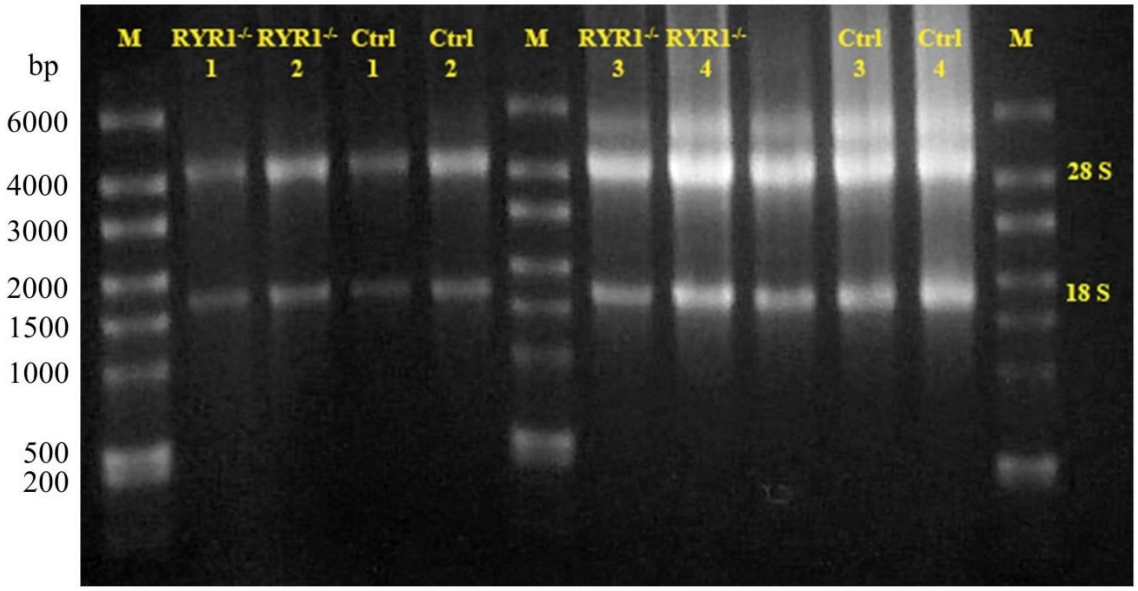

Sample	c [ng/µl]	Sample	c [ng/µl]
RYR1$^{-/-}$ 1	142.3	RYR1$^{-/-}$ 3	458.6
RYR1$^{-/-}$ 2	224.0	RYR1$^{-/-}$ 4	434.0
Ctrl 1	183.9	Ctrl 3	835.2
Ctrl 2	278.3	Ctrl 4	934.7

Fig. 15: RNA quality assessment.
Total RNA was extracted from the skeletal muscles of the fore- and hind limbs of 4 RYR1$^{-/-}$ (RYR1$^{-/-}$ samples 1 to 4) and 4 control (Ctrl samples 1-4) E18.5 mouse fetuses and 5 µl of each RNA sample were tested via an electrophoretic run on a 2% agarose gel next to 5 µl of RiboRuler High Range RNA Ladder as size marker (marked as "M" with bp size of each band given on the left, Thermo Fisher Scientific). The RNA concentration of each sample is given in the table under the photograph. For each sample clear and distinct bands corresponding to the 18S and 28S rRNAs were observed indicating a high degree of RNA integrity. Modified from (Filipova et al., 2016).

After background correction, summarization and normalization via a Robust Multi-array Analysis (RMA), the microarrays yielded information about the expression of 41,101 transcript clusters, spanning 21,569 unique annotated genetic loci. A subsequent t-test statistical analysis combined with a Benjamini-Hochberg false discovery rate (FDR) test revealed that the expression of 417 genomic loci was significantly differentially regulated in the RYR1$^{-/-}$ limb skeletal muscle, meeting the criteria of fold change FC $\geq$ 1.5 or $\leq$ -1.5 and an FDR-adjusted P-value $\leq$ 0.05. Of these 417 genomic loci, 394 mapped within annotated genes and after correcting for genes which were detected multiple times, 318 unique genes were identified as differentially expressed genes (DEGs). Interestingly,

exactly 50% of the DEGs (159 DEGs) were negatively regulated and 50% (159 DEGs) were positively regulated in RYR1$^{-/-}$ skeletal muscle (Table 10).

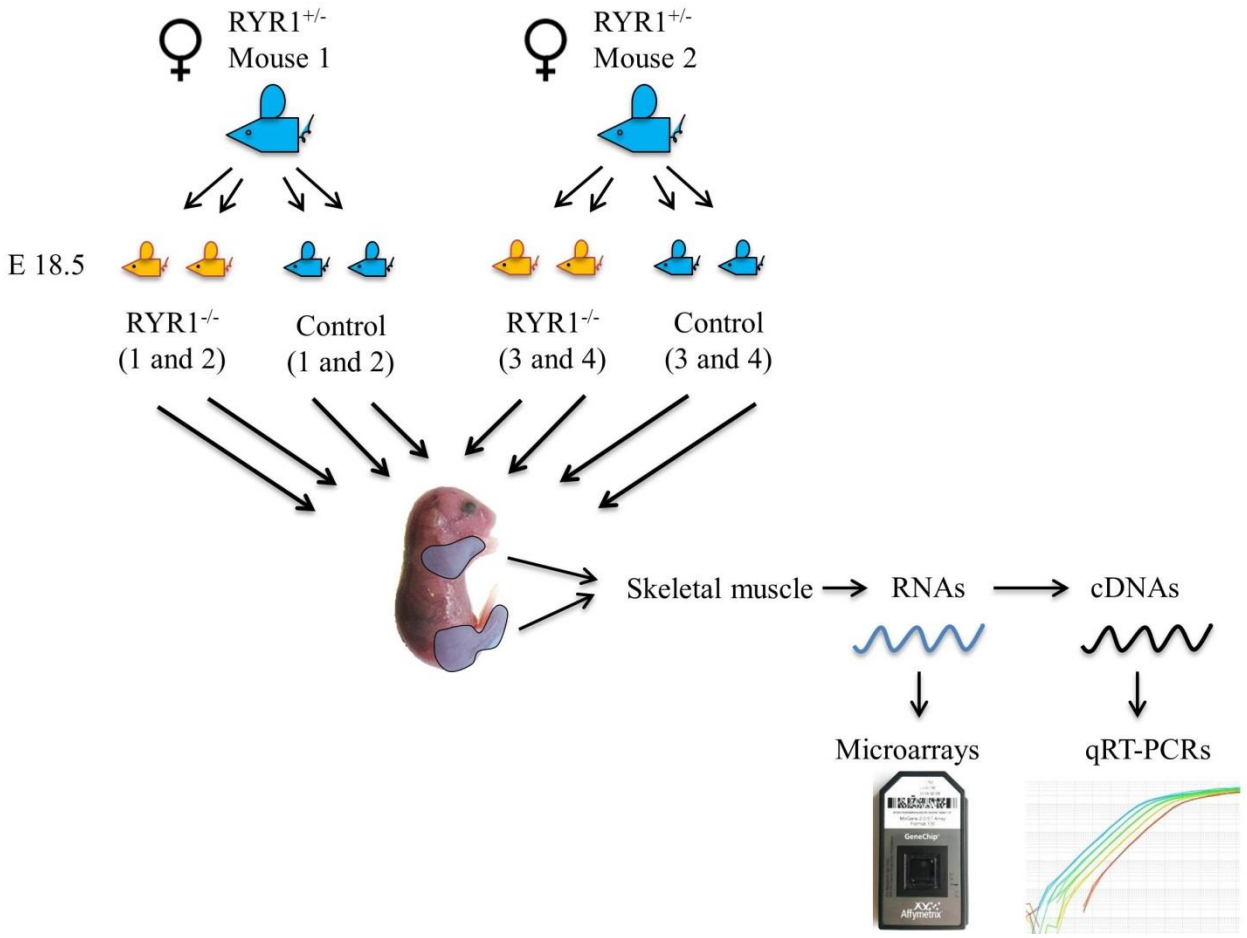

Fig. 16: Workflow scheme for the gene expression analysis of E18.5 RYR1$^{-/-}$ vs. RYR$^{+/-}$ limb skeletal muscle. Two heterozygous RYR1$^{+/-}$ male and female mice were subjected to timed pairings. The pregnant females were sacrificed at day 18.5 post coitum (E18.5)and the skeletal muscles from the front- and hind limbs of 2 RYR1$^{-/-}$ and 2 control (RYR1$^{+/-}$) E18.5 fetuses were collected and used for RNA extractions. Equal amounts of total RNA from each sample were used for individual hybridizations to Affymetrix Mouse Genome 430 2.0 array chips and microarray analysis was performed as described in Materials and Methods. Additionally, equal amounts of the total RNAs were used in reverse transcription reactions and the resulting cDNAs were used in qRT-PCR analyses. Modified from (Filipova et al., 2016).

Table 10. E18.5 RYR1$^{-/-}$ vs. RYR$^{+/-}$ DEGs.

	Total DEGs	Annotated DEGs	Unique annotated DEGs
All	417	394	318
Downregulated	205	202	159
Upregulated	212	192	159

Numbers of the total, annotated and total annotated DEGs (FC ≤ -1.5 or ≥ 1.5; FDR-adjusted P-value ≤ 0.05) identified in the RYR1$^{-/-}$ vs. RYR1$^{+/-}$ microarray analysis.

3.1.3 Principal component analysis (PCA) shows segregation of RYR1$^{-/-}$ and control samples in discrete groups

In order to assess the similarity and the variation between the individual samples based on their global transcriptomic profiles, a two-dimensional PCA plot was generated using the intensity levels of all transcripts detected in the MAs for all probes (i.e. the entire limb skeletal muscle transcriptome of each sample, Fig. 17A).

The PCA is a mathematical algorithm that reduces the dimensionality of data sets which contain a high number of variables, but retains most of the variation in the data set (Ringner, 2008). Each of the biological RYR1$^{-/-}$ and control replicates can be viewed as a data set, in which the different transcripts (genes) are the variables that differ in respect to their expression levels. Thus, the PCA algorithm combines the original variables for each data set (i.e. each biological sample), resulting in much fewer new variables – the principal components (PCs) – that still represent most of the variation of the original data sets. By definition, the principal component 1 (PC1) is the direction representing the highest percentage of the original variation between the samples. The principal component 2 (PC2) is defined as the direction uncorrelated to PC1 along which the samples show the second highest percentage of variation.

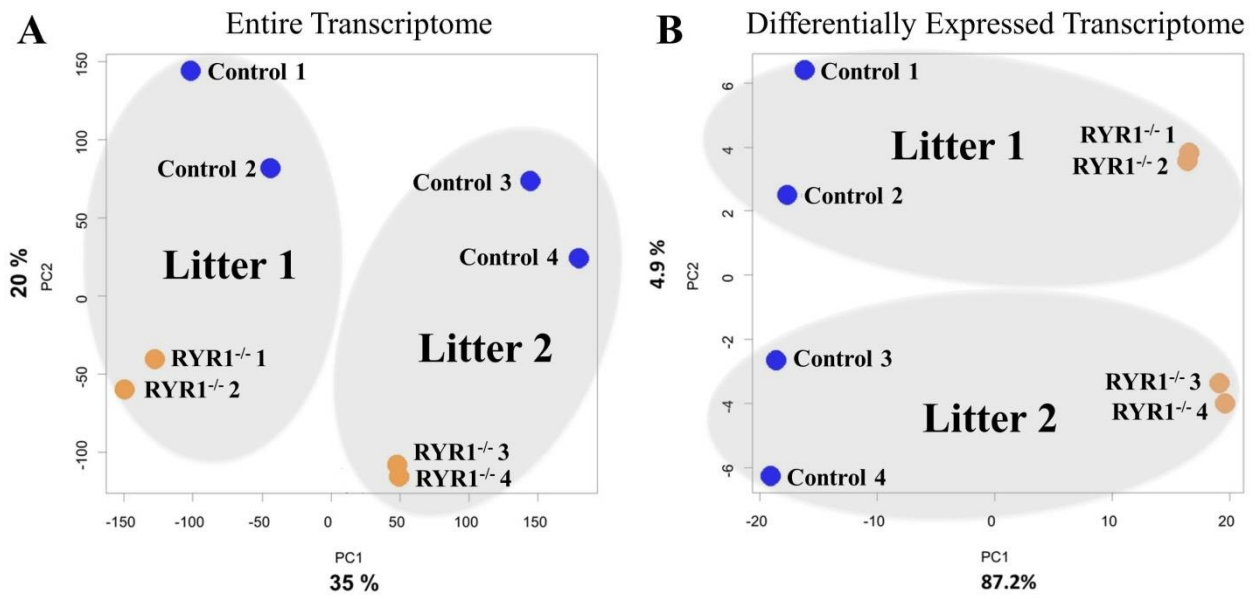

Fig. 17: E18.5 RYR1$^{-/-}$ vs. RYR$^{+/-}$ – PCA plots.
Two-dimensional principal component analysis (PCA) of the RYR1$^{-/-}$ (orange dots) and control (blue dots) samples (biological replicates 1 to 4) subjected to MAs. The expression of the entire transcriptome **(A)** and of the detected DEGs **(B)** was plotted. Samples from animals of the same litter (Litters 1 and 2) occupy the same shaded area. PCAs were performed with the help of Dr. John A. Gaspar. Modified from (Filipova et al., 2016).

The PCA plot generated from the data of the entire skeletal muscle transcriptome for all samples (Fig. 17A) showed a significant separation along PC1 (35%) between the samples obtained from animals of the two different litters. This suggests that the variation of the transcriptomic signature of the limb skeletal muscle samples is highly impacted by the specific sets of individual characteristics of the parents (genotype, SNPs, mutation pool, etc.) and probably by the small differences in the time of gestation time (± 0.5 day) of the individual litters. However, a clear separation between RYR1$^{-/-}$ and control samples was observed along PC2 (20%), indicating that the RYR1$^{-/-}$ skeletal muscles exhibits evident global transcriptomic changes when compared to the skeletal muscle of the control animals.

Next, a PCA was performed with the values of the DEGs (FC ≥ 1.5 or ≤ -1.5 and P-value ≤ 0.05) found in the RYR1$^{-/-}$ samples (Fig. 17B). This time the most significant proportion of the variation (PC1 = 87.2%) between the sample was evidently due to the samples' genotype as the RYR1$^{-/-}$ and the control biological replicates formed two distinct sample groups along PC1. Still, a smaller but present variation (4.9%) between the samples coming from different litters was observed along PC2.

These results indicate that the absence of RYR1 changes the global transcriptomic profile of the developing limb skeletal muscle and more specific, that it highly impacts the expression of the 318

DEGs identified in the MAs. Between-litter variability also influences the global transcriptomic profile of murine E18.5 limb skeletal muscles.

3.1.4 Validation of the MAs via qRT-PCR

In order to validate the results obtained by the MAs, the relative expression levels of 4 downregulated (*Trib1*, *c-Jun*, *c-Fos* and *Myl2*) and 3 upregulated (*Flcn*, *Bai3* and *Col19a1*) genes were analyzed via qRT-PCRs. These genes were randomly chosen to cover the whole spectrum of detected DEGs in respect to the direction (down- and upregulated) and FC magnitude (high or low FC). For both, the MA and qRT-PCR analyses, the FC of the control samples was set to 1. *Gapdh* was used as an endogenous control in the qRT-PCRs. The qRT-PCR results demonstrated that all tested genes exhibit the same direction of regulation (down- or upregulation) and similar FCs as detected in the MAs (Fig. 16) and thus, validated the results obtained by the MAs.

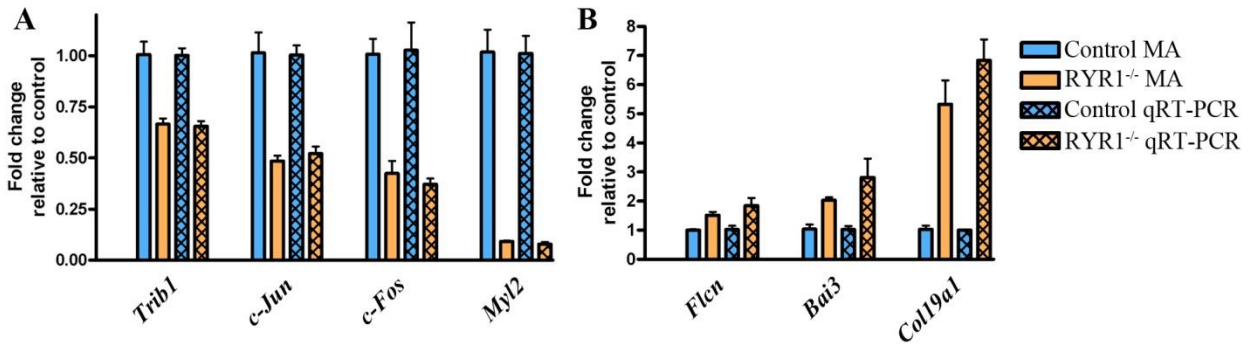

Fig. 18: Validation of the results obtained in the MA analysis via qRT-PCRs.
The expression level of **(A)** four downregulated DEGs: *Trib1* (FC -1.50), *c-Jun* (FC -2.07), *c-Fos* (FC -2.43), *Myl2* (FC -10.85); as well as **(B)** three upregulated DEGs: *Flcn* (FC 1.50), *Bai3* (FC 2.02), *Col19a1* (FC 5.13) were tested via qRT-PCRs. *Gapdh* was used as an endogenous control. The mean relative expression levels of the four control ($RYR1^{+/-}$) samples were set as FC = 1. The FC of each of the 4 biological replicates per group ($RYR1^{-/-}$ and control) were normalized to the mean FC of the control group. Error bars are S.E.M. Modified from (Filipova et al., 2016).

3.1.5 The DEGs with the highest FCs are related to muscle and ECM structure

Next, the ten DEGs with the highest positive and negative FCs in the $RYR1^{-/-}$ skeletal muscle were analyzed (Table 11). The strongest downregulation was observed for the genes encoding the cardiac slow myosin light chain 2 (*Myl2*, FC = -10.85) and smoothelin-like 1 (*Smtnl1*, FC = -9.68). Among the top 10 downregulated DEGs were also other genes encoding proteins associated with the structure and function of muscle and the the musculoskeletal system like– *Tppp3* (FC = -4.56), encoding a marker for tendon sheath and synovial joints differentiation (Staverosky, Pryce, Watson, & Schweitzer, 2009); *Irf6* (FC = -3.58), encoding a transcription factor (TF) involved in limb,

craniofacial and tongue development (Goudy et al., 2013; Ingraham et al., 2006); and *Cnn1* (FC = -3.25), encoding a marker for smooth muscle differentiation in late embryonic development (Duband, Gimona, Scatena, Sartore, & Small, 1993). The DEG showing the highest upregulation in the $RYR1^{-/-}$ samples was a collagen-coding gene (*Col25a1*, FC = 6.51). and the expression of another collagen-coding gene found in the top 10 most upregulated genes (*Col19a1*, FC = 5.11 and 5.13) has been demonstrated to diminish towards the final stages of differentiation of fetal limb skeletal muscle (Sumiyoshi, Laub, Yoshioka, & Ramirez, 2001). Other highly upregulated genes included the gene encoding myoglobin (*Mb*, FC = 4.75), controlled by hypoxia and Ca^{2+} signaling in skeletal muscle (Kanatous et al., 2009). Additionally, the gene encoding the RUNX1 TF (*Runx1*, FC = 3.94 and 4.08) known for its protective functions against muscle wasting, myofibrillar disorganization and autophagy in skeletal muscle (Wang et al., 2005) was highly upregulated as well.

Table 11. E18.5 $RYR1^{-/-}$ vs. $RYR^{+/-}$ – Top 10 DEGs.

Probe Set ID	Gene Title	Gene Symbol	FC
Downregulated genes			
1448394_at	myosin, light polypeptide 2, regulatory, cardiac, slow	Myl2	-10.85
1419145_at	smoothelin-like 1	Smtnl1	-9.68
1416713_at	tubulin polymerization-promoting protein family member 3	Tppp3	-4.56
1452766_at	tubulin polymerization promoting protein	Tppp	-3.91
1418395_at	solute carrier family 47, member 1	Slc47a1	-3.66
1418301_at	interferon regulatory factor 6	Irf6	-3.58
1418714_at	dual specificity phosphatase 8	Dusp8	-3.37
1418511_at	Dermatopontin	Dpt	-3.34
1455203_at	RIKEN cDNA A930003A15 gene	A930003A15Rik	-3.30
1417917_at	calponin 1	Cnn1	-3.25
Upregulated genes			
1438540_at	collagen, type XXV, alpha 1	Col25a1	6.51
1440085_at	ectodysplasin A2 receptor	Eda2r	5.73
1438059_at	cortexin 3	Ctxn3	5.23
1421698_a_at	collagen, type XIX, alpha 1	Col19a1	5.13
1456953_at	collagen, type XIX, alpha 1	Col19a1	5.11
1451203_at	myoglobin	Mb	4.75
1447807_s_at	pleckstrin homology domain containing, family H (with MyTH4 domain) member 1	Plekhh1	4.52
1422864_at	runt-related transcription factor 1	Runx1	4.08
1422865_at	runt-related transcription factor 1	Runx1	3.94
1418203_at	phorbol-12-myristate-13-acetate-induced protein 1	Pmaip1	3.69

The ten DEGs exhibiting the highest down- and upregulation in $RYR1^{-/-}$ fetal limb skeletal muscle. Modified from (Filipova et al., 2016).

3.1.6 Processes and pathways enriched with RYR1$^{-/-}$ specific DEGs

In order to gain a better understanding of the biological processes which were affected in the RYR1$^{-/-}$ skeletal muscle, the detected DEGs were subjected to a Gene Ontology enrichment analysis for Biological Process (GO BP, Fig. 19A). Interestingly, the most significantly enriched GO BP category was "Skeletal muscle cell differentiation". Other processes related to differentiation and development like "Oligodendrocyte differentiation", "Regulation of cell growth", "Glial cell differentiation" and "Regulation of endothelial cell proliferation" were also detected as being significantly enriched with DEGs. Two categories – "Response to oxygen levels" and "Response to decreased oxygen levels" suggested significant changes in the expression of genes related to oxygen metabolism in the RYR1$^{-/-}$ samples. Indications for changes in the expression of genes involved in the structure and composition of the ECM were represented by the presence of the GO BP categories "Extracellular matrix organization" and "Extracellular structure organization". Those were among the 10 most significantly affected biological processes in RYR1$^{-/-}$ samples.

Next, to assess which processes and signaling pathways were most significantly affected in the RYR1$^{-/-}$ skeletal muscle, the DEGs found in the RYR1$^{-/-}$ samples were used in enrichment analyses utilizing the KEGG (Fig. 19B), Reactome (Fig. 19C), and Panther (Fig. 19D) databases. These data bases resemble and are partly connected to the GO database, however their focus differs in respect to type of interactions, functional categories and analyzed organisms (Chowdhury & Sarkar, 2015).

The KEGG enrichment analysis indicated the „MAPK signaling pathway" as the most significantly represented with DEGs (Fig. 19B). The MAPK pathway was also among the 10 most significantly enriched categories in Reactome ("MAPK targets / Nuclear events mediated by MAP kinases") and Panther ("p38 MAPK pathway" and "Insulin / IGF pathway / MAP kinase cascade"). Other processes and pathways found multiple times as very significantly enriched in the different databases include processes related to muscle contraction (Reactome: "Muscle contraction" and "Striated muscle contraction"), oxidative stress (Panther: "Oxidative stress response" and GO BP categories "Response to oxygen levels" and "Response to decreased oxygen levels") and the ECM (KEGG: "Focal adhesion" and "ECM receptor interaction"; Reactome: "Extracellular matrix organization" and "Collagen formation").

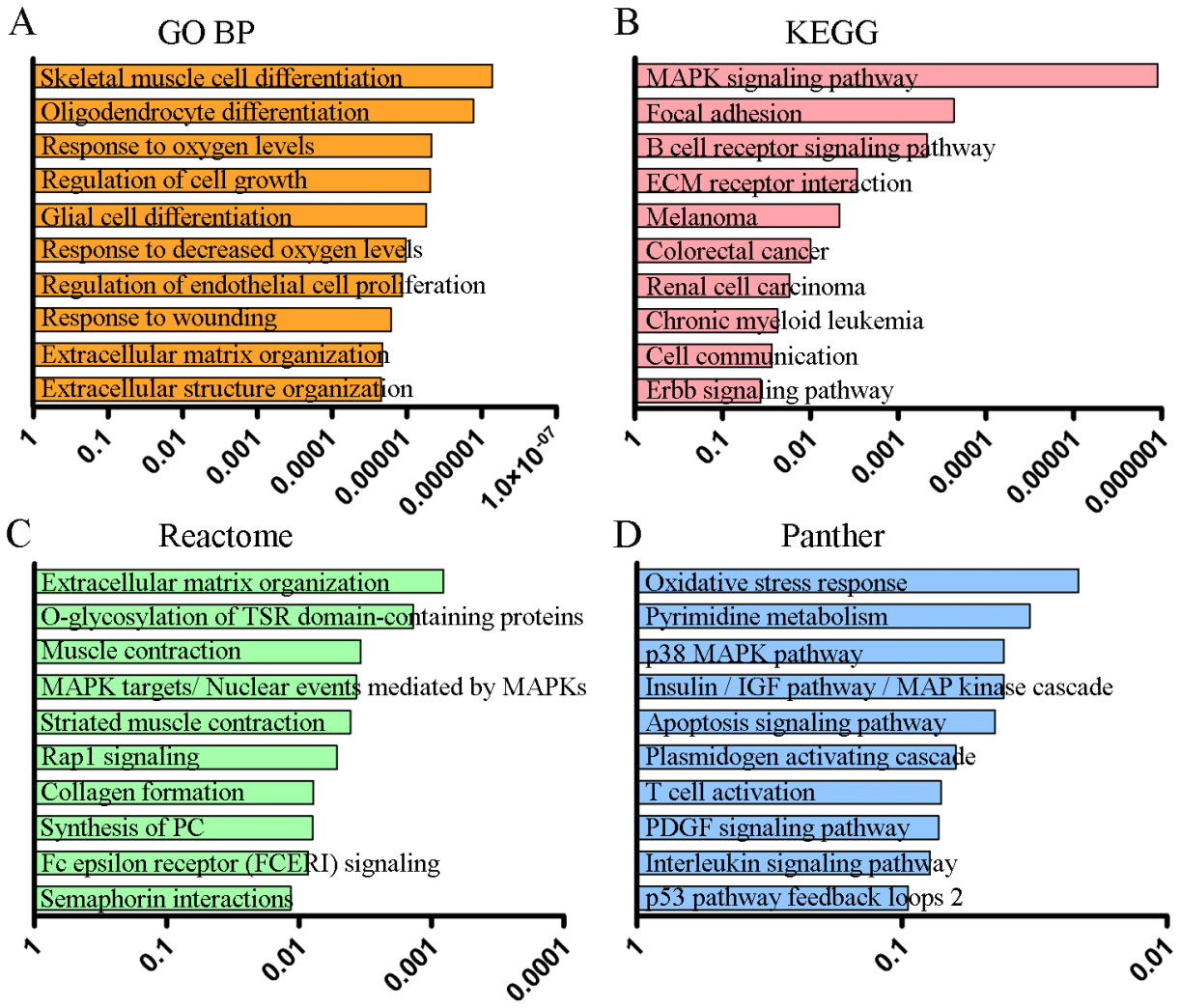

Fig. 19: Enrichment analysis of the DEGs detected in the RYR1$^{-/-}$ vs. RYR1$^{+/-}$ MAs.
The DEGs were subjected to an enrichment analysis using the GO BP **(A)**, KEGG **(B)**, Reactome **(C)** and Panther **(D)** databases using the Enrichr online gene list analysis tool (Chen et al., 2013; Kuleshov et al., 2016). P-value ranking was used in the analyses, represented by the bar length **(A – D)**. The values on the x-axis correspond to the measured P-values. Modified from (Filipova et al., 2016).

3.1.7 Signaling pathways enriched with DEGs in RYR1$^{-/-}$ skeletal muscle

The enrichment analyses of the DEGs found in RYR1$^{-/-}$ skeletal muscle at E18.5 (Fig. 19A-D) identified several affected major signaling pathways and networks that. In order to gain a deeper insight into the degree and the direction in which these signaling pathways were regulated, the DEGs encoding proteins and peptides involved in the MAPK, Wnt, PI3K/Akt/mTOR, G protein-coupled receptors (GPCRs) pathways and other TFs were closely examined (Table 12).

Table 12. E18.5 RYR1$^{-/-}$ vs. RYR$^{+/-}$ – DEGs involved in signaling pathways.

Probe Set ID	Gene Title	Gene Symbol	FC
MAPK signaling pathway			
1418714_at	dual specificity phosphatase 8	Dusp8	-3.37
1438933_x_at	RAS, guanyl releasing protein 2	Rasgrp2	-2.94
1419625_at	heat shock protein 1-like	Hspa1l	-2.81
1423100_at	FBJ osteosarcoma oncogene	Fos	-2.43
1448694_at	Jun oncogene	Jun	-2.07
1417164_at	dual specificity phosphatase 10	Dusp10	-2.06
1438883_at	fibroblast growth factor 5	Fgf5	-2.05
1427582_at	fibroblast growth factor 6	Fgf6	-2.03
1448830_at	dual specificity phosphatase 1	Dusp1	-1.95
1418401_a_at	dual specificity phosphatase 16	Dusp16	-1.76
1449117_at	Jun proto-oncogene related gene D	Jund	-1.75
1439205_at	nuclear factor of activated T cells, cytoplasmic, calcineurin dependent 2	Nfatc2	-1.64
1438030_at	RAS, guanyl releasing protein 3	Rasgrp3	-1.63
1449773_s_at	growth arrest and DNA-damage-inducible 45 beta	Gadd45b	-1.62
1435196_at	neurotrophic tyrosine kinase, receptor, type 2	Ntrk2	1.52
1421897_at	ELK1, member of ETS oncogene family	Elk1	1.56
1417856_at	avian reticuloendotheliosis viral (v-rel) oncogene related B	Relb	1.58
1421324_a_at	thymoma viral proto-oncogene 2	Akt2	1.65
1420895_at	transforming growth factor, beta receptor I	Tgfbr1	1.72
1440343_at	ribosomal protein S6 kinase, polypeptide 5	Rps6ka5	1.75
1436912_at	calcium channel, voltage-dependent, beta 4 subunit	Cacnb4	1.83
Wnt signaling pathway			
1449425_at	wingless-related MMTV integration site 2	Wnt2	-2.54
1423760_at	CD44 antigen	Cd44	-2.29
1451031_at	secreted frizzled-related protein 4	Sfrp4	-2.20
1418136_at	transforming growth factor beta-1-induced transcript 1	Tgfb1i1	-1.82
1427138_at	coiled-coil domain containing 88C	Ccdc88c	-1.80
1417985_at	Notch-regulated ankyrin repeat protein	Nrarp	-1.72
1455689_at	frizzled homolog 10 (Drosophila)	Fzd10	-1.56
1429506_at	naked cuticle 1 homolog (Drosophila)	Nkd1	1.53
1451689_a_at	SRY-box containing gene 10	Sox10	1.59
1460187_at	secreted frizzled-related protein 1	Sfrp1	2.36
PI3K/Akt/mTOR signaling pathway			
1451038_at	apelin	Apln	-1.96
1449022_at	nestin	Nes	-1.62
1421679_a_at	cyclin-dependent kinase inhibitor 1A (P21)	Cdkn1a	1.52
1421324_a_at	thymoma viral proto-oncogene 2	Akt2	1.65

Probe Set ID	Gene Title	Gene Symbol	FC
1425515_at	phosphatidylinositol 3-kinase, regulatory subunit, polypeptide 1 (p85 alpha)	Pik3r1	1.73
G protein-coupled signaling			
1444409_at	rabphilin 3A-like (without C2 domains)	Rph3al	-2.37
1417625_s_at	chemokine (C-X-C motif) receptor 7	Cxcr7	-2.18
1455466_at	G protein-coupled receptor 133	Gpr133	-2.10
1451038_at	apelin	Apln	-1.96
1440009_at	olfactory receptor 78	Olfr78	-1.81
1431326_a_at	tropomodulin 2	Tmod2	-1.68
1455689_at	frizzled homolog 10 (Drosophila)	Fzd10	-1.56
1418394_a_at	CD97 antigen	Cd97	-1.56
1420940_x_at	regulator of G-protein signaling 5	Rgs5	-1.54
1417327_at	caveolin 2	Cav2	-1.53
1416286_at	regulator of G-protein signaling 4	Rgs4	-1.50
1460440_at	latrophilin 3	Lphn3	1.62
1451411_at	G protein-coupled receptor, family C, group 5, member B	Gprc5b	1.63
1456833_at	G protein-coupled receptor 17	Gpr17	1.68
1442082_at	complement component 3a receptor 1	C3ar1	1.81
1436912_at	calcium channel, voltage-dependent, beta 4 subunit	Cacnb4	1.83
1420401_a_at	receptor (calcitonin) activity modifying protein 3	Ramp3	1.86
1454782_at	brain-specific angiogenesis inhibitor 3	Bai3	2.02
1434172_at	cannabinoid receptor 1 (brain)	Cnr1	2.11
1432466_a_at	apolipoprotein E	Apoe	2.17
1460123_at	G protein-coupled receptor 1	Gpr1	2.37
1450875_at	G protein-coupled receptor 37	Gpr37	2.54
1436889_at	gamma-aminobutyric acid (GABA) A receptor, subunit alpha 1	Gabra1	2.54
Other transcription factors and transcriptional modulators			
1455267_at	estrogen-related receptor gamma	Esrrg	-3.04
1449363_at	activating transcription factor 3	Atf3	-2.58
1418572_x_at	tumor necrosis factor receptor superfamily, member 12a	Tnfrsf12a	-2.39
1418762_at	CD55 antigen	Cd55	-2.14
1425518_at	Rap guanine nucleotide exchange factor (GEF) 4	Rapgef4	-1.73
1422742_at	human immunodeficiency virus type I enhancer binding protein 1	Hivep1	-1.72
1420696_at	sema domain, immunoglobulin domain (Ig), short basic domain, secreted, (semaphorin) 3C	Sema3c	-1.68
1456796_at	snail homolog 3 (Drosophila)	Snai3	-1.66
1418936_at	v-maf musculoaponeurotic fibrosarcoma oncogene family, protein F (avian)	Maff	-1.61
1451932_a_at	ADAMTS-like 4	Adamtsl4	-1.58
1425896_a_at	fibrillin 1	Fbn1	-1.57
1418394_a_at	CD97 antigen	Cd97	-1.56

Probe Set ID	Gene Title	Gene Symbol	FC
1459372_at	neuronal PAS domain protein 4	Npas4	-1.51
1424880_at	tribbles homolog 1 (Drosophila)	Trib1	-1.50
1428983_at	scleraxis	Scx	1.53
1429841_at	multiple EGF-like-domains 10	Megf10	1.53
1422210_at	forkhead box D3	Foxd3	1.57
1441107_at	doublesex and mab-3 related transcription factor like family A2	Dmrta2	1.58
1435775_at	circadian locomotor output cycles kaput	Clock	1.60
1457342_at	IKAROS family zinc finger 4	Ikzf4	1.60
1452650_at	tripartite motif-containing 62	Trim62	1.61
1449164_at	CD68 antigen	Cd68	1.61
1452021_a_at	hairy and enhancer of split 6	Hes6	1.66
1434458_at	follistatin	Fst	1.93
1450042_at	aristaless related homeobox	Arx	2.18
1454693_at	histone deacetylase 4	Hdac4	2.36
1418937_at	deiodinase, iodothyronine, type II	Dio2	2.87
1422864_at	runt related transcription factor 1	Runx1	4.08
1440085_at	ectodysplasin A2 receptor	Eda2r	5.73

DEGs in RYR1$^{-/-}$ skeletal muscle involved in the MAPK, Wnt, PI3K/mTor, GPCR and other signaling pathways. Downregulated DEGs are highlighted in blue and upregulated DEGs – in orange. Modified from (Filipova et al., 2016).

The MAPK pathway, identified as one of the most significantly affected pathways in all four enrichment analyses (GO, KEGG, Reactome and Panther, Fig. 19), was represented by 21 DEGs, 14 of which were negatively and 7 were positively regulated (Fig. 20). The observed DEGs encode proteins from the MAPK/ERK and the p38/JNK pathways. Interestingly, the majority of the downregulated DEGs encode proteins that are involved in the late and final steps of the pathway, like the calcineurin-dependent nuclear factor of activated T cells 2 (*Nfatc2*), the Jun oncogene (*c-Jun*), the FBJ osteosarcoma oncogene (*c-Fos*), and the Jun proto-oncogene-related gene D (*Jund*). The products of these genes are global TFs involved in the regulation and modulation of multiple physiological cellular processes like differentiation, proliferation, programmed cell death and inflammation. The products of *c-Fos*, *c-Jun* and *JunD* can exert their regulatory functions alone or after dimerization with one another participating in the composition of the activating protein 1 (AP-1). AP-1 is a pleiotropic TF that is involved, among other things, in muscle cell differentiation and during pathological alternations – in muscle wasting (Andreucci et al., 2002; Moore-Carrasco et al., 2006). On the other hand, three upregulated DEGs from the MAPK pathway encoded cell surface receptor proteins – the beta 4 subunit of voltage-dependent calcium channels (*Cacnb4*), the neurotrophic tyrosine kinase receptor type 2 (*Ntrk2*), and the transforming growth factor beta

receptor I (*Tgfbr1*). A downregulation was observed for four dual specificity phosphatase transcripts (*Dusp1, Dusp8, Dusp10 and Dusp16*), and one heat shock protein (*Hspa1l*) gene, all of which inactivate ERK, JNK or p38.

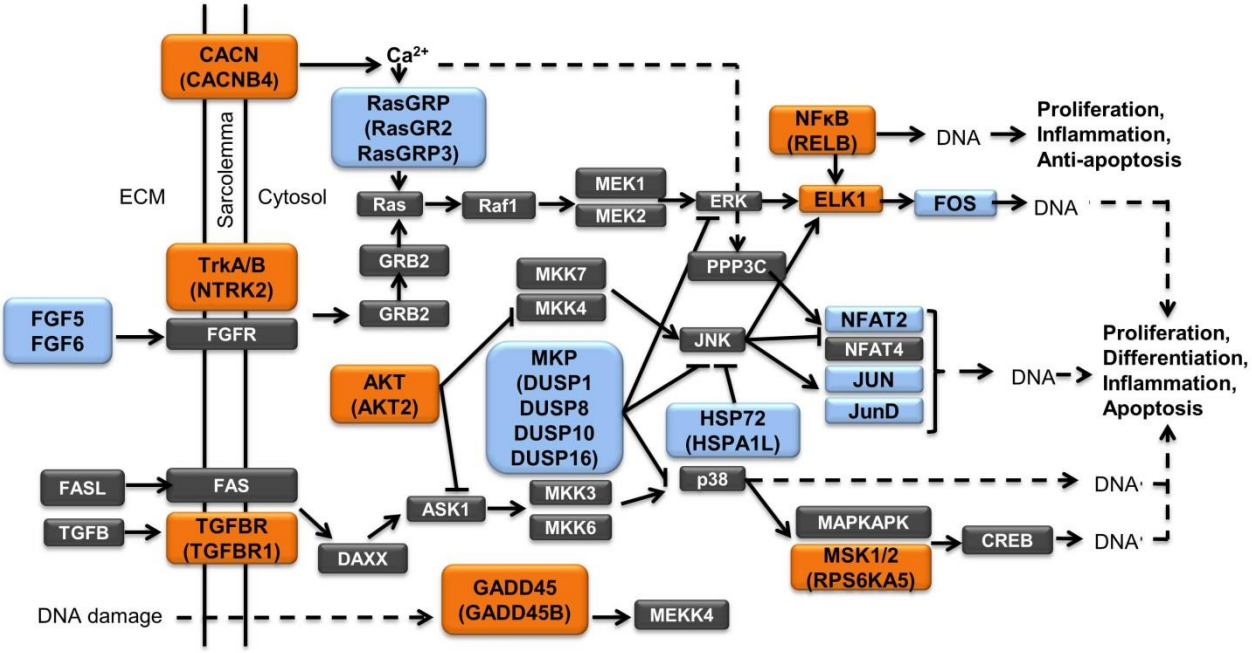

Fig. 20: DEGs in the MAPK pathway.
A simplified schematic representation of the MAPK pathway in KEGG pathways. The proteins encoded by downregulated DEGs are shown as blue boxes, the ones encoded by upregulated DEGs – as orange boxes, and those proteins for which no change in expression was detected – by grey boxes. If multiple genes encoding proteins from the same category or protein subunits were detected as differentially expressed, these genes are shown in brackets in the respective boxes. Solid lines stand for direct and broken lines – for indirect interactions. Arrowhead ends indicate activation and blunt ends represent inhibition.

Furthermore, among the DEGs related to signaling processes, several altered genes encoded key proteins connecting the MAPK cascade to other signaling pathways. For example, the upregulated thymoma viral proto-oncogene 2 (*Akt2*) encodes a central member of the PI3K/Akt/mTOR pathway, a pathway regulating skeletal muscle hypertrophy (Bodine et al., 2001). Other DEGs from this pathway included the Akt's activator p85 alpha regulatory subunit of the phosphatidylinositol 3-kinase (Pik3r1) and a Akt's target, the gene encoding the cyclin-dependent kinase inhibitor 1A (P21) (Cdkn1a). All three (*Akt2*, *Pik3r1* and *Cdkn1a*) were upregulated in RYR1$^{-/-}$ samples. Annother major signaling pathway in muscle development, the Wnt pathway, was represented by 10 DEGs, 7 of wich were downregulated, including the wingless-related MMTV integration site 2 (Wnt2), secreted frizzled-related protein 4 (Sfrp4) and the induced transcript 1 of transforming growth factor

beta 1 (Tgfb1i1). Three DEGs from the Wnt pathways were upregulated, on e of which – the secreted frizzled-related protein 1 (Sfrp1), inhibits myoblast fusion (Descamps et al., 2008).

Other DEGs encode GPCRs or modulators of GPCR-mediated signaling, as well as various TFs, revealing a complex and entangled network of expression changes influencing the majority of the cellular signaling pathways in the RYR1$^{-/-}$ skeletal muscle.

3.1.8 DEGs in processes related to muscle function and structure

The enrichment analyses of the DEGs found in the RYR1$^{-/-}$ samples revealed multiple processes and pathways related to muscle structure, functions and development (Fig. 19A-D). Changes in these processes are of special interest in the frame of this project, since they can directly infer which physiological parameters of the skeletal muscle organ are most likely affected by the absence of RYR1, the RYR1-mediated Ca^{2+} release and the resulting excitation-contraction uncoupling. Therefore, the entire set of DEGs identified in the MAs was subjected to additional enrichment analyses using the David GO and MGI GO databases (Huang da et al., 2009; Smith et al., 2014), as well as to manual data mining in order to assess which and how many DEGs were directly connected to skeletal muscle. The results were sorted in two main groups – muscle contraction and mechanical force generation, and muscle structure and morphogenesis (Table 13), although many DEGs contribute to both categories. Multiple genes involved in muscle contraction, additionally take part in the structure of the sarcomeres. The majority of them were systematically downregulated, especially genes coding myosin light chain isoforms (*Myl2*, *Myl3*, Myl9) and coding Z-disc and costamere proteins (*Ankrd1*, *Krt8*, *Nrap*, *Csrp3*, *Pdlim1*, *Fhl1*, *Crip1*). Only one DEG involved in the sarcomere structure was mildly upregulated – *Tnnt2* (FC = 1.59), coding for a troponin T isoform. The expression of the *Dbndd1* gene, encoding a protein participating in the costamere structure, was also slightly higher in the RYR1$^{-/-}$ samples (FC = 1.75). Some of the detected DEGs encode protein isoforms that are described as typically expressed not in skeletal, but rather in cardiac muscle. However, during embryonic and fetal development many such genes, like for example the genes encoding the myosin light chain and actin isoforms, are expressed in skeletal, cardiac and smooth muscle and their specific expression pattern is laid later during the postnatal development (Takano-Ohmuro, Obinata, Kawashima, Masaki, & Tanaka, 1985; Woodcockmitchell et al., 1988).

The transcription levels of multiple genes related to focal adhesion, ECM structure and organization, collagen matrix formation and ECM-receptor interactions were also changed in the RYR1$^{-/-}$ samples.

Since these processes are also intimately connected to the function and morphogenesis of the skeletal muscle organ, the detected DEGs were analyzed and listed under "Muscle morphogenesis" (Table 13). A total of 22 such DEGs were identified, 14 of which were downregulated and 8 – upregulated. A strong upregulation was observed for two collagen genes – *Col19a1* and *Col25a1* – both associated with the development of the skeletal muscle organ.

Table 13. DEGs in RYR1$^{-/-}$ skeletal muscle involved in muscle contraction, structure and morphogenesis.

Probe Set ID	Gene Title	Gene Symbol	Fold Change	Localization / Function / Reference
Muscle contraction and mechanical force				
1448394_at	myosin, light polypeptide 2, regulatory, cardiac, slow	Myl2	-10.85	Sarcomere; part of myosin filaments (Sheikh, Lyon, & Chen, 2015) (Schiaffino, Rossi, Smerdu, Leinwand, & Reggiani, 2015)
1419145_at	smoothelin-like 1	Smtnl1	-9.68	Sarcomere; binds calmodulin and tropomyosin (Ulke-Lemee, Ishida, Chappellaz, Vogel, & MacDonald, 2014)
1417917_at	calponin 1	Cnn1	-3.25	Sarcomere; binds tropomyosin and inhibits cross-bridge cycle in a Ca^{2+}-dependent manner (Winder, Walsh, Vasulka, & Johnson, 1993)
1449996_a_at	tropomyosin 3, gamma	Tpm3	-3.24	Sarcomere; actin filament associated; increases contractility and decreases Ca^{2+}-sensitivity (Pieples et al., 2002)
1420991_at	ankyrin repeat domain 1 (cardiac muscle)	Ankrd1	-2.99	Sarcomere; Z-disc, Part of titin-N2A mechanosensory complex (Miller et al., 2003)
1427768_s_at	myosin, light polypeptide 3	Myl3	-2.93	Sarcomere; part of myosin filaments (Schiaffino et al., 2015)
1439204_at	sodium channel, voltage-gated, type III, alpha	Scn3a	-2.93	Sarcolemma; Na^{+} channel; binds to CaM, and is regulated by CaM and Ca^{2+} (Lee-Kwon, Goo, Zhang, Silldorff, & Pallone, 2007); regulates ECC (Aronsen, Swift, & Sejersted, 2013)
1452670_at	myosin, light polypeptide 9, regulatory	Myl9	-2.65	Involved in actomyosin contractility and stress fiber assembly (Licht et al., 2010)
1420647_a_at	keratin 8	Krt8	-2.58	Sacomere; Z-disc and M-line domains, at costameres, at the sarcolemmal membrane (Ursitti et al., 2004)
1421253_at	nebulin-related anchoring protein	Nrap	-2.41	Sarcomere; Z-disc; terminal actin binding (Luo, Herrera, & Horowits, 1999)
1460318_at	cysteine and glycine-rich protein 3	Csrp3	-2.37	Sarcomere; Z-disc (Knoll, Buyandelger, & Lab, 2011)

Probe Set ID	Gene Title	Gene Symbol	Fold Change	Localization / Function / Reference
1416554_at	PDZ and LIM domain 1 (elfin)	Pdlim1	-2.31	Sarcomere; Z-disc; Interaction with α-actinin (Knoll et al., 2011)
1435767_at	sodium channel, voltage-gated, type III, beta	Scn3b	-2.23	Sarcolemma; Na^+ channel; regulates ECC (Aronsen et al., 2013)
1417872_at	four and a half LIM domains 1	Fhl1	-1.94	Sarcomere; Z-disc (Knoll et al., 2011)
1416326_at	cysteine-rich protein 1 (intestinal)	Crip1	-1.76	Sarcomere; Z-disc; Interaction with α-actinin (Knoll et al., 2011)
1422635_at	acetylcholinesterase	Ache	-1.71	Neuromuscular junctions; Regulation of ECC (Quinn, 1987)
1450650_at	myosin X	Myo10	1.57	Link between integrins and cytoskeleton (Marotta et al., 2009)
1424967_x_at	troponin T2, cardiac	Tnnt2	1.59	Sarcomere; interaction with tropomyosin of actin filaments
1449307_at	dysbindin (dystrobrevin binding protein 1) domain containing 1	Dbndd1	1.75	Costamere; part of dystrophin-glycoprotein complex (DGC) (Hijikata et al., 2008)
1436912_at	calcium channel, voltage-dependent, beta 4 subunit	Cacnb4	1.83	Sarcolemma; couples electrical activity to gene expression (Tadmouri et al., 2012)
1418852_at	cholinergic receptor, nicotinic, alpha polypeptide 1 (muscle)	Chrna1	2.28	Neuromuscular junctions; muscle excitation (Beeson, Jeremiah, West, Povey, & Newsom-Davis, 1990)
Muscle structure and morphogenesis				
1418511_at	dermatopontin	Dpt	-3.34	Cell-matrix adhesion (Okamoto & Fujiwara, 2006)
1449082_at	microfibrillar associated protein 5	Mfap5	-3.13	ECM; glycoprotein associated with microfibrils like elastin (Llano-Diez, Gustafson, Olsson, Goransson, & Larsson, 2011)
1450798_at	tenascin XB	Tnxb	-2.85	ECM; collagen formation (Voermans, Gerrits, van Engelen, & de Haan, 2014)
1456344_at	tenascin C	Tnc	-2.63	ECM; glycoprotein; interaction with fibronectin (Mackey et al., 2011)
1416697_at	dipeptidylpeptidase 4	Dpp4	-2.25	Cell surface peptidase; cell-cell connections (Lambeir, Durinx, Scharpe, & De Meester, 2003)
1424701_at	protocadherin 20	Pcdh20	-2.35	Transmembrane protein; cell-cell connections (Suzuki, 2000)
1423760_at	CD44 antigen	Cd44	-2.29	Cell surface glycoprotein; migration and myoblast fusion (Mylona, Jones, Mills, & Pavlath, 2006)
1449388_at	thrombospondin 4	Thbs4	-2.14	ECM glycoprotein; Ca^{2+} binding (Greco et al., 2010)
1426529_a_at	transgelin 2	Tagln2	-1.93	Cytoskeleton; Actin-gelling protein (Shapland, Hsuan, Totty,

Probe Set ID	Gene Title	Gene Symbol	Fold Change	Localization / Function / Reference
				& Lawson, 1993)
1437218_at	fibronectin 1	Fn1	-1.74	ECM glycoprotein; cell adhesion; regulation of fiber organization (Snow, Peterson, Khalil, & Henry, 2008)
1434928_at	growth arrest-specific 2 like 1	Gas2l1	-1.72	Cytoskeleton; Crosslinking of microfilaments and microtubules (Goriounov, Leung, & Liem, 2003)
1449022_at	nestin	Nes	-1.62	Cytoskeleton; intermediate filament, co-localized with desmin in Z-disc of embryonic skeletal muscle (Sejersen & Lendahl, 1993)
1451932_a_at	ADAMTS-like 4	Adamtsl4	-1.58	ECM; glycoprotein; microfibril biogenesis (Gabriel et al., 2012)
1425896_a_at	fibrillin 1	Fbn1	-1.57	ECM glycoprotein; microfibril biogenesis (Gabriel et al., 2012)
1436425_at	KN motif and ankyrin repeat domains 4	Kank4	1.56	Control of actin polymerization (Zhu, Kakinuma, Wang, & Kiyama, 2008)
1434709_at	neuron-glia-CAM-related cell adhesion molecule	Nrcam	1.64	Transmembrane cell adhesion protein; axon guidance (Kostrominova, Dow, Dennis, Miller, & Faulkner, 2005)
1418204_s_at	allograft inflammatory factor 1	Aif1	1.68	Actin-polymerizing protein (Autieri, Kelemen, & Wendt, 2003)
1419050_at	transmembrane protein 8C	Tmem8c	1.74	Transmembrane cell surface protein; myoblast fusion (Millay et al., 2013)
1429861_at	protocadherin 9	Pcdh9	1.90	Transmembrane protein; Ca^{2+} - dependent cell-cell communication (Wang et al., 2012)
1418139_at	doublecortin	Dcx	2.03	Marker for Pax7+MyoD− subpopulation contributing to myofiber maturation during muscle regeneration (Ogawa et al., 2015)
1456953_at	collagen, type XIX, alpha 1	Col19a1	5.11	ECM; expressed during muscle development (Sumiyoshi et al., 2001)
1438540_at	collagen, type XXV, alpha 1	Col25a1	6.51	ECM; branching of axon bundles within the muscle (Tanaka et al., 2014)

Downregulated DEGs are highlighted in blue and upregulated DEGs – in orange. Modified from (Filipova et al., 2016).

3.1.9 Elevated mRNA levels of several MRFs

The complex multistep skeletal myogenic program is regulated by a variety of extrinsic and intrinsic signals (Bentzinger et al., 2012). Eight TFs transmit some of the most potent intrinsic signals in the

progression of the skeletal myogenesis and thus constitute canonical myogenic regulatory factors (MRFs). These MRFs are encoded by the genes *Six1*, *Six4*, *Pax3*, *Pax7*, *Myf5 MyoD*, *MyoG* and *Mrf4*, each expressed in a particular cell population from the myogenic lineage. Their spatiotemporal expression patterns safeguards and reflects the proper developmental transitions during myogenesis (Bentzinger et al., 2012; Goulding, Chalepakis, Deutsch, Erselius, & Gruss, 1991; Grifone et al., 2005; Jostes, Walther, & Gruss, 1990; Pownall, Gustafsson, & Emerson, 2002; Sassoon et al., 1989) (Fig. 21A). The MAs detected no significant changes in the expression for any of these genes (FC ≥ ± 1.5, FDR-adjusted P-value ≤ 0.05), although there were indications for a putative tendencies for some of them: *Six4* (FC = 1.38, P = 0.0027), *Pax7* (FC = 1.27, P = 0.0074), *Myf5* (FC = 1.25, P = 0.04), *MyoD* (FC = 1.53, P = 0.0018) and *MyoG* (FC = 1.46, P = 0.0001). Because of the eminent importance of these MRFs for muscle development, their mRNA levels in the $RYR1^{-/-}$ and $RYR1^{+/-}$ samples were more precisely examined via qRT-PCRs (Fig. 21B). Significant ($p \leq 0.05$) upregulation in $RYR1^{-/-}$ vs. $RYR1^{+/-}$ samples was observed for *Six1*, *Six4*, *Pax7*, *MyoD*, *MyoG* and *Mrf4* (Table 14). These increases in the MRFs expression levels, that are physiologically downregulated in differentiated myofibers, indicate a delay in $RYR1^{-/-}$ skeletal myogenesis.

Table 14. MRFs expression levels.

	Microarray analyses			**qRT-PCR analyses**		
Gene	FC	S.E.M.	P-value	FC	S.E.M.	P-value
Six1	1.04	± 0.05	0.717	1.27	± 0.07	0.014
Six4	1.38	± 0.09	0.003**	1.66	± 0.19	0.014*
Pax3	0.93	± 0.02	0.165	0.69	± 0.19	0.234
Pax7	1.27	± 0.02	0.007**	1.57	± 0.18	0.018*
Myf5	1.25	± 0.04	0.040*	1.40	± 0.23	0.139
MyoD	1.53	± 0.08	0.002**	2.39	± 0.30	0.005**
MyoG	1.46	± 0.05	0.0001***	1.97	± 0.18	0.002**
Mrf4	1.38	± 0.18	0.217	1.50	± 0.19	0.034*

Comparison of MAs and qRT-PCR analysis. FC, S.E.M. and P-value (from unpaired t-tests) of the examined MRFs found in the $RYR1^{-/-}$ samples in the MAs and in the qRT-PCR analyses. FC values are relative to the expression in control samples. * represents a P-value ≤ 0.05, ** represents a P-value ≤ 0.01 and *** represents a P-value ≤ 0.001.

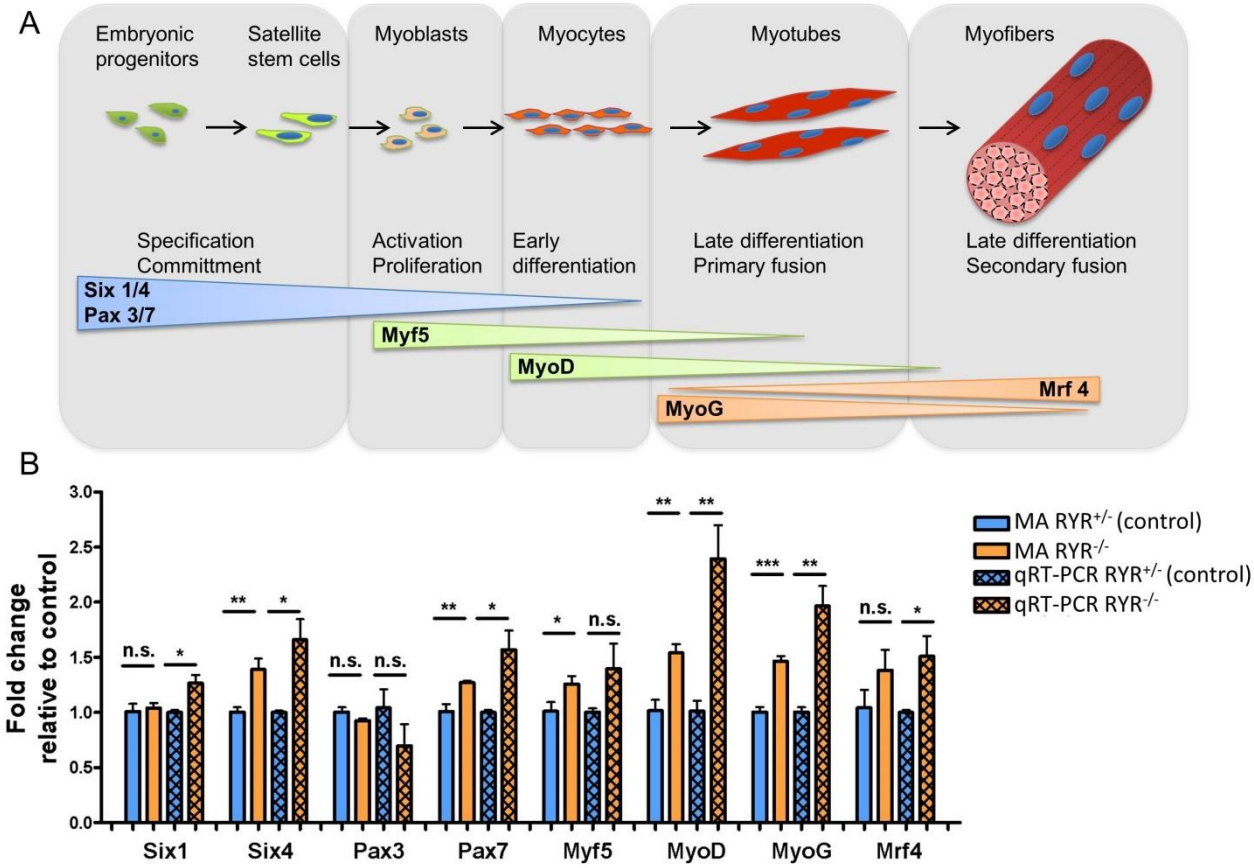

Fig. 21: MRFs expression during myogenesis.
(A) Progression of the skeletal myogenic lineage throughout myogenesis and expression levels of the MRFs *Six1*, *Six4*, *Pax3*, *Pax7*, *Myf5*, *MyoD*, *MyoG* and *Mrf4* (modified from (Bentzinger et al., 2012)). **(B)** Expression levels of the MRFs shown in (A) in RYR1$^{-/-}$ skeletal muscle measured as FC of the respective MRF mRNA levels in RYR1$^{+/-}$ (control) skeletal muscle samples. Four biological replicates (n = 4) were tested in each group. Hollow bars represent the results from the MAs and crossed bars represent the results of the qRT-PCRs using the *Gapdh* transcript as endogenous control. For each gene the FCs were normalized to the mean FC of the control group, thus each RYR1$^{+/-}$ control group (in MAs and qRT-PCRs) has a mean FC = 1. Unpaired t-tests were performed for RYR1$^{-/-}$ vs. control for each gene, * represents a P-value ≤ 0.05, ** represents a P-value ≤ 0.01 and *** represents a P-value ≤ 0.001. Error bars are S.E.M.

3.2 Part II: Analysis of the embryonic (E14.5) and fetal (E18.5) skeletal muscle lacking RYR1 or $Ca_v1.1$

The second part of this thesis analyzes the changes occurring in the developing murine limb skeletal muscle in the absence of either RYR1 or $Ca_v1.1$. Precisely, the end of the embryonic marking the beginning of fetal development (E14.5) and the end of fetal development shortly before birth (E18.5) were analyzed and compared. The limb skeletal muscle morphology, developmental markers, and global gene expression were closely examined and evaluated. At both time points – E14.5 and E18.5 – WT ($^{+/+}$), heterozygous ($^{+/-}$) and homozygous ($^{-/-}$) mutant animals from the RYR1 and $Ca_v1.1$ mouse model were examined. Thus, the physiological changes in limb skeletal muscle morphology and gene expression during fetal development were compared to those in the absence of $RYR1^{-/-}$ and $Ca_v1.1^{-/-}$ limb skeletal muscle. The main findings of this part of the results were reported in (Filipova et al., 2018).

3.2.1 Gross morphology of WT, $RYR1^{+/-}$, $RYR1^{-/-}$, $Ca_v1.1^{+/-}$ and $Ca_v1.1^{-/-}$ fetuses at E14.5 and E18.5

First, the gross morphological appearance of entire mouse fetuses was analyzed at embryonic days E14.5 and E18.5. For this analysis whole embryos preparations were performed with 3 littermates from each genotype, $RYR1^{+/+}$ (WT), $RYR1^{+/-}$ and $RYR1^{-/-}$, as well as $Ca_v1.1^{+/+}$ (WT), $Ca_v1.1^{+/-}$ and $Ca_v1.1^{-/-}$ (Fig. 22). At E14.5, no apparent macroscopic differences in the morphology were observed between the WT, heterozygous ($^{+/-}$) and homozygous ($^{-/-}$) mutants. At E18.5 the heterozygous $RYR1^{+/-}$ and $Ca_v1.1^{+/-}$ mutants were undistinguishable from their WT littermates which is in accordance with previously reports (Pai, 1965a; Takeshima et al., 1994) and the results described in the previous Results part. In contrast, homozygous $RYR1^{-/-}$ and $Ca_v1.1^{-/-}$ mutants exhibited severe morphological changes comprising a characteristic spinal curvature, smaller limbs and enlarged necks, as well as a smaller body size (Fig. 22).

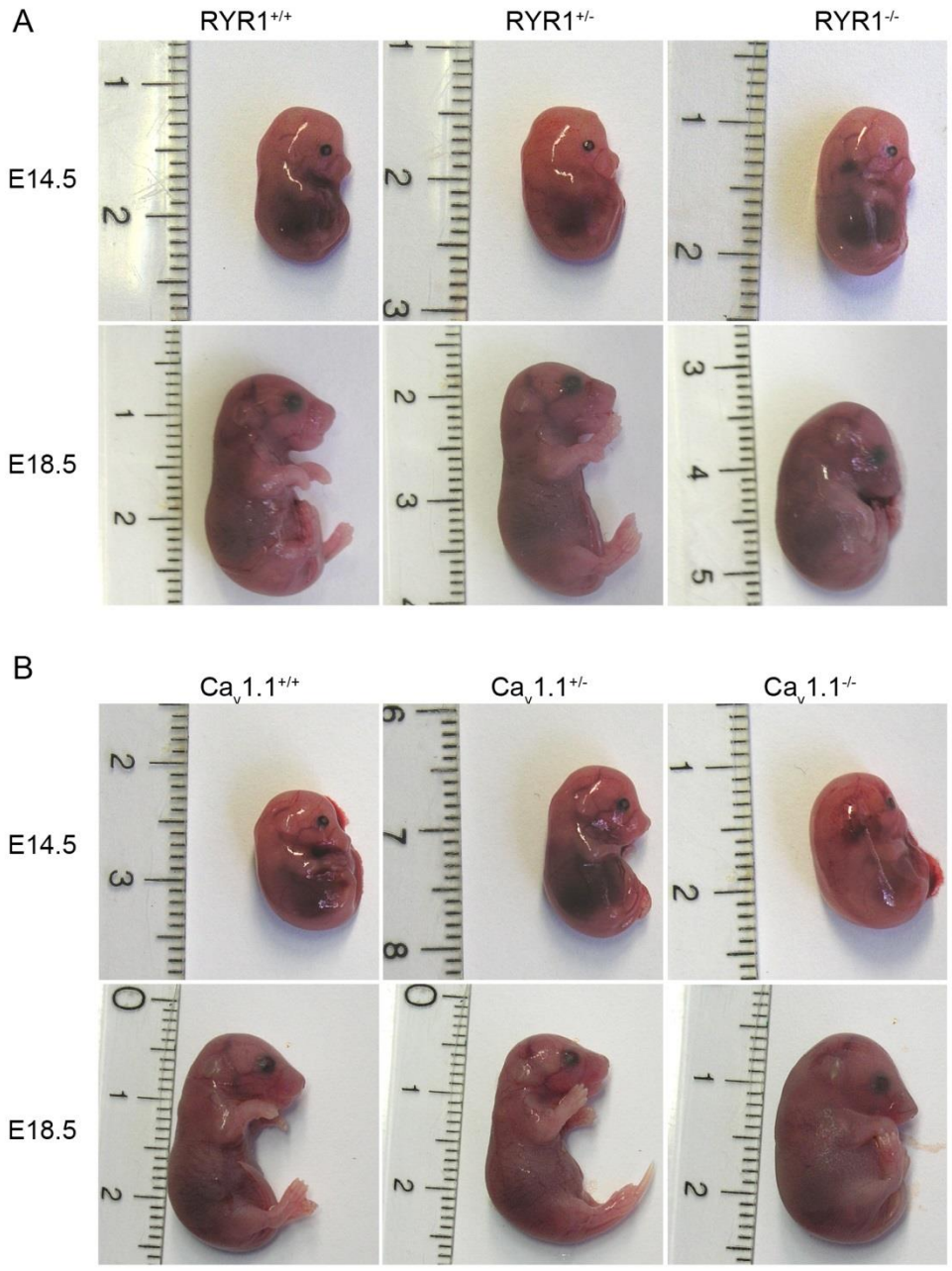

Fig. 22: Gross fetal morphological appearance at E14.5 and E18.5.
Whole mouse fetuses were photographed at E14.5 and E18.5. Three littermates from each genotype **(A)** $RYR1^{+/+}$ (WT), $RYR1^{+/-}$ and $RYR1^{-/-}$; as well as **(B)** $Ca_v1.1^{+/+}$ (WT), $Ca_v1.1^{+/-}$ and $Ca_v1.1^{-/-}$ were analyzed. Representative photographs are shown. Modified from (Filipova et al., 2018).

3.2.2 Histological alterations in RYR1$^{-/-}$, Ca$_v$1.1$^{+/-}$ and Ca$_v$1.1$^{-/-}$ fetuses at E14.5 and E18.5

In order to examine the structure and composition of the limb skeletal muscle at E14.5 and E18.5 in more detail, histological cross sections from the hind limbs of WT, heterozygous ($^{+/-}$), and homozygous ($^{-/-}$) RYR1 and Ca$_v$1.1 mouse fetuses were analyzed. At E14.5, fascicle formation was already initiated in WT muscles (Fig. 23A, B), the predominant cell type was myotubes but some primary muscle fibers were detectable. As expected, the RYR1$^{+/-}$ muscle morphology closely resembled that of WT fetuses (Fig. 23D, E), whereas the hind limb muscles of homozygous RYR1$^{-/-}$ mutants were characterized by multiple unorganized myotubes and only few, individual muscle fibers with small fiber caliber (Fig. 23G, H). No indication of any organization of muscle fascicles in the RYR1$^{-/-}$ muscles was detectable. Similar morphological alterations were found in muscles from Ca$_v$1.1$^{-/-}$ animals at E14.5 (Fig. 23M, N). However, while the muscles of heterozygous RYR1$^{+/-}$ animals were morphologically identical to those of the WT fetuses, the muscles of heterozygous Ca$_v$1.1$^{+/-}$ animals exhibited similar but less severe disorganization of the muscle fascicles as Ca$_v$1.1$^{-/-}$ animals (Fig. 23J, K). Thus, the most severe phenotype was observed in homozygous Ca$_v$1.1$^{-/-}$ fetuses, with skeletal muscles consisting almost exclusively of small caliber myotubes and myoblasts while mature muscle fibers were virtually absent (Fig. 23M, N). Additionally, only in Ca$_v$1.1$^{-/-}$ skeletal muscle there was an indication for ongoing apoptosis, revealed by a positive nuclear activated caspase-3 staining in a small fraction of myotubes (Fig. 23O, arrows), which was absent in the other fetuses.

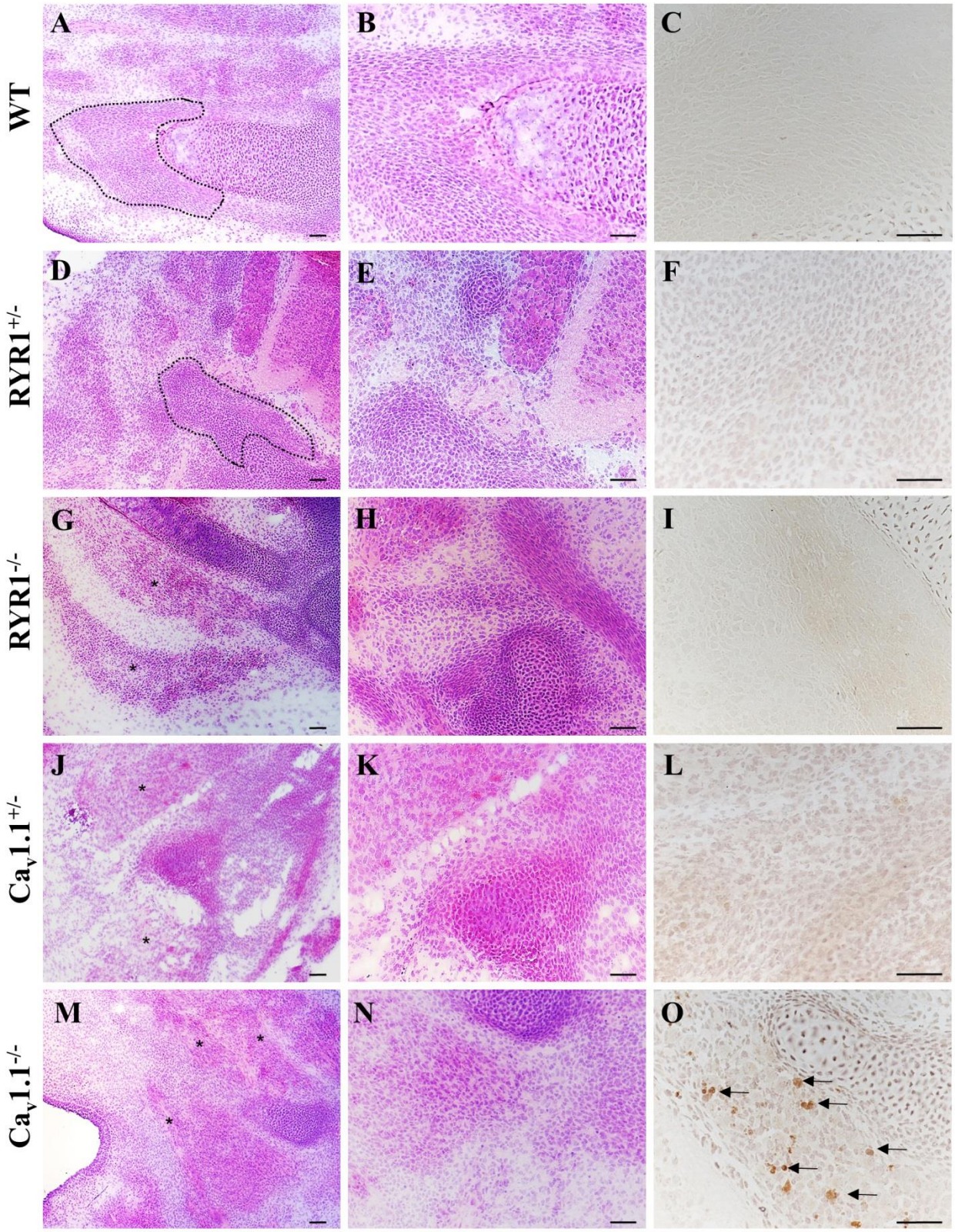

Fig. 23: Histological cross sections of mouse hind limb skeletal muscle at E14.5.
Cross sections of the lower hind limb of a WT fetus **(A-C)**, a $RYR1^{+/-}$ fetus **(D-F)**, a $RYR1^{-/-}$ fetus **(G-I)**, a $Ca_v1.1^{+/-}$ fetus **(J-L)**, and a $Ca_v1.1^{-/-}$ fetus **(M-O)** at E14.5, respectively.

At E14.5, the skeletal muscle of the WT fetus **(A, B)** and RYR1$^{+/-}$ fetus **(D, E**) already exhibited muscle fascicles (surrounded by dotted line) comprised of primary muscle fibers with almost no myoblasts. In contrast, the skeletal muscle of the RYR1$^{-/-}$ **(G, H)**, $Ca_v1.1^{+/-}$ **(J, K)**, and $Ca_v1.1^{-/-}$ **(M, N)** fetuses had either disorganized (asterisks) or completely lacking muscle fascicles and contained numerous myoblasts. Immunohistochemistry with anti-activated caspase-3 revealed prominent apoptosis only in nuclei of the myotubes of a $Ca_v1.1^{-/-}$ fetus **(O, arrows)**. H&E staining **(A, B, D, E, G, H, J, K, M, and N)**; original magnification x100 **(A, D, G, J, M)** and x200 **(B, E, H, K, N)**. Immunohistochemistry **(C, F, I, L, O)** with rabbit anti-mouse activated caspase-3 (clone C92-605; BD Biosciences) and slight counterstaining with hemalum; original magnification x400. Scale bars correspond to 100 µm in all microphotographs. Micrographs were taken by PD Dr. Anna Brunn. Modified from (Filipova et al., 2018).

At E18.5, WT and RYR1$^{+/-}$ muscles exhibited a normal development and consisted almost entirely of differentiated muscle fibers organized in fascicles (Fig. 24A-F), whereas the RYR1$^{-/-}$ skeletal muscle lacked a distinct fascicle formation and consisted mostly of myotubes and small, disorganized fibers (Fig. 24G, H), as shown before (Fig. 14). In contrast to the WT and the unaffected RYR$^{+/-}$ fetuses, the skeletal muscles of the heterozygous $Ca_v1.1^{+/-}$ fetuses displayed a bigger percentage of small fibers and myotubes and a higher degree of disorganization as evident from the large spaces devoid of fibers within the fascicles (Fig. 24 asterisks in J and K). At E18.5 homozygous $Ca_v1.1^{-/-}$ skeletal muscle still exhibited the greatest signs of immaturity, consisting predominantly of myoblasts and myotubes and had virtually no differentiated muscle fibers. (Fig. 24M,N). Moreover, the hind limb of the E18.5 $Ca_v1.1^{-/-}$ fetuses also exhibited a retarded bone maturation, as the bones consisted of a hyaline cartilage at a time point when mineralization of bones should be active (Fig. 24; arrows in M). The activated caspase-3 stainings revealed no signs of apoptosis in any of the analyzed genotypes at E18.5 (Fig. 24C, F, I, L, O).

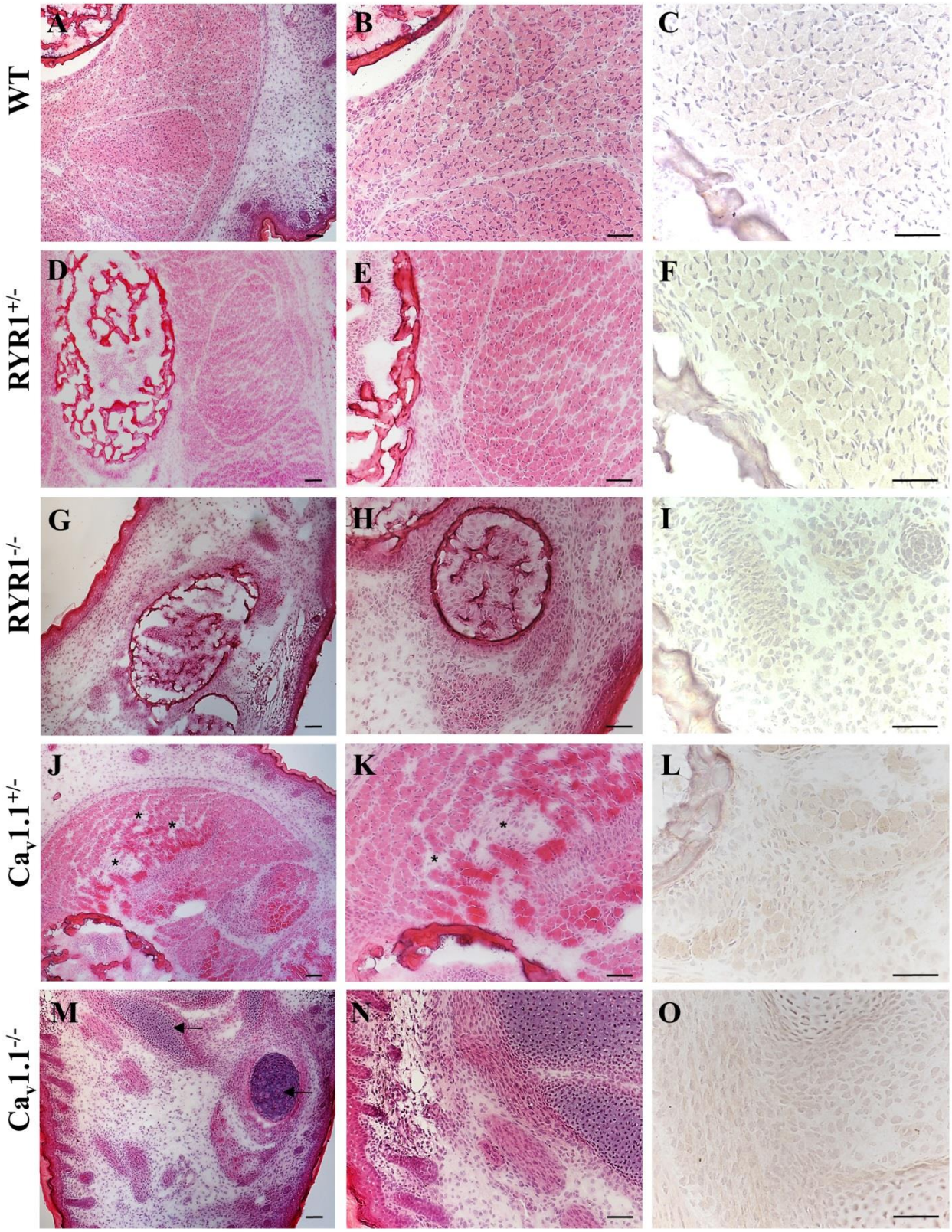
WT
RYR1+/-
RYR1-/-
CaV1.1+/-
CaV1.1-/-
A
B
C
D
E
F
G
H
I
J
K
L
M
N
O

Fig. 24: Histological cross sections of mouse hind limb skeletal muscle at E18.5.
Cross sections of the lower hind limb of a WT fetus **(A-C)**, a $RYR1^{+/-}$ fetus **(D-F)**, a $RYR1^{-/-}$ fetus **(G-I)**, a $Ca_v1.1^{+/-}$ fetus **(J-L)**, and a $Ca_v1.1^{-/-}$ fetus **(M-O)**, respectively. At E18.5, the fetal skeletal muscles of a WT fetus **(A-C)** was mature with regularly developed muscle fascicles consisting of differentiated muscle fibers. as well as inconspicuous bone having reached a normal state of mineralization. In a $RYR1^{+/-}$ fetus **(D-F)**, skeletal muscle and bone were normally developed, thus, being similar to WT mice. In contrast, the skeletal muscle of $RYR1^{-/-}$ **(G, H)** and $Ca_v1.1^{-/-}$ **(M, N)** fetuses, consisted predominantly of small, unorganized myotubes with a lack of fascicular organization. In addition, bone of the hind limb of a $Ca_v1.1^{-/-}$ **(M-O)** fetus was impaired in development as evidenced by persisting hyaline cartilage while mineralization had not been initiated **(arrows in M)**. The skeletal muscle of a $Ca_v1.1^{+/-}$ fetus exhibited milder signs of an incomplete development such as partial fiber disorganization within the fascicles **(asterisks in J, K)**. At day E18.5 apoptosis was completely absent from all mutant strains as evidenced by the absence of nuclear immunoreaction in immunohistochemistry with anti-activated caspase-3. H&E staining (**A, B, D, E, G, H, J, K, M, and N)**; original magnification x100 **(A, D, G, J, M)** and x200 **(B, E, H, K, N)**. Immunohistochemistry with rabbit anti-mouse activated caspase-3 (clone C92-605; BD Biosciences) and slight counterstaining with hemalum; original magnification x400. Scale bars correspond to 100 µm in all microphotographs. Micrographs were taken by PD Dr. Anna Brunn. Modified from (Filipova et al., 2018).

3.2.3 Global transcriptome analyses of limb skeletal muscle at E14.5 and E18.5

In order to elucidate the global transcriptomic changes accompanying fetal development and secondary myogenesis in mouse limb skeletal muscle from E14.5 – the beginning of fetal development and of secondary myogenesis – to E18.5 – the end of prenatal development and secondary myogenesis, microarray analyses (MAs) were performed as described in (Filipova et al., 2018). In particular, at E14.5 and E18.5 the skeletal muscles from the front and hind limbs of 3 littermates of each of the genotypes $RYR1^{+/+}$ (WT), $RYR1^{+/-}$ and $RYR1^{-/-}$, as well as $Ca_v1.1^{+/+}$ (WT), $Ca_v1.1^{+/-}$ and $Ca_v1.1^{-/-}$ were collected separately and used for total RNA extractions (Fig. 25). The RNA concentration was measured and the RNA integrity was analyzed on 2% agarose gels (Fig. 26). Subsequently, 250 ng of each sample were subjected to microarray analyses. The Affymetrix MoGene 2.0 ST array chips were used for the MAs, which provided information about the expression levels of 41,345 genomic loci. One advantage of these chips over the previously used Mouse Genome 430 2.0 chips (E18.5 $RYR1^{-/-}$ vs. $RYR1^{+/-}$) is, that they span not only the coding regions of the mouse transcriptome but also provide information about the expression of non-coding RNAs like micro RNAs (miRNAs) or long non-coding RNAs (lncRNAs).

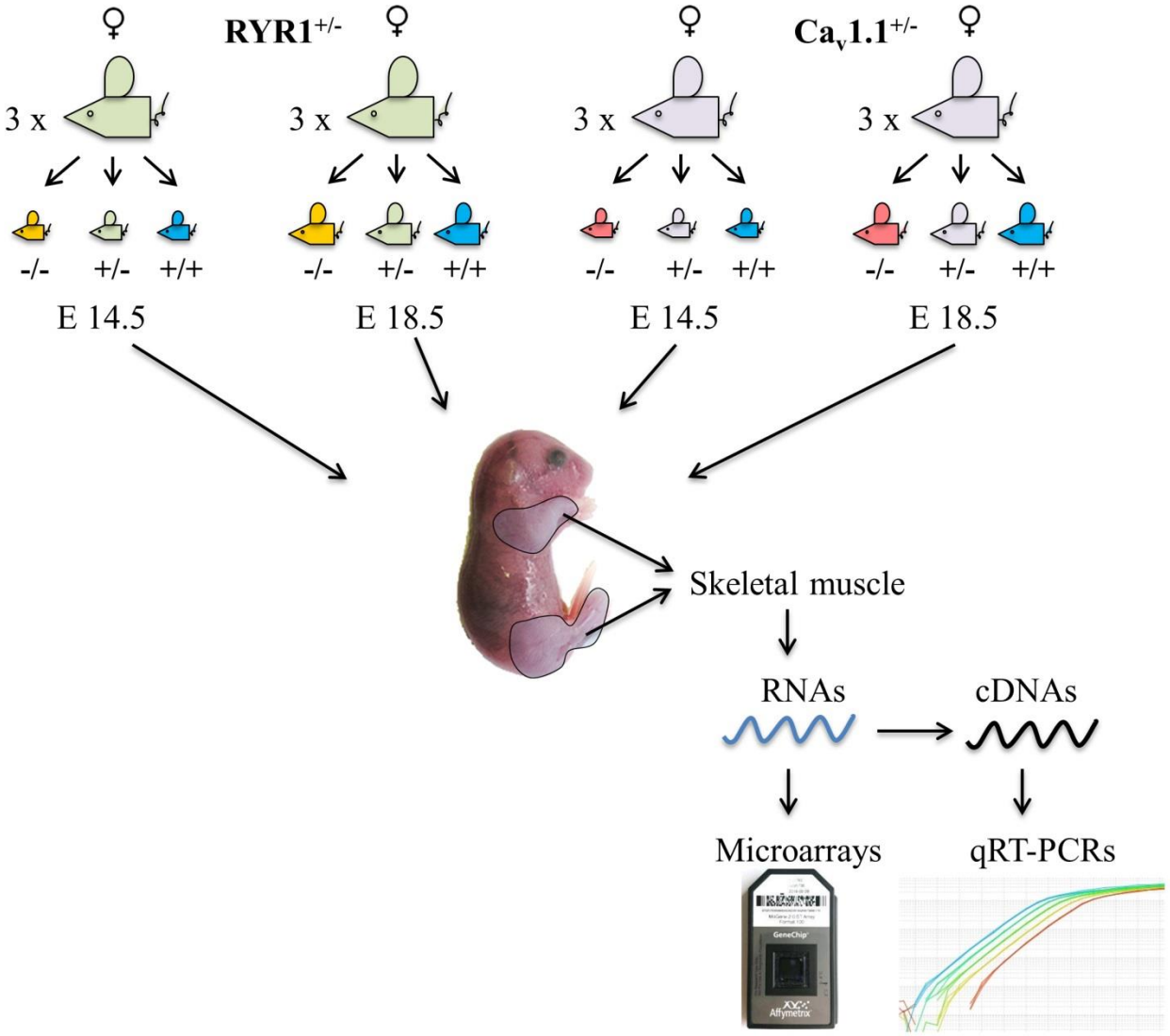

Fig. 25: Workflow scheme for the gene expression analysis of limb skeletal muscle at E14.5 and E18.5.
Six heterozygous RYR1$^{+/-}$ and Cav1.1$^{+/-}$ male and females mice were subjected to timed pairings (always RYR1$^{+/-}$ x RYR1$^{+/-}$ and Cav1.1$^{+/-}$ x Cav1.1$^{+/-}$). Three pregnant females were sacrifices at day 14.5 and three – at day 18.5 post coitum. From each litter the skeletal muscles from the front and hind limbs of one WT ($^{+/+}$), one heterozygous ($^{+/-}$) and one homozygous ($^{-/-}$) fetus were collected and used for RNA extractions. Equal amounts of total RNA from each sample were used for individual hybridizations to Affymetrix MoGene 2.0 ST array chips and MAs was performed as described in Materials and Methods. Additionally, equal amounts of the total RNAs were used in reverse transcription reactions and the resulting cDNAs were used in qRT-PCR analyses. Modified from (Filipova et al., 2018).

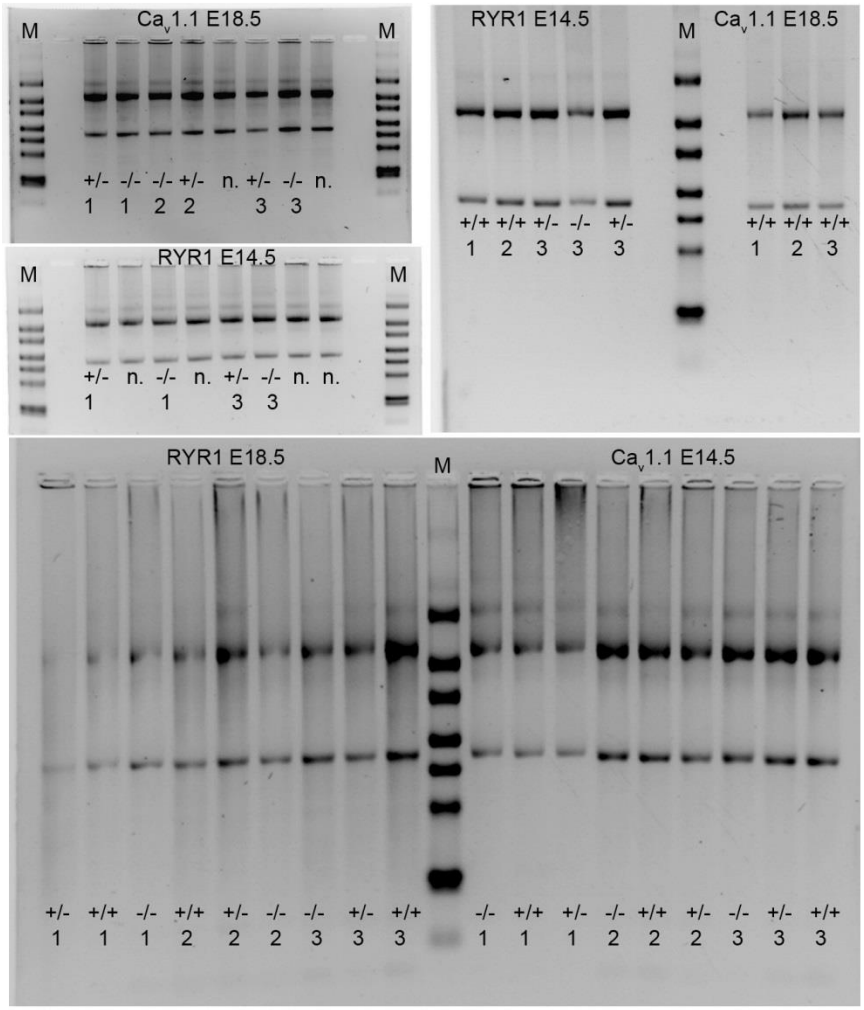

Fig. 26: RNA quality assessment for MAs.
RNA agarose electrophoresis. 250 ng or 500 ng total RNA extracted from the skeletal muscles of WT ($^{+/+}$), heterozygous ($^{+/-}$) or homozygous ($^{-/-}$) RYR1 and Cav1.1 fetuses were subjected to electrophoresis on 2% agarose gels next to 2 µl RiboRuler High Range RNA Ladder as size marker (marked as "M"). Animals from different genotypes belonging to the same litter at each time point (E14.5 or E18.5) were marked as 1, 2 and 3, standing for "litter 1", "litter 2" and "litter 3". Samples marked with "n." were not subjected to MAs. Modified from (Filipova et al., 2018).

3.2.3.1 PCA identifies distinct global transcriptomic profiles of RYR1$^{-/-}$ and Ca$_v$1.1$^{-/-}$ limb skeletal muscle at E18.5 but not E14.5

Next, the results of the MAs (.CEL files) were subjected to background correction, summarization and normalization via a robust Multi-array Analysis (RMA) using the Affymetrix Expression Console™ (Affymetrix® / Thermo Fisher). The resulting summarization files (.CHP) were used for the construction of a 3D PCA plot representing the variance between the samples on the basis of the detected expression levels for the entire transcriptome (Fig. 27). The PCA identified that the factor

responsible for the biggest part of the observed variance among the samples (PC1 = 47.2%) was the developmental stage – E14.5 or E18.5, as all samples separated along PC1 according to this criteria. At E14.5 no genotype-related separation was observed between the samples. In contrast, the samples taken at E18.5 segregated into two groups along PC2 (PC2 = 5.3%): in the first group are the $RYR1^{-/-}$ and $Ca_v1.1^{-/-}$ samples, which are grouped together and separated from the other group that consists of all of the other (WT and heterozygous) genotypes. This is best seen for the $Ca_v1.1.^{-/-}$ samples (green squares in Fig. 27) which are located most distantly from the samples of the WT and heterozygous fetuses. Additionally, the E18.5 $RYR1^{-/-}$ and $Ca_v1.1^{-/-}$ samples appeared slightly closer to the E14.5 sample group along PC1. This indicates that at E18.5 the $RYR1^{-/-}$ and $Ca_v1.1^{-/-}$ limb skeletal muscles possess similar global transcriptomic profiles, which differ significantly from those of WT and heterozygous ($RYR1^{+/-}$ and $Ca_v1.1^{+/-}$) limb skeletal muscle.

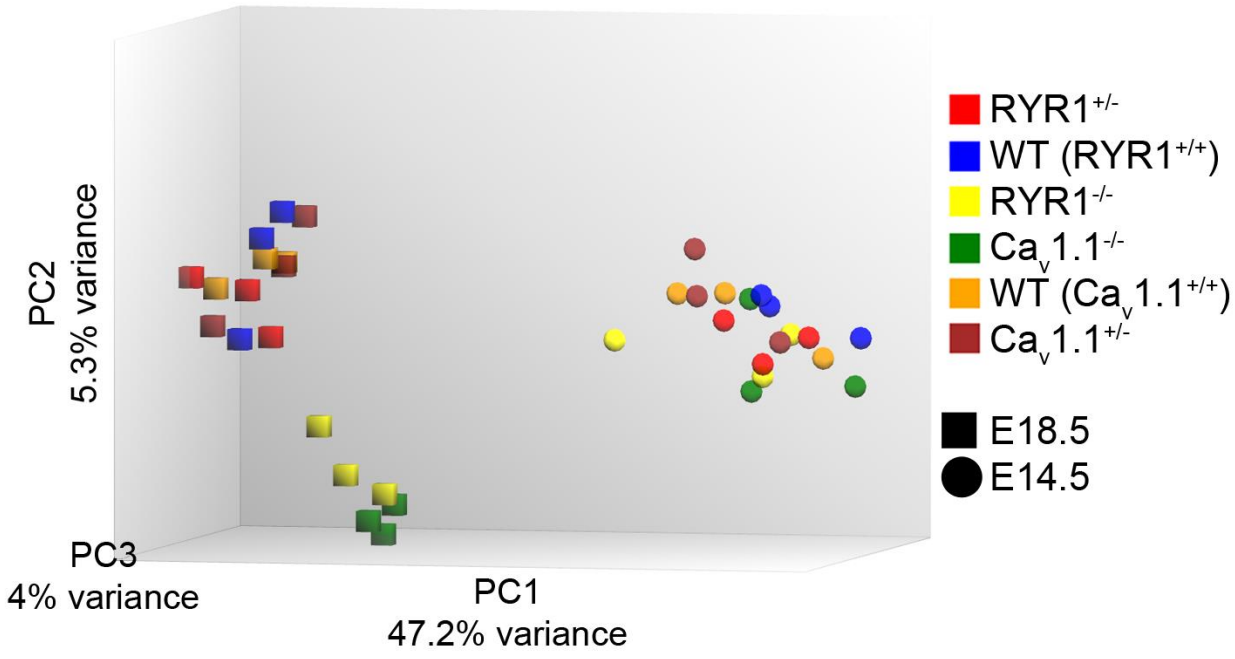

Fig. 27: A 3D PCA plot from the MAs results.
PCA was performed for all samples with all their genes detected by the MAs via the Expression Analysis Console 3.0 (Affymetrix® / Thermo Fisher). The shape of each sample corresponds to its embryonic day: E14.5 – circles, and E18.5 – squares. The color of each sample corresponds to its genotype. Modified from (Filipova et al., 2018).

3.2.3.2 DEGs criteria and numbers

The MAs summarization files (.CHP) were further subjected to one-way ANOVA analyses via the Transcriptome Analysis Console 3.0 (Affymetrix® / Thermo Fisher) for detection of differentially

regulated genes (DEGs). One major aim of this analysis was to identify and compare DEGs arising from E14.5 to E18.5 (E18.5 vs. E14.5 comparisons) within each genotype. In this aspect, a gene was considered to be differentially expressed if it had a P-value ≤ 0.05 and a linear FC ≤ -2 or ≥ 2 (Fig. 28A). Another main purpose of this work was to analyze the differences in gene expression between the different genotypes at each developmental point (E14.5 and E18.5). In order to be able to analyze less pronounced changes in gene expression, a gene was considered as a DEG if it had a P-value ≤ 0.05 and a linear FC ≤ -1.5 or ≥ 1.5 (Fig. 28B). Only genes meeting these criteria (Table 15) were subjected to further analyses.

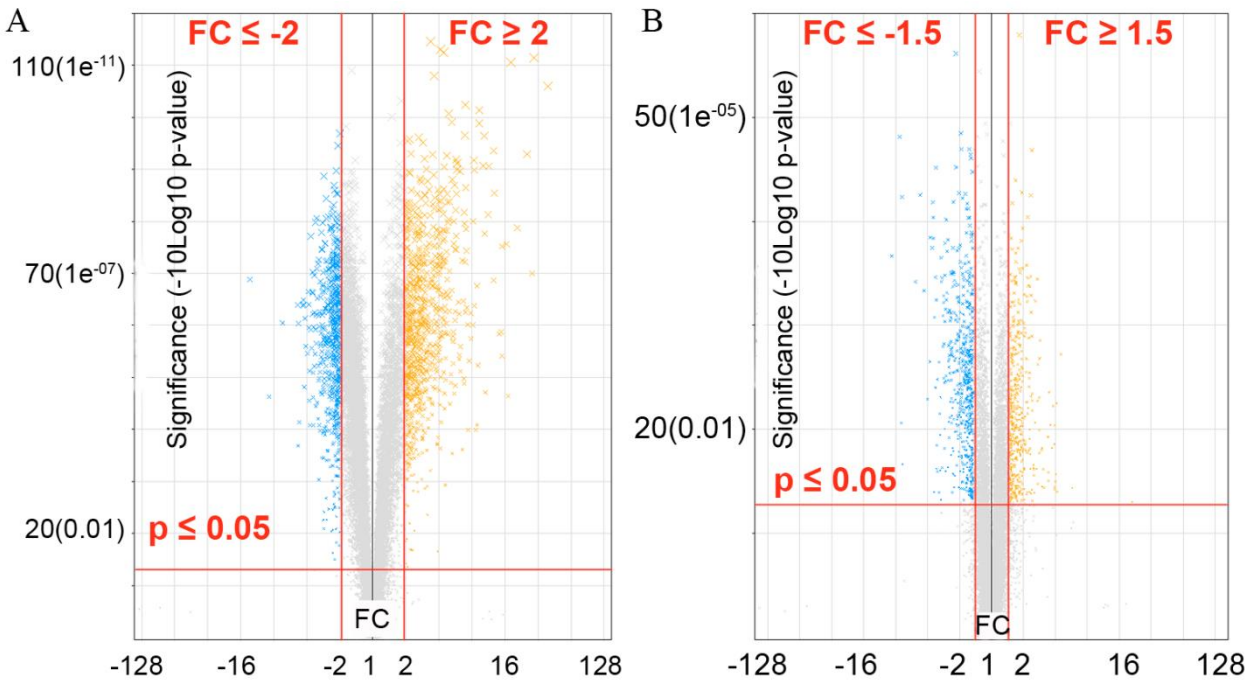

Fig. 28: Criteria for DEGs.
(A) When comparing different developmental stages (E18.5 vs. E14.5), the cut-off criteria for being considered as a DEG were a FC ≥ +2 or ≤-2, and a P-value ≤ 0.05 (the example shown is from the comparison WT E18.5 vs. WT E14.5). **(B)** When comparing groups from the same developmental stage, the cut-off criteria were a FC ≥ +1.5 or ≤-1.5, and a P-value ≤ 0.05 (the example shown is from the comparison Cav1.1$^{-/-}$ E18.5 vs. WT E18.5). Modified from (Filipova et al., 2018).

Table 15. Number of DEGs found in various comparisons.

Test group	Comparison (Test vs. Control group)	Total DEGs	Downregulated DEGs	Upregulated DEGs
WT	E18.5 vs. WT E14.5	1314	541	773
RYR1$^{+/-}$	E18.5 vs. RYR1$^{+/-}$ E14.5	1426	611	815
	E14.5 vs. WT E14.5	36	27	9
	E18.5 vs. WT E18.5	21	13	8
RYR1$^{-/-}$	E18.5 vs. RYR1$^{-/-}$ E14.5	812	311	501
	E14.5 vs. WT E14.5	61	32	29
	E18.5 vs. WT E18.5	493	304	189
Ca$_v$1.1$^{+/-}$	E18.5 vs. Ca$_v$1.1$^{+/-}$ E14.5	1079	433	646
	E14.5 vs. WT E14.5	8	5	3
	E18.5 vs. WT E18.5	33	10	23
Ca$_v$1.1$^{-/-}$	E18.5 vs. Ca$_v$1.1$^{-/-}$ E14.5	900	282	618
	E14.5 vs. WT E14.5	97	66	31
	E18.5 vs. WT E18.5	1047	571	476

As shown by Table 15, the highest numbers of DEGs were detected in the comparisons of the two developmental stages, E18.5 vs. E14.5, for WT (1314 DEGs), RYR1$^{+/-}$ (1426 DEGs) and Ca$_v$1.1$^{+/-}$ (1079 DEGs) samples. The homozygous RYR1$^{-/-}$ and Ca$_v$1.1$^{-/-}$ mutants exhibited a smaller number of DEGs (812 and 900 DEGs, respectively) in this comparison, going in line with the suggestion that the secondary myogenesis in these muscles is incomplete and therefore less genes are expected to be significantly changed. When comparing the RYR1$^{+/-}$ and Ca$_v$1.1$^{+/-}$ mutants to their WT littermates at E14.5 and E18.5, both heterozygous mutants revealed only a handful of DEGs, the majority of which had a FC between 1.5 and 2 or -1.5 and -2. Therefore, the gene expression changes in the RYR1$^{+/-}$ and Ca$_v$1.1$^{+/-}$ mutants were not further analyzed.

When comparing the homozygous RYR1$^{-/-}$ or Ca$_v$1.1$^{-/-}$ vs. WT samples at E14.5, 61 DEGs were identified in the RYR1$^{-/-}$ samples and 97 – in the Ca$_v$1.1 samples. At E18.5 these numbers grew by 8 to 10-fold comparing homozygous E18.5 RYR1$^{-/-}$ (493 DEGs) or Ca$_v$1.1$^{-/-}$ (1047) to the WT samples. Thus, this dramatic increase in DEGs indicated that the majority of the transcriptomic changes in limb skeletal muscle due to the absence of RYR1 or Ca$_v$1.1 occur between E14.5 and E18.5. In agreement with the slightly more severe phenotype of Ca$_v$1.1$^{-/-}$ skeletal muscle (Figs. 23 and 24) two times more DEGs were detected in the Ca$_v$1.1$^{-/-}$ as in the RYR1$^{-/-}$ vs. WT samples at both E14.5 and E18.5.

3.2.3.3 qRP-PCRs validation of the MAs

Next, the gene sets found as differentially regulated in the MAs were validated via qRT-PCRs. This required suitable reference genes, having stable expression levels in the two examined developmental stages, E14.5 and E18.5, and being not affected by the RYR1 and $Ca_v1.1$ deficiency. Many of the genes traditionally used as references in qRT-PCR analyses like *Gapdh* or *Actb* change their expression profiles during development or have been found to be regulated in muscle dystrophies or upon exercise (Hildyard & Wells, 2014; Mahoney et al., 2004; Rivers, Simpson, Robertson, Gaskell, & Beynon, 2007; Ruiz-Villalba et al., 2017; Seilertuyns, Eldridge, & Paterson, 1984). Since mouse development between E14.5 and E18.5 is connected to active growth and protein synthesis enhancement, it is to be expected that the majority of the genes alter their expression profiles. In order to find the best reference genes that could be utilized as endogenous controls in the qRT-PCRs, the expression levels of all detected genes (not only DEGs) in the analyzed mouse genotypes (RYR1 and $Ca_v1.1$: $^{+/+}$, $^{+/-}$ and $^{-/-}$) were compared between the two developmental stages – E18.5 and E14.5. Additionally, the expression levels of all heterozygous and homozygous mutants for each time point were compared to those of the WTs at the respective time point (i.e. E14.5 or E18.5 $^{+/-}$ vs. $^{+/-}$ and $^{-/-}$ vs. $^{+/+}$). The comparisons identified two genes, putatively suitable for being used as reference – *Cytb*, encoding cytochrome b, and *Uba52*, encoding ubiquitin A-52 residue ribosomal protein fusion product 1. qRT-PCRs were performed, measuring the expression of *Cytb*, *Uba52*, *Gapdh*, *Actb* and *Rplp0*, the latter encoding the large ribosomal protein P0. *Cytb* was used an endogenous control (Fig. 29). Indeed, the analysis revealed an upregulation of *Gapdh* and a downregulation of *Actb* in WT samples when comparing E18.5 vs. E14.5.Moreover, *Actb* was downregulated in $RYR1^{-/-}$ vs. WT samples at E14.5 and *Gapdh*, although not significantly, exhibited a tendency of a downregulation in $Ca_v1.1^{-/-}$ vs. WT samples at E18.5. However, *Uba52* and *Cytb* genes exhibited stable relative expression levels and could therefore be suitable for being used as reference (Fig. 29A). For consistancy, *Cytb* was used as an endogenous control in all subsequent qRT-PCRs.

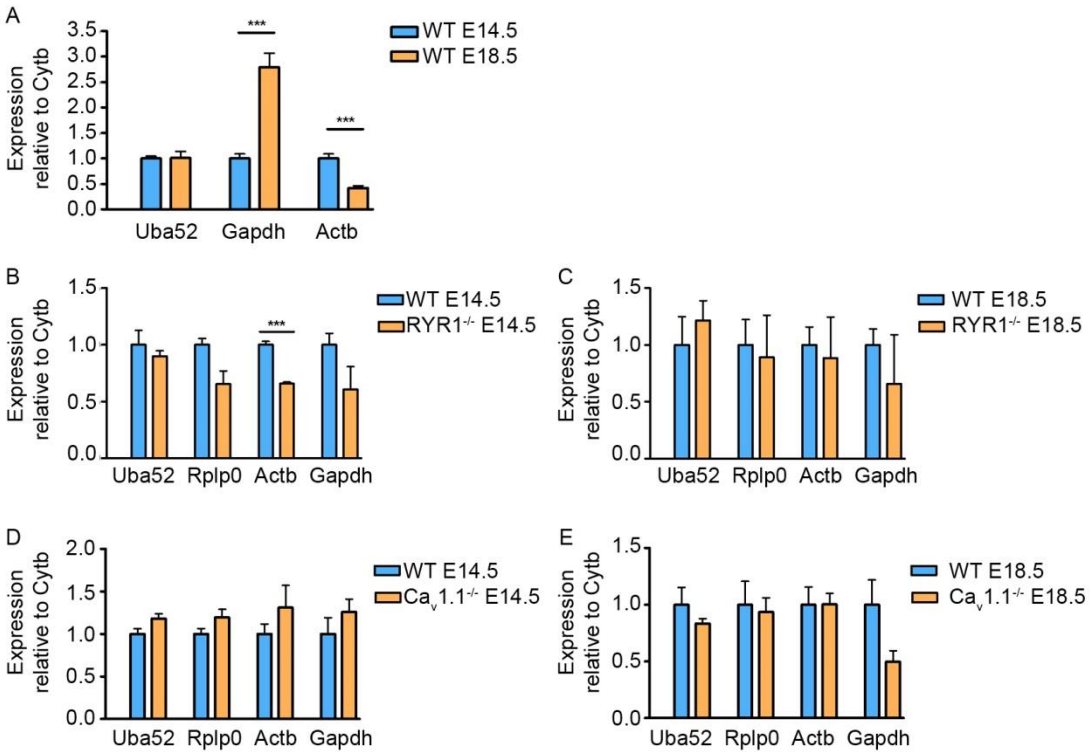

Fig. 29: qRT-PCR analyses of putative endogenous controls.
The relative expression levels of *Gapdh*, *Actb*, *Rplp0*, *Uba52* and *CytB* (used as endogenous control) were measured via qRT-PCRs for WT E18.5 vs. E14.5 samples (A), as well as for $RYR1^{-/-}$ vs. WT (B and C) and for $Ca_v1.1^{-/-}$ vs. WT (D and E) at E14.5 and E18.5. Expression levels of control samples (blue bars) were set to 1. Statistical *t*-tests were performed for each gene, ***represents a P-value ≤ 0.001. Error bars are S.E.M. Modified from (Filipova et al., 2018).

For validation of the MAs results which compared changes in the expression occurring between E14.5 and E18.5 in the WT, $RYR1^{-/-}$ and $Ca_v1.1^{-/-}$ samples, seven to eight DEGs were randomly chosen and subjected to qRT-PCR analysis (Fig. 30A-C). The DEGs spanned both directions of regulation (up- and downregulation), as well as the entire analyzed FC spectrum, containing genes exhibiting low, medium or high expression changes. Since much fewer DEGs were identified in the E14.5 $RYR1^{-/-}$ vs. WT and E14.5 $Ca_v1.1^{-/-}$ vs. WT analyses (See Table 15), four DEGs were used for the validation of these comparisons (Fig. 30D, E). Six DEGs were analyzed via qRT-PCRs in the E18.5 $RYR1^{-/-}$ vs. WT and E18.5 $Ca_v1.1^{-/-}$ vs. WT analyses (Fig. 30F, G). The results showed that all analyzed DEGs were regulated in the same direction and with a similar FC as observed in the MAs. The most clearly up- or downregulated DEGs tested revealed a much stronger differential regulation in the qRT-PCR experiments than in the MAs. This was most likely due to the much higher sensitivity of the qRT-PCR technique and its wider dynamic range (Morey, Ryan, & Van Dolah, 2006). Hence, the MA comparisons could be confirmed via qRT-PCR, suggesting validity of the MA analysis also for the genes not additionally tested by qRT-PCR.

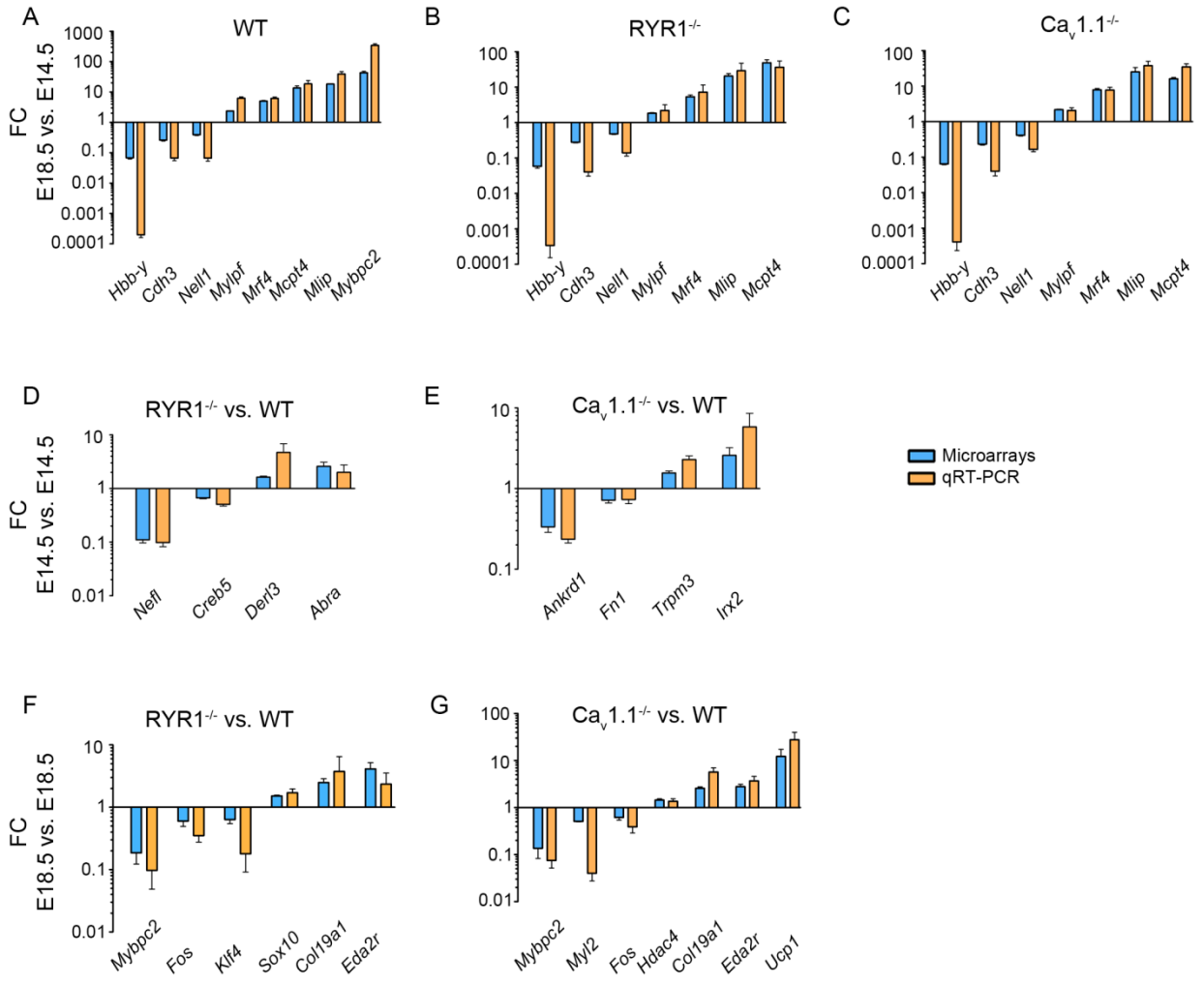

Fig. 30: Validation of the MAs results via qRT-PCRs.
DEGs found in the E18.5 vs. E14.5 analyses were validated in (A), WT vs. WT samples, 8 genes, n = 6 biological replicates per group (WTs from both the RYR1 and $Ca_v1.1$ lines); (B) $RYR1^{-/-}$ vs. $RYR1^{-/-}$, 7 genes, n =3 biological replicates per group; (C), $Ca_v1.1^{-/-}$ vs. $Ca_v1.1^{-/-}$, 7 genes, n =3 biological replicates per group. At E14.5 four DEGs were analyzed for the $RYR1^{-/-}$ vs. WT (D) and for the $Ca_v1.1^{-/-}$ vs. WT (E) analyses, n=3 biological replicates per group. At E18.5 six DEGs were analyzed for the $RYR1^{-/-}$ vs. WT (F) and seven DEGs for the $Ca_v1.1^{-/-}$ vs. WT (G) analyses, n=3 biological replicates per group. In all MAs and qRT-PCR analyses the FCs of the control samples were set to 1. The relative expression levels obtained by qRT-PCR analysis were normalized to *Cytb*, which was used as endogenous control. Error bars are S.E.M. Modified from (Filipova et al., 2018).

3.2.3.4 Distinct transcriptomic changes in the $RYR1^{-/-}$ and $Ca_v1.1^{-/-}$ skeletal muscle at E14.5

At E14.5 61 DEGs were detected in the samples from $RYR1^{-/-}$ skeletal muscle and 97 DEGS – in the samples from $Ca_v1.1^{-/-}$ skeletal muscle in comparison to samples from WT skeletal muscle (Table 15). This indicated that initial changes had already occurred in the global transcriptomes at the crucial transition phase of end of embryonic development respectively primary myogenesis towards

the beginning of fetal development, and respectively secondary myogenesis. GO BP enrichment analyses were performed with the detected DEGs in order to analyze which biological processes and pathways were affected (Fig. 31A, B). Interestingly, only 2 DEGs were found in both $RYR1^{-/-}$ and $Ca_v1.1^{-/-}$ samples – namely the solute carrier family 44, member 5 (*Slc44a5*) and Der1-like domain family, member 3 (*Derl3*), suggesting that the absence of RYR1 or $Ca_v1.1$ exerts differential effects on embryonic skeletal muscle development. The Go BP enrichment analyses indeed found no overlap between the most significantly enriched with DEGs in the $RYR1^{-/-}$ and in the $Ca_v1.1^{-/-}$ samples, and specific tendencies were observed in each genotype. In the $RYR1^{-/-}$ limb skeletal muscle the majority of the GO BP categories enriched with the highest significance were related to innervation and neurogenesis-related processes. "Regulation of neuron differentiation" was the most significantly affected process (Fig. 31A). The categories "Microtubule-based transport" and "Cytoskeleton-dependent intracellular transport" implicated putative changes in the cellular transport regulation. On the other hand, in the $Ca_v1.1^{-/-}$ samples almost all of the top 10 most significantly enriched biological processes were related to muscle contraction with the "Muscle contraction" category on position one (Fig. 31B). These results correlated with the slightly more severe phenotype and higher muscle disorganization observed in $Ca_v1.1^{-/-}$ skeletal muscle at E14.5 (Fig. 23).

In order to assess the direction in which these processes were affected, heatmaps were generated from the expression values of the genes associated with the two most significantly enriched processes (Fig. 31, arrows in A and B). Both heatmaps revealed a systemic downregulation of the genes involved in "Regulation of neuron differentiation" (for $RYR1^{-/-}$ vs. WT, Fig. 31C) and in "Muscle contraction" (for $Ca_v1.1^{-/-}$ vs. WT, Fig. 31D). In $Ca_v1.1^{-/-}$ vs. WT, *Myh6*, a gene, encoding cardiac myosin heavy polypeptide 6, alpha was the only upregulated DEG related to muscle contraction.. Thus, a general negative regulation or possibly a missing positive regulation of processes regulating innervation responses and muscle contraction was anticipated for the $RYR1^{-/-}$ and $Ca_v1.1^{-/-}$ limb skeletal muscle, respectively.

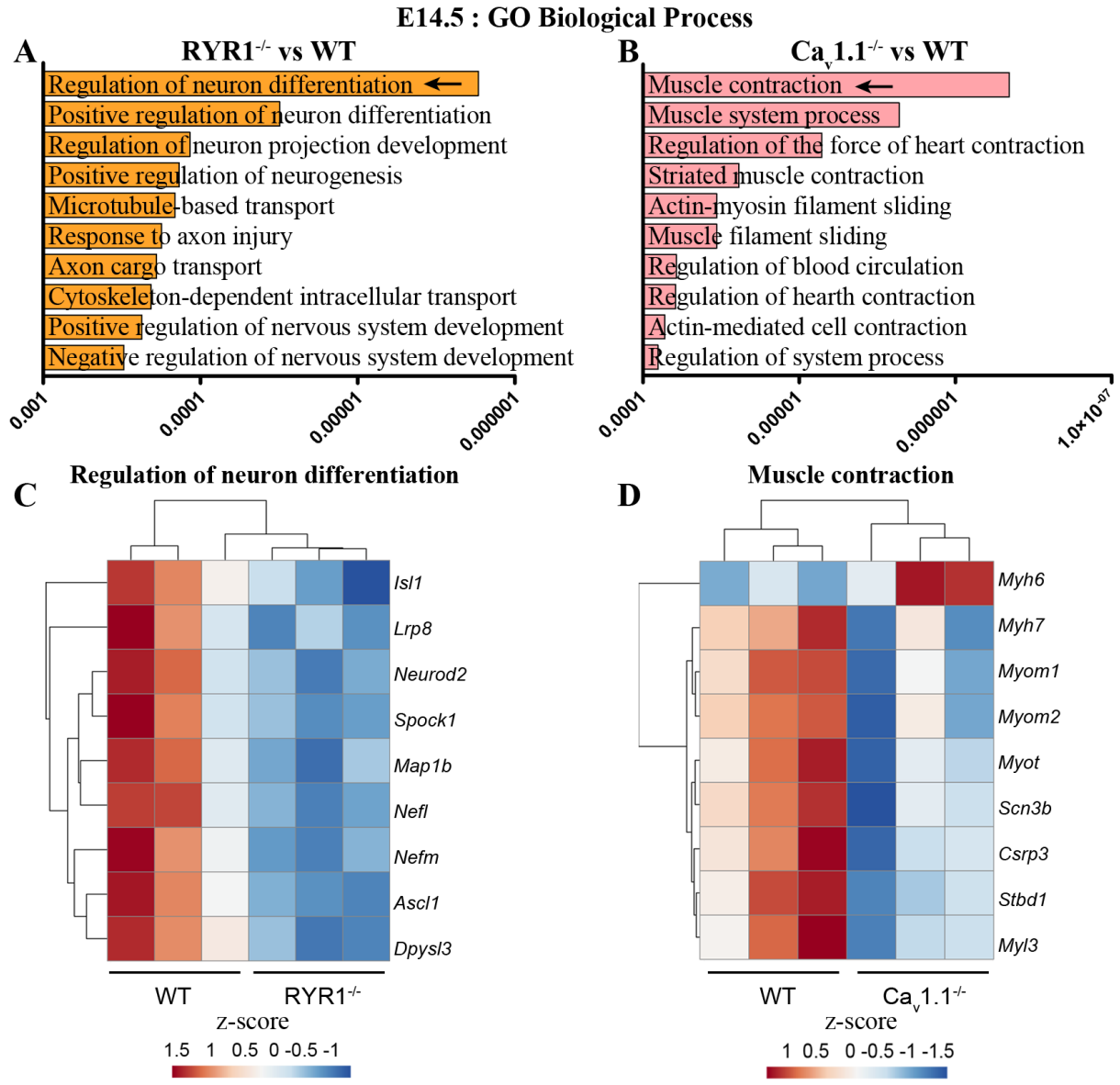

Fig. 31: Biological processes most affected by the RYR1$^{-/-}$ and Ca$_v$1.1$^{-/-}$ mutations at E14.5.
GO BP enrichment analyses were performed using the DEGs identified in the RYR1$^{-/-}$ vs. WT (A) and Ca$_v$1.1$^{-/-}$ vs. WT (B) samples at E14.5. The ten most significantly enriched categories for each analysis are shown. Arrows indicate categories presented as heat maps in (C) and (D). The enrichment analyses was performed via the Enrichr online tool (Chen et al., 2013), length of the bars represents the significance (P-value, shown on the x-axes in A,B). Heatmaps were generated for the DEGs enriched in the process "Regulation of neuron differentiation" in RYR1$^{-/-}$ samples (C) and for the DEGs enriched in the process "Muscle contraction" in Ca$_v$1.1$^{-/-}$ samples (D). The heatmaps were generated from the MAs intensity levels of each gene via *ClustVis* (Metsalu & Vilo, 2015). Hierarchical linkage clustering using the average Euclidean distance was performed for all rows and columns. Modified from (Filipova et al., 2018).

3.2.3.5 Substantial overlap in the transcriptomic changes occurring in RYR1$^{-/-}$ and Ca$_v$1.1$^{-/-}$ skeletal muscle at E18.5

At E18.5 the numbers of DEGs found in the samples from both mutants were 8- to 10-fold higher than at E14.5 (Table 15). Unlike the totally distinct sets of DEGs found in both mutants at E14.5, at E18.5 328 DEGs were shared by the RYR1$^{-/-}$ and Ca$_v$1.1$^{-/-}$ samples, which correspond to 66.5% of all RYR1$^{-/-}$ DEGs and 31.3% of all Ca$_v$1.1$^{-/-}$ DEGs, respectively. This suggested that the majority of the transcriptomic changes in the mutant limb skeletal muscles occur between E14.5 and E18.5 and that the absence of RYR1 or Ca$_v$1.1 initially causes divergent transcriptomic changes that converge towards E18.5.

To determine more precisely which biological processes are most influenced by the transcriptome changes at E18.5, the DEGs detected in the E18.5 RYR1$^{-/-}$ vs. WT and Ca$_v$1.1$^{-/-}$ vs. WT comparisons were also subjected to GO BP enrichment analyses (Fig. 32). The enrichment analyses showed that the overlap in DEGs found in both mutants corresponds to a substantial overlap in the most affected processes in RYR1$^{-/-}$ and Ca$_v$1.1$^{-/-}$ samples, since the 3 most significantly enriched processes were identical for both mutants and were related to muscle contraction. Further analyses also revealed major signaling pathways like the MAPK, PI3K-AKT, Wnt, peroxisome proliferator-activated receptor (PPAR), cAMP and cGMP-PKG pathways that were enriched with DEGs in both RYR1$^{-/-}$ and Ca$_v$1.1$^{-/-}$ samples (Suppl. Table 1). Additionally, the GO BP enrichment analyses also identified highly significantly enriched processes which were specific for the RYR$^{-/-}$ or for the Ca$_v$1.1$^{-/-}$ samples. In the RYR1$^{-/-}$ samples these processes were connected to the structure and composition of the extracellular matrix ECM (Fig. 32A), whereas in the Ca$_v$1.1$^{-/-}$ samples these were primarily related to lipid metabolism (Fig. 32B).

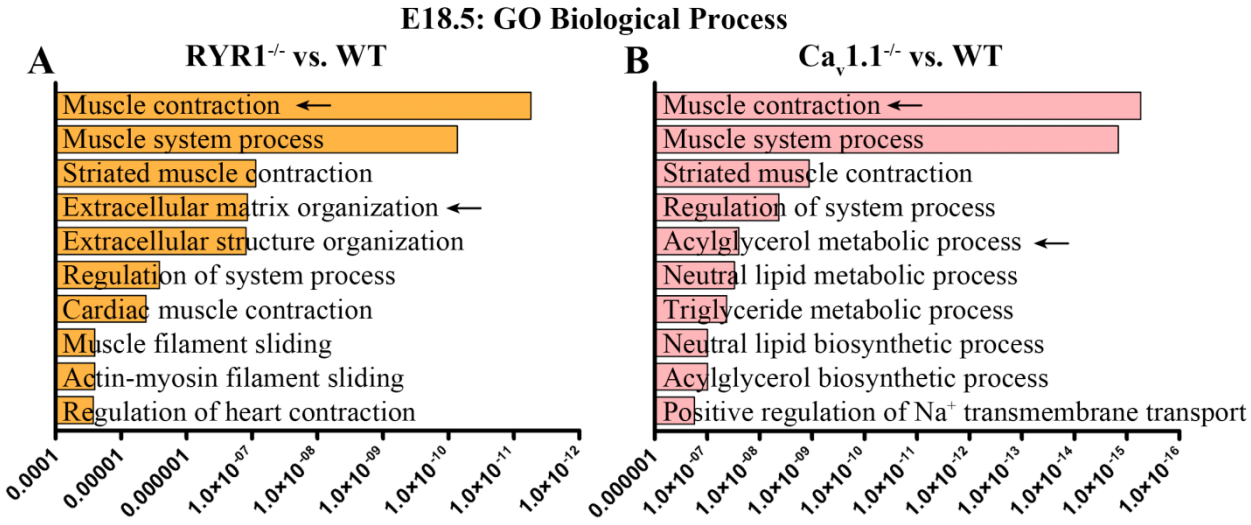

Fig. 32: Biological processes affected by the RYR1$^{-/-}$ and Ca$_v$1.1$^{-/-}$ mutations at E18.5.
GO BP enrichment analyses were performed for the DEGs identified in the RYR1$^{-/-}$ vs. WT **(A)** and Ca$_v$1.1$^{-/-}$ vs. WT **(B)** at E18.5. The ten most significantly enriched categories for each analysis are shown. Arrows indicate categories presented as heat maps in Fig. 33A-C. The enrichment analyses was performed via the Enrichr online tool (Chen et al., 2013), the length of the bars corresponds to the significance (P-value). Modified from (Filipova et al., 2018).

To evaluate the direction in which the common (found in both mutants) and the specific (found only in one of the mutants) processes were regulated, heatmaps were constructed for the DEGs from the "Muscle contraction" category – the most significantly enriched biological process in both mutants (Fig. 33A). Heatmaps were also generated for the DEGs from "Extracellular matrix organization" in RYR1$^{-/-}$ samples (Fig. 33B), and for the DEGs from "Acylglycerol metabolic process" in the Ca$_v$1.1$^{-/-}$ samples (Fig. 33C) – the most significantly affected processes specific for each mutant. 44 out of 49 DEGs identified under "Muscle contraction" were downregulated either in RYR1$^{-/-}$ or in Ca$_v$1.1$^{-/-}$, or in both mutants (Fig. 33A). Many of these DEGs, like *Myl2*, *Myl3*, *Myl6b*, *Myl9*, *Myh3*, *Myh7*, *Csrp3*, *Tcap*, *Tpm3*, *Myom1* and *Myom2* encode sarcomeric proteins suggesting significant defects in the buildup of the contractile machinery in the mutants. These findings are in line with the observed scarcity of myofibrils and the abnormalities in sarcomere arrangement in limb skeletal muscle from RYR1$^{-/-}$ and Ca$_v$1.1$^{-/-}$ mice at the perinatal stage (Pai, 1965b; Takeshima et al., 1994).

17 of 27 DEGs found in the "Extracellular matrix organization" in the RYR1$^{-/-}$ samples, were downregulated and 10 DEGs were upregulated compared to WT samples, suggesting a shift in the ECM structure and composition in RYR1$^{-/-}$ skeletal muscle (Fig. 33B).

20 DEGs detected in the E18.5 $Ca_v1.1^{-/-}$ vs. WT analysis participate in the "Acylglycerol metabolic process". The majority – 17 DEGs – were upregulated in the samples from $Ca_v1.1^{-/-}$ skeletal muscle (Fig. 22C), indicating an increased lipid metabolism in the limb skeletal muscle of these mutants.

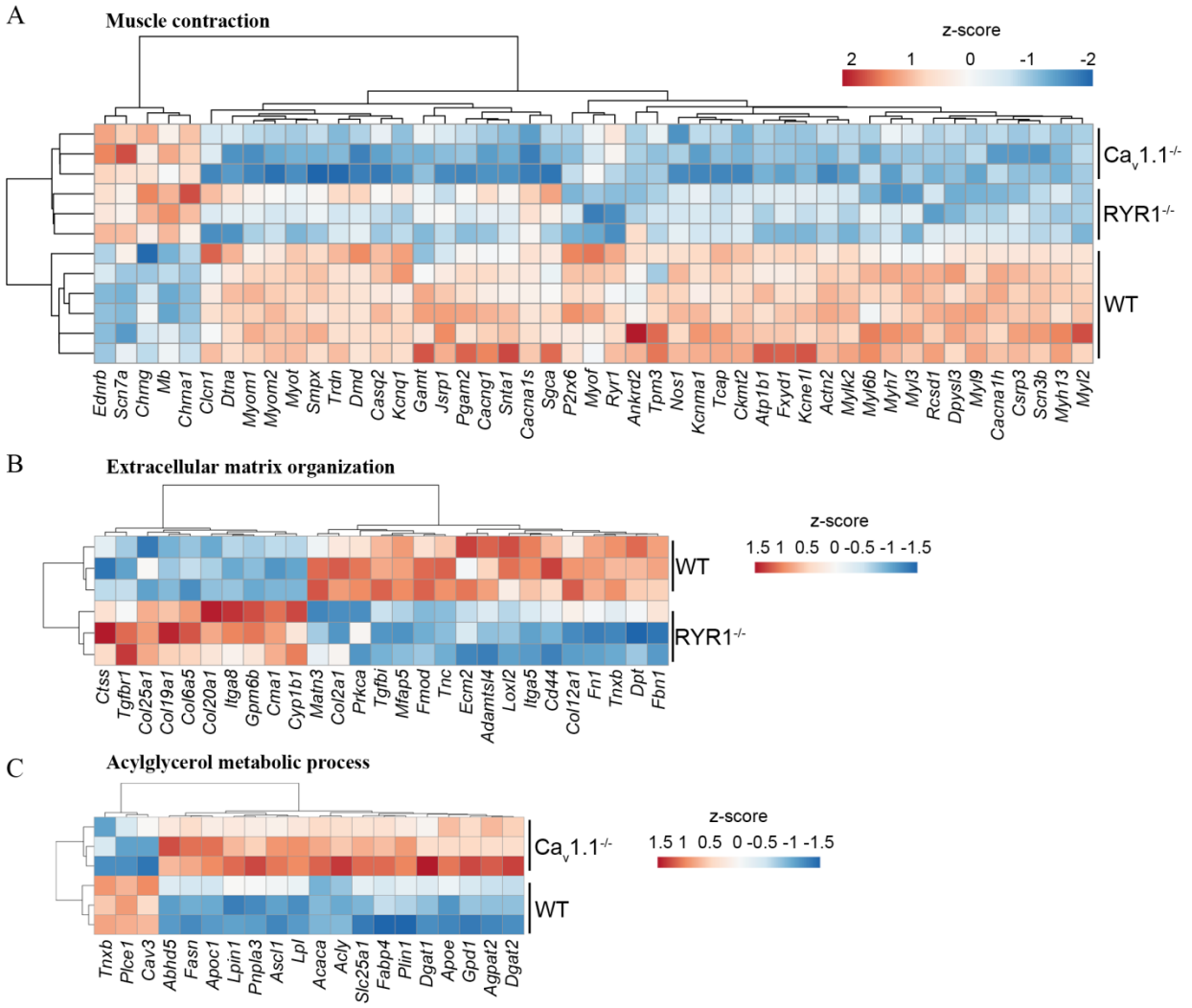

Fig. 33: Heatmaps for the most significant common and specific GO BP processes at E18.5.
Heatmaps were generated for the DEGs enriched in the "Muscle contraction" biological process in RYR1$^{-/-}$ and $Ca_v1.1^{-/-}$ samples **(A)**; for the DEGs enriched in "Extracellular matrix organization" biological process in RYR1$^{-/-}$ samples **(B)**; and for the DEGs enriched in "Acylglycerol metabolic process" biological process in $Ca_v1.1^{-/-}$ samples **(C)**. Heatmaps were generated from the MAs intensity levels of each included gene via *ClustVis* (Metsalu & Vilo, 2015). Hierarchical average linkage clustering using the Euclidean distance was performed for all rows and columns. Modified from (Filipova et al., 2018).

3.2.3.6 Global transcriptomic changes during fetal development in WT, RYR1$^{-/-}$ and $Ca_v1.1^{-/-}$ limb skeletal muscle

One main incentive while comparing the MAs results was to analyze the developmental changes occurring in limb skeletal muscle during fetal development and the simultaneous secondary

myogenesis. In order to assess the physiological transcriptomic changes accompanying this period in skeletal muscle development, the DEGs found in the WT samples from E14.5 to E18.5 (E18.5 vs. E14.5) were subjected to GO BP and Wiki Pathways enrichment analyses (Fig. 34A, B). The results exhibited a clear predominance of differently expressed genes related to processes associated with muscle structure and muscle contraction . Other significantly regulated pathways were related to energy metabolism, specifically to glycolysis, gluconeogenesis and fatty acid metabolism; as well as pathways related to the cell cycle. Similar results were found when these enrichment analyses were performed with the DEGs detected in the E18.5 vs. E14.5 comparisons of the $RYR1^{-/-}$ (Fig. 34C, D) and $Ca_v1.1^{-/-}$ (Fig. 34E, F) samples. However, in both mutants the processes connected to muscle contraction are represented by much fewer GO BP and WP categories. Instead, the pathways of fatty acid metabolism and beta oxidation seemed to be represented with a higher significance. Additional categories related to lipid metabolism and adipogenesis were identified in the mutants, especially in the samples from the $Ca_v1.1^{-/-}$ skeletal muscles. Furthermore, significantly enriched processes with the DEGs from the $RYR1^{-/-}$ E18.5 vs. E14.5 comparison were “DNA replication”, “Negative regulation of calcium ion transport”, “Cell-cell adhesion via plasma-membrane adhesion molecules”, and “Mesenchymal cell differentiation”. $Ca_v1.1^{-/-}$ samples, on the other hand, showed a specific GO BP enrichment in “Lipid storage”, “Carnitine shuttle” and “Glucose homeostasis”. The WP enrichment analyses revealed “Striated muscle contraction *Mus musculus*” as the most significantly engaged process in WT and $Ca_v1.1^{-/-}$ samples, whereas in the $RYR1^{-/-}$samples “Fatty acid and beta oxidation *Mus musculus/Homo sapiens*” were more significantly implicated. The “PPAR signaling pathway” was identified in the WP enrichment analysis of the $RYR1^{-/-}$ and $Ca_v1.1^{-/-}$ samples but not the WT samples.

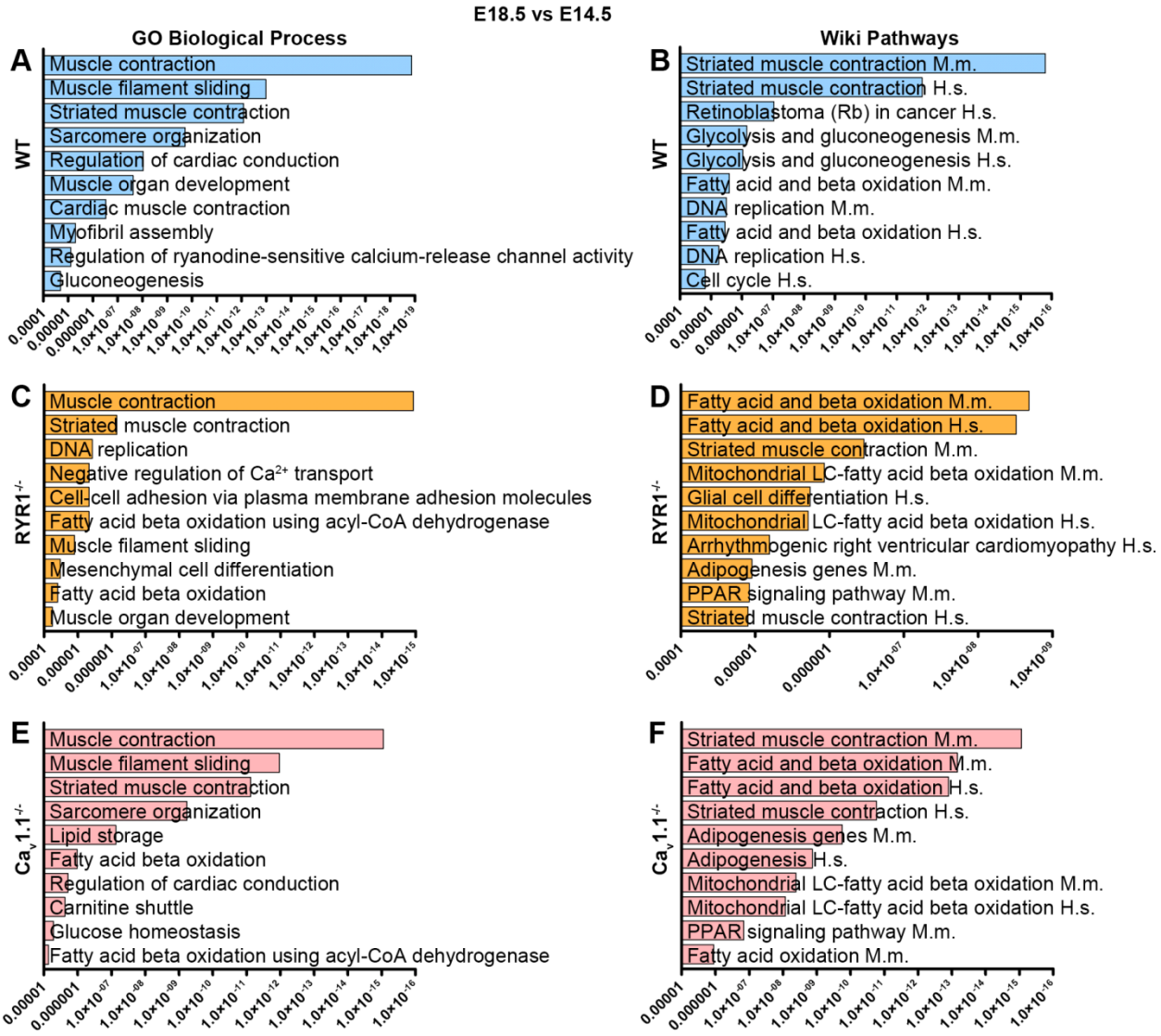

Fig. 34: Enrichment analysis of all DEGs found in skeletal muscle development from E14.5 to E18.5.
GO BP **(A, C and E)** and Wiki Pathways **(B, D, F)** enrichment analyses of all DEGs found in WT **(A, B)**, RYR1$^{-/-}$ **(C, D)** and $Ca_v1.1^{-/-}$ **(E, F)** from E14.5 (control) to E18.5. The ten most significantly enriched categories for each analysis are shown. Enrichment analyses **(A – F)** were performed via the Enrichr online tool (Chen et al., 2013), length of the bars is proportional to the significance (P-value). H.s. stands for *Homo sapiens*, and M.m. stands for *Mus musculus*. Modified from (Filipova et al., 2018).

3.2.3.7 Common and distinct DEGs during fetal development of WT, RYR1$^{-/-}$ and $Ca_v1.1^{-/-}$ skeletal muscle

To analyze to what degree the observed transcriptomic developmental changes from E14.5 to E18.5 were specific for each genotype, the DEGs detected in the E18.5 vs. E14.5 analyses in the WT, RYR1$^{-/-}$ and $Ca_v1.1^{-/-}$ skeletal muscles were compared (Fig. 35A). This analysis revealed that 429 DEGs were shared/observed in all analyzed genotypes from E14.5 to E18.5, 169 DEGs were

matching in the development of WT and RYR1$^{-/-}$ skeletal muscle, 164 DEGs – in the development of WT and $Ca_v1.1$ skeletal muscle, and 100 DEGs – in the development of RYR1$^{-/-}$ and $Ca_v1.1^{-/-}$ skeletal muscle. Additionally, 483 DEGs were exclusively found in WT; 91 DEGs – only in RYR1$^{-/-}$; and 171 DEGs – only in $Ca_v1.1^{-/-}$ skeletal muscle in the comparison of E18.5 vs. E14.5.

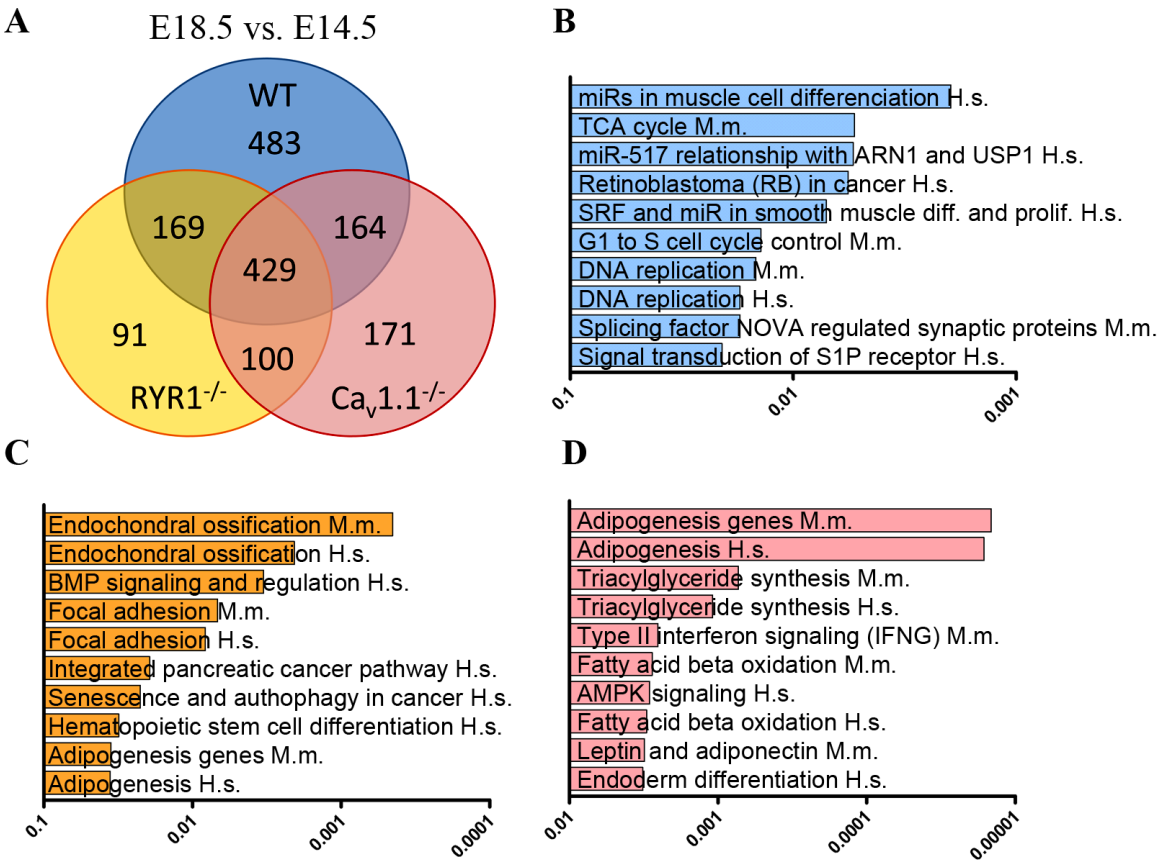

Fig. 35: DEGs specific for the E18.5 vs. E14.5 analyses of WT, RYR1$^{-/-}$ or $Ca_v1.1^{-/-}$ skeletal muscle.
(A) A Venn diagram, showing the number of DEGs identified in the MA analyses at E18.5 compared to E14.5 in WT, RYR1$^{-/-}$ and $Ca_v1.1^{-/-}$ limb skeletal muscle. Numbers in the overlapping and non-overlapping areas represent the amount of shared and not shared DEGs between genotypes, respectively. Wiki Pathways enrichment analyses of the DEGs found exclusively in **(B)** WT (483 DEGs); **(C)** RYR1$^{-/-}$ (91 DEGs); and **(D)** $Ca_v1.1^{-/-}$ (171 DEGs) from E14.5 (control) to E18.5, respectively. The ten most significantly enriched categories for each analysis are shown. Enrichment analyses **(B – D)** were performed via the Enrichr online tool (Chen et al., 2013), Modified from (Filipova et al., 2018).

WP enrichment analyses were performed with the specific DEGs in each genotype (Fig. 35B-D) to evaluate which signaling pathways were specifically affected in the development of the skeletal muscles of each genotype. The most significant WP pathway identified from the WT-specific DEGs was “miRs in muscle cell differentiation” (Fig. 35B). Two other miRNA-related pathways – “miR-517 relationship with ARN1 and USP1” and “SRF and miR in smooth muscle differentiation and proliferation” – were also among the most significantly regulated WT development-specific

pathways. Additionally, pathways related to metabolism, like the "TCA cycle", as well as to cell cycle and signal transduction like "G1 to S cell cycle control", "DNA replication" were also significantly affected WP categories by the WT-specific DEGs. Analyzing the $RYR1^{-/-}$-specific DEGs, the WP enrichment analysis identified "Endochondral ossification", "BMP signaling and regulation", "Focal adhesion" and "Adipogenesis" as very significantly affected pathways (Fig. 35C). In $Ca_v1.1^{-/-}$ pathways related to adipogenesis and lipid metabolism, such as "Adipogenesis", "Triglyceride synthesis" and "Fatty acid and beta oxidation" were most significantly affected.

In order to analyze in greater detail which biological processes and cellular structures were affected differently throughout the E14.5 to E18.5 skeletal muscle development, the genotype-specific DEGs found in the E18.5 vs. E14.5 analyses (Fig. 35A) were subjected to GO BP and GO CC enrichment analyses (Fig. 36).

In WT-specific DEGs, the results of the GO BP analyses were similar to those of the WP analyses, identifying "Positive regulation of rRNA processing" and several muscle- and cell cycle-related processes as highly enriched (Fig. 36A). The $RYR1^{-/-}$-specific DEGs showed a high enrichment for "Chondrocyte differentiation", and several other developmental processes (Fig. 36C). The $Ca_v1.1^{-/-}$-specific DEGs exhibited a very specific enrichment in "Acylglycerol acyl chain remodeling" and other lipid and fatty acid metabolic processes (Fig. 36E).

The GO CC enrichment analysis indicated specific changes in the "Sarcolemma" and other muscle-specific structures like "Costamere", "Sarcomere", "I-band", and "Z-disc" in the WT-specific DEGs analysis (Fig. 36B). The structures "Postsynaptic membrane", "Acetylcholine gated channel complex" and "Voltage-gated Ca^{2+} channel complex" were most significantly enriched with the $RYR1^{-/-}$-specific DEGs (Fig. 36D). The structures and cellular components most enriched with $Ca_v1.1^{-/-}$-specific DEGs were "Proteinaceous extracellular matrix", "Integral component of nuclear inner membrane" and "Integral component of plasma membrane" (Fig. 36F).

These results indicate that the $RYR1^{-/-}$ and $Ca_v1.1^{-/-}$ skeletal muscle only partially recapitulates the physiological transcriptomic changes characteristic for the WT fetal development and the secondary myogenesis from E14.5 to E18.5. Additionally, both mutants exhibited distinct changes perturbing signaling pathways, biological processes and cellular components that were not affected in the development of the WT skeletal muscle. Specifically, the $RYR1^{-/-}$ limb skeletal muscle development

was characterized by a dysregulation of processes and structures related to the muscle-bone and muscle-ECM interaction network.

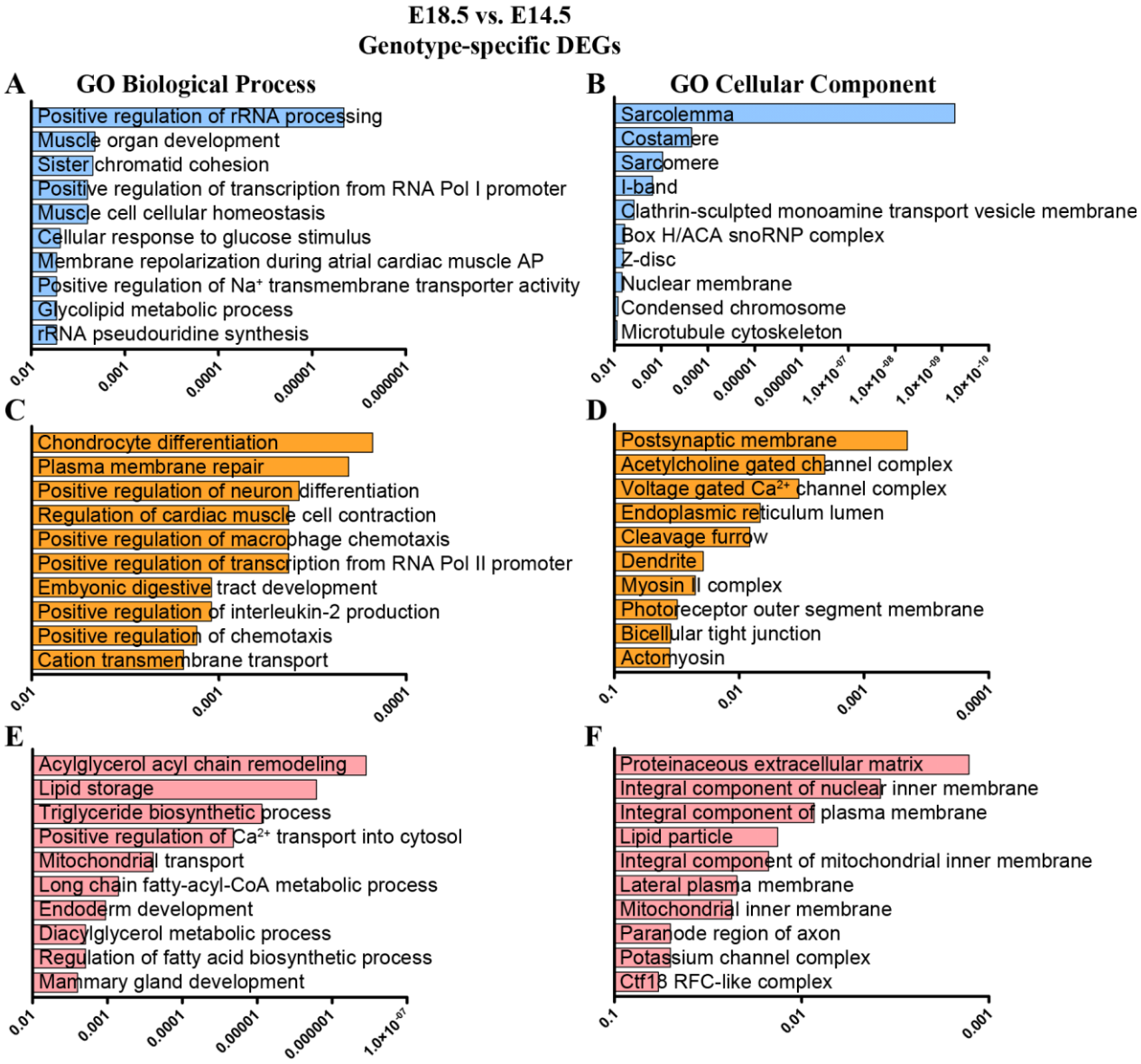

Fig. 36: GO BP and GO CC enrichment analyses of the E18.5 vs. E14.4 specific DEGs.
GO BP **(A, C, E)** and GO CC **(B, D, F)** enrichment analyses of the DEGs found exclusively in WT (483 DEGs, blue charts), $RYR1^{-/-}$ (91 DEGs, yellow charts) and $Ca_V1.1^{-/-}$ (171 DEGs, red charts) from E14.5 (control) to E18.5, respectively (see Fig. 35). The ten most significantly enriched categories for each analysis are shown. Enrichment analyses **(A–F)** were performed via the Enrichr online tool (Chen et al., 2013), length of the bars is proportional to the significance (P-value). Modified from (Filipova et al., 2018).

The development of the $Ca_V1.1^{-/-}$ limb skeletal muscle was displayed by dysregulation in adipogenesis and lipid metabolism. Thus, these data suggest that not only ECC but also additional

specific functions exerted by RYR1 and $Ca_v1.1$ play distinct roles during limb skeletal muscle development.

3.2.3.8 Differential miRNA expression profiles during limb secondary myogenesis

The WP enrichment analysis of the WT skeletal muscle development-specific DEGs (Fig. 35B) identified several pathways connected to miRNA regulation of different processes, the most significant of which was "Mirs in Muscle Cell Differentiation Homo sapiens". These results implied that multiple miRNAs and miRNA-related pathways are impacted by the absence of RYR1 or $Ca_v1.1$ during fetal development and secondary myogenesis. An in-depth analysis of the "Mirs in Muscle Cell Differentiation Homo sapiens" WP category revealed that 10 DEGs participating in this pathway were identified in WT skeletal muscle development between E14.5 and E18.5 and only three of them were found in the development of $RYR1^{-/-}$ or $Ca_v1.1^{-/-}$ limb skeletal muscle (Fig. 37A). Several of the WT-specific DEGs from this pathway encode regulators of the expression and activity of the canonical myogenic regulatory factors (MRFs) Pax7, Myf5 and MyoD; as well as the muscle-specific miRNAs (MyoMirs) *Mir206* and *Mir133a-2* implicated in skeletal muscle differentiation and development (Chen et al., 2006; Luo et al., 2013).

miRNAs are potent and versatile regulators of a wide range of processes, including muscle development (Luo et al., 2013). In order to better understand and describe the expression changes in miRNA genes accompanying secondary myogenesis, the expression levels changes of all miRNAs detected in the MAs were analyzed. More precisely, the miRNAs detected as DEGs in the E18.5 vs. E14.5 analyses in the WT, $RYR1^{-/-}$ and $Ca_v1.1^{-/-}$ skeletal muscles were closely examined (Fig. 37B, Table 16). From E14.5 to E18.5 61 miRNAs were differentially regulated in the WT samples, 16 of which were also found in the $Ca_v1.1^{-/-}$ samples and only 3 – in the $RYR1^{-/-}$ samples. Additionally, 1 miRNA was differentially regulated only in the $RYR1^{-/-}$ samples and 4 – only in the $Ca_v1.1^{-/-}$ samples. A hierarchical clustering analysis of all samples from the MAs based on their miRNA expression profiles revealed that all E18.5 WT samples were clustered together, whereas only a partial clustering was observed for the E18.5 $RYR1^{-/-}$ and $Ca_v1.1^{-/-}$ samples on one side, and for all E14.5 samples – on the other. However, one E18.5 $RYR1^{-/-}$ was clustered closer to the E14.5 samples than to the other E18.5 samples. Out of the 61 miRNAs detected in the WT E18.5 vs. E14.5 analysis, only 5 were downregulated, and the rest were upregulated, indicating a growing importance for the miRNA-mediated regulation for the secondary myogenesis. The $RYR1^{-/-}$ and $Ca_v1.1^{-/-}$ samples

exhibited a similar tendency of miRNA expression changes. However, the majority of these changes were not found to be significant by the MAs. Six of the canonical MyoMirs, Mir206, Mir133b, Mir133a-2, Mir1a-2, Mir133a-1 and Mir1a-1, were found to be upregulated in the WT samples from E14.5 to E18.5. Additionally, another 22 miRNAs differentially regulated in the E18.5 vs. E14.5 WT samples were related to muscle development or different myopathies (Table 16).). Interestingly, 32 (i.e., 52% of all) of the identified miRNAs which were upregulated in E18.5 relative to E14.5 in WT, which have been found by others to be downregulated in ageing skeletal muscle [37]. This suggests that these miRNAs might have important roles during skeletal muscle development and during subsequent adaptation or alteration. Moreover, 26 (43% of all) of the identified miRNAs originate from a miRNA cluster located within the imprinted Dlk-Dio3 genomic region on chromosome 12. This region might be of eminent importance for skeletal muscle development.

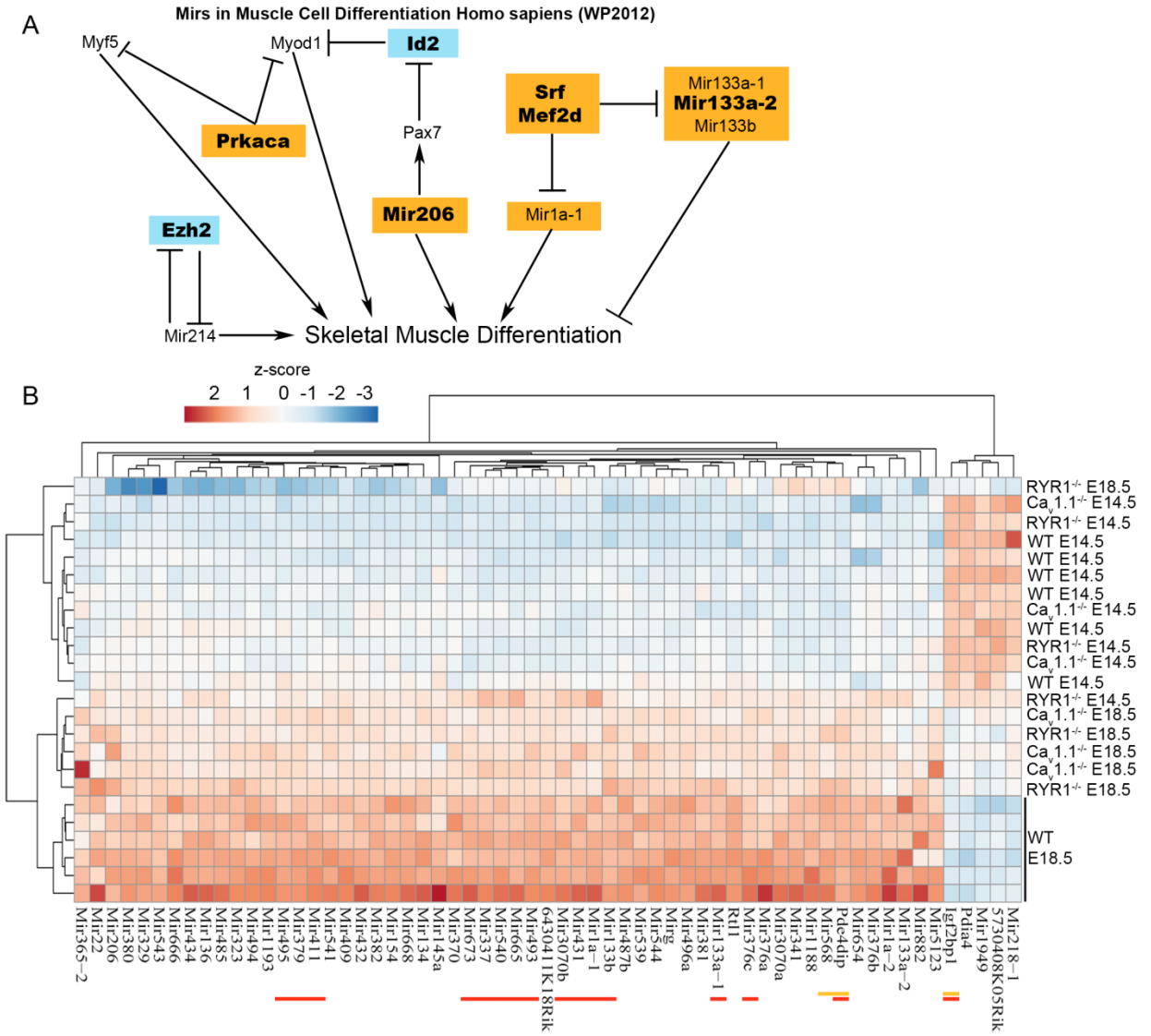

Fig. 37: Differentially expressed miRNAs during WT skeletal muscle development.
(A) Up (orange) and down (blue) regulated DEGs identified by the MAs for E18.5 vs. E14.5 (control) taking part in the Wiki pathway "Mirs in Muscle Cell Differentiation Homo sapiens" (see Fig. 35B). DEGs regulated only in WT samples from E14.5 to E18.5 are shown in bold. **(B)** A heatmap of all miRNAs, found to be differentially regulated at E18.5 compared to E14.5 in WT samples. Each row represents one biological replicate. miRNAs, found to be differentially regulated from E14.5 to E18.5 also in $RYR1^{-/-}$ samples, are underlined in yellow, and in the $Ca_v1.1^{-/-}$ samples – in red. The heatmap was generated from the MAs intensity levels of each of the Mir genes via *ClustVis* (Metsalu & Vilo, 2015). Modified from (Filipova et al., 2018).

Table 16. miRNAs differentially regulated from E14.5 to E18.5 in WT, RYR1$^{-/-}$ and Ca$_v$1.1$^{-/-}$.

Description	Gene Symbol	FC E18.5 vs. E14.5			Muscle-related functions	Reference
		WT	RYR1$^{-/-}$	Ca$_v$1.1$^{-/-}$		
Downregulated miRNAs						
microRNA 1949	Mir1949	-3.25	-	-		
insulin-like growth factor 2 mRNA binding protein 1; microRNA 3063	Igf2bp1	-3.23	-3	-2.43		
protein disulfide isomerase associated 4; microRNA 704	Pdia4	-2.59	-	-		
microRNA 218-1	Mir218-1	-2.58	-	-	involved in muscle-bone communication and Wnt signaling	(Qin et al., 2017)
RIKEN cDNA 5730408K05 gene; microRNA 5136	5730408K05 Rik	-2.1	-	-		
Upregulated miRNAs						
MyoMirs						
microRNA 206	Mir206	2.08	-	-	promotes myoblast entry into terminal differentiation	(Luo et al., 2013)
microRNA 133b	Mir133b	2.73	-	2.12	enhances myoblast proliferation	(Chen et al., 2006)
microRNA 133a-2	Mir133a-2	3.69	-	-	enhances myoblast proliferation	(Chen et al., 2006)
microRNA 1a-2	Mir1a-2	4.01	-	-	positive role in muscle development	(Luo et al., 2013)
microRNA 133a-1	Mir133a-1	5.36	-	2.83	enhances myoblast proliferation	(Chen et al., 2006)
microRNA 1a-1	Mir1a-1	6.29	-	2.32	positive roles in muscle development	(Luo et al., 2013)
miRNAs encoded in the Dlk-Dio3 genomic region						
microRNA 323	**Mir323**	**2.22**	**-**	**-**		
microRNA 668	**Mir668**	**2.32**	**-**	**-**		

Description	Gene Symbol	FC E18.5 vs. E14.5			Muscle-related functions	Reference
		WT	RYR1$^{-/-}$	$Ca_v1.1^{-/-}$		
microRNA 134; miRNA containing gene	Mir134	2.35	-	-	possibly targets *Pax7* and *Myf5*	(Lamon et al., 2017)
microRNA 485; miRNA containing gene	Mir485	2.4	-	-		
microRNA 494	Mir494	2.42	-	-		
microRNA 673	Mir673	2.48	-	2.24		
microRNA 544	Mir544	2.5	-	-		
microRNA 382	Mir382	2.53	-	-	increased in Becker muscular dystrophy	(Fiorillo et al., 2015)
microRNA 666	Mir666	2.55	-	-		
microRNA 539	Mir539	2.58	-	-	dysregulated in DMD dogs	(Jeanson-Leh et al., 2014)
microRNA 541	Mir541	2.71	-	-		
microRNA 381	Mir381	2.9	-	-	implicated in muscle differentiation	(Forterre et al., 2014)
microRNA 487b	Mir487b	2.98	-	-	delays myogenic differentiation in C2C12	(Katase, Terada, Suzuki, Nishimatsu, & Nohno, 2015)
microRNA 431	Mir431	2.98	-	2	promotes differentiation and regeneration of old skeletal muscle	(Wu et al., 2015)
miRNA containing gene; microRNA 410; microRNA 412; microRNA 369	Mirg	3	-	-		
microRNA 409	Mir409	3.17	-	-	upregulated in nemaline myopathy	(Eisenberg et al., 2007)
microRNA 495	Mir495	3.5		2.4		
microRNA 496a	Mir496a	3.51	-	-		

Description	Gene Symbol	FC E18.5 vs. E14.5			Muscle-related functions	Reference
		WT	RYR1$^{-/-}$	$Ca_v1.1^{-/-}$		
microRNA 379	**Mir379**	**3.8**	**-**	**2.28**		
microRNA 411	**Mir411**	**3.8**	**-**	**2.64**	**involved in myogenic proliferation in FSHD and rhabdomyosarcoma**	**(Harafuji, Schneiderat , Walter, & Chen, 2013; Sun et al., 2015)**
microRNA 341	Mir341	2.15	-	-		
microRNA 380	Mir380	2.57	-	-		
microRNA 654	Mir654	2.85	-	-		
microRNA 154	Mir154	3.2	-	-	downregulated by TNF-α in skeletal muscle differentiation	(Meyer et al., 2015)
microRNA 376c	Mir376c	3.35	-	3.34		
microRNA 376b	Mir376b	3.69	-	-	a role in cardioprotection	(Pan et al., 2012)
Other miRNAs implicated in skeletal muscle development						
RIKEN cDNA 6430411K18 gen; microRNA 127; microRNA 433	**6430411K18 Rik**	**2.78**	**-**	**-**	**enhances myogenic cell differentiation**	**(Zhai, Wu, Han, Zhang, & Zhu, 2017)**
microRNA 376a	**Mir376a**	**2.81**	**-**	**-**	**involved in skeletal muscle development**	**(McDaneld et al., 2009)**
microRNA 665	**Mir665**	**2.92**		**2.04**	**associated in secondary myogenesis in pigs**	**(Verardo et al., 2013)**
microRNA 136	**Mir136**	**3.41**	**-**	**-**	**downregulated in mouse skeletal muscle after birth**	**(Lamon et al., 2017)**
microRNA 434	**Mir434**	**3.55**	**-**	**-**	**influences AChR expression in rat hind limb**	**(Shang et al., 2016)**
microRNA 540	**Mir540**	**3.56**	**-**	**2.05**	**induces hypertrophy in C2C12**	**(Hitachi & Tsuchida, 2017)**

Description	Gene Symbol	FC E18.5 vs. E14.5			Muscle-related functions	Reference
		WT	RYR1$^{-/-}$	$Ca_v1.1^{-/-}$		
microRNA 432	Mir432	2.04	-	-	regulates myoblast proliferation and differentiation	(Ren, Liu, Zhao, & Cao, 2016)
microRNA 365-2	Mir365-2	2.04	-	-	putative inhibition of myogenic differentiation in C2C12	(Sun et al., 2011)
microRNA 145a	Mir145a	2.1	-	-	promotes myoblast differentiation	(Du et al., 2016)
microRNA 22; Mir22 host gene (non-protein coding); TLC domain containing 2	Mir22	2.24	-	-	up-regulated during myocyte differentiation	(Huang et al., 2013)
microRNA 5123	Mir5123	2.29	-	-	upregulated in ageing muscle	(Soriano-Arroquia, House, Tregilgas, Canty-Laird, & Goljanek-Whysall, 2016)
miRNAs not yet described in skeletal muscle development						
microRNA 1193	**Mir1193**	**2.01**	**-**	**-**		
microRNA 329	**Mir329**	**2.15**	**-**	**-**		
microRNA 1188	**Mir1188**	**2.16**	**-**	**-**		
microRNA 543	**Mir543**	**2.43**	**-**	**-**		
retrotransposon-like 1; microRNA 3071	**Rtl1**	**3.54**	**-**	**-**		
microRNA 337	**Mir337**	**5.61**	**-**	**3.06**		
microRNA 882	Mir882	2.01	-	-		
microRNA 3070b	Mir3070b	2.81	-	2.01		
microRNA 3070a	Mir3070a	2.83	-	-		
microRNA 370	Mir370	3.02	-	-		

Description	Gene Symbol	FC E18.5 vs. E14.5			Muscle-related functions	Reference
		WT	RYR1$^{-/-}$	Ca$_v$1.1$^{-/-}$		
microRNA 493	Mir493	3.76	-	2.52		
microRNA 568; zinc finger and BTB domain containing 20	Mir568	4.41	2.65	-		
phosphodiesterase 4D interacting protein (myomegalin); microRNA 7225	Pde4dip	4.49	4.1	3.79		
miRNAs found exclusively in RYR1$^{-/-}$ skeletal muscle development (E18.5 vs. E14.5)						
microRNA 125b-1	Mir125b-1	-	-2.11	-	represses myocyte differentiation	(Ge, Sun, & Chen, 2011)
miRNAs found exclusively in Ca$_v$1.1$^{-/-}$ skeletal muscle development (E18.5 vs. E14.5)						
microRNA 205; RIKEN cDNA 4631405K08 gene	Mir205	-	-	-2.38		
microRNA 669d	Mir669d	-	-	-2.07		
glutamate-ammonia ligase (glutamine synthetase); microRNA 8114	Glul	-	-	2.14		
microRNA 130a	Mir130a	-	-	2.28		

miRNAs reported as downregulated in ageing skeletal muscle are written in bold text (Lee et al., 2015b). The FCs of miRNAs not detected as differentially regulated in some of the conditions are marked as "-". Modified from (Filipova et al., 2018).

3.2.4 Minor MRFs expression changes in RYR1$^{-/-}$ and Ca$_v$1.1$^{-/-}$ at E14.5 and E18.5.

Next, putative changes in the expression levels of the canonical MRFs – genes *Six1*, *Six4*, *Pax3*, *Pax7*, *Myf5*, *MyoD*, *MyoG* and *Mrf4* – in the samples from RYR1$^{-/-}$ and Ca$_v$1.1$^{-/-}$ skeletal muscle at E14.5 and E18.5 were examined via qRT-PCRs and compared to WT (Fig. 38). At E14.5 a slight decrease in the expression of *Six1* (0.7-fold of WT) was observed in the RYR1$^{-/-}$ samples and of *Mrf4* (0.33-fold of WT) – in the Ca$_v$1.1$^{-/-}$ samples. *Pax3* exhibited a tendency towards downregulation in the RYR1$^{-/-}$ samples, which was insignificant at E14.5 and gained significance at E18.5. The

expression levels of none of the other MRFs were changed in both mutants at both E14.5 and E18.5. These discrepancies with the previous results showing an upregulation in almost all MRFs in E18.5 RYR1$^{-/-}$ vs. WT (Fig. 21B) might be caused by the different endogenous controls used for both analyses – *Gapdh* and *CytB*. Since the *CytB* gene was found to have a more stable expression across the examined genotypes and developmental stages (Fig. 29) the present data probably reflects more accurately the changes observed in the MRFs expression.

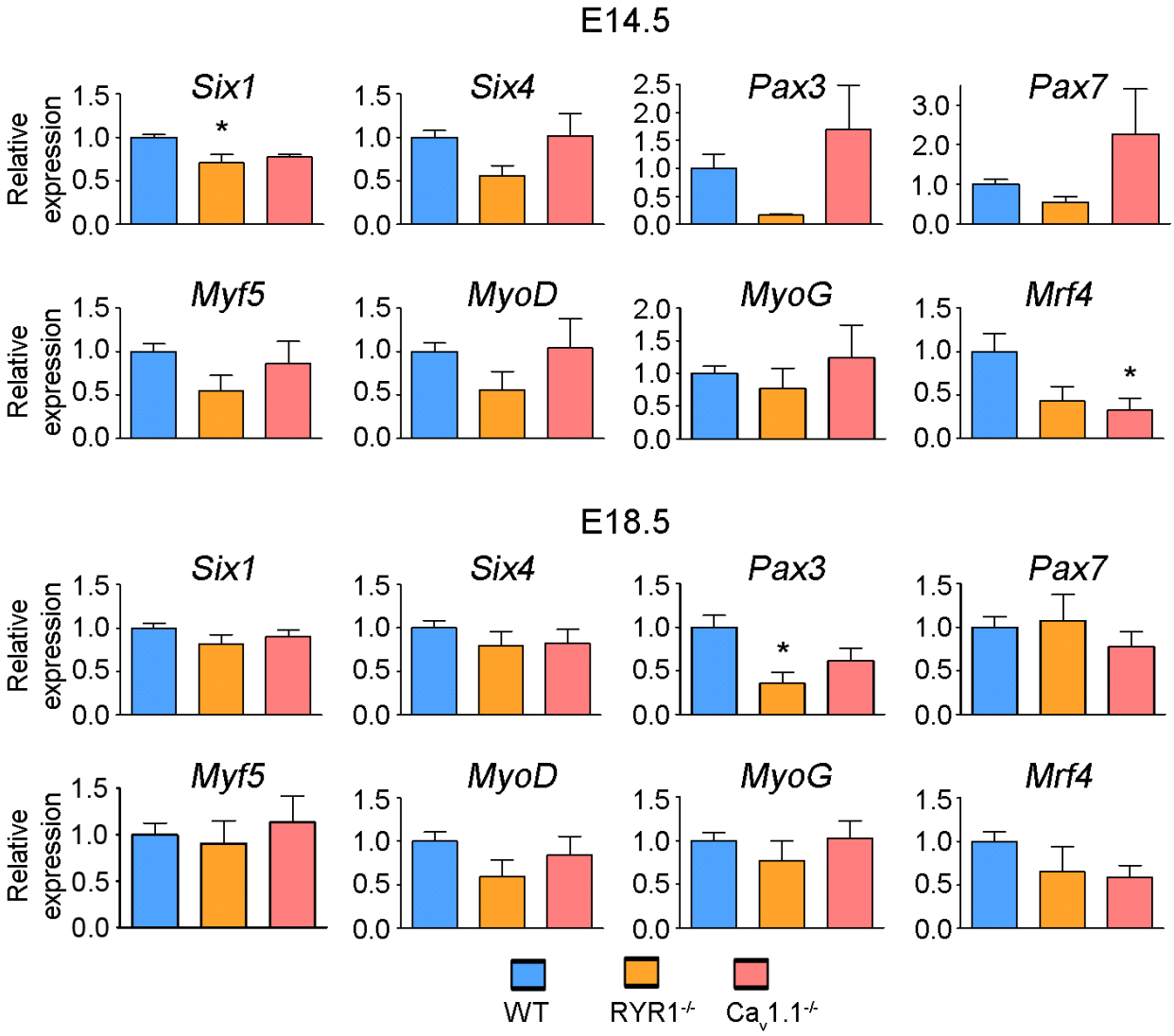

Fig. 38: MRFs expression in limb skeletal muscle from WT, RYR1$^{-/-}$ and Ca$_v$1.1$^{-/-}$ mice at E14.5 and at E18.5. Relative expression levels of *Six1*, *Six4*, *Pax3*, *Pax7*, *Myf5*, *MyoD*, *MyoG* and *Mrf4* in WT, RYR1$^{-/-}$ and Ca$_v$1.1$^{-/-}$ samples (each n = 6) at E14.5 (upper part) and E18.5 (lower part) were obtained by qRT-PCR analyses using *Cytb* as endogenous control. Expression levels of WT samples were set to 1. One-way ANOVA with Bonferroni's Multiple Comparison tests were performed for each gene, *represents a P-value ≤ 0.05. Error bars are S.E.M. Modified from (Filipova et al., 2018).

3.2.5 Attenuated $Ca_v1.1$ isoform-switch at E14.5 and lower $Ca_v1.1$ mRNA levels at E18.5 in $RYR1^{-/-}$ limb skeletal muscle

It has been previously shown that a $Ca_v1.1$ splice variant missing exon 29 ($Ca_v1.1$ Δ29) is highly expressed during embryonic skeletal muscle development and that its expression is gradually attenuated with the myogenic progression, being only weakly expressed at birth and ultimately lost until the third week of postnatal development (Flucher & Tuluc, 2011; Tuluc et al., 2009). Unlike the full length $Ca_v1.1$ that has poor Ca^{2+} conducting properties and predominates in fully differentiated skeletal muscles, the Δ29 $Ca_v1.1$ conducts strong Ca^{2+} currents and has putative roles in the development of the neuromuscular junctions (Flucher & Tuluc, 2011). Thus, changes in the ratio between Δ29 and full length $Ca_v1.1$ might be a factor affecting skeletal muscle development.

To analyze whether this ratio is changed in the samples from $RYR1^{-/-}$ skeletal muscle the region between exons e28 and e32 of the $Ca_v1.1$ mRNA was analyzed via PCRs (Fig. 39A-C). Total mRNA from the limb skeletal muscle of 6 WT and 6 $RYR1^{-/-}$ fetuses at E14.5 and E18.5 was subjected to reverse transcription and the resulting cDNA was used as template in the PCR reactions. The amplification products of the full length $Ca_v1.1$ and the $Ca_v1.1$ Δ29 mRNAs were 343 bp and 286 bp, respectively. The PCR products were visualized on 2% agarose gels, the intensities of the bands in each sample were measured and used for calculation of the relative amount of each splice variant as a percentage of the total $Ca_v1.1$ transcript (Fig. 39C). At E14.5, each splice variant (full length and Δ29) accounted for approximately 50% of the total $Ca_v1.1$ mRNA in WT samples. However, in $RYR1^{-/-}$ samples the amount of the $Ca_v1.1$ Δ29 (70% of the total $Ca_v1.1$) was significantly higher that this of the full length $Ca_v1.1$ (30% of the total $Ca_v1.1$). At E18.5 both WT and $RYR1^{-/-}$ sample groups exhibited higher transcript levels for the full length $Ca_v1.1$ (77% in WT and 69% in $RYR1^{-/-}$). The relative $Ca_v1.1$ expression levels were examined in the $RYR1^{-/-}$ vs. WT samples at E14.5 and E18.5 via qRT-PCRs (Fig. 39D). While at E14.5 there was no significant differences in the expression of $Ca_v1.1$ in the WT and $RYR1^{-/-}$ samples, at E18.5 the $RYR1^{-/-}$ samples exhibited approximately 2-fold lower $Ca_v1.1$ transcript levels than in WT. These results are in agreement with previous studies demonstrating a 2-fold reduced $Ca_v1.1$ protein expression, as well as a strong

decrease of L-type Ca^{2+} current density and charge movements in skeletal muscle from $RYR1^{-/-}$ neonates (Avila, O'Connell, Groom, & Dirksen, 2001; Buck et al., 1997; Nakai et al., 1996).

Thus, the increased $Ca_v1.1$ Δ29 to full length $Ca_v1.1$ at E14.5 and the decreased total $Ca_v1.1$ expression in the $RYR1^{-/-}$ samples may be indicative of an impaired skeletal muscle development. These results also infer possible defects in proper neuromuscular junction formation that might have various downstream effects on the myogenic program.

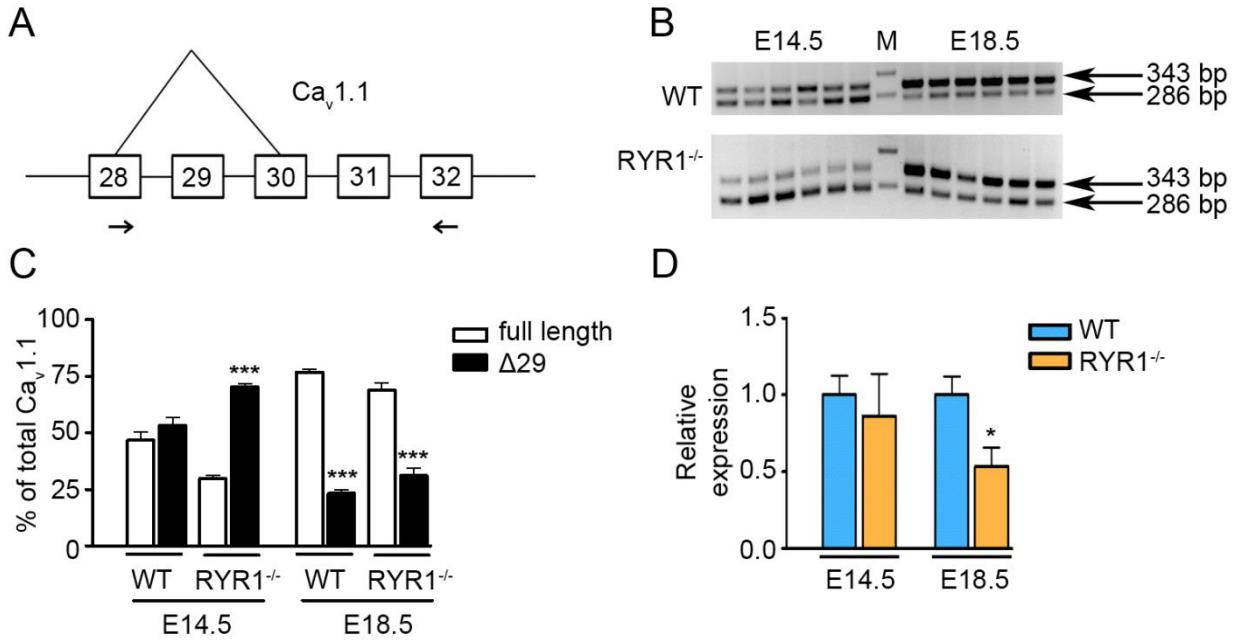

Fig. 39: $Ca_v1.1$ splice variants in WT and $RYR1^{-/-}$ skeletal muscle.
(A) Graphical representation of the genomic exon 29 vicinity of murine full length and Δ29 $Ca_v1.1$ (NCBI Reference Sequence: NM_001081023.1) splice variants. Arrows indicate the primer binding positions used for amplification of exons 28-32. (B) PCR products of the full length (343 bp) and Δ29 (286 bp) $Ca_v1.1$ splice variants from 6 WT and 6 $RYR1^{-/-}$ at each time point (E14.5 and E18.5, n = 6). (C) Full length (343 bp) and Δ29 (286 bp) splice variants as percentage of total $Ca_v1.1$ mRNA in limb skeletal muscle from WT and $RYR1^{-/-}$ animals at E14.5 and E18.5. (D) Relative expression of total $Ca_v1.1$ mRNA measured via qRT-PCR in $RYR1^{-/-}$ vs. WT skeletal muscle at E14.5 and E18.5, using *Cytb* as endogenous control. T-tests were performed for comparison of Δ29 vs. full length splice variants (C) and for WT vs. $RYR1^{-/-}$ (D) in each group; * indicates P-values <0.05 and *** P-values < 0.001; error bars are S.E.M. Modified from (Filipova et al., 2018).

4 Discussion

In the present work I examined how the absence of each of the two Ca^{2+} channels necessary for muscle contraction, RYR1 and $Ca_v1.1$, will affect structure and gene expression of developing limb skeletal muscle on a global scale. In situ, the term skeletal muscle comprises diverse tissues and cell types, the majority of which is devoted to the muscle lineage at different stages of differentiation. Even though myofibers make up most of the mass of the skeletal muscle organ, it also contains fibroblasts, neurons, blood vessels and connective tissue. All of these contribute to muscle organ development, structure and functions. Therefore, it is not only unavoidable, but also desirable to have their transcriptomic impact integrated in the present analysis. This analysis yielded valuable in-depth information about biological processes, signaling pathways and cellular structures that dependent on the presence or on the proper functioning of the two critical components of the ECC machinery, RYR1 and $Ca_v1.1$, throughout skeletal muscle development.

The first part of this work demonstrated that loss of the type 1 ryanodine receptor (RYR1) – the SR Ca^{2+} release unit in ECC – has detrimental effects on skeletal muscle structure at the end of fetal development and of secondary myogenesis – at E18.5 (Filipova et al., 2016). Moreover, RYR1's absence altered the global transcriptomic profile of E18.5 limb skeletal muscle, resulting in over 300 differentially expressed genes (DEGs) identified in a microarray (MA) analysis. Enrichment analysis of these DEGs pointed to their involvement in skeletal muscle's structure and central signaling pathways. Furthermore, the expression of six major myogenic regulatory factors (MRFs) – *Six1*, *Six4*, *Pax7*, *MyoD*, *MyoG* and *Mrf4* – was upregulated, although these results were not reproduced in my succeeding study, using *Cytb* as a reference gene. Thus, RYR1-deficient skeletal muscle is characterized by a distinct transcriptomic signature at E18.5.

The second part of this work compared the structural and transcriptomic alterations caused either by the loss of RYR1 or that of its upstream activator during ECC – $Ca_v1.1$ (Filipova et al., 2018). An analysis of WT ($^{+/+}$), heterozygous ($^{+/-}$) and homozygous ($^{-/-}$) RYR1 and $Ca_v1.1$ fetuses at E14.5 revealed that their absence of either Ca^{2+} channel leads to structural and transcriptomic changes already at the end of primary and the beginning of secondary myogenesis. Interestingly, at E14.5 around twice as many DEGs were found in $Ca_v1.1^{-/-}$ compared to $RYR1^{-/-}$ samples and completely different sets of genes and biological processes were dysregulated in the two mutants (Table 15, Fig. 31). Much more pronounced structural alterations were observed in the $RYR1^{-/-}$ and $Ca_v1.1^{-/-}$ skeletal

muscles at E18.5. At this stage an 8- to 10-fold increase in the total number of DEGs for both mutants was observed, while the number of DEGs remained 2 times higher in $Ca_v1.1^{-/-}$ than in $RYR1^{-/-}$ muscles (Table 15). Moreover, a significant overlap of the differentially regulated gene sets and processes was observed for both mutants (Fig. 32), although some genotype-specific patterns of regulation were still detected (Fig. 33). Furthermore, the overall transcriptome dynamics between the beginning (E14.5) and the end (E18.5) of secondary myogenesis significantly differed in $RYR1^{-/-}$ and $Ca_v1.1^{-/-}$ in comparison to WT skeletal muscle (Fig. 35). This analysis showed that both mutants failed to regulate multiple genes connected to muscle differentiation, structure and signaling. Enrichment analyses of the respective DEGs hinted at altered metabolism, focal adhesion and formation of the musculoskeletal system. Moreover, expression changes of a large set of microRNAs (miRNAs) were observed from E14.5 to E18.5 only in WT, but neither in $RYR1^{-/-}$, nor in $Ca_v1.1^{-/-}$ skeletal muscle. Finally, this thesis demonstrates that these two Ca^{2+} channels exert modulatory effects on one another showing that the absence of RYR1 alters the ratio of $Ca_v1.1$ mRNA splice variants at E14.5, and their total content at E18.5 (Fig. 39). Taken together, these results reveal that RYR1 and $Ca_v1.1$ play complex and in part also divergent roles during secondary skeletal myogenesis.

The impact of RYR1 and $Ca_v1.1$ absence on different aspects of skeletal muscle development are discussed in detail below. Full lists of all DEGs from both gene profiling experiments are available as a "Supplementary Table 1" in the respective publications (Filipova et al., 2016) and (Filipova et al., 2018).

4.1 Divergent effects of the absence of RYR1 and $Ca_v1.1$ in the beginning of secondary myogenesis

At E14.5 – the stage of transition from embryonic to fetal development, as well as from primary to secondary myogenesis, the limb skeletal muscle of $RYR1^{-/-}$ and $Ca_v1.1^{-/-}$ mice already displayed initial structural abnormalities (Fig. 23). Specifically, both mutants exhibited an impaired fascicle organization, as well as smaller, unaligned fibers. Interestingly, active apoptosis at this stage was detected only in the $Ca_v1.1^{-/-}$ skeletal muscle (Fig. 23O). These findings are contrary to earlier observations that necrosis and not apoptosis was responsible for the cell death of extraocular muscles of $Ca_v1.1^{-/-}$ mice at E16.5 (Heimann, Kuschel, & Jockusch, 2004). However, the authors of this study did not report any cell death at E14.5, which might be due to differences in the experimental design

or between extraocular and limb muscles (Sekulic-Jablanovic, Palmowski-Wolfe, Zorzato, & Treves, 2015). Histology of developmentally paralyzed muscle suggests a high degree of fiber degeneration (Gonzalez de Aguilar et al., 2008). Apoptosis is a common, stringently controlled event during normal skeletal muscle development but it also occurs in response to a large variety of factors such as muscle loading or disuse, denervation and ER stress (Nakanishi, Sudo, & Morishima, 2005; Schwartz, 2008). Therefore, the signaling alterations caused by the ablation of ECC-mediated Ca^{2+} release at the onset of muscle contraction, E14.5, probably affect the apoptosis rate in $Ca_v1.1^{-/-}$ skeletal muscle, thus introducing changes in the equilibrium between cellular differentiation, degeneration and regeneration. The observed apoptosis in the present work might be caused by altered signaling due to the lack of Ca^{2+} entry through $Ca_v1.1$ that is not necessary for ECC but which has been implicated in CamKII activation and downstream signaling pathways like MAPK and PI3K/Akt/mTOR (Lee et al., 2015a). This notion is supported by a report that the downregulation of $Ca_v1.1$ from regions on the sarcolemma, different than the T-tubules, that does not impair ECC, leads to skeletal muscle atrophy (Pietri-Rouxel et al., 2010). In addition, at rest $Ca_v1.1$ seems to have a stabilizing effect on RYR1, preventing or minimizing passive Ca^{2+} leak from the SR: Eltit et al. reported higher basal intracellular Ca^{2+} concentrations, $[Ca^{2+}]_i$, in $Ca_v1.1^{-/-}$ cultured myotubes as compared to WT myotubes (Eltit et al., 2011). Hence, a higher $[Ca^{2+}]_i$ could be a contributing factor to the apoptosis observed in $Ca_v1.1^{-/-}$ skeletal muscle.

At E14.5 less than 100 DEGs were detected in the $RYR1^{-/-}$ and $Ca_v1.1^{-/-}$ skeletal muscles compared to WT littermates (Table 15). The modesty of these transcriptomic changes was confirmed by a principal component analysis (PCA), which did not display a significant variance between the global transcriptomic profiles of WTs, homozygous and heterozygous mutants at this stage. Nevertheless, the identified DEGs indicate that RYR1 and $Ca_v1.1$ have important developmental functions already at the beginning of secondary myogenesis. Interestingly, only two DEGs were found both in $RYR1^{-/-}$ and $Ca_v1.1^{-/-}$ vs. WT, suggesting that the absence of each Ca^{2+} channel has distinct effects during early myogenesis at the mRNA level, although the changes in muscle structure observed in both mutants were not very different at this stage. These findings were reflected by the completely different sets of biological processes, identified as significantly affected by the DEGs in each mutant by the Gene Ontology (GO) enrichment analyses (Fig. 31). E14.5 is the stage at which the first limb muscle contractions take place (Kodama & Sekiguchi, 1984). Thus, although the primary roles of RYR1 and $Ca_v1.1$ are related to ECC, the different transcriptomic changes in both mutants at this

early stage imply additional, non-contractile functions of each channel during the myogenic process. The absence of RYR1 seems to negatively regulate multiple processes connected to neurogenesis (Fig. 31A, C). This indicates a possible impairment of proper muscle innervation and of the communication between nerves and skeletal muscle. In $Ca_v1.1^{-/-}$ samples from the same developmental stage, however, a clear downregulation of processes related to muscle contraction had already started (Fig. 31B, D). A possible explanation for these differences between $RYR1^{-/-}$ and $Ca_v1.1^{-/-}$ samples might be that the absence of $Ca_v1.1$ alters Ca^{2+} release from the SR not only through RYR1, but also through the inositol 1,4,5-triphosphate receptor (IP3R). IP3Rs are relatively abundant in non-differentiated muscle fibers (see below), co-reside with RYR1s on the SR membrane and, unlike the fast Ca^{2+} release kinetics of RYR1 in ECC, mediate a so called "slow" Ca^{2+} release, generating cytosolic Ca^{2+} transients that can last tens of seconds but do not trigger muscle contraction (Powell et al., 2001). Rather, the IP3R-mediated slow Ca^{2+} release has been implicated in regulation of gene expression and different signaling pathways related to myogenesis (Carrasco et al., 2003; Juretic et al., 2007). $Ca_v1.1$ is expressed prior to RYR1 in cell culture (Kyselovic, Leddy, Ray, Wigle, & Tuana, 1994) and can activate phospholipase C (PLC), which triggers Ca^{2+} release from the SR via IP3Rs (Eltit et al., 2006). Furthermore, IP3R is highly expressed in mice during early embryonic development and its expression is reduced towards the late myogenic stages, whereas RYR1 expression roughly follows the opposite pattern (Rosemblit et al., 1999). Thus, some of the transcriptomic changes observed in $Ca_v1.1^{-/-}$ muscle could probably be linked to changes in IP3R expression and/or activity.

Another possible reason for the distinct transcriptomic changes in $RYR1^{-/-}$ vs. $Ca_v1.1^{-/-}$ mutants at E14.5 may be ascribed to an altered Ca^{2+} influx from the extracellular space through the embryonic $Ca_v1.1$ Δ29 splice variant. $Ca_v1.1$ Δ29 is highly expressed in early fetal stages and its expression dwindles with the progressing muscle development. It has been implicated in acetylcholine receptor (AChR) pre-patterning of developing skeletal muscle (Flucher & Tuluc, 2011). At E14.5 a higher ratio of Δ29 to full length $Ca_v1.1$ mRNA was observed in $RYR1^{-/-}$ compared to WT skeletal muscle, which might increase the $Ca_v1.1$-mediated Ca^{2+} influx into these muscles upon spontaneous or motor neuron-caused depolarization. In contrast, no $Ca_v1.1$-mediated Ca^{2+} influx can occur in $Ca_v1.1^{-/-}$ muscle, which might also be a reason for the observed genotype-specific expression changes. Nevertheless, a recent study of a mouse model expressing exclusively a non-conducting $Ca_v1.1$ has found no phenotypical, developmental or contractile changes in the skeletal muscle of these animals

(Dayal et al., 2017). Thus, the extent to which changes in the $Ca_v1.1$-mediated Ca^{2+} influx contribute to the transcriptomic changes of $RYR1^{-/-}$ or $Ca_v1.1^{-/-}$ muscles remains unclear.

Surprisingly, structural alterations similar to these in $Ca_v1.1^{-/-}$ and $RYR1^{-/-}$ mice were also observed in heterozygous $Ca_v1.1^{+/-}$ mice (but not in heterozygous $RYR1^{+/-}$ mice) at E14.5 (Fig. 23J, K). This was unexpected since these mice have long been regarded to have no phenotype and have been used as "normal" controls alongside WTs in many studies (Bannister, Papadopoulos, Haarmann, & Beam, 2009; Chaudhari & Beam, 1989; Flucher et al., 1993; Herring & Lakars, 1982). These defects partly persist at E18.5, observed as an incomplete fascicular organization and higher fiber caliber variability in $Ca_v1.1^{+/-}$ skeletal muscle (Fig. 24J, K). Nevertheless, at E18.5 these muscles are far better developed than the ones of homozygous $RYR1^{-/-}$ and $Ca_v1.1^{-/-}$ mutants and an insignificant number of DEGs was detected in $Ca_v1.1^{+/-}$ vs. WT samples at both E14.5 and E18.5. Postnatally $Ca_v1.1^{+/-}$ mice develop normally and do not seem to be impacted by the presence of only a single functional copy of the *Cacna1s* gene (encoding $Ca_v1.1$) with regard to activity, fertility or lifespan. One study, however, describes an impairment of mandible development in $Ca_v1.1^{+/-}$ mice (Atchley, Herring, Riska, & Plummer, 1984). This, together with the severe bone phenotype observed in $Ca_v1.1^{-/-}$ mice at E18.5, suggests that besides triggering ECC, $Ca_v1.1$ might also be implicated in bone development. Thus, it seems that the correct gene dosage of *Cacna1s* could play a wider role during early fetal development. It is possible that reduced levels of the embryonic splice variant $Ca_v1.1\ \Delta29$ in $Ca_v1.1^{+/-}$ mice could be a factor in the formation of this phenotype.

4.2 The effects of the absence of RYR1 and $Ca_v1.1$ converge towards the end of secondary myogenesis

In accordance with the original characterization of $RYR1^{-/-}$ and $Ca_v1.1^{-/-}$ neonates (Buck et al., 1997; Pai, 1965a), this study also reports severe morphological aberrations in both mutants at E18.5, a stage marking the end of fetal development, shortly prior to birth (E19 – E20.5) (Figs. 13 and R22). Histological analysis of the hind limb reveal a terminal prenatal muscle differentiation in WT and $RYR1^{+/-}$ mice (and partially also in $Ca_v1.1^{+/-}$ mice, as discussed above), exhibiting a predominance of differentiated myofibers, organized into fascicles (Figs. 14A and 24A,B,D,E). In contrast, limb skeletal muscle of $RYR1^{-/-}$ and $Ca_v1.1^{-/-}$ mice are represented with features of degeneration and / or impaired development – mainly myotubes were detected and only a few small, unorganized fibers could be seen (Figs. 14B and 24G, H, M, N). Furthermore, fascicle formation was almost completely

absent in both mutants, with the larger volume of extracellular space that might be indicative of fibrosis. At E18.5 no activated caspase-3 was present in any of the analyzed mouse muscles (Fig. 24C, F, I, L, O). This suggests that the higher apoptosis levels detected in $Ca_v1.1^{-/-}$ muscles at E14.5 had declined until E18.5, probably due to the death of all affected cells at an earlier stage.

The severe structural abnormalities of $RYR1^{-/-}$ and $Ca_v1.1^{-/-}$ limb skeletal muscle at E18.5 are accompanied by a remarkable increase in the numbers of detected DEGs in both mutants vs. their WT littermates (Table 15). This indicates that the majority of changes caused by the absence of each of the Ca^{2+} channels occurs during fetal development and thus influences secondary myogenesis. Furthermore, unlike the DEGs detected at E14.5, those detected at E18.5 display a significant overlap in the two mutants – 66.5% of all $RYR1^{-/-}$ DEGs were equal to 31.3% of all $Ca_v1.1^{-/-}$ DEGs. These similarities are recapitulated in the GO enrichment analyses performed for the affected biological processes (BPs) in both mutants, showing that the most significantly affected BPs at the transcriptomic level are the same in $RYR1^{-/-}$ and $Ca_v1.1^{-/-}$ muscle (Fig. 32). Specifically, these are processes mainly related to muscle contraction. In addition, global changes are found in diverse signaling pathways like MAPK, PI3K/Akt/mTOR, Wnt and peroxisome proliferator-activated receptor (PPAR) pathways, as well as cAMP and cGMP-PKG signaling (Suppl. Table 1). The observed similarities are probably due to the absence of mechanotransduction signaling, triggered by muscle contraction in WT mice, as well as to associated Ca^{2+} signaling changes (discussed below). This notion is supported by the fact that spontaneous intrauterine movements in mice begin around E14.5 (Kodama & Sekiguchi, 1984). These results demonstrate that the distinct transcriptomic changes in E14.5 mouse skeletal muscle lacking RYR1 or $Ca_v1.1$ converge at E18.5 (Filipova et al., 2018). Still, some mutant-specific changes were also observed (Figs. 32 and 33). Furthermore, more than twice as many DEGs were found in $Ca_v1.1^{-/-}$ than in $RYR1^{-/-}$ vs. WT samples (Table 15), probably due to an additional impairment of the slow Ca^{2+} release through IP3Rs (as mentioned above, 4.1). The most prominent transcriptomic changes at E18.5 in each of the $RYR1^{-/-}$ and $Ca_v1.1^{-/-}$ mutants or in both, are discussed below.

4.2.1 Severe alterations in the structure of E18.5 skeletal muscle in the absence of RYR1 and $Ca_v1.1$

The absence of RYR1 and $Ca_v1.1$ at E18.5 changes the expression of numerous genes encoding intracellular and extracellular structural proteins that participate in the buildup and composition of

the skeletal muscle organ. As stated above, the most explicit transcriptomic changes found in both mutants affect the muscle's contractile apparatus. Previous analyses indicated that RYR1$^{-/-}$ skeletal muscle expresses major elements of the triadic junction (Buck et al., 1997; Takeshima et al., 1994). However, both MA analyses performed on RYR1$^{-/-}$ skeletal muscle at E18.5 reveal 34 DEGs involved in the formation, organization, structure and function of the muscle contractile machinery (Fig. 33A). Almost all of the 34 genes displayed a lower expression, with the exception of *Ednrb, Chrna1, Chrng, Mb* and *Tnnt2*. Most of these genes were also differentially expressed in the samples from $Ca_v1.1^{-/-}$ skeletal muscle, displaying a total of 41 downregulated and 3 upregulated (*Chrna1, Scn7a, Ednrb*) contraction-related DEGs (Fig. 33A). Functionally these DEGs encode thick (*Myl2, Myh13, Myl9, Myh7, Myl6b*) and thin (*Tpm3, Cnn1, Tnnt2*) filament proteins, M-line proteins (*Myom1, Myom2*), Z-disc proteins (*Csrp3, Rcsd1, Actn2, Tcap*), as well as proteins taking part in the structure of costameres (*Myof, Ankrd1, Ankrd2, Dmd, Sgca, Myot*) and ion channels (*Cacna1h, Kcne1l, Kcnma1, Ryr1, P2rx6, Cacna1s, Cacng1, Kcnq1, Clcn1*). Interestingly, the expression of some of these genes is already changed at E14.5 in $Ca_v1.1^{-/-}$ but not in RYR1$^{-/-}$ samples, indicating the earlier onset of pathological changes in the muscles of $Ca_v1.1^{-/-}$ mutants, as discussed above.

Some of the products of the detected DEGs in RYR1$^{-/-}$ and $Ca_v1.1^{-/-}$ samples at E18.5 have dual functions, like the gene encoding myosin light chain 2 (*Myl2*), which is an essential component of the contraction machinery, as well as a regeneration marker (Sifringer et al., 2004). Regulators of muscle contraction like smoothelin-like 1 (*Smtnl1*), a calmodulin-binding modulator of smooth and skeletal muscle contractility (Ulke-Lemee et al., 2014) and calponin 1 (*Cnn1*), a thin filament-associated protein of muscle contraction that binds tropomyosin and calmodulin and inhibits myosin cross-bridge cycling (Winder et al., 1993), are also downregulated in both RYR1$^{-/-}$ and Ca1.1$^{-/-}$ samples. These results exemplify the perturbed synthesis of contractile proteins in the absence of the ECC-mediating Ca^{2+} channels in limb skeletal muscle. Notably, many of the negatively regulated DEGs encode proteins that localize to the Z-discs of sarcomeres or participate in the formation of costameres, connecting the sarcomeres to the sarcolemma. In addition to their important function related to contraction, these proteins are critical elements of cellular mechanosensing, transmitting the signals induced by mechanical loading between the ECM, the sarcolemma and the myofibrils (Danowski, Imanaka-Yoshida, Sanger, & Sanger, 1992; Frank et al., 2006). They are also connected to signaling cascades contributing to muscle development and hypertrophy like calcineurin/NFAT (nuclear factor of activated T cells), MAPK, PI3K/AKT/mTOR and GPCR-mediated signaling

(Gehlert et al., 2015; Knoll et al., 2011; Tidball, 2005; Yamada, Verlengia, & Bueno Junior, 2012). Moreover, these proteins interact with each other and with the products of other DEGs identified by the MAs, such as the a basic helix-loop-helix transcription factor CLOCK (upregulated in $RYR1^{-/-}$), a key factor in the circadian regulation of gene expression (Schroder & Esser, 2013) and the histone deacetylase HDAC4 (upregulated in $RYR1^{-/-}$ and $Ca_v1.1^{-/-}$), which modulates the Ca^{2+} sensitivity of certain Z-disc proteins, as well as negatively regulates the myogenic program (Knoll et al., 2011; Miska et al., 2001). Thus, the absence of RYR1 and $Ca_v1.1$ also strongly impacts on different hierarchical levels of muscle cell function, structure and organization.

The changes in the $RYR1^{-/-}$ and $Ca_v1.1^{-/-}$ skeletal muscle transcriptomes do not spare the extracellular matrix. ECM structure and composition is crucial for proper muscle formation and differentiation (Fry, Kirby, Kosmac, McCarthy, & Peterson, 2017; Gillies & Lieber, 2011; Hinds, Bian, Dennis, & Bursac, 2011; Yeung et al., 2015; Yi et al., 2017). Both mutants exhibit a dysregulation of multiple ECM protein-coding genes. However, the GO BP enrichment analyses identified more significant ECM organization-related changes in the $RYR1^{-/-}$ samples (Figs. 32 and 33). In them, the downregulation of the *Mfap5, Tnxb, Tnc, Fn1, Adamtsl4* and *Fbn1* genes, encoding ECM proteins involved in microfibrillar assembly and matrix structuring (Bayle et al., 2008; Gabriel et al., 2012; Sabatier et al., 2009; Zweers et al., 2004), suggests an impaired elastic fiber formation. This concept is supported by the repression of *Loxl2* in $RYR1^{-/-}$ muscle, a gene encoding a member of the lysyl oxidases family, proteins which bind and crosslink elastin monomers into an insoluble amorphous tissue (Xiao & Ge, 2012). Conversely, the expression levels of four collagen species (*Col6a5, Col19a1, Col20a1,* and *Col25a1*) are upregulated in samples from $RYR1^{-/-}$ and $Ca_v1.1^{-/-}$ mice. These changes may indicate a shift in the ECM composition towards collagen fibers at the expense of elastic fibers. However, two other collagen-coding DEGs in $RYR1^{-/-}$ samples, Col2a1 and Col12a1, were downregulated. The organization and turnover rate of ECM in skeletal muscle is highly regulated by mechanical loading (Kjaer, 2004). Thus, the paralysis of $RYR1^{-/-}$ and $Ca_v1.1^{-/-}$ skeletal muscle is certainly an important factor in the above-mentioned changes and might contribute to the observed tissue disorganization (Figs. 14 and 24). Nevertheless, it seems that the absence of RYR1 induces additional downstream changes influencing the ECM. It is possible that due to its numerous interactions with other proteins and molecules, RYR1 represents a hub for communication between different signaling pathways, influencing the ECM composition.

Interestingly, the development of the skeleton was also challenged in $Ca_v1.1^{-/-}$ mice. At E18.5 the bones of the hind limbs of these mice consisted of hyaline cartilage with no signs of mineralization (Fig. 24M, N). Previous studies argue that the absence of contraction in $Ca_v1.1^{-/-}$ mice affects tendon, bone and joint development (Blitz et al., 2009; Huang et al., 2015; Kahn et al., 2009). However, since both $RYR1^{-/-}$ and $Ca_v1.1^{-/-}$ mutants are paralyzed, the defects in $Ca_v1.1^{-/-}$ bones cannot be caused by the mere absence of mechanical loading. One possible explanation could be that the absence of $Ca_v1.1$ has downstream effects on the expression, activity or targeting of morphogens and signaling molecules in skeletal muscle that aid ossification and bone mineralization. This hypothesis is partly supported by a study showing that E18.5 $Ca_v1.1^{-/-}$ mice have an incomplete bone ridge formation due to a block of bone morphogenic protein (*Bmp4*) signaling (Blitz et al., 2009). Indeed, the MAs identified *Bmp4* as being 1.9-fold downregulated in $Ca_v1.1^{-/-}$ at E18.5 (S1 Table in (Filipova et al., 2018)). However, the authors argue that BMP4 (the product of *Bmp4*) necessary for bone ridge development originates from the tendons (Blitz et al., 2009), the signal from which can also contribute to the observed *Bmp4* downregulation in the MAs. This implies that either $Ca_v1.1$ is normally also expressed and has functions in the tendons and/or skeleton; or that its absence in skeletal muscle triggers a more intricate downstream cascade of events, resulting in a lower *Bmp4* expression in the tendons.

4.2.2 Absence of RYR1 or $Ca_v1.1$ at E18.5 alters the transcriptomic signature of skeletal muscle metabolism

The high energy demand during muscle contraction is met via the particularly high metabolic capacity of the skeletal muscle organ. As one of the organs with highest plasticity capabilities, skeletal muscle adapts its volume, composition and versatile metabolic pathways according to the levels of contractile activity (Hood, Irrcher, Ljubicic, & Joseph, 2006). Thus, it is not surprising that at E18.5 the muscle paralysis caused by the absence of RYR1 or $Ca_v1.1$ changes the expression levels of many genes related to different metabolic processes. In particular, the results of the MAs indicate that both $RYR1^{-/-}$ and $Ca_v1.1^{-/-}$ skeletal muscles undergo metabolic adaptations related to fatty acids metabolism and β-oxidation (Fig. 34). A particular upregulation of key constituents of these processes was observed in the $Ca_v1.1^{-/-}$ skeletal muscle at E18.5, as exemplified by DEGs from the "Acylglycerol metabolic process" category (Fig. 33C). Among the upregulated DEGs are typical modulators of lipid metabolism like the gene for lipoprotein lipase (*Lpl*) and apolipoprotein E (*Apoe*)

(Huang & Mahley, 2014; Olivecrona, 2016). Furthermore, multiple genes from the peroxisome proliferator-activated receptor (PPAR) signaling pathway are also specifically upregulated only in the $Ca_v1.1^{-/-}$ skeletal muscle at E18.5 (Suppl. Table 1). PPARs are a family of lipid-activated nuclear receptors that regulate the expression and activity of multiple proteins participating in fatty acid metabolism (Desvergne & Wahli, 1999). Pathologic alterations in the PPAR signaling cause changes in skeletal muscle glucose uptake and are associated with insulin resistance and obesity-related diabetes (Finck et al., 2005; Leonardini, Laviola, Perrini, Natalicchio, & Giorgino, 2009). Therefore, the upregulation of the PPAR signaling pathway in the $Ca_v1.1^{-/-}$ mice may induce expression changes related to an increased accumulation of adipose tissue in these muscles. Accordingly, differences in $[Ca^{2+}]_i$ have been implicated in the commitment of progenitor cells either towards the myogenic or to the adipogenic lineage (Sun et al., 2017). Thus, the altered basal $[Ca^{2+}]_i$ resulting from the absence of RYR1 or $Ca_v1.1$ may be directing the metabolism of $RYR1^{-/-}$ and $Ca_v1.1^{-/-}$ skeletal muscle towards an adipogenic fate. The more pronounced effects on metabolic gene regulation in $Ca_v1.1^{-/-}$ skeletal muscles might, once again, be related to the additional inhibition of the IP3R-mediated Ca^{2+} release in these animals.

The DEGs indicating global metabolic alterations in the $RYR1^{-/-}$ and especially in the $Ca_v1.1^{-/-}$ skeletal muscles also suggest changes in mitochondrial biogenesis, content and stability in these muscles. This is not surprising if one considers the important role of Ca^{2+} for mitochondrial (patho)physiology in skeletal muscle (Elustondo, Nichols, Robertson, & Pavlov, 2016; Lundby & Jacobs, 2016). Moreover, mitochondria are important regulators of Ca^{2+} signaling (Rizzuto, De Stefani, Raffaello, & Mammucari, 2012). Furthermore, mitochondria are associated with the ECC Ca^{2+} release units (CRUs) in skeletal muscle in an age- and exercise-dependent manner (Protasi, 2015). In the C2C12 myocyte cell culture, mitochondrial genetic and metabolic stress induces the expression of RYR1 and Ca^{2+}-responsive factors (Biswas et al., 1999). Thus, absence of ECC-mediated Ca^{2+} release in $RYR1^{-/-}$ and $Ca_v1.1^{-/-}$ muscle may cause mitochondrial stress and impair the mitochondrial regulation of myogenesis (Wagatsuma & Sakuma, 2013). Surprisingly, no changes in the mRNA levels were detected for any mitochondrially-encoded proteins in either mutant. This suggests that putative mitochondrial alterations are caused by expression changes in the nuclear-encoded genes or are the result of post-transcriptional modifications.

4.2.3 Changes in global signaling networks: the role of Ca^{2+}

As discussed above, upon membrane depolarization $Ca_v1.1$ triggers a "fast" and a "slow" Ca^{2+} release from RYR1 and IP3R, respectively. Experimental evidence suggests that in myotubes, both the IP3R and RYR1 are involved in Ca^{2+} signaling not immediately related to contraction (Arias-Calderon et al., 2016; Juretic et al., 2007; Witherspoon & Meilleur, 2016). However, it is not clear to what extent the Ca^{2+} signaling functions of the two channels are interwoven: Upon depolarization, primarily IP3R-mediated Ca^{2+} release from the SR of C2C12 myotubes caused long lasting elevation in nuclear $[Ca^{2+}]$, leading to extracellular signal–regulated kinases 1 and 2 (ERK1/2) activation and phosphorylation of the cAMP response element-binding protein (CREB) (Powell et al., 2001). Depolarization of primary myotubes, on the other hand, resulted in reactive oxygen species (ROS) generation, increased ERK1/2 and CREB phosphorylation, as well as increase in mRNA for *c-Fos* and *c-Jun*, and these effects could specifically be blocked by RYR1 inhibition (Espinosa et al., 2006). In this respect, changes in the interplay between the RYR1- and IP3R-mediated Ca^{2+} release could account for the observed downregulation of *c-Fos* and *c-Jun* in specific, and in MAPK-related genes in general, in $RYR1^{-/-}$ skeletal muscle.

$[Ca^{2+}]_i$ in skeletal muscle is characterized by ~100nM resting levels and by its ~100-fold rise upon activation of RYR1 (Berchtold, Brinkmeier, & Muntener, 2000). Increased $[Ca^{2+}]_i$ levels will increase Ca^{2+} binding by calmodulin (CaM), leading to activation of calcineurin and calmodulin kinases II (CAMKII) and IV (CAMKIV), with various effects on downstream signaling (Gehlert et al., 2015). Interestingly, unlike $Ca_v1.1^{-/-}$ primary muscle cells, where the resting $[Ca^{2+}]_i$ is elevated relative to WT, it is ~2-fold lower in $RYR1^{-/-}$ compared to WT myotubes (Eltit et al., 2011; Eltit et al., 2010). Thus, the absence of RYR1 vs. $Ca_v1.1$ is likely to differentially affect the resting-state $[Ca^{2+}]_i$ availability, and thus, to differently change various resting-state Ca^{2+} signaling mechanisms. For instance, the 2.2-fold downregulation of the gene encoding CAMKIIβ, *Camk2b*, in $Ca_v1.1^{-/-}$ but not in $RYR1^{-/-}$ samples at E18.5 could somehow be related to the differences in resting Ca^{2+} (Suppl. Table 1). Since numerous signaling molecules are regulated by phosphorylation (Cardenas et al., 2004; Enslen, Tokumitsu, & Soderling, 1995; Kramer & Goodyear, 2007), changes in CAMKII and CAMKIV activity, resulting in an altered cAMP, cGMP and protein kinases A, C or G (PKA, PKC, PKG) signaling, could contribute to the distinct expression profile of genes in $RYR1^{-/-}$ and $Ca_v1.1^{-/-}$ skeletal muscle. Yet, multiple DEGs participating in all these signaling cascades have been identified in both mutants (Suppl. Table 1). Significant differences in the identified DEGs were observed in

some pathways like mitogen-activated protein kinase (MAPK) pathway. A consistent downregulation of *c-Fos*, *c-Jun*, *Jund* and *Nfatc2*, encoding phosphorylation targets of ERK1/2, JNK and p38 was observed in $RYR1^{-/-}$ samples, but *c-Jun*, *Jund* were not detected as DEGs in $Ca_v1.1^{-/-}$ samples at E18.5, implying more pronounced MAPK signaling changes in $RYR1^{-/-}$ skeletal muscle. Interestingly, *Jund* was downregulated in $Ca_v1.1^{-/-}$ samples at E14.5. The products of *c-Fos*, *c-Jun* and *Jund* take part in the composition of the AP-1 complex, a major transcription factor that can exert either positive or negative functions on muscle development and differentiation, depending on its composition (Andreucci et al., 2002). Thus, some of the differences between the DEGs found in the $RYR1^{-/-}$ and $Ca_v1.1^{-/-}$ samples at E18.5 can be caused by putative changes in the composition of AP-1. At E18.5 multiple DEGs identified only in $Ca_v1.1^{-/-}$ samples encode membrane proteins and ion channels acting upstream of the MAPK cascades. These findings could imply a disturbed regulation of the three central MAPK branches, ERK1/2, JNK and p38, which are activated in a Ca^{2+}-dependent manner (Chuderland & Seger, 2008; Enslen, Tokumitsu, Stork, Davis, & Soderling, 1996). Moreover, all of these are also activated via mechanical stress like cell stretching and play a crucial role in myogenesis (Benavides Damm & Egli, 2014). Furthermore, DEGs identified in both $RYR1^{-/-}$ and $Ca_v1.1^{-/-}$ samples have been shown to be under the influence of p38γ in the context of exercise-induced metabolic adaptation (Pogozelski et al., 2009). Alterations in the activity of p38y in both mutant models are likely to have an impact on mitochondrial biogenesis and oxidative metabolism. In this line of thought, some of the downregulated DEGs in both mutants encode proteins participating in oxidative reactions, like the gene encoding methionine sulfoxide reductase B3 (*Msrb3*), or genes regulated by oxidative stress, like the gene encoding thrombospondin 4 (*Thbs4*). Moreover, the expression of *c-Jun* and *c-Fos* is positively regulated by oxidative stress in a RYR1-dependent manner (Espinosa et al., 2006), further indicating that the absence of RYR1 or RYR1 activation via $Ca_v1.1$ may influence various ROS-sensitive signaling cascades. ROS-mediated signaling furthermore influences the expression and modifications of many contractile proteins, including multiple thick, thin and titin filament proteins (Beckendorf & Linke, 2014), detected as downregulated DEGs in both mutant models at E18.5. Interestingly, the gene encoding myoglobin (*Mb*), a classical oxidative stress response protein, is highly upregulated in $RYR1^{-/-}$ skeletal muscle. This is unexpected in view of the missing mechanical loading in $RYR1^{-/-}$ samples and the observed downregulation of *Nfatc2*, a major activator of *Mb* expression (Wittenberg, 2009). However, an increase of *Mb* expression has been observed in immobilized rat muscles (Lee et al., 2013).

Other signaling pathways, enriched with DEGs in RYR1$^{-/-}$ and Ca$_v$1.1$^{-/-}$ skeletal muscles, like the Wnt and the PI3K/AKT/mTOR pathways (Suppl. Table 1), are also influenced by Ca^{2+} (Drenning et al., 2009; Kohn & Moon, 2005). Factors promoting the Wnt signaling (*Wnt2, Cd44, Fzd10, Tgfb1i1*) were downregulated in RYR1$^{-/-}$ samples at E18.5 (Table 12), whereas *Sfrp1*, an inhibitor of Wnt signaling, was upregulated, suggesting an overall repression of Wnt signaling in RYR1$^{-/-}$ skeletal muscle. Furthermore, in RYR1$^{-/-}$ samples an overexpression was observed for *Nkd1* (Table 12), encoding an intracellular switch which suppresses the canonical and promotes the non-canonical Wnt pathway (Ekici et al., 2010). This may indicate a shift towards the non-canonical pathway in E18.5 RYR1$^{-/-}$ muscle. The downregulation of the non-transforming Wnt ligand gene *Wnt2*, associated with the activation of the non-canonical pathway, is another indication of a dysregulation between the canonical and non-canonical Wnt pathway. A repression of the canonical Wnt pathway suggests inhibition of the Wnt myogenic activity which is mediated mainly through the β-catenin pathway (Yann Fedon, 2012). The Wnt pathway seems to be affected also by the absence of Ca$_v$1.1 (Suppl. Table 1). In E18.5 Ca$_v$1.1$^{-/-}$ samples, the gene *Dkk2*, encoding a member of the dickkopf family – potent inhibitors of the canonical Wnt signaling, was 1.6-fold upregulated. Furthermore, *Dkk2* is a target of different miRNAs and has been shown to regulate the cell cycle and apoptosis (Sun et al., 2016) (Lou, Liu, Zhan, Wang, & Fan, 2016; Mu et al., 2017). The observed Wnt regulation, combined with follistatin (*Fst)* overexpression, might reflect an attempt to prevent negative regulation of muscle mass by myostatin in RYR1$^{-/-}$ and Ca$_v$1.1$^{-/-}$ muscles. A putative shift towards the non-canonical Wnt/calcium pathway in the RYR1$^{-/-}$ muscle might also be a compensatory effect to raise the intracellular Ca^{2+} concentrations via activation of IP3Rs.

The Wnt non-canonical pathway, together with G protein signaling, have been implicated in the activation of the PI3K/Akt/mTOR pathway, involved in increased anabolic activity and in hypertrophy of skeletal muscle (von Maltzahn, Bentzinger, & Rudnicki, 2012). Accordingly, an upregulation of DEGs taking part in the central (*Pik3r1, Akt2*) and late (*Cdkn1a*) stages of this pathway was observed in RYR1$^{-/-}$ samples at E18.5 (Table 12). The PI3K/Akt/mTOR pathway was represented by many more DEGs in the Ca$_v$1.1$^{-/-}$ E18.5 samples (Suppl. Table 1). This observation is probably related to the more prominent metabolic changes (as indicated by the number of the respective DEGs) in muscle samples from Ca$_v$1.1$^{-/-}$ mice.

The Notch and BMP signaling pathways, also involved in the regulation of myogenesis, are represented among the DEGs of RYR1$^{-/-}$ and Ca$_v$1.1$^{-/-}$ at E18.5 to a lesser extent. The upregulation of

Megf10 and *Hes6*, positive regulators of Notch signaling, both of which have been shown to suppress myogenic differentiation (Cossins, Vernon, Zhang, Philpott, & Jones, 2002; Holterman, Le Grand, Kuang, Seale, & Rudnicki, 2007), indicates an impaired terminal differentiation of $RYR1^{-/-}$ skeletal muscle (Table 12).

These findings demonstrate that the crosstalk between many intracellular global signaling pathways is significantly altered in skeletal muscles of $RYR1^{-/-}$ and $Ca_v1.1^{-/-}$ mice. These substantial alterations in signaling are very likely to be causative for the myogenic impairment observed in limb skeletal muscle of these animals.

4.2.4 The effects of paralysis – comparison to other models

As a consequence of EC uncoupling, the $RYR1^{-/-}$ and $Ca_v1.1^{-/-}$ mice are characterized by both a lack of ECC-mediated Ca^{2+}signaling and, consequently, a lack of mechanical movement. The two deficits may have far-reaching consequences, an obvious one being the complete skeletal muscle paralysis of the embryo. Paralysis itself, in turn, impairs the embryonic development of cartilage and bones (Nowlan, Sharpe, Roddy, Prendergast, & Murphy, 2010). The latter leads to neuromuscular degeneration due to the absence of mechanotransduction-associated signaling, which significantly alters global gene expression in skeletal muscle (Rodriguez, Garcia-Alix, Palacios, & Paniagua, 1988; Rolfe et al., 2014). Concomitantly, Ca^{2+} itself is a crucial second messenger in diverse signaling pathways, as discussed above. Thus, the observed phenotype of the $RYR1^{-/-}$ and $Ca_v1.1^{-/-}$ muscle, especially at E18.5, could be a direct effect of missing ECC-dependent Ca^{2+} signaling, a secondary effect due to the lack of mechanotransduction, or most likely – a combination of both. This leads to a dilemma of cause or consequence. To address this problem, the present results are compared to other studies involving models that share the characteristics of paralysis, like denervation, amyotrophic lateral sclerosis (ALS), or toxin-paralyzed models. Although the adult models for neuromuscular degeneration recapitulate many aspects of prenatal paralysis, one should be aware that the (predominantly reactive) processes in differentiated, adult muscle models are not necessarily all homologous to the ones taking place in fetal skeletal muscle. Furthermore, the effects of species-specific differences (e.g. patient-derived samples vs. mouse models) should also be considered.

Multiple typical denervation markers, consisting of genes of the post-synaptic end-plate, are upregulated in the $RYR1^{-/-}$ and $Ca_v1^{-/-}$ mutants at E18.5. Such are the acetylcholine receptor subunit

AChRα (*Chrna1*), upregulated in both RYR1$^{-/-}$ and $Ca_v1.1^{-/-}$ samples; the fetal subunit AChRγ (*Chrng*), upregulated in RYR1$^{-/-}$ samples; and receptor-associated protein of the synapse (*Rapsn*), which is clustered with the nAChR complex and is also upregulated in RYR1$^{-/-}$ samples (Ohno, Sadeh, Blatt, Brengman, & Engel, 2003). In further analogy to paralysis models, the ECM genes, which are responsive to muscle loading and training, tenascin C (*Tnc*) and microfibrillar associated protein 5 (*Mfap5*), were down-regulated in RYR1$^{-/-}$ and $Ca_v1.1^{-/-}$ mice at E18.5 (Irintchev, Salvini, Faissner, & Wernig, 1993; Llano-Diez et al., 2011). Conversely, another ECM gene, coding for collagen type XIXα1 (*Col19a1*), which plays a role in muscle organ development, is up-regulated in both RYR1$^{-/-}$ and $Ca_v1.1^{-/-}$ muscle at E18.5, and is also found to be elevated in ALS and other denervation models (Shtilbans et al., 2011). Shtilbans et al. (2011) further reported an upregulation of the myostatin antagonist follistatin (*Fst*) – also upregulated in both mutants – which is linked to muscle regeneration after injury, mediating myoblast recruitment and subsequent fusion into myotubes (Shtilbans et al., 2011). The upregulation of these genes in RYR1$^{-/-}$ and $Ca_v1.1^{-/-}$ skeletal muscle might result from compensatory mechanisms attempting to counteract the processes leading to the observed muscle degeneration in the mutants.

The transcription factor-coding gene *Runx1* is upregulated in both RYR1$^{-/-}$ and $Ca_v1.1^{-/-}$ skeletal muscle at E18.5 (Table 11; S1 Table in (Filipova et al., 2018)). *Runx1* regulation in the same direction was also observed in skeletal muscle of ALS and other denervation models (Gonzalez de Aguilar et al., 2008). In the context of muscle disuse, *Runx1* upregulation may occur in differentiated muscle fibers and could compensate to a certain extent the lack of muscle movement, preventing muscle wasting, autophagy and myofibrillar disorganization (Wang et al., 2005).

Similar changes were observed in the expression of one cytoskeletal and three contraction-related DEGs, comprising *Tppp* (downregulated in RYR1$^{-/-}$ and $Ca_v1.1^{-/-}$ at E18.5), *Tnnt2* (upregulated in RYR1$^{-/-}$ at E18.5), *Fhl1* and *Myl3* (both downregulated in RYR1$^{-/-}$ at E18.5 and in $Ca_v1.1^{-/-}$ at E14.5 and E18.5) (Loughna, Mason, Bayol, & Brownson, 2000; Petrie, Suneja, Faidley, & Shields, 2014; Saggin, Gorza, Ausoni, & Schiaffino, 1990; Toivonen et al., 2014). The downregulation of *Fhl1* and *Myl3* in $Ca_v1.1^{-/-}$ but not RYR1$^{-/-}$ samples at the early (E14.5) stage implies that their regulation is not exclusively dictated by muscle paralysis. Furthermore, this can indicate that gene expression changes caused by absence of $Ca_v1.1^{-/-}$ occur earlier than those caused by the absence of RYR1$^{-/-}$.

Other DEGs implicated in paralysis and signaling include *Hdac4, Mylk2, Actn3, Mybpc2, Fmod* (in RYR1$^{-/-}$ and $Ca_v1.1^{-/-}$); *Cd44*, *Cdkn1a*, *Lphn3*, *Trib1* and *Sfrp1* (only in RYR1$^{-/-}$); *Eno3*, *Pgam2*, *Asb2*, *Klhl38*, *Fbp2*, *Tcea3* (only in $Ca_v1.1$) (Cohen et al., 2007; de Oliveira et al., 2014; Gonzalez de Aguilar et al., 2008; Qin, Pan, Bauman, & Cardozo, 2010; Shtilbans et al., 2011; Svensson, Norrby, Libelius, & Tagerud, 2008; Uyan et al., 2013). In addition, the expression of *Prr32* gene, encoding a protein named proline rich 32, is increased in muscles from ALS patients and decreased in muscles from multifocal motor neuropathy patients, is also downregulated in $Ca_v1.1^{-/-}$ at E18.5 (Shtilbans et al., 2011). These similarities imply that the missing contraction and respectively, mechanotransduction causes many of the observed transcriptomic changes in the RYR1$^{-/-}$ and $Ca_v1.1^{-/-}$ mutants.

However, some DEGs in the RYR1$^{-/-}$ and $Ca_v1.1^{-/-}$ samples at E18.5 are regulated in the opposite direction compared to the above mentioned models for paralysis and denervation. Such a DEGs is *Ankrd1*, the product of which – ankyrin repeat domain protein 1 – is a member of the titin-N2A mechanosensory complex of the Z-disc (Miller et al., 2003). It participates in the mechanical response to stress and stretching, influencing muscle morphogenesis and remodeling and can also translocate to the nucleus and regulate gene expression (Jeyaseelan et al., 1997). Thus, *Ankrd1* represents a downstream target gene for multiple myogenic regulators like MyoD, MyoG and MEF2 (Blais et al., 2005). Furthermore, it was shown to be a p53 target, as well as an interaction partner of p53 for regulation of downstream expression (Kojic et al., 2010). In different studies, an upregulation of *Ankrd1* was observed in ALS muscle and after denervation (Gonzalez de Aguilar et al., 2008; Shtilbans et al., 2011), whereas a strong downregulation of this gene is found in $Ca_v1.1^{-/-}$ at E14.5 and in both RYR1$^{-/-}$ and $Ca_v1.1^{-/-}$ skeletal muscle at E18.5. However, one study also reported a strong down-regulation of mouse Ankrd1, but only 35 days post denervation (Qin et al., 2010).

The *Tnfrsf12a* transcript, coding for the TWEAK receptor, is upregulated upon denervation (Mittal et al., 2010) but, like *Ankrd1*, is downregulated in RYR1$^{-/-}$ and $Ca_v1.1^{-/-}$ skeletal muscle at E18.5. Both, TWEAK and Ankrd1 are Bcl-3 targets and are repressed by the MAPK p38γ (Pogozelski et al., 2009). Thus, alterations in p38 signaling in the mutants, might be causing the observed expression changes of *Ankrd1* and *Tnfrsf12a* in RYR1$^{-/-}$ and $Ca_v1.1^{-/-}$ mice.

The *Anxa1* gene encodes annexin A1 – a protein binding biological membranes in a Ca^{2+}-dependent manner, that has been implicated in muscle differentiation and regeneration (Bizzarro, Petrella, &

Parente, 2012). While the expression of *Anxa1* was increased in ALS, it is decreased in RYR1$^{-/-}$ skeletal muscle at E18.5.

Deletion or mutations of the gene for prolyl endopeptidase-like, *Prepl*, have been linked to myasthenic disorders at birth, possibly affecting the ACh presynaptic vesicles (Regal et al., 2014), and *Prepl* KO mice exhibit growth impairment and neonatal hypotonia (Lone et al., 2014). *Prepl* was overexpressed in the skeletal muscle of ALS patients (Shtilbans et al., 2011) but interestingly, it is downregulated in Ca$_v$1.1$^{-/-}$ muscles at E14.5 and in both RYR1$^{-/-}$ and Ca$_v$1.1$^{-/-}$ muscles at E18.5. Thus, lower levels of *Prepl* mRNA may be involved in the formation of the RYR1$^{-/-}$ and Ca$_v$1.1$^{-/-}$ phenotype, characterized by smaller body size and reduced skeletal muscle content. Furthermore, the detection of *Prepl* downregulation already at E14.5 in Ca$_v$1.1$^{-/-}$ samples, substantiates the assumption of an earlier onset of pathological muscle alterations in Ca$_v$1.1$^{-/-}$ than in RYR1$^{-/-}$ muscles.

The inhibitor of DNA binding 2 protein (*Id2*) was downregulated in gastrocnemius muscle of a 40-day old presymptomatic ALS mouse model (de Oliveira et al., 2014), but was upregulated both in RYR1$^{-/-}$ and Ca$_v$1.1$^{-/-}$ samples at E18.5 (S1 Table in (Filipova et al., 2018)). *Id2* encodes a myogenic repressor and its upregulation may be responsible for some of the developmental abnormalities observed in the RYR1$^{-/-}$ and Ca$_v$1.1$^{-/-}$ skeletal muscle.

The multiple similarities between gene expression changes in muscles of paralysis models and RYR1$^{-/-}$ and Ca$_v$1.1$^{-/-}$ muscles highlight the great importance of ECC-triggered mechanotransduction for the developing skeletal muscle. As in RYR1$^{-/-}$ and Ca$_v$1.1$^{-/-}$ mice, the skeletal muscles of many of the models above display pathological alteration of muscle structure, myofibrillar disorganization and muscle atrophy. Thus, the DEGs common for both mutants and the paralysis models, might be directly connected to the observed phenotype of RYR1$^{-/-}$ and Ca$_v$1.1$^{-/-}$ skeletal muscles at E18.5. Interestingly, some paralysis-associated DEGs, were found only in one of the mutants. Since both mutants are paralyzed, this would suggest that additional levels govern the expression of these DEGs. However, some differences, especially for the DEGs with low FCs, might also be caused by the technical handling and the dynamic range of the MAs. In addition, the paralysis-related DEGs that were detected in the RYR1$^{-/-}$ or Ca$_v$1.1$^{-/-}$ samples at E14.5, the time point of the first movements in mouse fetuses, might be involved in the early steps of the mechanotransduction-induced signaling and hence, have downstream effects at later developmental stages like E18.5.

4.3 Changes in the developmental transcriptome of RYR1$^{-/-}$ and Ca$_v$1.1$^{-/-}$ mice: effects on secondary myogenesis

The proper spatio-temporal coordination of intra- and extracellular signaling networks is essential for embryonic and fetal development. Hence, the plethora of signaling-related DEGs, detected in RYR1$^{-/-}$ and Ca$_v$1.1$^{-/-}$ limb skeletal muscles, strongly indicates that the observed pathological structural alterations in these muscles are caused by a failure in myogenesis. Accordingly, the first part of this work detected a differential expression of various genes involved in the regulation of satellite cells motility, proliferation and differentiation (*Six1, Six4, Pax7, Sfrp4, Dusp10, Nes, Rgs5, Cav2, Megf10, Hgf, Ptpz1, Aif1, Cnr1*); myoblast differentiation and fusion (*Mfap5, Nov, Dpysl3, Wnt2, Cd44, Nfatc2, Cdkn1a, Hes6, Akt2, Adamtsl2, Hdac4, Fst, Sfrp1, Bai3, Marveld2*) and terminal muscle differentiation (*MyoD, MyoG, Mrf4, Hes6, Csrp3,Bcl6, Fgf6, Nfatc2*) in the limb skeletal muscles of RYR1$^{-/-}$ mice at E18.5 (Supplementary Table1 in (Filipova et al., 2016)). Furthermore, an upregulation was observed for the canonical myogenic regulatory factors (MRFs) *Six1, Six4, Pax7, MyoD, MyoG* and *Mrf4* (Fig. 21), the expression of which (except for *Mrf4*) is attenuated in terminally differentiated skeletal muscle (Bentzinger et al., 2012), pointing to a delay in myogenic development. However, this upregulation could not be reproduced in the second part of this work, analyzing the MRFs expression relative to *Cytb* (Fig. 38). This is probably caused by slight difference in the expression levels of the used endogenous controls – *Gapdh* vs. *Cytb*, the first of which is also developmentally regulated and may be therefore unsuitable for the analysis of developmentally-challenged mutants (Hildyard & Wells, 2014). However, at E18.5, the end of secondary myogenesis, the observed morphological and transcriptomic changes in RYR1$^{-/-}$ and Ca$_v$1.1$^{-/-}$ mice might also be the result of skeletal muscle degeneration in the late stages of fetal development.

In order to examine the putative changes in transcriptome dynamics from the beginning to the end of secondary myogenesis, the global transcriptomic changes occurring between E14.5 and E18.5 (E18.5, test vs. E14.5, control) were analyzed for WT, RYR1$^{-/-}$ and Ca$_v$1.1$^{-/-}$ limb skeletal muscles. These comparisons revealed a higher number of DEGs for WT than for either mutant (Table 15). Thus, a considerable fraction of the DEGs found in the mutants vs. WT at E18.5, might emerge from a failure in the two mutants to activate the normal developmental expression program. Supporting this notion are the processes associated with the DEGs emerging from the E18.5 vs. E14.5

enrichment analyses (Figs. 34, 35, 36). A general analysis of all DEGs in the E18.5 vs. E14.5 comparisons suggests that in all three genotypes – WT, RYR1$^{-/-}$ and Ca$_v$1.1$^{-/-}$ an induction of differential regulation connected to muscle contraction takes place (Fig. 34). However, the same analysis also indicates that myogenic and contractile processes like "Muscle organ development" and "Myofibril assembly", as well as processes related to DNA replication and the cell cycle, were preferentially regulated in the WTs, but not in the mutants, indicated an incomplete developmental progression in the mutants. On the other hand, more significant changes related to fatty acids metabolism and β-oxidation were observed in both mutants, and especially in the Ca$_v$1.1$^{-/-}$ (Fig. 34), which is in line with the observed metabolic changes in Ca$_v$1.1$^{-/-}$ muscles at E18.5. These differences clearly stand out in the analyses of the WT, RYR1$^{-/-}$ and Ca$_v$1.1$^{-/-}$ specific DEGs in the E18.5 vs. E14.5 analyses (Figs. 35 and 36). Specifically, multiple genes involved in the cell cycle control (*Prim2, Ccnd2, Mcm7, Cdk4, Mcm2, Plk1, Mad2l1*) were downregulated only in WT samples – a typical sign for terminal differentiation. The failure of RYR1$^{-/-}$ and Ca$_v$1.1$^{-/-}$ skeletal muscles to downregulate these genes is an indication of a disturbed terminal muscle differentiation. Furthermore, many cellular compartments (CCs) related to the buildup of the contractile machinery like the sarcolemma, costameres, sarcomeres and I-band are differentially regulated only in the WTs from E14.5 to E18.5 (Fig. 36). These findings are supported by the detection of contraction-related DEGs upregulated from E14.5 to E18.5 exclusively in the WTs samples; or to be upregulated with a much smaller FC in the mutants like *Mybpc2*, *Ckmt2*, *Myh2*, *Myh4* and *Mylk2* (S1 Table in (Filipova et al., 2018)). These observations strongly imply that the secondary myogenesis, normally involving an increased level and organization of contractile structures, and accompanied by the exit from the cell cycle during fetal development, is impaired in RYR1$^{-/-}$ and Ca$_v$1.1$^{-/-}$ limb skeletal muscle.

Various differentiation-related processes were affected by the RYR1$^{-/-}$ specific DEGs in the E18.5 vs. E14.5 analyses (Figs. 35 and 36), further suggesting that the absence of RYR1 leads to changes in the global developmental program. Most of the affected cellular processes and structures were related to bone, cartilage and neuron differentiation, focal adhesion and ion channels. Interestingly, several processes related to ossification, were detected as significantly enriched with RYR1$^{-/-}$- and not with Ca$_v$1.1$^{-/-}$-specific DEGs (Figs. 35 and 36). A possible reason for this might be compensatory paralysis-triggered processes that could not be set in action in the Ca$_v$1.1$^{-/-}$ skeletal muscles.

The DEGs specific for the fetal development of Ca$_v$1.1$^{-/-}$ muscles these were predominantly associated with processes linked to adipogenesis and lipid metabolism (Figs. 35 and 36). Thus, the

elevation of the expression levels of lipid-metabolism in $Ca_v1.1^{-/-}$ vs. WT muscles at E18.5 (Fig. 33C) seems to be a result of an active developmental upregulation of these genes in the $Ca_v1.1^{-/-}$ mutants. The higher $[Ca^{2+}]_i$ in $Ca_v1.1^{-/-}$ compared to WT and $RYR1^{-/-}$ myotubes due to a higher rate of RYR1-mediated passive Ca^{2+} leak from the SR (Eltit et al., 2011; Eltit et al., 2010) may be the cause of some of these $Ca_v1.1^{-/-}$ specific expression changes during secondary myogenesis. These changes suggest significant alterations in the mitochondrial Ca^{2+} content, and hence also in their functions, volume or stability in the muscles of these animals. Accordingly, the increased mitochondrial Ca^{2+} and decreased SR Ca^{2+} content have been implicated in mitochondrial myopathy, arguing that higher mitochondrial Ca^{2+} concentrations can stimulate metabolic events but in the same time can trigger cell damage (Aydin et al., 2009). Thus, a mitochondrial Ca^{2+} overload might be the cause of the observed apoptosis in the skeletal muscle of $Ca_v1.1^{-/-}$ mice at E14.5, and lipotoxicity might also be a contributing factor (Akhmedov & Berdeaux, 2013). Furthermore, an upregulation of the paralysis hallmarks *Musk*, *Chrnd* and *Chrng*, is detected only during development of $RYR1^{-/-}$ skeletal muscle. Reduced $[Ca^{2+}]_i$ in $RYR1^{-/-}$ and increased $[Ca^{2+}]_i$ in $Ca_v1.1^{-/-}$ muscles can explain this observation, as these genes are negatively regulated by increased $[Ca^{2+}]_i$ and in turn regulate proper neuromuscular synaptic pre-patterning (Chen et al., 2011).

At least 61 miRNAs are differentially expressed in WT limb skeletal muscle from E14.5 to E18.5 (Fig. 37, Table 16). Only 3 of these miRNAs undergo a parallel regulation in $RYR1^{-/-}$ and 16 miRNAs – in $Ca_v1.1^{-/-}$ skeletal muscle from E14.5 to E18.5 (Table 16). In addition, one miRNA (Mir125b-1, downregulated) was found exclusively in $RYR1^{-/-}$ and four (Mir205, Mir669d, Glul and Mir130a) – in $Ca_v1.1^{-/-}$ muscles in the course of secondary myogenesis. Mir125b-1 is a negative regulator of myoblast differentiation and its levels decline with progression of the myogenic program (Ge et al., 2011). Classically, miRNAs function as potent regulators of gene expression in general and of muscle differentiation, in particular (Goljanek-Whysall, Sweetman, & Munsterberg, 2012). Therefore, the altered miRNA developmental patterns in $RYR1^{-/-}$ and $Ca_v1.1^{-/-}$ limb skeletal muscle are likely to have contributed to the observed transcriptomic changes. The vast majority of differentially expressed miRNAs identified in the WT showed an upregulation at E18.5 vs. E14.5. Among the upregulated miRNAs are six of the MyoMirs (Mir206, Mir133b, Mir133a-1, Mir133a-2, Mir1a-1 and Mir1a-2), named after their pivotal role in muscle development and differentiation (Luo et al., 2013). The expression of all of them is regulated by the late MRFs MyoD and myogenin, as well as by other myogenic TFs like the myocyte enhancer factor 2 (MEF-2) (Luo et al., 2013). None

of the MyoMirs were significantly upregulated in the development of RYR1$^{-/-}$ skeletal muscle from E14.5 to E18.5. In Ca$_v$1.1$^{-/-}$ only Mir133b, Mir133a-1 and Mir1a-1 were developmentally upregulated, all of which exhibit a lower FC than in WT. Furthermore, both Mir133b and Mir133a-1 suppress differentiation and promote myoblast proliferation (Chen et al., 2006; Luo et al., 2013). The MyoMirs of the Mir1 and Mir206 families have opposing actions, promoting terminal muscle differentiation by targeting HDAC4, an inhibitor of MEF2 expression, as well as of muscle differentiation and growth (Luo et al., 2013). However, these two miRNAs do not show functional redundancy, as they cannot replace each other (Luo et al., 2013). Although Mir1a-1 is 2.3-fold upregulated in Ca$_v$1.1$^{-/-}$ samples from E14.5 to E18.5, it is 6.3-fold upregulated in WT samples in the same period. Accordingly, Mir1a-1 is 3.3-fold downregulated in Ca$_v$1.1$^{-/-}$ vs. WT samples at E18.5. Insufficient action of Mir1 and Mir206 is also suggested by the upregulation of *Hdac4* in both RYR1$^{-/-}$ and Ca$_v$1.1$^{-/-}$ skeletal muscle at E18.5. Additionally, multiple other miRNAs that were implicated in the regulation of muscle development and differentiation were only upregulated in WT skeletal muscle during secondary myogenesis (Table 16). Thus, a global failure of the RYR1$^{-/-}$ and Ca$_v$1.1$^{-/-}$ skeletal muscle to induce a physiological upregulation of this multitude of miRNAs is very probably causing many of the transcriptional changes observed in these muscles at E18.5.

Interestingly, more than half of the miRNAs upregulated in the WT E18.5 vs. E14.5 comparison are also downregulated in ageing skeletal muscle (Table 16) (Lee et al., 2015b), suggesting important and dynamic roles for these miRNAs in myogenesis and in skeletal muscle maintenance. In this respect, the *Dlk-Dio3* genomic region – a miRNA megacluster encoding more than 50 miRNAs – appears to be of eminent importance (Glazov, McWilliam, Barris, & Dalrymple, 2008): 26 of the developmentally upregulated miRNAs found in WT skeletal muscle originate from this region (Table 16). Reduced expression of miRNAs from the *Dlk-Dio3* cluster has been implicated in the ageing process in gastrocnemius muscles (Kim et al., 2014), and myostatin deficiency has been shown to lead to a transcriptional activation of this locus (Hitachi & Tsuchida, 2017). Only 6 of the miRNAs from the *Dlk-Dio3* genomic locus upregulated in WT (E18.5 vs. E14.5) are also upregulated in Ca$_v$1.1$^{-/-}$ muscle, and none in RYR1$^{-/-}$ muscle (Table 16). These findings suggest that the increased expression level of multiple miRNAs from the *Dlk-Dio3* genomic region is a significant contributor to secondary myogenesis and that muscle contraction and ECC-mediated Ca^{2+} release probably drives their expression. All of these results highlight novel important roles for RYR1 and Ca$_v$1.1 in

the regulation of gene expression via an intricate network of signaling cascades during secondary myogenesis.

4.4 Putative similarities to RYR1- and $Ca_v1.1$-linked diseases

As main components of the ECC apparatus in skeletal muscle, multiple mutations in the genes of RYR1 and $Ca_v1.1$ have been associated with a range of diseases and neuromuscular disorders, often described as channelopathies, including malignant hyperthermia (MH) and hypokalemic periodic paralysis type 1 (HPP-1) (Cannon, 2015; Robinson, Carpenter, Shaw, Halsall, & Hopkins, 2006; Striessnig et al., 2010). Furthermore, a wide range of *Ryr1* (the gene encoding RYR1) mutations cause different congenital myopathies, the majority of which have an early onset – at birth, during infancy or childhood (Jungbluth et al., 2018). Autosomal dominant *Ryr1* mutations are associated with diverse core myopathies – a class of congenital myopathies, characterized by the presence of "cores" of reduced oxidative activity in skeletal muscle fibers (Snoeck et al., 2015). In addition, sarcomere disorganization and mitochondrial depletion are often observed in muscles from these patients. Two of the more prominent core myopathies caused by *Ryr1* mutations are central core disease (CCD) and multiminicore disease (MmD), commonly associated with malignant hyperthermia (MH) susceptibility (Robinson et al., 2006; Snoeck et al., 2015). Recently, mutations in *Cacna1s* (the gene encoding $Ca_v1.1$) have been linked to similar pathological alterations in patients with a so-called CACNA1S congenital myopathy (Schartner et al., 2017).

The complete absence of $Ca_v1.1$ or RYR1 in the homozygous mutant ($^{-/-}$) mice leads to EC uncoupling and perinatal lethality accompanied by abnormal alterations in muscle phenotype indicative of muscle degeneration (Figs. 13, 14, 23 and 24). Similarly, severe mutations leading to the functional abolishment of RYR1 have been linked to lethal multiple pterygium syndrome – a disease characterized by fetal akinesia and death *in utero* (Kariminejad et al., 2016; McKie et al., 2014). Ultrastructure studies of these skeletal muscles have revealed a myofibrillar disarray, loss of fibers and fibrosis, similar to the phenotype observed in $RYR1^{-/-}$ and $Ca_v1.1^{-/-}$ skeletal muscle at E18.5 (McKie et al., 2014). Hence, the transcriptomic changes in the muscle of $RYR1^{-/-}$ and $Ca_v1.1^{-/-}$ mice may be reconstituted to a different degree in patients carrying various mutations in the *Ryr1* and *Cacna1s* genes. If this is the case, the present analysis might aid future development of pharmaceuticals and therapies aiming to alleviate the symptoms of the respective RYR1- and $Ca_v1.1$-linked channelopathies.

4.5 Conclusions and outlook

In conclusion, this work provides the first extensive analysis of the global transcriptomic changes occurring in developing murine limb skeletal muscle in the absence of RYR1 or $Ca_v1.1$. As essential ECC components these two channels act as a team – $Ca_v1.1$ senses membrane depolarization and transmits this signal to RYR1 that in turn releases Ca^{2+} from the SR into the cytosol, resulting in muscle contraction. However, the present work suggests discrete roles of each channel for skeletal muscle gene expression and development, as observed by the consequences of their complete absence.

The loss of RYR1 or $Ca_v1.1$ causes morphological alterations in skeletal muscle already at E14.5 – the period of transition from primary to secondary myogenesis. These changes are accompanied by elevated levels of apoptosis in the $Ca_v1.1^{-/-}$ but not in the $RYR1^{-/-}$ limb skeletal muscle. Furthermore, at E14.5 the RYR1- and $Ca_v1.1$-deficient skeletal muscles are characterized by distinct transcriptomic changes, affecting neuronal development and innervation in $RYR1^{-/-}$ muscles, and muscle contraction – in $Ca_v1.1^{-/-}$ muscles. The ability of RYR1 and $Ca_v1.1$ to modulate each other's functions is demonstrated by the change of the Δ29 to full length $Ca_v1.1$ ratio in $RYR1^{-/-}$ muscle at E14.5 and by the 2-fold downregulation of total $Ca_v1.1$ mRNA in these samples at E18.5.

At E18.5, the end of secondary myogenesis and prenatal development in mice, the absence of RYR1 and $Ca_v1.1$ causes severe morphological abnormalities of skeletal muscle, as well as of the gross body appearance of $RYR1^{-/-}$ and $Ca_v1.1^{-/-}$ fetuses. The limb skeletal muscle of these animals is characterized by an impaired fascicle formation, a predominance of small, unaligned fibers, and an overall degeneration. Additionally, the bone development is disturbed in $Ca_v1.1^{-/-}$ fetuses. Microarray analyses identified an 8- to 10-fold increase in the number of DEGs in limb skeletal muscles of both mutants at E18.5. Moreover, at this stage the global transcriptomic changes in $RYR1^{-/-}$ and $Ca_v1.1^{-/-}$ skeletal muscle partially converge while still presenting with characteristic transcriptomic signatures, differing from those of WT muscles. Multiple genes involved in skeletal muscle contraction and in the buildup of the contractile machinery are downregulated while global signaling pathways like the MAPK, Wnt and PI3K/Akt/mTOR are markedly represented among the DEGs in both mutants. Mutant-specific transcriptomic changes suggest a shift of the ECM composition in $RYR1^{-/-}$ and an upregulation of fatty acid metabolism and adipogenesis in $Ca_v1.1^{-/-}$ skeletal muscle. Interestingly, a mild phenotype was observed in the morphological but not in the transcriptomic analysis of

heterozygous $Ca_v1.1^{+/-}$ skeletal muscle at both E14.5 and E18.5. This would suggest that the precise *Cacna1s* gene dosage may also be important for skeletal muscle development.

The RYR1 and $Ca_v1.1$ absence induces significant changes in the transcriptomic dynamics of skeletal muscle from the beginning (E14.5) to the end (E18.5) of secondary myogenesis. The transcriptomic development of $RYR1^{-/-}$ and $Ca_v1.1^{-/-}$ muscles in this period suggests that both mutants fail to exit the cell cycle and to appropriately upregulate the synthesis of components for the contractile machinery. Impaired Ca^{2+} signaling and lack of mechanotransduction are probably responsible for the majority of the observed transcriptomic changes. A profound differential regulation of miRNAs in WT but not in $RYR1^{-/-}$ and $Ca_v1.1^{-/-}$ muscles between E14.5 and E18.5 suggests that changes in the miRNA-mediated gene regulation are involved in the formation of the $RYR1^{-/-}$ and $Ca_v1.1^{-/-}$ transcriptomic signature.

Taken together, these results reveal that RYR1 and $Ca_v1.1$ play complex and partially discrete roles throughout secondary myogenesis in limb skeletal muscle. Future research should analyze the extent to which the observed transcriptomic changes are recapitulated on a proteomic level. A targeted analysis of the individual signaling pathways affected in both mutants will aid the elucidation of the precise molecular mechanisms behind the RYR1- and $Ca_v1.1$-mediated regulation of muscle organ development. Finally, a more in-depth analysis of the differentially regulated genes and processes, occurring during secondary myogenesis in WT skeletal muscle, will provide a valuable reference for the studies of the developmental changes caused by various treatments, mutations or diseases of the skeletal muscle organ.

5 References

Abmayr, S. M., & Pavlath, G. K. 2012. Myoblast fusion: lessons from flies and mice. ***Development***, 139(4): 641-656.

Adams, B. A., Tanabe, T., Mikami, A., Numa, S., & Beam, K. G. 1990. Intramembrane charge movement restored in dysgenic skeletal muscle by injection of dihydropyridine receptor cDNAs. ***Nature***, 346(6284): 569-572.

Agbulut, O., Noirez, P., Beaumont, F., & Butler-Browne, G. 2003. Myosin heavy chain isoforms in postnatal muscle development of mice. ***Biol Cell***, 95(6): 399-406.

Agrawal, G., Aung, A., & Varghese, S. 2017. Skeletal muscle-on-a-chip: an in vitro model to evaluate tissue formation and injury. ***Lab Chip***, 17(20): 3447-3461.

Akhmedov, D., & Berdeaux, R. 2013. The effects of obesity on skeletal muscle regeneration. ***Front Physiol***, 4: 371.

Al-Qusairi, L., & Laporte, J. 2011. T-tubule biogenesis and triad formation in skeletal muscle and implication in human diseases. ***Skelet Muscle***, 1(1): 26.

Allen, E. R., & Pepe, F. A. 1965. Ultrastructure of Developing Muscle Cells in the Chick Embryo. ***Am J Anat***, 116: 115-147.

Andreucci, J. J., Grant, D., Cox, D. M., Tomc, L. K., Prywes, R., Goldhamer, D. J., Rodrigues, N., Bedard, P. A., & McDermott, J. C. 2002. Composition and function of AP-1 transcription complexes during muscle cell differentiation. ***J Biol Chem***, 277(19): 16426-16432.

Araya, R., Liberona, J. L., Cardenas, J. C., Riveros, N., Estrada, M., Powell, J. A., Carrasco, M. A., & Jaimovich, E. 2003. Dihydropyridine receptors as voltage sensors for a depolarization-evoked, IP3R-mediated, slow calcium signal in skeletal muscle cells. ***J Gen Physiol***, 121(1): 3-16.

Argiles, J. M., Campos, N., Lopez-Pedrosa, J. M., Rueda, R., & Rodriguez-Manas, L. 2016. Skeletal Muscle Regulates Metabolism via Interorgan Crosstalk: Roles in Health and Disease. ***J Am Med Dir Assoc***, 17(9): 789-796.

Arias-Calderon, M., Almarza, G., Diaz-Vegas, A., Contreras-Ferrat, A., Valladares, D., Casas, M., Toledo, H., Jaimovich, E., & Buvinic, S. 2016. Characterization of a multiprotein complex involved in excitation-transcription coupling of skeletal muscle. ***Skelet Muscle***, 6: 15.

Armant, O., Gourain, V., Etard, C., & Strahle, U. 2016. Whole transcriptome data analysis of zebrafish mutants affecting muscle development. ***Data Brief***, 8: 61-68.

Armstrong, C. M., Bezanilla, F. M., & Horowicz, P. 1972. Twitches in the presence of ethylene glycol bis(-aminoethyl ether)-N,N'-tetracetic acid. ***Biochim Biophys Acta***, 267(3): 605-608.

Arnold, S. J., & Robertson, E. J. 2009. Making a commitment: cell lineage allocation and axis patterning in the early mouse embryo. ***Nat Rev Mol Cell Biol***, 10(2): 91-103.

Aronsen, J. M., Swift, F., & Sejersted, O. M. 2013. Cardiac sodium transport and excitation-contraction coupling. ***J Mol Cell Cardiol***, 61: 11-19.

Asfour, H. A., Allouh, M. Z., & Said, R. S. 2018. Myogenic regulatory factors: The orchestrators of myogenesis after 30 years of discovery. ***Exp Biol Med (Maywood)***, 243(2): 118-128.

Atchley, W. R., Herring, S. W., Riska, B., & Plummer, A. A. 1984. Effects of the Muscular Dysgenesis Gene on Developmental Stability in the Mouse Mandible. ***J Craniofac Genetic Dev Biol***, 4(3): 179-189.

Autieri, M. V., Kelemen, S. E., & Wendt, K. W. 2003. AIF-1 is an actin-polymerizing and Rac1-activating protein that promotes vascular smooth muscle cell migration. ***Circ Res***, 92(10): 1107-1114.

Avila, G., & Dirksen, R. T. 2000. Functional impact of the ryanodine receptor on the skeletal muscle L-type Ca(2+) channel. ***J Gen Physiol***, 115(4): 467-480.

Avila, G., O'Connell, K. M., Groom, L. A., & Dirksen, R. T. 2001. Ca2+ release through ryanodine receptors regulates skeletal muscle L-type Ca2+ channel expression. ***J Biol Chem***, 276(21): 17732-17738.

Aydin, J., Andersson, D. C., Hanninen, S. L., Wredenberg, A., Tavi, P., Park, C. B., Larsson, N. G., Bruton, J. D., & Westerblad, H. 2009. Increased mitochondrial Ca2+ and decreased sarcoplasmic reticulum Ca2+ in mitochondrial myopathy. ***Hum Mol Genet***, 18(2): 278-288.

Bang, M. L., Caremani, M., Brunello, E., Littlefield, R., Lieber, R. L., Chen, J., Lombardi, V., & Linari, M. 2009. Nebulin plays a direct role in promoting strong actin-myosin interactions. ***Faseb J***, 23(12): 4117-4125.

Bannister, R. A., & Beam, K. G. 2013. Ca(V)1.1: The atypical prototypical voltage-gated Ca(2)(+) channel. ***Biochim Biophys Acta***, 1828(7): 1587-1597.

Bannister, R. A., Papadopoulos, S., Haarmann, C. S., & Beam, K. G. 2009. Effects of inserting fluorescent proteins into the alpha1S II-III loop: insights into excitation-contraction coupling. ***J Gen Physiol***, 134(1): 35-51.

Barnard, R. J., Edgerton, V. R., Furukawa, T., & Peter, J. B. 1971. Histochemical, biochemical, and contractile properties of red, white, and intermediate fibers. ***Am J Physiol***, 220(2): 410-414.

Bartel, D. P. 2004. MicroRNAs: genomics, biogenesis, mechanism, and function. ***Cell***, 116(2): 281-297.

Bartoo, M. L., Linke, W. A., & Pollack, G. H. 1997. Basis of passive tension and stiffness in isolated rabbit myofibrils. ***Am J Physiol***, 273(1 Pt 1): C266-276.

Bayle, J., Fitch, J., Jacobsen, K., Kumar, R., Lafyatis, R., & Lemaire, R. 2008. Increased expression of Wnt2 and SFRP4 in Tsk mouse skin: role of Wnt signaling in altered dermal fibrillin deposition and systemic sclerosis. ***J Invest Dermatol***, 128(4): 871-881.

Beam, K. G., & Bannister, R. A. 2010. Looking for answers to EC coupling's persistent questions. ***J Gen Physiol***, 136(1): 7-12.

Beam, K. G., Knudson, C. M., & Powell, J. A. 1986. A lethal mutation in mice eliminates the slow calcium current in skeletal muscle cells. ***Nature***, 320(6058): 168-170.

Beckendorf, L., & Linke, W. A. 2014. Emerging importance of oxidative stress in regulating striated muscle elasticity. ***J Muscle Res Cell Motil***, 36(1):25-36.

Beeson, D., Jeremiah, S., West, L. F., Povey, S., & Newsom-Davis, J. 1990. Assignment of the human nicotinic acetylcholine receptor genes: the alpha and delta subunit genes to chromosome 2 and the beta subunit gene to chromosome 17. ***Ann Hum Genet***, 54(Pt 3): 199-208.

Benavides Damm, T., & Egli, M. 2014. Calcium's role in mechanotransduction during muscle development. ***Cell Physiol Biochem***, 33(2): 249-272.

Bentzinger, C. F., Wang, Y. X., & Rudnicki, M. A. 2012. Building muscle: molecular regulation of myogenesis. ***Cold Spring Harb Perspect Biol***, 4(2): a008342.

Berchtold, M. W., Brinkmeier, H., & Muntener, M. 2000. Calcium ion in skeletal muscle: its crucial role for muscle function, plasticity, and disease. ***Physiol Rev***, 80(3): 1215-1265.

Berkes, C. A., & Tapscott, S. J. 2005. MyoD and the transcriptional control of myogenesis. ***Seminars Cell & Dev Biol***, 16(4-5): 585-595.

Bertocchini, F., Ovitt, C. E., Conti, A., Barone, V., Scholer, H. R., Bottinelli, R., Reggiani, C., & Sorrentino, V. 1997. Requirement for the ryanodine receptor type 3 for efficient contraction in neonatal skeletal muscles. ***EMBO J***, 16(23): 6956-6963.

Bezanilla, F. 2000. The voltage sensor in voltage-dependent ion channels. ***Physiol Rev***, 80(2): 555-592.

Biressi, S., Molinaro, M., & Cossu, G. 2007a. Cellular heterogeneity during vertebrate skeletal muscle development. ***Dev Biol***, 308(2): 281-293.

Biressi, S., Tagliafico, E., Lamorte, G., Monteverde, S., Tenedini, E., Roncaglia, E., Ferrari, S., Ferrari, S., Cusella-De Angelis, M. G., Tajbakhsh, S., & Cossu, G. 2007b. Intrinsic phenotypic diversity of embryonic and fetal myoblasts is revealed by genome-wide gene expression analysis on purified cells. ***Dev Biol***, 304(2): 633-651.

Biswas, G., Adebanjo, O. A., Freedman, B. D., Anandatheerthavarada, H. K., Vijayasarathy, C., Zaidi, M., Kotlikoff, M., & Avadhani, N. G. 1999. Retrograde Ca2+ signaling in C2C12 skeletal myocytes in response to mitochondrial genetic and metabolic stress: a novel mode of inter-organelle crosstalk. ***EMBO J***, 18(3): 522-533.

Bizzarro, V., Petrella, A., & Parente, L. 2012. Annexin A1: novel roles in skeletal muscle biology. ***J Cell Physiol***, 227(8): 3007-3015.

Blais, A., Tsikitis, M., Acosta-Alvear, D., Sharan, R., Kluger, Y., & Dynlacht, B. D. 2005. An initial blueprint for myogenic differentiation. ***Genes Dev***, 19(5): 553-569.

Blitz, E., Viukov, S., Sharir, A., Shwartz, Y., Galloway, J. L., Pryce, B. A., Johnson, R. L., Tabin, C. J., Schweitzer, R., & Zelzer, E. 2009. Bone ridge patterning during musculoskeletal assembly is mediated through SCX regulation of Bmp4 at the tendon-skeleton junction. ***Dev Cell***, 17(6): 861-873.

Block, B. A., Imagawa, T., Campbell, K. P., & Franzini-Armstrong, C. 1988. Structural evidence for direct interaction between the molecular components of the transverse tubule/sarcoplasmic reticulum junction in skeletal muscle. ***J Cell Biol***, 107(6 Pt 2): 2587-2600.

Bober, E., Franz, T., Arnold, H. H., Gruss, P., & Tremblay, P. 1994. Pax-3 Is Required for the Development of Limb Muscles - a Possible Role for the Migration of Dermomyotomal Muscle Progenitor Cells. ***Development***, 120(3): 603-612.

Bodine, S. C., Stitt, T. N., Gonzalez, M., Kline, W. O., Stover, G. L., Bauerlein, R., Zlotchenko, E., Scrimgeour, A., Lawrence, J. C., Glass, D. J., & Yancopoulos, G. D. 2001. Akt/mTOR pathway is a crucial regulator of skeletal muscle hypertrophy and can prevent muscle atrophy in vivo. ***Nat Cell Biol***, 3(11): 1014-1019.

Bolstad, B. M., Irizarry, R. A., Astrand, M., & Speed, T. P. 2003. A comparison of normalization methods for high density oligonucleotide array data based on variance and bias. ***Bioinformatics***, 19(2): 185-193.

Borello, U., Berarducci, B., Murphy, P., Bajard, L., Buffa, V., Piccolo, S., Buckingham, M., & Cossu, G. 2006. The Wnt/beta-catenin pathway regulates Gli-mediated Myf5 expression during somitogenesis. ***Development***, 133(18): 3723-3732.

Braun, T., Buschhausen-Denker, G., Bober, E., Tannich, E., & Arnold, H. H. 1989. A novel human muscle factor related to but distinct from MyoD1 induces myogenic conversion in 10T1/2 fibroblasts. ***EMBO J***, 8(3): 701-709.

Braun, T., Rudnicki, M. A., Arnold, H. H., & Jaenisch, R. 1992. Targeted inactivation of the muscle regulatory gene Myf-5 results in abnormal rib development and perinatal death. ***Cell***, 71(3): 369-382.

Bryson-Richardson, R. J., & Currie, P. D. 2008. The genetics of vertebrate myogenesis. ***Nat Rev Genet***, 9(8): 632-646.

Buchthal, F., & Schmalbruch, H. 1980. Motor unit of mammalian muscle. ***Physiol Rev***, 60(1): 90-142.

Buck, E., Zimanyi, I., Abramson, J. J., & Pessah, I. N. 1992. Ryanodine stabilizes multiple conformational states of the skeletal muscle calcium release channel. ***J Biol Chem***, 267(33): 23560-23567.

Buck, E. D., Nguyen, H. T., Pessah, I. N., & Allen, P. D. 1997. Dyspedic mouse skeletal muscle expresses major elements of the triadic junction but lacks detectable ryanodine receptor protein and function. ***J Biol Chem***, 272(11): 7360-7367.

Buckingham, M., Bajard, L., Chang, T., Daubas, P., Hadchouel, J., Meilhac, S., Montarras, D., Rocancourt, D., & Relaix, F. 2003. The formation of skeletal muscle: from somite to limb. ***J Anat***, 202(1): 59-68.

Burattini, S., Ferri, P., Battistelli, M., Curci, R., Luchetti, F., & Falcieri, E. 2004. C2C12 murine myoblasts as a model of skeletal muscle development: morpho-functional characterization. ***Eur J Histochem***, 48(3): 223-233.

Campbell, K. P., & Stull, J. T. 2003. Skeletal muscle basement membrane-sarcolemma-cytoskeleton interaction minireview series. ***J Biol Chem***, 278(15): 12599-12600.

Cannon, S. C. 2015. Channelopathies of skeletal muscle excitability. ***Compr Physiol***, 5(2): 761-790.

Cardenas, C., Muller, M., Jaimovich, E., Perez, F., Buchuk, D., Quest, A. F., & Carrasco, M. A. 2004. Depolarization of skeletal muscle cells induces phosphorylation of cAMP response element binding protein via calcium and protein kinase Calpha. ***J Biol Chem***, 279(37): 39122-39131.

Carrasco, M. A., Riveros, N., Rios, J., Muller, M., Torres, F., Pineda, J., Lantadilla, S., & Jaimovich, E. 2003. Depolarization-induced slow calcium transients activate early genes in skeletal muscle cells. ***Am J Physiol Cell Physiol***, 284(6): C1438-1447.

Castel, D., Baghdadi, M. B., Mella, S., Gayraud-Morel, B., Marty, V., Cavaille, J., Antoniewski, C., & Tajbakhsh, S. 2018. Small-RNA sequencing identifies dynamic microRNA deregulation during skeletal muscle lineage progression. ***Sci Rep***, 8(1): 4208.

Catterall, W. A. 1988. Structure and Function of Voltage-Sensitive Ion Channels. ***Science***, 242(4875): 50-61.

Catterall, W. A. 1995. Structure and function of voltage-gated ion channels. ***Annu Rev Biochem***, 64: 493-531.

Catterall, W. A. 2000. Structure and regulation of voltage-gated Ca2+ channels. ***Annu Rev Cell Dev Biol***, 16: 521-555.

Chal, J., & Pourquie, O. 2017. Making muscle: skeletal myogenesis in vivo and in vitro. ***Development***, 144(12): 2104-2122.

Chandra, M., Mamidi, R., Ford, S., Hidalgo, C., Witt, C., Ottenheijm, C., Labeit, S., & Granzier, H. 2009. Nebulin alters cross-bridge cycling kinetics and increases thin filament activation: a novel mechanism for increasing tension and reducing tension cost. ***J Biol Chem***, 284(45): 30889-30896.

Chaudhari, N. 1992. A single nucleotide deletion in the skeletal muscle-specific calcium channel transcript of muscular dysgenesis (mdg) mice. ***J Biol Chem***, 267(36): 25636-25639.

Chaudhari, N., & Beam, K. G. 1989. The Muscular Dysgenesis Mutation in Mice Leads to Arrest of the Genetic Program for Muscle Differentiation. ***Dev Biol***, 133(2): 456-467.

Chelu, M. G., Goonasekera, S. A., Durham, W. J., Tang, W., Lueck, J. D., Riehl, J., Pessah, I. N., Zhang, P. M., Bhattacharjee, M. B., Dirksen, R. T., & Hamilton, S. L. 2005. Heat- and anesthesia-induced malignant hyperthermia in an RyR1 knock-in mouse. ***FASEB J***, 19(13): 329-+.

Chen, E. Y., Tan, C. M., Kou, Y., Duan, Q., Wang, Z., Meirelles, G. V., Clark, N. R., & Ma'ayan, A. 2013. Enrichr: interactive and collaborative HTML5 gene list enrichment analysis tool. ***BMC Bioinformat***, 14: 128.

Chen, F., Liu, Y., Sugiura, Y., Allen, P. D., Gregg, R. G., & Lin, W. 2011. Neuromuscular synaptic patterning requires the function of skeletal muscle dihydropyridine receptors. ***Nat Neurosci***, 14(5): 570-577.

Chen, J. F., Mandel, E. M., Thomson, J. M., Wu, Q., Callis, T. E., Hammond, S. M., Conlon, F. L., & Wang, D. Z. 2006. The role of microRNA-1 and microRNA-133 in skeletal muscle proliferation and differentiation. ***Nat Genet***, 38(2): 228-233.

Chiang, C., Litingtung, Y., Lee, E., Young, K. E., Corden, J. L., Westphal, H., & Beachy, P. A. 1996. Cyclopia and defective axial patterning in mice lacking Sonic hedgehog gene function. ***Nature***, 383(6599): 407-413.

Chowdhury, S., & Sarkar, R. R. 2015. Comparison of human cell signaling pathway databases--evolution, drawbacks and challenges. ***Database (Oxford)***, 2015.

Chuderland, D., & Seger, R. 2008. Calcium regulates ERK signaling by modulating its protein-protein interactions. ***Commun Integr Biol***, 1(1): 4-5.

Church, V. L., & Francis-West, P. 2002. Wnt signalling during limb development. ***Int J Dev Biol***, 46(7): 927-936.

Clapham, D. E. 2007. Calcium signaling. ***Cell***, 131(6): 1047-1058.

Clark, K. A., McElhinny, A. S., Beckerle, M. C., & Gregorio, C. C. 2002. Striated muscle cytoarchitecture: an intricate web of form and function. ***Annu Rev Cell Dev Biol***, 18: 637-706.

Cohen, T. J., Waddell, D. S., Barrientos, T., Lu, Z., Feng, G., Cox, G. A., Bodine, S. C., & Yao, T. P. 2007. The histone deacetylase HDAC4 connects neural activity to muscle transcriptional reprogramming. ***J Biol Chem***, 282(46): 33752-33759.

Conti, A., Gorza, L., & Sorrentino, V. 1996. Differential distribution of ryanodine receptor type 3 (RyR3) gene product in mammalian skeletal muscles. ***Biochem J***, 316 (Pt 1): 19-23.

Cossins, J., Vernon, A. E., Zhang, Y., Philpott, A., & Jones, P. H. 2002. Hes6 regulates myogenic differentiation. ***Development***, 129(9): 2195-2207.

Danowski, B. A., Imanaka-Yoshida, K., Sanger, J. M., & Sanger, J. W. 1992. Costameres are sites of force transmission to the substratum in adult rat cardiomyocytes. ***J Cell Biol***, 118(6): 1411-1420.

Darabid, H., Perez-Gonzalez, A. P., & Robitaille, R. 2014. Neuromuscular synaptogenesis: coordinating partners with multiple functions. ***Nat Rev Neurosci***, 15(11): 703-718.

Davis, R. L., Weintraub, H., & Lassar, A. B. 1987. Expression of a single transfected cDNA converts fibroblasts to myoblasts. ***Cell***, 51(6): 987-1000.

Dayal, A., Schrotter, K., Pan, Y., Fohr, K., Melzer, W., & Grabner, M. 2017. The Ca(2+) influx through the mammalian skeletal muscle dihydropyridine receptor is irrelevant for muscle performance. ***Nat Commun***, 8(1): 475.

de Oliveira, G. P., Maximino, J. R., Maschietto, M., Zanoteli, E., Puga, R. D., Lima, L., Carraro, D. M., & Chadi, G. 2014. Early gene expression changes in skeletal muscle from SOD1(G93A) amyotrophic lateral sclerosis animal model. ***Cell Mol Neurobiol***, 34(3): 451-462.

Deries, M., & Thorsteinsdottir, S. 2016. Axial and limb muscle development: dialogue with the neighbourhood. ***Cell Mol Life Sci***, 73(23): 4415-4431.

Descamps, S., Arzouk, H., Bacou, F., Bernardi, H., Fedon, Y., Gay, S., Reyne, Y., Rossano, B., & Levin, J. 2008. Inhibition of myoblast differentiation by Sfrp1 and Sfrp2. ***Cell Tissue Res***, 332(2): 299-306.

Desvergne, B., & Wahli, W. 1999. Peroxisome proliferator-activated receptors: nuclear control of metabolism. ***Endocr Rev***, 20(5): 649-688.

Dias, J. M., & Vogel, P. D. 2009. Effects of Small Molecule Modulators on ATP Binding to Skeletal Ryanodine Receptor. ***Protein J***, 28(5): 240-246.

Drenning, J. A., Lira, V. A., Soltow, Q. A., Canon, C. N., Valera, L. M., Brown, D. L., & Criswell, D. S. 2009. Endothelial nitric oxide synthase is involved in calcium-induced Akt signaling in mouse skeletal muscle. ***Nitric Oxide***, 21(3-4): 192-200.

Du, G. G., Sandhu, B., Khanna, V. K., Guo, X. H., & MacLennan, D. H. 2002. Topology of the Ca2+ release channel of skeletal muscle sarcoplasmic reticulum (RyR1). ***Proc Natl Acad Sci USA***, 99(26): 16725-16730.

Du, J. J., Li, Q., Shen, L. Y., Lei, H. G., Luo, J., Liu, Y. H., Zhang, P. W., Pu, Q., Zhang, Y., Shuai, S. R., Li, X. W., Zhang, S. H., & Zhu, L. 2016. miR-145a-5p Promotes Myoblast Differentiation. ***Biomed Res Internat***, 2016:5276271.

Duband, J. L., Gimona, M., Scatena, M., Sartore, S., & Small, J. V. 1993. Calponin and SM 22 as differentiation markers of smooth muscle: spatiotemporal distribution during avian embryonic development. ***Diff***, 55(1): 1-11.

Dulhunty, A. F. 2006. Excitation-contraction coupling from the 1950s into the new millennium. ***Clin Exp Pharmacol Physiol***, 33(9): 763-772.

Durbeej, M., & Campbell, K. P. 2002. Muscular dystrophies involving the dystrophin-glycoprotein complex: an overview of current mouse models. ***Curr Opin Genet Dev***, 12(3): 349-361.

Duxson, M. J., Usson, Y., & Harris, A. J. 1989. The origin of secondary myotubes in mammalian skeletal muscles: ultrastructural studies. ***Development***, 107(4): 743-750.

Edgeworth, F. H. 1899. On the Medullated Fibres of some of the Cranial Nerves, and the Development of Certain Muscles of the Head. ***J Anat Physiol***, 34(Pt 1): 113-150 125.

Efremov, R. G., Leitner, A., Aebersold, R., & Raunser, S. 2014. Architecture and conformational switch mechanism of the ryanodine receptor. ***Nature***, 517(7532):39-43.

Eisenberg, I., Eran, A., Nishino, I., Moggio, M., Lamperti, C., Amato, A. A., Lidov, H. G., Kang, P. B., North, K. N., Mitrani-Rosenbaum, S., Flanigan, K. M., Neely, L. A., Whitney, D., Beggs, A. H., Kohane, I. S., & Kunkel, L. M. 2007. Distinctive patterns of microRNA expression in primary muscular disorders. ***Proc Natl Acad Sci USA***, 104(43): 17016-17021.

Ekici, A. B., Hilfinger, D., Jatzwauk, M., Thiel, C. T., Wenzel, D., Lorenz, I., Boltshauser, E., Goecke, T. W., Staatz, G., Morris-Rosendahl, D. J., Sticht, H., Hehr, U., Reis, A., & Rauch, A. 2010. Disturbed Wnt Signalling due to a Mutation in CCDC88C Causes an Autosomal Recessive Non-Syndromic Hydrocephalus with Medial Diverticulum. ***Mol Syndromol***, 1(3): 99-112.

el-Hayek, R., Antoniu, B., Wang, J., Hamilton, S. L., & Ikemoto, N. 1995. Identification of calcium release-triggering and blocking regions of the II-III loop of the skeletal muscle dihydropyridine receptor. ***J Biol Chem***, 270(38): 22116-22118.

Eltit, J. M., Garcia, A. A., Hidalgo, J., Liberona, J. L., Chiong, M., Lavandero, S., Maldonado, E., & Jaimovich, E. 2006. Membrane electrical activity elicits inositol 1,4,5-trisphosphate-dependent slow Ca2+ signals through a Gbetagamma/phosphatidylinositol 3-kinase gamma pathway in skeletal myotubes. ***J Biol Chem***, 281(17): 12143-12154.

Eltit, J. M., Li, H., Ward, C. W., Molinski, T., Pessah, I. N., Allen, P. D., & Lopez, J. R. 2011. Orthograde dihydropyridine receptor signal regulates ryanodine receptor passive leak. ***Proc Natl Acad Sci USA***, 108(17): 7046-7051.

Eltit, J. M., Yang, T., Li, H., Molinski, T. F., Pessah, I. N., Allen, P. D., & Lopez, J. R. 2010. RyR1-mediated Ca2+ leak and Ca2+ entry determine resting intracellular Ca2+ in skeletal myotubes. ***J Biol Chem***, 285(18): 13781-13787.

Elustondo, P. A., Nichols, M., Robertson, G. S., & Pavlov, E. V. 2016. Mitochondrial Ca2+ uptake pathways. ***J Bioenerg Biomembr***, 49(1):113-119.

Emery, A. E. 2002. The muscular dystrophies. ***Lancet***, 359(9307): 687-695.

Enslen, H., Tokumitsu, H., & Soderling, T. R. 1995. Phosphorylation of CREB by CaM-kinase IV activated by CaM-kinase IV kinase. ***Biochem Biophys Res Commun***, 207(3): 1038-1043.

Enslen, H., Tokumitsu, H., Stork, P. J., Davis, R. J., & Soderling, T. R. 1996. Regulation of mitogen-activated protein kinases by a calcium/calmodulin-dependent protein kinase cascade. ***Proc Natl Acad Sci USA***, 93(20): 10803-10808.

Ervasti, J. M. 2003. Costameres: the Achilles' heel of Herculean muscle. ***J Biol Chem***, 278(16): 13591-13594.

Espinosa, A., Leiva, A., Pena, M., Muller, M., Debandi, A., Hidalgo, C., Carrasco, M. A., & Jaimovich, E. 2006. Myotube depolarization generates reactive oxygen species through NAD(P)H oxidase; ROS-elicited Ca2+ stimulates ERK, CREB, early genes. ***J Cell Physiol***, 209(2): 379-388.

Fahrenbach, W. H. 1965. Sarcoplasmic Reticulum: Ultrastructure of the Triadic Junction. ***Science***, 147(3663): 1308-1309.

Filipova, D., Henry, M., Rotshteyn, T., Brunn, A., Carstov, M., Deckert, M., Hescheler, J., Sachinidis, A., Pfitzer, G., & Papadopoulos, S. 2018. Distinct transcriptomic changes in E14.5 mouse skeletal muscle lacking RYR1 or Cav1.1 converge at E18.5. ***PLoS One***, 13(3): e0194428.

Filipova, D., Walter, A. M., Gaspar, J. A., Brunn, A., Linde, N. F., Ardestani, M. A., Deckert, M., Hescheler, J., Pfitzer, G., Sachinidis, A., & Papadopoulos, S. 2016. Gene profiling of embryonic skeletal muscle lacking type I ryanodine receptor Ca(2+) release channel. ***Sci Rep***, 6: 20050.

Finck, B. N., Bernal-Mizrachi, C., Han, D. H., Coleman, T., Sambandam, N., LaRiviere, L. L., Holloszy, J. O., Semenkovich, C. F., & Kelly, D. P. 2005. A potential link between muscle peroxisome proliferator-activated receptor-alpha signaling and obesity-related diabetes. ***Cell Metabol***, 1(2): 133-144.

Fiorillo, A. A., Heier, C. R., Novak, J. S., Tully, C. B., Brown, K. J., Uaesoontrachoon, K., Vila, M. C., Ngheim, P. P., Bello, L., Kornegay, J. N., Angelini, C., Partridge, T. A., Nagaraju, K., & Hoffman, E. P. 2015. TNF-alpha-Induced microRNAs Control Dystrophin Expression in Becker Muscular Dystrophy. ***Cell Rep***, 12(10): 1678-1690.

Flucher, B. E., Andrews, S. B., Fleischer, S., Marks, A. R., Caswell, A., & Powell, J. A. 1993. Triad formation: organization and function of the sarcoplasmic reticulum calcium release channel and triadin in normal and dysgenic muscle in vitro. ***J Cell Biol***, 123(5): 1161-1174.

Flucher, B. E., & Daniels, M. P. 1989. Distribution of Na+ Channels and Ankyrin in Neuromuscular-Junctions Is Complementary to That of Acetylcholine-Receptors and the 43 Kd Protein. ***Neuron***, 3(2): 163-175.

Flucher, B. E., & Tuluc, P. 2011. A new L-type calcium channel isoform required for normal patterning of the developing neuromuscular junction. ***Channels (Austin)***, 5(6): 518-524.

Forterre, A., Jalabert, A., Chikh, K., Pesenti, S., Euthine, V., Granjon, A., Errazuriz, E., Lefai, E., Vidal, H., & Rome, S. 2014. Myotube-derived exosomal miRNAs downregulate Sirtuin1 in myoblasts during muscle cell differentiation. ***Cell Cycle***, 13(1): 78-89.

Fox, R. M., Watson, J. D., Von Stetina, S. E., McDermott, J., Brodigan, T. M., Fukushige, T., Krause, M., & Miller, D. M., 3rd. 2007. The embryonic muscle transcriptome of Caenorhabditis elegans. ***Genome Biol***, 8(9): R188.

Frank, D., Kuhn, C., Katus, H. A., & Frey, N. 2006. The sarcomeric Z-disc: a nodal point in signalling and disease. ***J Mol Med (Berl)***, 84(6): 446-468.

Fredette, B. J., & Landmesser, L. T. 1991. A reevaluation of the role of innervation in primary and secondary myogenesis in developing chick muscle. ***Dev Biol***, 143(1): 19-35.

Freise, D., Held, B., Wissenbach, U., Pfeifer, A., Trost, C., Himmerkus, N., Schweig, U., Freichel, M., Biel, M., Hofmann, F., Hoth, M., & Flockerzi, V. 2000. Absence of the gamma subunit of the skeletal muscle dihydropyridine receptor increases L-type Ca2+ currents and alters channel inactivation properties. ***J Biol Chem***, 275(19): 14476-14481.

Frontera, W. R., & Ochala, J. 2015. Skeletal muscle: a brief review of structure and function. ***Calcif Tissue Int***, 96(3): 183-195.

Fry, C. S., Kirby, T. J., Kosmac, K., McCarthy, J. J., & Peterson, C. A. 2017. Myogenic Progenitor Cells Control Extracellular Matrix Production by Fibroblasts during Skeletal Muscle Hypertrophy. ***Cell Stem Cell***, 20(1): 56-69.

Gaarenstroom, T., & Hill, C. S. 2014. TGF-beta signaling to chromatin: How Smads regulate transcription during self-renewal and differentiation. ***Seminars Cell & Dev Biol***, 32: 107-118.

Gabriel, L. A., Wang, L. W., Bader, H., Ho, J. C., Majors, A. K., Hollyfield, J. G., Traboulsi, E. I., & Apte, S. S. 2012. ADAMTSL4, a secreted glycoprotein widely distributed in the eye, binds fibrillin-1 microfibrils and accelerates microfibril biogenesis. ***Invest Ophthalmol Vis Sci***, 53(1): 461-469.

Gach, M. P., Cherednichenko, G., Haarmann, C., Lopez, J. R., Beam, K. G., Pessah, I. N., Franzini-Armstrong, C., & Allen, P. D. 2008. Alpha2delta1 dihydropyridine receptor subunit is a critical element for excitation-coupled calcium entry but not for formation of tetrads in skeletal myotubes. ***Biophys J***, 94(8): 3023-3034.

Garcia, J., Tanabe, T., & Beam, K. G. 1994. Relationship of calcium transients to calcium currents and charge movements in myotubes expressing skeletal and cardiac dihydropyridine receptors. ***J Gen Physiol***, 103(1): 125-147.

Ge, Y., & Chen, J. 2012. Mammalian target of rapamycin (mTOR) signaling network in skeletal myogenesis. ***J Biol Chem***, 287(52): 43928-43935.

Ge, Y. J., Sun, Y. T., & Chen, J. 2011. IGF-II is regulated by microRNA-125b in skeletal myogenesis. ***J Cell Biol***, 192(1): 69-81.

Gehlert, S., Bloch, W., & Suhr, F. 2015. Ca2+-Dependent Regulations and Signaling in Skeletal Muscle: From Electro-Mechanical Coupling to Adaptation. ***Int J Mol Sci***, 16(1): 1066-1095.

Gillies, A. R., & Lieber, R. L. 2011. Structure and function of the skeletal muscle extracellular matrix. ***Muscle Nerve***, 44(3): 318-331.

Glazov, E. A., McWilliam, S., Barris, W. C., & Dalrymple, B. P. 2008. Origin, evolution, and biological role of miRNA cluster in DLK-DIO3 genomic region in placental mammals. ***Mol Biol Evol***, 25(5): 939-948.

Goljanek-Whysall, K., Sweetman, D., & Munsterberg, A. E. 2012. microRNAs in skeletal muscle differentiation and disease. ***Clin Sci (Lond)***, 123(11): 611-625.

Gonzalez de Aguilar, J. L., Niederhauser-Wiederkehr, C., Halter, B., De Tapia, M., Di Scala, F., Demougin, P., Dupuis, L., Primig, M., Meininger, V., & Loeffler, J. P. 2008. Gene profiling of skeletal muscle in an amyotrophic lateral sclerosis mouse model. ***Physiol Genomics***, 32(2): 207-218.

Goriounov, D., Leung, C. L., & Liem, R. K. 2003. Protein products of human Gas2-related genes on chromosomes 17 and 22 (hGAR17 and hGAR22) associate with both microfilaments and microtubules. ***J Cell Sci***, 116(Pt 6): 1045-1058.

Goudy, S., Angel, P., Jacobs, B., Hill, C., Mainini, V., Smith, A. L., Kousa, Y. A., Caprioli, R., Prince, L. S., Baldwin, S., & Schutte, B. C. 2013. Cell-autonomous and non-cell-autonomous roles for IRF6 during development of the tongue. ***PLoS One***, 8(2): e56270.

Goulding, M. D., Chalepakis, G., Deutsch, U., Erselius, J. R., & Gruss, P. 1991. Pax-3, a novel murine DNA binding protein expressed during early neurogenesis. ***EMBO J***, 10(5): 1135-1147.

Grabner, M., Dirksen, R. T., Suda, N., & Beam, K. G. 1999. The II-III loop of the skeletal muscle dihydropyridine receptor is responsible for the bi-directional coupling with the ryanodine receptor. ***J Biol Chem***, 274(31): 21913-21919.

Greco, S. A., Chia, J., Inglis, K. J., Cozzi, S. J., Ramsnes, I., Buttenshaw, R. L., Spring, K. J., Boyle, G. M., Worthley, D. L., Leggett, B. A., & Whitehall, V. L. 2010. Thrombospondin-4 is a putative tumour-suppressor gene in colorectal cancer that exhibits age-related methylation. ***BMC Cancer***, 10: 494.

Gregg, R. G., Messing, A., Strube, C., Beurg, M., Moss, R., Behan, M., Sukhareva, M., Haynes, S., Powell, J. A., Coronado, R., & Powers, P. A. 1996. Absence of the beta subunit (cchb1) of the skeletal muscle dihydropyridine receptor alters expression of the alpha 1 subunit and eliminates excitation-contraction coupling. ***Proc Natl Acad Sci USA***, 93(24): 13961-13966.

Greising, S. M., Gransee, H. M., Mantilla, C. B., & Sieck, G. C. 2012. Systems biology of skeletal muscle: fiber type as an organizing principle. ***Wiley Inter Rev Sys Biol Med***, 4(5): 457-473.

Grifone, R., Demignon, J., Giordani, J., Niro, C., Souil, E., Bertin, F., Laclef, C., Xu, P. X., & Maire, P. 2007. Eya1 and Eya2 proteins are required for hypaxial somitic myogenesis in the mouse embryo. ***Dev Biol***, 302(2): 602-616.

Grifone, R., Demignon, J., Houbron, C., Souil, E., Niro, C., Seller, M. J., Hamard, G., & Maire, P. 2005. Six1 and Six4 homeoproteins are required for Pax3 and Mrf expression during myogenesis in the mouse embryo. ***Development***, 132(9): 2235-2249.

Gros, J., Manceau, M., Thome, V., & Marcelle, C. 2005. A common somitic origin for embryonic muscle progenitors and satellite cells. ***Nature***, 435(7044): 954-958.

Harafuji, N., Schneiderat, P., Walter, M. C., & Chen, Y. W. 2013. miR-411 is up-regulated in FSHD myoblasts and suppresses myogenic factors. ***Orphanet J Rare Dis***, 8: 55.

Hartung, T. 2008. Thoughts on limitations of animal models. ***Parkinsonism Relat Disord***, 14 Suppl 2: S81-83.

Hasty, P., Bradley, A., Morris, J. H., Edmondson, D. G., Venuti, J. M., Olson, E. N., & Klein, W. H. 1993. Muscle deficiency and neonatal death in mice with a targeted mutation in the myogenin gene. ***Nature***, 364(6437): 501-506.

Hauser, J., Saarikettu, J., & Grundstrom, T. 2008. Calcium regulation of myogenesis by differential calmodulin inhibition of basic helix-loop-helix transcription factors. ***Mol Biol Cell***, 19(6): 2509-2519.

Heimann, P., Kuschel, T., & Jockusch, H. 2004. Elimination by necrosis, not apoptosis, of embryonic extraocular muscles in the muscular dysgenesis mutant of the mouse. ***Cell Tissue Res***, 315(2): 243-247.

Herring, S. W., & Lakars, T. C. 1982. Craniofacial development in the absence of muscle contraction. ***J Craniofac Genet Dev Biol***, 1(4): 341-357.

Hescheler, J. 2008. Quergestreifte Muskulatur. In J. H. E. J. Speckmann, R. Köhlig (Ed.), ***Physiologie***, 5 ed.: Urban & Fischer Verlag/Elsevier GmbH.

Hijikata, T., Nakamura, A., Isokawa, K., Imamura, M., Yuasa, K., Ishikawa, R., Kohama, K., Takeda, S., & Yorifuji, H. 2008. Plectin 1 links intermediate filaments to costameric sarcolemma through beta-synemin, alpha-dystrobrevin and actin. ***J Cell Sci***, 121(Pt 12): 2062-2074.

Hildyard, J. C., & Wells, D. J. 2014. Identification and validation of quantitative PCR reference genes suitable for normalizing expression in normal and dystrophic cell culture models of myogenesis. ***PLoS Curr***, 6.

Hinds, S., Bian, W., Dennis, R. G., & Bursac, N. 2011. The role of extracellular matrix composition in structure and function of bioengineered skeletal muscle. ***Biomaterials***, 32(14): 3575-3583.

Hitachi, K., & Tsuchida, K. 2017. Myostatin-deficiency in mice increases global gene expression at the Dlk1-Dio3 locus in the skeletal muscle. ***Oncotarget***, 8(4): 5943-5953.

Hofmann, M., Schuster-Gossler, K., Watabe-Rudolph, M., Aulehla, A., Herrmann, B. G., & Gossler, A. 2004. WNT signaling, in synergy with T/TBX6, controls Notch signaling by regulating DII1 expression in the presomitic mesoderm of mouse embryos. ***Genes & Dev***, 18(22): 2712-2717.

Holterman, C. E., Le Grand, F., Kuang, S., Seale, P., & Rudnicki, M. A. 2007. Megf10 regulates the progression of the satellite cell myogenic program. ***J Cell Biol***, 179(5): 911-922.

Hood, D. A., Irrcher, I., Ljubicic, V., & Joseph, A. M. 2006. Coordination of metabolic plasticity in skeletal muscle. ***J Exp Biol***, 209(Pt 12): 2265-2275.

Hoppeler, H. 2016. Molecular networks in skeletal muscle plasticity. ***J Exp Biol***, 219(Pt 2): 205-213.

Horak, M., Novak, J., & Bienertova-Vasku, J. 2016. Muscle-specific microRNAs in skeletal muscle development. ***Dev Biol***, 410(1): 1-13.

Hoshijima, M. 2006. Mechanical stress-strain sensors embedded in cardiac cytoskeleton: Z disk, titin, and associated structures. ***Am J Physiol Heart Circ Physiol***, 290(4): H1313-1325.

Huang, A. H., Riordan, T. J., Pryce, B., Weibel, J. L., Watson, S. S., Long, F. X., Lefebvre, V., Harfe, B. D., Stadler, H. S., Akiyama, H., Tufa, S. F., Keene, D. R., & Schweitzer, R. 2015. Musculoskeletal integration at the wrist underlies the modular development of limb tendons. ***Development***, 142(14): 2431-2441.

Huang da, W., Sherman, B. T., & Lempicki, R. A. 2009. Systematic and integrative analysis of large gene lists using DAVID bioinformatics resources. ***Nat Protoc***, 4(1): 44-57.

Huang, Y., & Mahley, R. W. 2014. Apolipoprotein E: structure and function in lipid metabolism, neurobiology, and Alzheimer's diseases. ***Neurobiol Dis***, 72 Pt A: 3-12.

Huang, Z. P., Chen, J., Seok, H. Y., Zhang, Z., Kataoka, M., Hu, X., & Wang, D. Z. 2013. MicroRNA-22 regulates cardiac hypertrophy and remodeling in response to stress. ***Circ Res***, 112(9): 1234-1243.

Hutcheson, D. A., Zhao, J., Merrell, A., Haldar, M., & Kardon, G. 2009. Embryonic and fetal limb myogenic cells are derived from developmentally distinct progenitors and have different requirements for beta-catenin. ***Genes Dev***, 23(8): 997-1013.

Huxley, A. F. 2000. Cross-bridge action: present views, prospects, and unknowns. ***J Biomech***, 33(10): 1189-1195.

Huxley, H., & Hanson, J. 1954. Changes in the Cross-Striations of Muscle during Contraction and Stretch and Their Structural Interpretation. ***Nature***, 173(4412): 973-976.

Huxley, H. E. 1961. The contractile structure of cardiac and skeletal muscle. ***Circulation***, 24: 328-335.

Ingraham, C. R., Kinoshita, A., Kondo, S., Yang, B., Sajan, S., Trout, K. J., Malik, M. I., Dunnwald, M., Goudy, S. L., Lovett, M., Murray, J. C., & Schutte, B. C. 2006. Abnormal skin, limb and craniofacial morphogenesis in mice deficient for interferon regulatory factor 6 (Irf6). ***Nat Genet***, 38(11): 1335-1340.

Inui, M., Saito, A., & Fleischer, S. 1987. Purification of the ryanodine receptor and identity with feet structures of junctional terminal cisternae of sarcoplasmic reticulum from fast skeletal muscle. ***J Biol Chem***, 262(4): 1740-1747.

Irintchev, A., Salvini, T. F., Faissner, A., & Wernig, A. 1993. Differential expression of tenascin after denervation, damage or paralysis of mouse soleus muscle. ***J Neurocytol***, 22(11): 955-965.

Irizarry, R. A., Gautier, L., & Cope, L. M. 2003. An R Package for Analyses of Affymetrix Oligonucleotide Arrays. In G. Parmigiani, Garrett, E. S., Irizarry, R. A., Zeger, S. L. (Ed.), ***Anal Gen Expres Data: Met Soft***, 102-119. New York, NY: Springer.

Janssen, I., Heymsfield, S. B., Wang, Z. M., & Ross, R. 2000. Skeletal muscle mass and distribution in 468 men and women aged 18-88 yr. ***J Appl Physiol (1985)***, 89(1): 81-88.

Javan, R., Horvath, J. J., Case, L. E., Austin, S., Corderi, J., Dubrovsky, A., Kishnani, P. S., & Bashir, M. R. 2013. Generating color-coded anatomic muscle maps for correlation of quantitative magnetic resonance imaging analysis with clinical examination in neuromuscular disorders. ***Muscle Nerve***, 48(2): 293-295.

Jeanson-Leh, L., Lameth, J., Krimi, S., Buisset, J., Amor, F., Le Guiner, C., Barthelemy, I., Servais, L., Blot, S., Voit, T., & Israeli, D. 2014. Serum profiling identifies novel muscle miRNA and cardiomyopathy-related miRNA biomarkers in Golden Retriever muscular dystrophy dogs and Duchenne muscular dystrophy patients. ***Am J Pathol***, 184(11): 2885-2898.

Jeyaseelan, R., Poizat, C., Baker, R. K., Abdishoo, S., Isterabadi, L. B., Lyons, G. E., & Kedes, L. 1997. A novel cardiac-restricted target for doxorubicin - CARP, a nuclear modulator of gene expression in cardiac progenitor cells and cardiomyocytes. ***J Biol Chem***, 272(36): 22800-22808.

Jones, N. C., Fedorov, Y. V., Rosenthal, R. S., & Olwin, B. B. 2001. ERK1/2 is required for myoblast proliferation but is dispensable for muscle gene expression and cell fusion. ***J Cell Physiol***, 186(1): 104-115.

Jostes, B., Walther, C., & Gruss, P. 1990. The murine paired box gene, Pax7, is expressed specifically during the development of the nervous and muscular system. ***Mech Dev***, 33(1): 27-37.

Jungbluth, H., Treves, S., Zorzato, F., Sarkozy, A., Ochala, J., Sewry, C., Phadke, R., Gautel, M., & Muntoni, F. 2018. Congenital myopathies: disorders of excitation-contraction coupling and muscle contraction. ***Nat Rev Neurol***, 14(3):151-167.

Juretic, N., Urzua, U., Munroe, D. J., Jaimovich, E., & Riveros, N. 2007. Differential gene expression in skeletal muscle cells after membrane depolarization. ***J Cell Physiol***, 210(3): 819-830.

Kablar, B., & Rudnicki, M. A. 2000. Skeletal muscle development in the mouse embryo. ***Histol Histopathol***, 15(2): 649-656.

Kahn, J., Shwartz, Y., Blitz, E., Krief, S., Sharir, A., Breitel, D. A., Rattenbach, R., Relaix, F., Maire, P., Rountree, R. B., Kingsley, D. M., & Zelzer, E. 2009. Muscle Contraction Is Necessary to Maintain Joint Progenitor Cell Fate. ***Dev Cell***, 16(5): 734-743.

Kanatous, S. B., Mammen, P. P., Rosenberg, P. B., Martin, C. M., White, M. D., Dimaio, J. M., Huang, G., Muallem, S., & Garry, D. J. 2009. Hypoxia reprograms calcium signaling and regulates myoglobin expression. ***Am J Physiol Cell Physiol***, 296(3): C393-402.

Kariminejad, A., Ghaderi-Sohi, S., Hossein-Nejad Nedai, H., Varasteh, V., Moslemi, A. R., & Tajsharghi, H. 2016. Lethal multiple pterygium syndrome, the extreme end of the RYR1 spectrum. ***BMC Musculoskelet Disord***, 17(1): 109.

Katase, N., Terada, K., Suzuki, T., Nishimatsu, S., & Nohno, T. 2015. miR-487b, miR-3963 and miR-6412 delay myogenic differentiation in mouse myoblast-derived C2C12 cells. ***BMC Cell Biol***, 16: 13.

Kim, J. H., Jin, P., Duan, R., & Chen, E. H. 2015. Mechanisms of myoblast fusion during muscle development. ***Curr Opin Genet Dev***, 32: 162-170.

Kim, J. Y., Park, Y. K., Lee, K. P., Lee, S. M., Kang, T. W., Kim, H. J., Dho, S. H., Kim, S. Y., & Kwon, K. S. 2014. Genome-wide profiling of the microRNA-mRNA regulatory network in skeletal muscle with aging. ***Aging (Albany NY)***, 6(7): 524-544.

Kjaer, M. 2004. Role of extracellular matrix in adaptation of tendon and skeletal muscle to mechanical loading. ***Physiol Rev***, 84(2): 649-698.

Klinke, R., Pape, H-C., Silbernagl, St. 2005. ***Physiologie***: Georg Thieme Verlag Stuttgart.

Knoll, R., Buyandelger, B., & Lab, M. 2011. The sarcomeric Z-disc and Z-discopathies. ***J Biomed Biotechnol***, 2011: 569628.

Kodama, N., & Sekiguchi, S. 1984. The Development of Spontaneous Body Movement in Prenatal and Perinatal Mice. ***Dev Psychobiol***, 17(2): 139-150.

Kohn, A. D., & Moon, R. T. 2005. Wnt and calcium signaling: beta-catenin-independent pathways. ***Cell Calcium***, 38(3-4): 439-446.

Kojic, S., Nestorovic, A., Rakicevic, L., Belgrano, A., Stankovic, M., Divac, A., & Faulkner, G. 2010. A novel role for cardiac ankyrin repeat protein Ankrd1/CARP as a co-activator of the p53 tumor suppressor protein. ***Arch Biochem Biophys***, 502(1): 60-67.

Kostrominova, T. Y., Dow, D. E., Dennis, R. G., Miller, R. A., & Faulkner, J. A. 2005. Comparison of gene expression of 2-mo denervated, 2-mo stimulated-denervated, and control rat skeletal muscles. ***Physiol Genomics***, 22(2): 227-243.

Kramer, H. F., & Goodyear, L. J. 2007. Exercise, MAPK, and NF-kappaB signaling in skeletal muscle. ***J Appl Physiol (1985)***, 103(1): 388-395.

Kruger, M., & Kotter, S. 2016. Titin, a Central Mediator for Hypertrophic Signaling, Exercise-Induced Mechanosignaling and Skeletal Muscle Remodeling. ***Front Physiol***, 7: 76.

Kuleshov, M. V., Jones, M. R., Rouillard, A. D., Fernandez, N. F., Duan, Q., Wang, Z., Koplev, S., Jenkins, S. L., Jagodnik, K. M., Lachmann, A., McDermott, M. G., Monteiro, C. D., Gundersen, G. W., & Ma'ayan, A. 2016. Enrichr: a comprehensive gene set enrichment analysis web server 2016 update. ***Nucleic Acids Res***, 44(W1): W90-97.

Kuroda, K., Tani, S., Tamura, K., Minoguchi, S., Kurooka, H., & Honjo, T. 1999. Delta-induced notch signaling mediated by RBP-J inhibits MyoD expression and myogenesis. ***J Biol Chem***, 274(11): 7238-7244.

Kyselovic, J., Leddy, J. J., Ray, A., Wigle, J., & Tuana, B. S. 1994. Temporal differences in the induction of dihydropyridine receptor subunits and ryanodine receptors during skeletal muscle development. ***J Biol Chem***, 269(34): 21770-21777.

Lacerda, A. E., Kim, H. S., Ruth, P., Perez-Reyes, E., Flockerzi, V., Hofmann, F., Birnbaumer, L., & Brown, A. M. 1991. Normalization of current kinetics by interaction between the alpha 1 and beta subunits of the skeletal muscle dihydropyridine-sensitive Ca2+ channel. ***Nature***, 352(6335): 527-530.

Laclef, C., Hamard, G., Demignon, J., Souil, E., Houbron, C., & Maire, P. 2003. Altered myogenesis in Six1-deficient mice. ***Development***, 130(10): 2239-2252.

Lamb, G. D. 2000. Excitation-contraction coupling in skeletal muscle: comparisons with cardiac muscle. ***Clin Exp Pharmacol Physiol***, 27(3): 216-224.

Lambeir, A. M., Durinx, C., Scharpe, S., & De Meester, I. 2003. Dipeptidyl-peptidase IV from bench to bedside: an update on structural properties, functions, and clinical aspects of the enzyme DPP IV. ***Crit Rev Clin Lab Sci***, 40(3): 209-294.

Lamon, S., Zacharewicz, E., Butchart, L. C., Orellana, L., Mikovic, J., Grounds, M. D., & Russell, A. P. 2017. MicroRNA expression patterns in post-natal mouse skeletal muscle development. ***BMC Genomics***, 18(1): 52.

Lang, F., Thews, G., & Schmidt, R. F. 2000. Physiologie des Menschen.

Lee-Kwon, W., Goo, J. H., Zhang, Z., Silldorff, E. P., & Pallone, T. L. 2007. Vasa recta voltage-gated Na+ channel Nav1.3 is regulated by calmodulin. ***Am J Physiol Renal Physiol***, 292(1): F404-414.

Lee, C. S., Dagnino-Acosta, A., Yarotskyy, V., Hanna, A., Lyfenko, A., Knoblauch, M., Georgiou, D. K., Poche, R. A., Swank, M. W., Long, C., Ismailov, II, Lanner, J., Tran, T., Dong, K., Rodney, G. G., Dickinson, M. E., Beeton, C., Zhang, P., Dirksen, R. T., & Hamilton, S. L. 2015a. Ca(2+) permeation and/or binding to CaV1.1 fine-tunes skeletal muscle Ca(2+) signaling to sustain muscle function. ***Skelet Muscle***, 5: 4.

Lee, J. U., Kim, J. H., Kim, M. Y., Lee, L. K., Yang, S. M., Jeon, H. J., Lee, W. D., Noh, J. W., Lee, T. H., Kwak, T. Y., Kim, B., & Kim, J. 2013. Increase of Myoglobin in Rat Gastrocnemius Muscles with Immobilization-induced Atrophy. ***J Phys Ther Sci***, 25(12): 1617-1620.

Lee, K. P., Shin, Y. J., Panda, A. C., Abdelmohsen, K., Kim, J. Y., Lee, S. M., Bahn, Y. J., Choi, J. Y., Kwon, E. S., Baek, S. J., Kim, S. Y., Gorospe, M., & Kwon, K. S. 2015b. miR-431 promotes differentiation and regeneration of old skeletal muscle by targeting Smad4. ***Genes Dev***, 29(15): 1605-1617.

Leonardini, A., Laviola, L., Perrini, S., Natalicchio, A., & Giorgino, F. 2009. Cross-Talk between PPAR gamma and Insulin Signaling and Modulation of Insulin Sensitivity. ***Ppar Res***, 2009:818945.

Li, J., & Johnson, S. E. 2006. ERK2 is required for efficient terminal differentiation of skeletal myoblasts. ***Biochem Biophys Res Commun***, 345(4): 1425-1433.

Licht, A. H., Nubel, T., Feldner, A., Jurisch-Yaksi, N., Marcello, M., Demicheva, E., Hu, J. H., Hartenstein, B., Augustin, H. G., Hecker, M., Angel, P., Korff, T., & Schorpp-Kistner, M. 2010. Junb regulates arterial contraction capacity, cellular contractility, and motility via its target Myl9 in mice. ***J Clin Invest***, 120(7): 2307-2318.

Lieber, R. L., & Friden, J. 2000. Functional and clinical significance of skeletal muscle architecture. ***Muscle Nerve***, 23(11): 1647-1666.

Linke, W. A., & Kruger, M. 2010. The giant protein titin as an integrator of myocyte signaling pathways. ***Physiol (Bethesda)***, 25(3): 186-198.

Llano-Diez, M., Gustafson, A. M., Olsson, C., Goransson, H., & Larsson, L. 2011. Muscle wasting and the temporal gene expression pattern in a novel rat intensive care unit model. ***BMC Genomics***, 12: 602.

Lluis, F., Perdiguero, E., Nebreda, A. R., & Munoz-Canoves, P. 2006. Regulation of skeletal muscle gene expression by p38 MAP kinases. ***Trends Cell Biol***, 16(1): 36-44.

Lone, A. M., Leidl, M., McFedries, A. K., Horner, J. W., Creemers, J., & Saghatelian, A. 2014. Deletion of Prepl Causes Growth Impairment and Hypotonia in Mice. ***PloS One***, 9(2).

Lou, Y., Liu, L., Zhan, L. H., Wang, X. W., & Fan, H. 2016. miR-187-5p Regulates Cell Growth and Apoptosis in Acute Lymphoblastic Leukemia via DKK2. ***Oncol Res***, 24(2): 89-97.

Loughna, P. T., Mason, P., Bayol, S., & Brownson, C. 2000. The LIM-domain protein FHL1 (SLIM 1) exhibits functional regulation in skeletal muscle. ***Mol Cell Biol Res Commun***, 3(3): 136-140.

Lundby, C., & Jacobs, R. A. 2016. Adaptations of skeletal muscle mitochondria to exercise training. ***Exp Physiol***, 101(1): 17-22.

Luo, G., Herrera, A. H., & Horowits, R. 1999. Molecular interactions of N-RAP, a nebulin-related protein of striated muscle myotendon junctions and intercalated disks. ***Biochem***, 38(19): 6135-6143.

Luo, W., Nie, Q., & Zhang, X. 2013. MicroRNAs involved in skeletal muscle differentiation. ***J Genet Genomics***, 40(3): 107-116.

MacIntosh, B. R., Holash, R. J., & Renaud, J. M. 2012. Skeletal muscle fatigue--regulation of excitation-contraction coupling to avoid metabolic catastrophe. ***J Cell Sci***, 125(Pt 9): 2105-2114.

Mackey, A. L., Brandstetter, S., Schjerling, P., Bojsen-Moller, J., Qvortrup, K., Pedersen, M. M., Doessing, S., Kjaer, M., Magnusson, S. P., & Langberg, H. 2011. Sequenced response of extracellular matrix deadhesion and fibrotic regulators after muscle damage is involved in protection against future injury in human skeletal muscle. ***FASEB J***, 25(6): 1943-1959.

Mahoney, D. J., Carey, K., Fu, M. H., Snow, R., Cameron-Smith, D., Parise, G., & Tarnopolsky, M. A. 2004. Real-time RT-PCR analysis of housekeeping genes in human skeletal muscle following acute exercise. ***Physiol Genomics***, 18(2): 226-231.

Marks, A. R., Tempst, P., Hwang, K. S., Taubman, M. B., Inui, M., Chadwick, C., Fleischer, S., & Nadal-Ginard, B. 1989. Molecular cloning and characterization of the ryanodine receptor/junctional channel complex cDNA from skeletal muscle sarcoplasmic reticulum. ***Proc Natl Acad Sci USA***, 86(22): 8683-8687.

Marotta, M., Ruiz-Roig, C., Sarria, Y., Peiro, J. L., Nunez, F., Ceron, J., Munell, F., & Roig-Quilis, M. 2009. Muscle genome-wide expression profiling during disease evolution in mdx mice. ***Physiol Genomics***, 37(2): 119-132.

Martinez-Ortiz, W., & Cardozo, T. J. 2018. An Improved Method for Modeling Voltage-Gated Ion Channels at Atomic Accuracy Applied to Human Cav Channels. ***Cell Rep***, 23(5): 1399-1408.

Marx, S. O., Ondrias, K., & Marks, A. R. 1998. Coupled gating between individual skeletal muscle Ca2+ release channels (ryanodine receptors). ***Science***, 281(5378): 818-821.

Massari, M. E., & Murre, C. 2000. Helix-loop-helix proteins: Regulators of transcription in eucaryotic organisms. ***Mol Cell Biol***, 20(2): 429-440.

Mathews, K. D., & Moore, S. A. 2004. Multiminicore myopathy, central core disease, malignant hyperthermia susceptibility, and RYR1 mutations: one disease with many faces? ***Arch Neurol***, 61(1): 27-29.

McDaneld, T. G., Smith, T. P., Doumit, M. E., Miles, J. R., Coutinho, L. L., Sonstegard, T. S., Matukumalli, L. K., Nonneman, D. J., & Wiedmann, R. T. 2009. MicroRNA transcriptome profiles during swine skeletal muscle development. ***BMC Genomics***, 10: 77.

McKie, A. B., Alsaedi, A., Vogt, J., Stuurman, K. E., Weiss, M. M., Shakeel, H., Tee, L., Morgan, N. V., Nikkels, P. G., van Haaften, G., Park, S. M., van der Smagt, J. J., Bugiani, M., & Maher, E. R. 2014. Germline mutations in RYR1 are associated with foetal akinesia deformation sequence/lethal multiple pterygium syndrome. ***Acta Neuropathol Commun***, 2: 148.

McLennan, I. S. 1983. Differentiation of muscle fiber types in the chicken hindlimb. ***Dev Biol***, 97(1): 222-228.

Metsalu, T., & Vilo, J. 2015. ClustVis: a web tool for visualizing clustering of multivariate data using Principal Component Analysis and heatmap. ***Nucleic Acids Res***, 43(W1): W566-570.

Meyer, S. U., Thirion, C., Polesskaya, A., Bauersachs, S., Kaiser, S., Krause, S., & Pfaffl, M. W. 2015. TNF-alpha and IGF1 modify the microRNA signature in skeletal muscle cell differentiation. ***Cell Commun Signal***, 13: 4.

Millay, D. P., O'Rourke, J. R., Sutherland, L. B., Bezprozvannaya, S., Shelton, J. M., Bassel-Duby, R., & Olson, E. N. 2013. Myomaker is a membrane activator of myoblast fusion and muscle formation. ***Nature***, 499(7458): 301-305.

Miller, M. K., Bang, M. L., Witt, C. C., Labeit, D., Trombitas, C., Watanabe, K., Granzier, H., McElhinny, A. S., Gregorio, C. C., & Labeit, S. 2003. The muscle ankyrin repeat proteins: CARP, ankrd2/Arpp and DARP as a family of titin filament-based stress response molecules. ***J Mol Biol***, 333(5): 951-964.

Miska, E. A., Langley, E., Wolf, D., Karlsson, C., Pines, J., & Kouzarides, T. 2001. Differential localization of HDAC4 orchestrates muscle differentiation. ***Nucleic Acids Res***, 29(16): 3439-3447.

Mittal, A., Bhatnagar, S., Kumar, A., Lach-Trifilieff, E., Wauters, S., Li, H., Makonchuk, D. Y., Glass, D. J., & Kumar, A. 2010. The TWEAK-Fn14 system is a critical regulator of denervation-induced skeletal muscle atrophy in mice. ***J Cell Biol***, 188(6): 833-849.

Moore-Carrasco, R., Garcia-Martinez, C., Busquets, S., Ametller, E., Barreiro, E., Lopez-Soriano, F. J., & Argiles, J. M. 2006. The AP-1/CJUN signaling cascade is involved in muscle differentiation: implications in muscle wasting during cancer cachexia. ***FEBS Lett***, 580(2): 691-696.

Morey, J. S., Ryan, J. C., & Van Dolah, F. M. 2006. Microarray validation: factors influencing correlation between oligonucleotide microarrays and real-time PCR. ***Biol Proced Online***, 8: 175-193.

Mu, J. H., Hui, T. L., Shao, B. F., Li, L. L., Du, Z. F., Lu, L., Ye, L., Li, S. M., Li, Q. Q., Xiao, Q., Qiu, Z., Zhang, Y., Fan, J. X., Ren, G. S., Tao, Q., & Xiang, T. X. 2017. Dickkopf-related protein 2 induces G0/G1 arrest and apoptosis through suppressing Wnt/beta-catenin signaling and is frequently methylated in breast cancer. ***Oncotarget***, 8(24): 39443-39459.

Munsterberg, A. E., Kitajewski, J., Bumcrot, D. A., McMahon, A. P., & Lassar, A. B. 1995. Combinatorial signaling by Sonic hedgehog and Wnt family members induces myogenic bHLH gene expression in the somite. ***Genes Dev***, 9(23): 2911-2922.

Mylona, E., Jones, K. A., Mills, S. T., & Pavlath, G. K. 2006. CD44 regulates myoblast migration and differentiation. ***J Cell Physiol***, 209(2): 314-321.

Nakai, J., Dirksen, R. T., Nguyen, H. T., Pessah, I. N., Beam, K. G., & Allen, P. D. 1996. Enhanced dihydropyridine receptor channel activity in the presence of ryanodine receptor. ***Nature***, 380(6569): 72-75.

Nakai, J., Tanabe, T., Konno, T., Adams, B., & Beam, K. G. 1998. Localization in the II-III loop of the dihydropyridine receptor of a sequence critical for excitation-contraction coupling. ***J Biol Chem***, 273(39): 24983-24986.

Nakanishi, K., Sudo, T., & Morishima, N. 2005. Endoplasmic reticulum stress signaling transmitted by ATF6 mediates apoptosis during muscle development. ***J Cell Biol***, 169(4): 555-560.

Nakashima, Y., Nishimura, S., Maeda, A., Barsoumian, E. L., Hakamata, Y., Nakai, J., Allen, P. D., Imoto, K., & Kita, T. 1997. Molecular cloning and characterization of a human brain ryanodine receptor. ***FEBS Lett***, 417(1): 157-162.

Nassari, S., Duprez, D., & Fournier-Thibault, C. 2017. Non-myogenic Contribution to Muscle Development and Homeostasis: The Role of Connective Tissues. ***Front Cell Dev Biol***, 5: 22.

Noll, M. 1993. Evolution and role of Pax genes. ***Curr Opin Genet Dev***, 3(4): 595-605.

Nowlan, N. C., Sharpe, J., Roddy, K. A., Prendergast, P. J., & Murphy, P. 2010. Mechanobiology of embryonic skeletal development: Insights from animal models. ***Birth Defects Res C Embryo Today***, 90(3): 203-213.

Obermair, G. J., Kugler, G., Baumgartner, S., Tuluc, P., Grabner, M., & Flucher, B. E. 2005. The Ca2+ channel alpha2delta-1 subunit determines Ca2+ current kinetics in skeletal muscle but not targeting of alpha1S or excitation-contraction coupling. ***J Biol Chem***, 280(3): 2229-2237.

Obermair, G. J., Tuluc, P., & Flucher, B. E. 2008. Auxiliary Ca(2+) channel subunits: lessons learned from muscle. ***Curr Opin Pharmacol***, 8(3): 311-318.

Ogawa, R., Ma, Y., Yamaguchi, M., Ito, T., Watanabe, Y., Ohtani, T., Murakami, S., Uchida, S., De Gaspari, P., Uezumi, A., Nakamura, M., Miyagoe-Suzuki, Y., Tsujikawa, K., Hashimoto, N., Braun, T., Tanaka, T.,

Takeda, S., Yamamoto, H., & Fukada, S. 2015. Doublecortin marks a new population of transiently amplifying muscle progenitor cells and is required for myofiber maturation during skeletal muscle regeneration. ***Development***, 142(1): 51-61.

Ohno, K., Sadeh, M., Blatt, I., Brengman, J. M., & Engel, A. G. 2003. E-box mutations in the RAPSN promoter region in eight cases with congenital myasthenic syndrome. ***Hum Mol Genet***, 12(7): 739-748.

Okamoto, O., & Fujiwara, S. 2006. Dermatopontin, a novel player in the biology of the extracellular matrix. ***Connect Tissue Res***, 47(4): 177-189.

Olivecrona, G. 2016. Role of lipoprotein lipase in lipid metabolism. ***Curr Opin Lipidol***, 27(3): 233-241.

Ono, Y., Calhabeu, F., Morgan, J. E., Katagiri, T., Amthor, H., & Zammit, P. S. 2011. BMP signalling permits population expansion by preventing premature myogenic differentiation in muscle satellite cells. ***Cell Death Differ***, 18(2): 222-234.

Ottenheijm, C. A. C., & Granzier, H. 2010. Lifting the Nebula: Novel Insights into Skeletal Muscle Contractility. ***Physiol***, 25(5): 304-310.

Ozaki, H., Watanabe, Y., Takahashi, K., Kitamura, K., Tanaka, A., Urase, K., Momoi, T., Sudo, K., Sakagami, J., Asano, M., Iwakura, Y., & Kawakami, K. 2001. Six4, a putative myogenin gene regulator, is not essential for mouse embryonal development. ***Mol Cell Biol***, 21(10): 3343-3350.

Pai, A. C. 1965a. Developmental Genetics of a Lethal Mutation, Muscular Dysgenesis (Mdg), in the Mouse. I. Genetic Analysis and Gross Morphology. ***Dev Biol***, 11: 82-92.

Pai, A. C. 1965b. Developmental Genetics of a Lethal Mutation, Muscular Dysgenesis (Mdg), in the Mouse. Ii. Developmental Analysis. ***Dev Biol***, 11: 93-109.

Pan, Z., Guo, Y., Qi, H., Fan, K., Wang, S., Zhao, H., Fan, Y., Xie, J., Guo, F., Hou, Y., Wang, N., Huo, R., Zhang, Y., Liu, Y., & Du, Z. 2012. M3 subtype of muscarinic acetylcholine receptor promotes cardioprotection via the suppression of miR-376b-5p. ***PLoS One***, 7(3): e32571.

Pearson, G., Robinson, F., Beers Gibson, T., Xu, B. E., Karandikar, M., Berman, K., & Cobb, M. H. 2001. Mitogen-activated protein (MAP) kinase pathways: regulation and physiological functions. ***Endocr Rev***, 22(2): 153-183.

Perdiguero, E., Ruiz-Bonilla, V., Gresh, L., Hui, L., Ballestar, E., Sousa-Victor, P., Baeza-Raja, B., Jardi, M., Bosch-Comas, A., Esteller, M., Caelles, C., Serrano, A. L., Wagner, E. F., & Munoz-Canoves, P. 2007. Genetic analysis of p38 MAP kinases in myogenesis: fundamental role of p38 alpha in abrogating myoblast proliferation. ***EMBO J***, 26(5): 1245-1256.

Perez, C. F., Mukherjee, S., & Allen, P. D. 2003. Amino acids 1-1,680 of ryanodine receptor type 1 hold critical determinants of skeletal type for excitation-contraction coupling - Role of divergence domain D2. ***J Biol Chem***, 278(41): 39644-39652.

Petrie, M. A., Suneja, M., Faidley, E., & Shields, R. K. 2014. Low force contractions induce fatigue consistent with muscle mRNA expression in people with spinal cord injury. ***Physiol Rep***, 2(2): e00248.

Pieples, K., Arteaga, G., Solaro, R. J., Grupp, I., Lorenz, J. N., Boivin, G. P., Jagatheesan, G., Labitzke, E., DeTombe, P. P., Konhilas, J. P., Irving, T. C., & Wieczorek, D. F. 2002. Tropomyosin 3 expression leads to hypercontractility and attenuates myofilament length-dependent Ca(2+) activation. ***Am J Physiol Heart Circ Physiol***, 283(4): H1344-1353.

Pietri-Rouxel, F., Gentil, C., Vassilopoulos, S., Baas, D., Mouisel, E., Ferry, A., Vignaud, A., Hourde, C., Marty, I., Schaeffer, L., Voit, T., & Garcia, L. 2010. DHPR alpha1S subunit controls skeletal muscle mass and morphogenesis. ***EMBO J***, 29(3): 643-654.

Pogozelski, A. R., Geng, T., Li, P., Yin, X., Lira, V. A., Zhang, M., Chi, J. T., & Yan, Z. 2009. p38gamma mitogen-activated protein kinase is a key regulator in skeletal muscle metabolic adaptation in mice. ***PLoS One***, 4(11): e7934.

Pollard, T. D. 1990. Actin. ***Curr Opin Cell Biol***, 2(1): 33-40.

Polster, A., Nelson, B. R., Papadopoulos, S., Olson, E. N., & Beam, K. G. 2018a. Stac proteins associate with the critical domain for excitation-contraction coupling in the II-III loop of CaV1.1. ***J Gen Physiol***, 150(4): 613-624.

Polster, A., Perni, S., Filipova, D., Moua, O., Ohrtman, J. D., Bichraoui, H., Beam, K. G., & Papadopoulos, S. 2018b. Junctional trafficking and restoration of retrograde signaling by the cytoplasmic RyR1 domain. ***J Gen Physiol***, 150(2): 293-306.

Powell, J. A., Carrasco, M. A., Adams, D. S., Drouet, B., Rios, J., Muller, M., Estrada, M., & Jaimovich, E. 2001. IP(3) receptor function and localization in myotubes: an unexplored Ca(2+) signaling pathway in skeletal muscle. ***J Cell Sci***, 114(Pt 20): 3673-3683.

Powell, J. A., Petherbridge, L., & Flucher, B. E. 1996. Formation of triads without the dihydropyridine receptor alpha subunits in cell lines from dysgenic skeletal muscle. ***J Cell Biol***, 134(2): 375-387.

Pownall, M. E., Gustafsson, M. K., & Emerson, C. P., Jr. 2002. Myogenic regulatory factors and the specification of muscle progenitors in vertebrate embryos. ***Annu Rev Cell Dev Biol***, 18: 747-783.

Protasi, F. 2015. Mitochondria association to Calcium Release Units is controlled by age and muscle activity. ***Eur J Transl Myol***, 25(4): 257-262.

Protasi, F., Takekura, H., Wang, Y., Chen, S. R., Meissner, G., Allen, P. D., & Franzini-Armstrong, C. 2000. RYR1 and RYR3 have different roles in the assembly of calcium release units of skeletal muscle. ***Biophys J***, 79(5): 2494-2508.

Qin, W., Pan, J., Bauman, W. A., & Cardozo, C. P. 2010. Differential alterations in gene expression profiles contribute to time-dependent effects of nandrolone to prevent denervation atrophy. ***BMC Genomics***, 11: 596.

Qin, Y., Peng, Y., Zhao, W., Pan, J., Ksiezak-Reding, H., Cardozo, C., Wu, Y., Divieti Pajevic, P., Bonewald, L. F., Bauman, W. A., & Qin, W. 2017. Myostatin inhibits osteoblastic differentiation by suppressing osteocyte-derived exosomal microRNA-218: A novel mechanism in muscle-bone communication. ***J Biol Chem***, 292(26): 11021-11033.

Quinn, D. M. 1987. Acetylcholinesterase: enzyme structure, reaction dynamics, and virtual transition states. ***Chem Rev***, 87(5): 955–979.

Rao, T. P., & Kuhl, M. 2010. An updated overview on Wnt signaling pathways: a prelude for more. ***Circ Res***, 106(12): 1798-1806.

Rawls, A., Valdez, M. R., Zhang, W., Richardson, J., Klein, W. H., & Olson, E. N. 1998. Overlapping functions of the myogenic bHLH genes MRF4 and MyoD revealed in double mutant mice. ***Development***, 125(13): 2349-2358.

Read, S. E., Takeda, M., & Kirkaldy-Willis, W. H. 1971. Myogenesis and neurogenesis in the chick embryo: A comparative study. ***Wilhelm Roux Arch Entwickl Mech Org***, 167(3): 187-198.

Rebbeck, R. T., Karunasekara, Y., Gallant, E. M., Board, P. G., Beard, N. A., Casarotto, M. G., & Dulhunty, A. F. 2011. The beta(1a) subunit of the skeletal DHPR binds to skeletal RyR1 and activates the channel via its 35-residue C-terminal tail. ***Biophys J***, 100(4): 922-930.

Regal, L., Shen, X. M., Selcen, D., Verhille, C., Meulemans, S., Creemers, J. W. M., & Engel, A. G. 2014. PREPL deficiency with or without cystinuria causes a novel myasthenic syndrome. ***Neurology***, 82(14): 1254-1260.

Relaix, F., Rocancourt, D., Mansouri, A., & Buckingham, M. 2005. A Pax3/Pax7-dependent population of skeletal muscle progenitor cells. ***Nature***, 435(7044): 948-953.

Ren, R. M., Liu, H., Zhao, S. H., & Cao, J. H. 2016. Targeting of miR-432 to myozenin1 to regulate myoblast proliferation and differentiation. ***Genet Mol Res***, 15(4).

Reshef, R., Maroto, M., & Lassar, A. B. 1998. Regulation of dorsal somitic cell fates: BMPs and Noggin control the timing and pattern of myogenic regulator expression. ***Genes Dev***, 12(3): 290-303.

Reuter, H., Porzig, H., Kokubun, S., & Prodhom, B. 1985. 1,4-Dihydropyridines as Tools in the Study of Ca-2+ Channels. ***Trends Neurosci***, 8(9): 396-400.

Rhodes, S. J., & Konieczny, S. F. 1989. Identification of Mrf4 - a New Member of the Muscle Regulatory Factor Gene Family. ***Genes Dev***, 3(12B): 2050-2061.

Ringner, M. 2008. What is principal component analysis? ***Nature Biotechnol*** 26(3): 303-304.

Rios, E., & Brum, G. 1987. Involvement of dihydropyridine receptors in excitation-contraction coupling in skeletal muscle. ***Nature***, 325(6106): 717-720.

Rivers, J., Simpson, D. M., Robertson, D. H. L., Gaskell, S. J., & Beynon, R. J. 2007. Absolute multiplexed quantitative analysis of protein expression during muscle development using QconCAT. ***Mol Cell Proteom***, 6(8): 1416-1427.

Rizzuto, R., De Stefani, D., Raffaello, A., & Mammucari, C. 2012. Mitochondria as sensors and regulators of calcium signalling. ***Nat Rev Mol Cell Biol***, 13(9): 566-578.

Robinson, R., Carpenter, D., Shaw, M. A., Halsall, J., & Hopkins, P. 2006. Mutations in RYR1 in malignant hyperthermia and central core disease. ***Hum Mutat***, 27(10): 977-989.

Rodriguez, J. I., Garcia-Alix, A., Palacios, J., & Paniagua, R. 1988. Changes in the long bones due to fetal immobility caused by neuromuscular disease. A radiographic and histological study. ***J Bone Joint Surg Am***, 70(7): 1052-1060.

Rolfe, R. A., Nowlan, N. C., Kenny, E. M., Cormican, P., Morris, D. W., Prendergast, P. J., Kelly, D., & Murphy, P. 2014. Identification of mechanosensitive genes during skeletal development: alteration of genes associated with cytoskeletal rearrangement and cell signalling pathways. ***BMC Genomics***, 15: 48.

Rosemblit, N., Moschella, M. C., Ondriasova, E., Gutstein, D. E., Ondrias, K., & Marks, A. R. 1999. Intracellular calcium release channel expression during embryogenesis. ***Dev Biol***, 206(2): 163-177.

Rudnicki, M. A., Braun, T., Hinuma, S., & Jaenisch, R. 1992. Inactivation of MyoD in mice leads to up-regulation of the myogenic HLH gene Myf-5 and results in apparently normal muscle development. ***Cell***, 71(3): 383-390.

Rudnicki, M. A., Schnegelsberg, P. N., Stead, R. H., Braun, T., Arnold, H. H., & Jaenisch, R. 1993. MyoD or Myf-5 is required for the formation of skeletal muscle. ***Cell***, 75(7): 1351-1359.

Ruiz-Villalba, A., Mattiotti, A., Gunst, Q. D., Cano-Ballesteros, S., van den Hoff, M. J. B., & Ruijter, J. M. 2017. Reference genes for gene expression studies in the mouse heart. ***Sci Rep***, 7.

Sabatier, L., Chen, D., Fagotto-Kaufmann, C., Hubmacher, D., McKee, M. D., Annis, D. S., Mosher, D. F., & Reinhardt, D. P. 2009. Fibrillin assembly requires fibronectin. ***Mol Biol Cell***, 20(3): 846-858.

Saggin, L., Gorza, L., Ausoni, S., & Schiaffino, S. 1990. Cardiac troponin T in developing, regenerating and denervated rat skeletal muscle. ***Development***, 110(2): 547-554.

Sahlin, K., Tonkonogi, M., & Soderlund, K. 1998. Energy supply and muscle fatigue in humans. ***Acta Physiol Scand***, 162(3): 261-266.

Sandow, A. 1952. Excitation-contraction coupling in muscular response. ***Yale J Biol Med***, 25(3): 176-201.

Sassoon, D., Lyons, G., Wright, W. E., Lin, V., Lassar, A., Weintraub, H., & Buckingham, M. 1989. Expression of two myogenic regulatory factors myogenin and MyoD1 during mouse embryogenesis. ***Nature***, 341(6240): 303-307.

Schartner, V., Romero, N. B., Donkervoort, S., Treves, S., Munot, P., Pierson, T. M., Dabaj, I., Malfatti, E., Zaharieva, I. T., Zorzato, F., Abath Neto, O., Brochier, G., Lornage, X., Eymard, B., Taratuto, A. L., Bohm, J., Gonorazky, H., Ramos-Platt, L., Feng, L., Phadke, R., Bharucha-Goebel, D. X., Sumner, C. J., Bui, M. T., Lacene, E., Beuvin, M., Labasse, C., Dondaine, N., Schneider, R., Thompson, J., Boland, A., Deleuze, J. F., Matthews, E., Pakleza, A. N., Sewry, C. A., Biancalana, V., Quijano-Roy, S., Muntoni, F., Fardeau, M., Bonnemann, C. G., & Laporte, J. 2017. Dihydropyridine receptor (DHPR, CACNA1S) congenital myopathy. ***Acta Neuropathol***, 133(4): 517-533.

Schiaffino, S., & Reggiani, C. 2011. Fiber types in mammalian skeletal muscles. ***Physiol Rev***, 91(4): 1447-1531.

Schiaffino, S., Rossi, A. C., Smerdu, V., Leinwand, L. A., & Reggiani, C. 2015. Developmental myosins: expression patterns and functional significance. ***Skelet Muscle***, 5: 22.

Schroder, E. A., & Esser, K. A. 2013. Circadian rhythms, skeletal muscle molecular clocks, and exercise. ***Exerc Sport Sci Rev***, 41(4): 224-229.

Schwartz, L. M. 2008. Atrophy and programmed cell death of skeletal muscle. ***Cell Death Differ***, 15(7): 1163-1169.

Scott, W., Stevens, J., & Binder-Macleod, S. A. 2001. Human skeletal muscle fiber type classifications. ***Phys Ther***, 81(11): 1810-1816.

Seale, P., Sabourin, L. A., Girgis-Gabardo, A., Mansouri, A., Gruss, P., & Rudnicki, M. A. 2000. Pax7 is required for the specification of myogenic satellite cells. ***Cell***, 102(6): 777-786.

Seilertuyns, A., Eldridge, J. D., & Paterson, B. M. 1984. Expression and Regulation of Chicken Actin Genes Introduced into Mouse Myogenic and Nonmyogenic Cells. ***Proc Natl Acad Sci USA***, 81(10): 2980-2984.

Sejersen, T., & Lendahl, U. 1993. Transient expression of the intermediate filament nestin during skeletal muscle development. ***J Cell Sci***, 106 (Pt 4): 1291-1300.

Sekulic-Jablanovic, M., Palmowski-Wolfe, A., Zorzato, F., & Treves, S. 2015. Characterization of excitation-contraction coupling components in human extraocular muscles. ***Biochem J***, 466(1): 29-36.

Shah, S. B., Su, F. C., Jordan, K., Milner, D. J., Friden, J., Capetanaki, Y., & Lieber, R. L. 2002. Evidence for increased myofibrillar mobility in desmin-null mouse skeletal muscle. ***J Experiment Biol***, 205(3): 321-325.

Shang, F. F., Xia, Q. J., Liu, W., Xia, L., Qian, B. J., You, L., He, M., Yang, J. L., & Wang, T. H. 2016. miR-434-3p and DNA hypomethylation co-regulate eIF5A1 to increase AChRs and to improve plasticity in SCT rat skeletal muscle. ***Sci Rep***, 6.

Shapland, C., Hsuan, J. J., Totty, N. F., & Lawson, D. 1993. Purification and properties of transgelin: a transformation and shape change sensitive actin-gelling protein. ***J Cell Biol***, 121(5): 1065-1073.

Sheikh, F., Lyon, R. C., & Chen, J. 2015. Functions of myosin light chain-2 (MYL2) in cardiac muscle and disease. ***Gene***, 569(1): 14-20.

Shellswell, G. B. 1977. The formation of discrete muscles from the chick wing dorsal and ventral muscle masses in the absence of nerves. ***J Embryol Exp Morphol***, 41: 269-277.

Sheridan, D. C., Takekura, H., Franzini-Armstrong, C., Beam, K. G., Allen, P. D., & Perez, C. F. 2006. Bidirectional signaling between calcium channels of skeletal muscle requires multiple direct and indirect interactions. ***Proc Natl Acad Sci USA***, 103(52): 19760-19765.

Shtilbans, A., Choi, S. G., Fowkes, M. E., Khitrov, G., Shahbazi, M., Ting, J., Zhang, W., Sun, Y., Sealfon, S. C., & Lange, D. J. 2011. Differential gene expression in patients with amyotrophic lateral sclerosis. ***Amyotroph Lateral Scler***, 12(4): 250-256.

Sifringer, M., Uhlenberg, B., Lammel, S., Hanke, R., Neumann, B., von Moers, A., Koch, I., & Speer, A. 2004. Identification of transcripts from a subtraction library which might be responsible for the mild phenotype in an intrafamilially variable course of Duchenne muscular dystrophy. ***Hum Genet***, 114(2): 149-156.

Sine, S. M. 2012. End-plate acetylcholine receptor: structure, mechanism, pharmacology, and disease. ***Physiol Rev***, 92(3): 1189-1234.

Smith, C. M., Finger, J. H., Hayamizu, T. F., McCright, I. J., Xu, J., Berghout, J., Campbell, J., Corbani, L. E., Forthofer, K. L., Frost, P. J., Miers, D., Shaw, D. R., Stone, K. R., Eppig, J. T., Kadin, J. A., Richardson, J. E., & Ringwald, M. 2014. The mouse Gene Expression Database (GXD): 2014 update. ***Nucleic Acids Res***, 42(Database issue): D818-824.

Smyth, G. K. 2004. Linear models and empirical bayes methods for assessing differential expression in microarray experiments. ***Stat Appl Genet Mol Biol***, 3: Article3.

Snoeck, M., van Engelen, B. G., Kusters, B., Lammens, M., Meijer, R., Molenaar, J. P., Raaphorst, J., Verschuuren-Bemelmans, C. C., Straathof, C. S., Sie, L. T., de Coo, I. F., van der Pol, W. L., de Visser, M., Scheffer, H., Treves, S., Jungbluth, H., Voermans, N. C., & Kamsteeg, E. J. 2015. RYR1-related myopathies: a wide spectrum of phenotypes throughout life. ***Eur J Neurol***, 22(7): 1094-1112.

Snow, C. J., Peterson, M. T., Khalil, A., & Henry, C. A. 2008. Muscle development is disrupted in zebrafish embryos deficient for fibronectin. ***Dev Dyn***, 237(9): 2542-2553.

Soriano-Arroquia, A., House, L., Tregilgas, L., Canty-Laird, E., & Goljanek-Whysall, K. 2016. The functional consequences of age-related changes in microRNA expression in skeletal muscle. ***Biogerontology***, 17(3): 641-654.

Sparrow, J., Hughes, S. M., & Segalat, L. 2008. Other model organisms for sarcomeric muscle diseases. ***Adv Exp Med Biol***, 642: 192-206.

Staverosky, J. A., Pryce, B. A., Watson, S. S., & Schweitzer, R. 2009. Tubulin polymerization-promoting protein family member 3, Tppp3, is a specific marker of the differentiating tendon sheath and synovial joints. ***Dev Dyn***, 238(3): 685-692.

Striessnig, J., Bolz, H. J., & Koschak, A. 2010. Channelopathies in Cav1.1, Cav1.3, and Cav1.4 voltage-gated L-type Ca2+ channels. ***Pflugers Arch***, 460(2): 361-374.

Sumiyoshi, H., Laub, F., Yoshioka, H., & Ramirez, F. 2001. Embryonic expression of type XIX collagen is transient and confined to muscle cells. ***Dev Dyn***, 220(2): 155-162.

Sun, L., Xie, H. M., Mori, M. A., Alexander, R., Yuan, B. B., Hattangadi, S. M., Liu, Q. Q., Kahn, C. R., & Lodish, H. F. 2011. Mir193b-365 is essential for brown fat differentiation. ***Nature Cell Biology***, 13(8): 958-U198.

Sun, L. Y., Bie, Z. D., Zhang, C. H., Li, H., Li, L. D., & Yang, J. 2016. MiR-154 directly suppresses DKK2 to activate Wnt signaling pathway and enhance activation of cardiac fibroblasts. ***Cell Biol Internat***, 40(12): 1271-1279.

Sun, M., Huang, F., Yu, D., Zhang, Y., Xu, H., Zhang, L., Li, L., Dong, L., Guo, L., & Wang, S. 2015. Autoregulatory loop between TGF-beta1/miR-411-5p/SPRY4 and MAPK pathway in rhabdomyosarcoma modulates proliferation and differentiation. ***Cell Death Dis***, 6: e1859.

Sun, W., He, T., Qin, C., Qiu, K., Zhang, X., Luo, Y., Li, D., & Yin, J. 2017. A potential regulatory network underlying distinct fate commitment of myogenic and adipogenic cells in skeletal muscle. ***Sci Rep***, 7: 44133.

Suzuki, S. T. 2000. Recent progress in protocadherin research. ***Exp Cell Res***, 261(1): 13-18.

Svensson, A., Norrby, M., Libelius, R., & Tagerud, S. 2008. Secreted frizzled related protein 1 (Sfrp1) and Wnt signaling in innervated and denervated skeletal muscle. ***J Mol Histol***, 39(3): 329-337.

Tadmouri, A., Kiyonaka, S., Barbado, M., Rousset, M., Fablet, K., Sawamura, S., Bahembera, E., Pernet-Gallay, K., Arnoult, C., Miki, T., Sadoul, K., Gory-Faure, S., Lambrecht, C., Lesage, F., Akiyama, S., Khochbin, S., Baulande, S., Janssens, V., Andrieux, A., Dolmetsch, R., Ronjat, M., Mori, Y., & De Waard, M. 2012. Cacnb4 directly couples electrical activity to gene expression, a process defective in juvenile epilepsy. ***EMBO J***, 31(18): 3730-3744.

Tajbakhsh, S. 2009. Skeletal muscle stem cells in developmental versus regenerative myogenesis. ***J Intern Med***, 266(4): 372-389.

Takano-Ohmuro, H., Obinata, T., Kawashima, M., Masaki, T., & Tanaka, T. 1985. Embryonic chicken skeletal, cardiac, and smooth muscles express a common embryo-specific myosin light chain. ***J Cell Biol***, 100(6): 2025-2030.

Takekura, H., Bennett, L., Tanabe, T., Beam, K. G., & Franzini-Armstrong, C. 1994. Restoration of junctional tetrads in dysgenic myotubes by dihydropyridine receptor cDNA. ***Biophys J***, 67(2): 793-803.

Takekura, H., Nishi, M., Noda, T., Takeshima, H., & Franziniarmstrong, C. 1995. Abnormal Junctions between Surface-Membrane and Sarcoplasmic-Reticulum in Skeletal-Muscle with a Mutation Targeted to the Ryanodine Receptor. ***Proc Natl Acad Sci USA***, 92(8): 3381-3385.

Takeshima, H., Iino, M., Takekura, H., Nishi, M., Kuno, J., Minowa, O., Takano, H., & Noda, T. 1994. Excitation-contraction uncoupling and muscular degeneration in mice lacking functional skeletal muscle ryanodine-receptor gene. ***Nature***, 369(6481): 556-559.

Takeshima, H., Nishimura, S., Matsumoto, T., Ishida, H., Kangawa, K., Minamino, N., Matsuo, H., Ueda, M., Hanaoka, M., Hirose, T., & et al. 1989. Primary structure and expression from complementary DNA of skeletal muscle ryanodine receptor. ***Nature***, 339(6224): 439-445.

Tanabe, T., Beam, K. G., Adams, B. A., Niidome, T., & Numa, S. 1990. Regions of the skeletal muscle dihydropyridine receptor critical for excitation-contraction coupling. ***Nature***, 346(6284): 567-569.

Tanabe, T., Beam, K. G., Powell, J. A., & Numa, S. 1988. Restoration of excitation-contraction coupling and slow calcium current in dysgenic muscle by dihydropyridine receptor complementary DNA. ***Nature***, 336(6195): 134-139.

Tanabe, T., Takeshima, H., Mikami, A., Flockerzi, V., Takahashi, H., Kangawa, K., Kojima, M., Matsuo, H., Hirose, T., & Numa, S. 1987. Primary structure of the receptor for calcium channel blockers from skeletal muscle. ***Nature***, 328(6128): 313-318.

Tanaka, T., Wakabayashi, T., Oizumi, H., Nishio, S., Sato, T., Harada, A., Fujii, D., Matsuo, Y., Hashimoto, T., & Iwatsubo, T. 2014. CLAC-P/collagen type XXV is required for the intramuscular innervation of motoneurons during neuromuscular development. ***J Neurosci***, 34(4): 1370-1379.

Te, K. G., & Reggiani, C. 2002. Skeletal muscle fibre type specification during embryonic development. ***J Muscle Res Cell Motil***, 23(1): 65-69.

Tickle, C., & Towers, M. 2017. Sonic Hedgehog Signaling in Limb Development. ***Front Cell Dev Biol***, 5: 14.

Tidball, J. G. 2005. Mechanical signal transduction in skeletal muscle growth and adaptation. ***J Appl Physiol***, 98(5): 1900-1908.

Toivonen, J. M., Manzano, R., Olivan, S., Zaragoza, P., Garcia-Redondo, A., & Osta, R. 2014. MicroRNA-206: a potential circulating biomarker candidate for amyotrophic lateral sclerosis. ***PLoS One***, 9(2): e89065.

Tondeleir, D., Vandamme, D., Vandekerckhove, J., Ampe, C., & Lambrechts, A. 2009. Actin isoform expression patterns during mammalian development and in pathology: insights from mouse models. ***Cell Motil Cytoskeleton***, 66(10): 798-815.

Tripathy, A., Xu, L., Mann, G., & Meissner, G. 1995. Calmodulin Activation and Inhibition of Skeletal-Muscle Ca2+ Release Channel (Ryanodine Receptor). ***Biophys J***, 69(1): 106-119.

Tuluc, P., Molenda, N., Schlick, B., Obermair, G. J., Flucher, B. E., & Jurkat-Rott, K. 2009. A CaV1.1 Ca2+ channel splice variant with high conductance and voltage-sensitivity alters EC coupling in developing skeletal muscle. ***Biophys J***, 96(1): 35-44.

Ulke-Lemee, A., Ishida, H., Chappellaz, M., Vogel, H. J., & MacDonald, J. A. 2014. Two domains of the smoothelin-like 1 protein bind apo- and calcium-calmodulin independently. ***Biochim Biophys Acta***, 1844(9): 1580-1590.

Ursitti, J. A., Lee, P. C., Resneck, W. G., McNally, M. M., Bowman, A. L., O'Neill, A., Stone, M. R., & Bloch, R. J. 2004. Cloning and characterization of cytokeratins 8 and 19 in adult rat striated muscle. Interaction with the dystrophin glycoprotein complex. ***J Biol Chem***, 279(40): 41830-41838.

Ursu, D., Schuhmeier, R. P., Freichel, M., Flockerzi, V., & Melzer, W. 2004. Altered inactivation of Ca2+ current and Ca2+ release in mouse muscle fibers deficient in the DHP receptor gamma1 subunit. ***J Gen Physiol***, 124(5): 605-618.

Uyan, O., Omur, O., Agim, Z. S., Ozoguz, A., Li, H., Parman, Y., Deymeer, F., Oflazer, P., Koc, F., Tan, E., Ozcelik, H., & Basak, A. N. 2013. Genome-wide copy number variation in sporadic amyotrophic lateral sclerosis in the Turkish population: deletion of EPHA3 is a possible protective factor. ***PLoS One***, 8(8): e72381.

Van Petegem, F. 2012. Ryanodine receptors: structure and function. ***J Biol Chem***, 287(38): 31624-31632.

Van Petegem, F. 2015. Ryanodine receptors: allosteric ion channel giants. ***J Mol Biol***, 427(1): 31-53.

Vasyutina, E., Lenhard, D. C., & Birchmeier, C. 2007. Notch function in myogenesis. ***Cell Cycle***, 6(12): 1451-1454.

Verardo, L. L., Nascimento, C. S., Silva, F. F., Gasparino, E., Toriyama, E., Barbosa, A. R., Perisse, I. V., Costa, K. A., Lopes, P. S., & Guimaraes, S. E. F. 2013. Identification and expression levels of pig miRNAs in skeletal muscle. ***Livestock Sci***, 154(1-3): 45-54.

Voermans, N. C., Gerrits, K., van Engelen, B. G., & de Haan, A. 2014. Compound heterozygous mutations of the TNXB gene cause primary myopathy. ***Neuromuscul Disord***, 24(1): 88-89.

von Maltzahn, J., Bentzinger, C. F., & Rudnicki, M. A. 2012. Wnt7a-Fzd7 signalling directly activates the Akt/mTOR anabolic growth pathway in skeletal muscle. ***Nat Cell Biol***, 14(2): 186-191.

Voronova, A., Coyne, E., Al Madhoun, A., Fair, J. V., Bosiljcic, N., St-Louis, C., Li, G., Thurig, S., Wallace, V. A., Wiper-Bergeron, N., & Skerjanc, I. S. 2013. Hedgehog signaling regulates MyoD expression and activity. ***J Biol Chem***, 288(6): 4389-4404.

Wagatsuma, A., & Sakuma, K. 2013. Mitochondria as a potential regulator of myogenesis. ***Sci World J***, 2013: 593267.

Wang, C., Yu, G., Liu, J., Wang, J., Zhang, Y., Zhang, X., Zhou, Z., & Huang, Z. 2012. Downregulation of PCDH9 predicts prognosis for patients with glioma. ***J Clin Neurosci***, 19(4): 541-545.

Wang, X. X., Blagden, C., Fan, J. H., Nowak, S. J., Taniuchi, I., Littman, D. R., & Burden, S. J. 2005. Runx1 prevents wasting, myofibrillar disorganization, and autophagy of skeletal muscle. ***Genes & Development***, 19(14): 1715-1722.

Watson, S. S., Riordan, T. J., Pryce, B. A., & Schweitzer, R. 2009. Tendons and muscles of the mouse forelimb during embryonic development. ***Dev Dyn***, 238(3): 693-700.

Wei, L., Gallant, E. M., Dulhunty, A. F., & Beard, N. A. 2009. Junctin and triadin each activate skeletal ryanodine receptors but junctin alone mediates functional interactions with calsequestrin. ***Internat J Biochem Cell Biol***, 41(11): 2214-2224.

Westerblad, H., Bruton, J. D., & Katz, A. 2010. Skeletal muscle: energy metabolism, fiber types, fatigue and adaptability. ***Exp Cell Res***, 316(18): 3093-3099.

Winder, S. J., Walsh, M. P., Vasulka, C., & Johnson, J. D. 1993. Calponin-calmodulin interaction: properties and effects on smooth and skeletal muscle actin binding and actomyosin ATPases. ***Biochem***, 32(48): 13327-13333.

Witherspoon, J. W., & Meilleur, K. G. 2016. Review of RyR1 pathway and associated pathomechanisms. ***Acta Neuropathol Commun***, 4(1): 121.

Wittenberg, B. A. 2009. Both hypoxia and work are required to enhance expression of myoglobin in skeletal muscle. Focus on "Hypoxia reprograms calcium signaling and regulates myoglobin expression". ***Am J Physiol Cell Physiol***, 296(3): C390-392.

Wolfe, R. R. 2006. The underappreciated role of muscle in health and disease. ***Am J Clin Nutr***, 84(3): 475-482.

Woodcockmitchell, J., Mitchell, J. J., Low, R. B., Kieny, M., Sengel, P., Rubbia, L., Skalli, O., Jackson, B., & Gabbiani, G. 1988. Alpha-Smooth Muscle Actin Is Transiently Expressed in Embryonic Rat Cardiac and Skeletal-Muscles. ***Differentiation***, 39(3): 161-166.

Wright, W. E., Sassoon, D. A., & Lin, V. K. 1989. Myogenin, a Factor Regulating Myogenesis, Has a Domain Homologous to Myod. ***Cell***, 56(4): 607-617.

Wu, J., Yan, Z., Li, Z., Qian, X., Lu, S., Dong, M., Zhou, Q., & Yan, N. 2016. Structure of the voltage-gated calcium channel Cav1.1 at 3.6 A resolution. ***Nature***, 537(7619): 191-196.

Wu, R., Li, H., Zhai, L., Zou, X., Meng, J., Zhong, R., Li, C., Wang, H., Zhang, Y., & Zhu, D. 2015. MicroRNA-431 accelerates muscle regeneration and ameliorates muscular dystrophy by targeting Pax7 in mice. ***Nat Commun***, 6: 7713.

Xiao, Q., & Ge, G. 2012. Lysyl oxidase, extracellular matrix remodeling and cancer metastasis. ***Cancer Microenviron***, 5(3): 261-273.

Xie, S. J., Li, J. H., Chen, H. F., Tan, Y. Y., Liu, S. R., Zhang, Y., Xu, H., Yang, J. H., Liu, S., Zheng, L. L., Huang, M. B., Guo, Y. H., Zhang, Q., Zhou, H., & Qu, L. H. 2018. Inhibition of the JNK/MAPK signaling pathway by myogenesis-associated miRNAs is required for skeletal muscle development. ***Cell Death Differ***.

Yamada, A. K., Verlengia, R., & Bueno Junior, C. R. 2012. Mechanotransduction pathways in skeletal muscle hypertrophy. ***J Recept Signal Transduct Res***, 32(1): 42-44.

Yan, Z., Bai, X. C., Yan, C., Wu, J., Li, Z., Xie, T., Peng, W., Yin, C. C., Li, X., Scheres, S. H., Shi, Y., & Yan, N. 2014. Structure of the rabbit ryanodine receptor RyR1 at near-atomic resolution. ***Nature***.

Yang, D., Pan, Z., Takeshima, H., Wu, C., Nagaraj, R. Y., Ma, J., & Cheng, H. 2001. RyR3 amplifies RyR1-mediated Ca(2+)-induced Ca(2+) release in neonatal mammalian skeletal muscle. ***J Biol Chem***, 276(43): 40210-40214.

Yang, W., Chen, Y., Zhang, Y., Wang, X., Yang, N., & Zhu, D. 2006. Extracellular signal-regulated kinase 1/2 mitogen-activated protein kinase pathway is involved in myostatin-regulated differentiation repression. ***Cancer Res***, 66(3): 1320-1326.

Yann Fedon, A. B., Stéphanie Gay, Barbara Vernus, Francis Bacou and Henri Bernardi 2012. Role and Function of Wnts in the Regulation of Myogenesis: When Wnt Meets Myostatin, Skeletal Muscle - From Myogenesis to Clinical Relations,. In J. Cseri (Ed.).

Ye, J., Coulouris, G., Zaretskaya, I., Cutcutache, I., Rozen, S., & Madden, T. L. 2012. Primer-BLAST: a tool to design target-specific primers for polymerase chain reaction. ***BMC Bioinformatics***, 13: 134.

Yeung, C. Y., Zeef, L. A., Lallyett, C., Lu, Y., Canty-Laird, E. G., & Kadler, K. E. 2015. Chick tendon fibroblast transcriptome and shape depend on whether the cell has made its own collagen matrix. ***Sci Rep***, 5: 13555.

Yi, H., Forsythe, S., He, Y., Liu, Q., Xiong, G., Wei, S., Li, G., Atala, A., Skardal, A., & Zhang, Y. 2017. Tissue-specific extracellular matrix promotes myogenic differentiation of human muscle progenitor cells on gelatin and heparin conjugated alginate hydrogels. ***Acta Biomater***.

Yin, C. C., D'Cruz, L. G., & Lai, F. A. 2008. Ryanodine receptor arrays: not just a pretty pattern? ***Trends Cell Biol***, 18(4): 149-156.

Yin, C. C., & Lai, F. A. 2000. Intrinsic lattice formation by the ryanodine receptor calcium-release channel. ***Nat Cell Biol***, 2(9): 669-671.

Yuan, J. S., Reed, A., Chen, F., & Stewart, C. N., Jr. 2006. Statistical analysis of real-time PCR data. ***BMC Bioinformatics***, 7: 85.

Zalk, R., Clarke, O. B., Georges, A. D., Grassucci, R. A., Reiken, S., Mancia, F., Hendrickson, W. A., Frank, J., & Marks, A. R. 2014. Structure of a mammalian ryanodine receptor. ***Nature***, 517(7532):44-9.

Zhai, L., Wu, R., Han, W., Zhang, Y., & Zhu, D. 2017. miR-127 enhances myogenic cell differentiation by targeting S1PR3. ***Cell Death Dis***, 8(3): e2707.

Zhu, Y., Kakinuma, N., Wang, Y., & Kiyama, R. 2008. Kank proteins: a new family of ankyrin-repeat domain-containing proteins. ***Biochim Biophys Acta***, 1780(2): 128-133.

Zvaritch, E., Depreux, F., Kraeva, N., Loy, R. E., Goonasekera, S. A., Boncompagni, S., Kraev, A., Gramolini, A. O., Dirksen, R. T., Franzini-Armstrong, C., Seidman, C. E., Seidman, J. G., & Maclennan, D. H. 2007. An Ryr1I4895T mutation abolishes Ca2+ release channel function and delays development in homozygous offspring of a mutant mouse line. ***Proc Natl Acad Sci USA***, 104(47): 18537-18542.

Zweers, M. C., van Vlijmen-Willems, I. M., van Kuppevelt, T. H., Mecham, R. P., Steijlen, P. M., Bristow, J., & Schalkwijk, J. 2004. Deficiency of tenascin-X causes abnormalities in dermal elastic fiber morphology. ***J Invest Dermatol***, 122(4): 885-891.

6 Supplement

Suppl. Table 1. DEGs at E18.5 involved in signaling cascades

Transcript Cluster ID	Description	Gene Symbol	Fold Change	
			E18.5 $RYR1^{-/-}$ vs. WT	E18.5 $Ca_v1.1^{-/-}$ vs. WT
MAPK signaling pathway				
17498041	dual specificity phosphatase 8	Dusp8	-2.06	-2.29
17277387	FBJ osteosarcoma oncogene	Fos	-2.05	-1.55
17463332	fibroblast growth factor 6	Fgf6	-2.01	-1.72
17345465	serum response factor	Srf	-1.76	-1.87
17342642	dual specificity phosphatase 1	Dusp1	-1.73	-1.66
17220475	dual specificity phosphatase 10; predicted gene, 39725	Dusp10	-1.7	-1.65
17480420	p21 protein (Cdc42/Rac)-activated kinase 1	Pak1	-1.69	-2.27
17336824	heat shock protein 1-like	Hspa1l	-1.68	-2.08
17342249	calcium channel, voltage-dependent, T type, alpha 1H subunit	Cacna1h	-1.56	-1.6
17212185	interleukin 1 receptor, type I	Il1r1	1.52	1.63
17502001	jun D proto-oncogene	Jund	-1.93	NA
17427312	jun proto-oncogene	Jun	-1.76	NA
17332974	ribosomal protein S6 kinase, polypeptide 2	Rps6ka2	-1.62	NA
17271168	protein kinase C, alpha	Prkca	-1.5	NA
17339772	RAS, guanyl releasing protein 3	Rasgrp3	-1.5	NA
17283270	ribosomal protein S6 kinase, polypeptide 5	Rps6ka5	1.52	NA
17413915	transforming growth factor, beta receptor I	Tgfbr1	1.56	NA
17443342	heat shock protein 1	Hspb1	NA	-2.86
17217678	calcium channel, voltage-dependent, L type, alpha 1S subunit	Cacna1s	NA	-2.67
17271143	calcium channel, voltage-dependent, gamma subunit 1	Cacng1	NA	-1.92
17264960	fibroblast growth factor 11	Fgf11	NA	-1.77
17439517	fibroblast growth factor 5	Fgf5	NA	-1.72
17320307	mitogen-activated protein kinase 12	Mapk12	NA	-1.71
17473166	calcium channel, voltage-dependent, gamma subunit 6	Cacng6	NA	-1.7
17390079	phospholipase A2, group IVE	Pla2g4e	NA	-1.69
17456627	filamin C, gamma	Flnc	NA	-1.6
17235511	growth arrest and DNA-damage-inducible 45 beta	Gadd45b	NA	-1.59
17406031	Rap guanine nucleotide exchange factor (GEF) 2	Rapgef2	NA	-1.56
17371912	sterile alpha motif and leucine zipper containing kinase AZK	Zak	NA	-1.5

Transcript Cluster ID	Description	Gene Symbol	Fold Change	
			E18.5 $RYR1^{-/-}$ vs. WT	E18.5 $Ca_v1.1^{-/-}$ vs. WT
17290111	fibroblast growth factor 10	Fgf10	NA	1.5
17252013	arrestin, beta 2	Arrb2	NA	1.51
17482766	protein kinase C, beta	Prkcb	NA	1.55
17500535	dual specificity phosphatase 4	Dusp4	NA	1.79
PI3K/Akt/mTOR signaling pathway				
17321094	collagen, type II, alpha 1	Col2a1	-5.57	-3.25
17336681	tenascin XB	Tnxb	-2.81	-2.32
17399347	thrombospondin 3	Thbs3	-2.61	-2.02
17426365	tenascin C	Tnc	-2.35	-2.58
17294934	thrombospondin 4	Thbs4	-2.31	-2.8
17463332	fibroblast growth factor 6	Fgf6	-2.01	-1.72
17458682	cAMP responsive element binding protein 5	Creb5	-1.61	-1.83
17322369	integrin alpha 5 (fibronectin receptor alpha)	Itga5	-1.6	-1.5
17530159	protein phosphatase 2, regulatory subunit B, alpha	Ppp2r3a	-1.51	-1.69
17434933	hepatocyte growth factor	Hgf	1.58	1.97
17295796	phosphatidylinositol 3-kinase, regulatory subunit, polypeptide 1 (p85 alpha)	Pik3r1	1.63	1.84
17381717	integrin alpha 8	Itga8	1.64	1.52
17530540	collagen, type VI, alpha 5	Col6a5	2.23	2.41
17224071	fibronectin 1	Fn1	-1.74	NA
17271168	protein kinase C, alpha	Prkca	-1.5	NA
17501919	cartilage oligomeric matrix protein	Comp	NA	-3.48
17255227	chondroadherin	Chad	NA	-3.31
17211458	collagen, type IX, alpha 1	Col9a1	NA	-3.13
17228712	tenascin N	Tnn	NA	-1.79
17264960	fibroblast growth factor 11	Fgf11	NA	-1.77
17439517	fibroblast growth factor 5	Fgf5	NA	-1.72
17427746	protein kinase, AMP-activated, alpha 2 catalytic subunit	Prkaa2	NA	-1.72
17385654	integrin beta 6	Itgb6	NA	-1.58
17226043	B cell leukemia/lymphoma 2	Bcl2	NA	-1.57
17290111	fibroblast growth factor 10	Fgf10	NA	1.5
17507799	angiopoietin 2	Angpt2	NA	1.53
17211043	serum/glucocorticoid regulated kinase 3	Sgk3	NA	1.57
17316780	angiopoietin 1	Angpt1	NA	1.65
17301886	lysophosphatidic acid receptor 6	Lpar6	NA	1.69
17457310	cholinergic receptor, muscarinic 2, cardiac	Chrm2	NA	1.71
17310259	prolactin receptor	Prlr	NA	1.75

Transcript Cluster ID	Description	Gene Symbol	Fold Change	
			E18.5 $RYR1^{-/-}$ vs. WT	E18.5 $Ca_v1.1^{-/-}$ vs. WT
17351053	colony stimulating factor 1 receptor	Csf1r	NA	1.93
17284839	integrin beta 8	Itgb8	NA	2.26
17380222	phosphoenolpyruvate carboxykinase 1, cytosolic	Pck1	NA	3.12
Wnt signaling pathway				
17285546	secreted frizzled-related protein 4	Sfrp4	-2.11	-2.12
17237701	Wnt inhibitory factor 1	Wif1	-1.7	-2.45
17394806	nuclear factor of activated T cells, cytoplasmic, calcineurin dependent 2	Nfatc2	-1.56	-1.57
17427312	jun proto-oncogene	Jun	-1.76	NA
17271168	protein kinase C, alpha	Prkca	-1.5	NA
17500068	secreted frizzled-related protein 1	Sfrp1	1.78	NA
17260261	calcium/calmodulin-dependent protein kinase II, beta	Camk2b	NA	-2.23
17420154	wingless-type MMTV integration site family, member 4	Wnt4	NA	-1.53
17482766	protein kinase C, beta	Prkcb	NA	1.55
17402698	dickkopf homolog 2 (Xenopus laevis)	Dkk2	NA	1.65
17307738	frizzled homolog 3 (Drosophila)	Fzd3	NA	1.81
PPAR signaling pathway				
17501633	lipoprotein lipase	Lpl	1.63	2.33
17529398	malic enzyme 1, NADP(+)-dependent, cytosolic	Me1	2	2.28
17233384	fatty acid binding protein 7, brain	Fabp7	2.43	2.13
17404091	fatty acid binding protein 4, adipocyte	Fabp4	NA	1.74
17400862	3-hydroxy-3-methylglutaryl-Coenzyme A synthase 2	Hmgcs2	NA	1.74
17427994	sterol carrier protein 2, liver	Scp2	NA	1.97
17500996	acyl-CoA synthetase long-chain family member 1	Acsl1	NA	2.72
17461942	peroxisome proliferator activated receptor gamma	Pparg	NA	2.97
17380222	phosphoenolpyruvate carboxykinase 1, cytosolic	Pck1	NA	3.12
17492406	perilipin 1	Plin1	NA	4.02
17324404	adiponectin, C1Q and collagen domain containing	Adipoq	NA	4.12
17502899	uncoupling protein 1 (mitochondrial, proton carrier)	Ucp1	NA	21.17
cAMP signaling pathway				
17277387	FBJ osteosarcoma oncogene	Fos	-2.05	-1.55
17378663	myosin, light polypeptide 9, regulatory	Myl9	-1.76	-2.23
17480420	p21 protein (Cdc42/Rac)-activated kinase 1	Pak1	-1.69	-2.27
17458682	cAMP responsive element binding protein 5	Creb5	-1.61	-1.83

Transcript Cluster ID	Description	Gene Symbol	Fold Change	
			E18.5 $RYR1^{-/-}$ vs. WT	E18.5 $Ca_v1.1^{-/-}$ vs. WT
17534337	ATPase, (Na+)/K+ transporting, beta 4 polypeptide	Atp1b4	-1.61	-1.97
17359160	phospholipase C, epsilon 1	Plce1	-1.6	-1.77
17295796	phosphatidylinositol 3-kinase, regulatory subunit, polypeptide 1 (p85 alpha)	Pik3r1	1.63	1.84
17510772	Hedgehog-interacting protein	Hhip	1.89	2.07
17427312	jun proto-oncogene	Jun	-1.76	NA
17217678	calcium channel, voltage-dependent, L type, alpha 1S subunit	Cacna1s	NA	-2.67
17260261	calcium/calmodulin-dependent protein kinase II, beta	Camk2b	NA	-2.23
17264792	ATPase, Na+/K+ transporting, beta 2 polypeptide	Atp1b2	NA	-1.87
17535572	ATPase, Ca++ transporting, plasma membrane 3	Atp2b3	NA	-1.72
17229178	ATPase, Na+/K+ transporting, beta 1 polypeptide	Atp1b1	NA	-1.68
17489420	FXYD domain-containing ion transport regulator 1	Fxyd1	NA	-1.6
17331918	T cell lymphoma invasion and metastasis 1	Tiam1	NA	1.54
17403866	prostaglandin E receptor 3 (subtype EP3)	Ptger3	NA	1.56
17325206	adenylate cyclase 5	Adcy5	NA	1.58
17245874	GLI-Kruppel family member GLI1	Gli1	NA	1.63
17406145	glutamate receptor, ionotropic, AMPA2 (alpha 2)	Gria2	NA	1.7
17457310	cholinergic receptor, muscarinic 2, cardiac	Chrm2	NA	1.71
17482021	phosphodiesterase 3B, cGMP-inhibited	Pde3b	NA	1.77
17355264	melanocortin 2 receptor	Mc2r	NA	1.97
17452709	hydrocarboxylic acid receptor 1	Hcar1	NA	2.5
cGMP-PKG signaling pathway				
17377816	myosin, light polypeptide kinase 2, skeletal muscle	Mylk2	-2.4	-2.82
17306577	myosin, heavy polypeptide 7, cardiac muscle, beta	Myh7	-1.79	-1.72
17345465	serum response factor	Srf	-1.76	-1.87
17378663	myosin, light polypeptide 9, regulatory	Myl9	-1.76	-2.23
17458682	cAMP responsive element binding protein 5	Creb5	-1.61	-1.83
17534337	ATPase, (Na+)/K+ transporting, beta 4 polypeptide	Atp1b4	-1.61	-1.97
17394806	nuclear factor of activated T cells, cytoplasmic, calcineurin dependent 2	Nfatc2	-1.56	-1.57

Transcript Cluster ID	Description	Gene Symbol	Fold Change	
			E18.5 $RYR1^{-/-}$ vs. WT	E18.5 $Ca_v1.1^{-/-}$ vs. WT
17304012	potassium large conductance calcium-activated channel, subfamily M, alpha member 1	Kcnma1	-1.53	-1.78
17295796	phosphatidylinositol 3-kinase, regulatory subunit, polypeptide 1 (p85 alpha)	Pik3r1	1.63	1.84
17309268	endothelin receptor type B	Ednrb	1.66	2.18
17217678	calcium channel, voltage-dependent, L type, alpha 1S subunit	Cacna1s	NA	-2.67
17264792	ATPase, Na+/K+ transporting, beta 2 polypeptide	Atp1b2	NA	-1.87
17535572	ATPase, Ca++ transporting, plasma membrane 3	Atp2b3	NA	-1.72
17229178	ATPase, Na+/K+ transporting, beta 1 polypeptide	Atp1b1	NA	-1.68
17282309	solute carrier family 8 (sodium/calcium exchanger), member 3	Slc8a3	NA	-1.62
17363903	protein kinase, cGMP-dependent, type I	Prkg1	NA	-1.6
17496211	ATPase, Ca++ transporting, cardiac muscle, fast twitch 1	Atp2a1	NA	-1.58
17304010	potassium large conductance calcium-activated channel, subfamily M, alpha member 1; RIKEN cDNA A830039N20 gene	Kcnma1	NA	-1.5
17325206	adenylate cyclase 5	Adcy5	NA	1.58
17482021	phosphodiesterase 3B, cGMP-inhibited	Pde3b	NA	1.77

Acknowledgements

I would like to express my deepest gratitude to my thesis adviser, **Prof. Dr. Symeon Papadopoulos** for giving me the opportunity to work on this project, his ceaseless help, guidance and patience. I also thank him for always supporting me, for his kindness, his calm attitude and for making the time spent on this project pleasant and fun. Without his help this work would not have been possible.

I sincerely thank my committee members **Prof. Dr. Niels Gehring** and **Prof. Dr. Stefan Herzig** for taking the time and effort to review my thesis. I thank my thesis committee chair **Prof. Dr. Berenike Maier** for her time, help, kindness and flexibility.

I want to thank and express my great appreciation to **Prof. Dr. Gabriele Pfitzer** for her constant support, wise advice and for the valuable discussion of my project. I sincerely thank **Dr. Lubomir Lubomirov** for his continuous help inside and outside the lab and for keeping the record during my dissertation. I thank **Anna Walter** for helping me develop the initial steps of this project, as well as for her friendship and for the fun time in the lab. I thank **Dr. Mechthild Schroeter**, **Dr. Robert Stehle** and **Stefan Zittrich** for the valuable scientific discussions. Many thanks to **Dr. Mostafa Ardestani**, **Nina Felizitas Linde, Claudia Kilter** and **Aline Wies** for their assistance and the nice atmosphere in the lab. I am grateful to **Dr. Desirée Möhner** for revising this thesis, her thoughtful remarks, her cheerfulness and friendship, and for teaching me all important phrases in German. I thank **Dr. Diana Cimiotti**, **Katharina Schuler** and **Anja Kahl** for all amusing moments at and after work. I am also thankful to all my other past and present colleagues from the **Institute for Vegetative Physiology** for the great atmosphere and work environment.

I sincerely thank our collaborators **Prof. Dr. Martina Deckert**, **PD Dr. Anna Brunn** and **Mariana Carstov** from their excellent work and assistance with all histological analyses. I also owe special thanks to **Prof. Dr. Agapios Sachinidis**, **Dr. John A. Gaspar**, **Margit Henry** and **Tamara Rotshteyn** for their impeccable work handling all array chips and the bioinformatical support.

I thank **Dr. Isabell Witt** and **Kathy Jörgens** from the **Graduate School for Biological Sciences** (**GSfBS**) for their constant help and the versatile opportunities presented to me as a graduate student.

I thank **Antonino Gambuzza** and all the other members of the **CMMC animal facility** for taking care of the health and wellbeing of my mice. I am forever in debt to **all experimental animals** enabling this work, whose sacrifice I do not take lightly.

I thank my parents **Marusya** and **Zlatko,** and my sister **Vencislava** for their lifelong love, support and encouragement to follow my dreams and for lighting the spark of curiosity in me. I thank **Presian** for sharing his life and love with me, for always being there for me, inspiring me to be a better person.

Erklärung

Ich versichere, dass ich die von mir vorgelegte Dissertation selbständig angefertigt, die benutzten Quellen und Hilfsmittel vollständig angegeben und die Stellen der Arbeit − einschließlich Tabellen, Karten und Abbildungen −, die anderen Werken im Wortlaut oder dem Sinn nach entnommen sind, in jedem Einzelfall als Entlehnung kenntlich gemacht habe; dass diese Dissertation noch keiner anderen Fakultät oder Universität zur Prüfung vorgelegen hat; dass sie − abgesehen von unten angegebenen Teilpublikationen − noch nicht veröffentlicht worden ist, sowie, dass ich eine solche Veröffentlichung vor Abschluss des Promotionsverfahrens nicht vornehmen werde.

Die Bestimmungen der Promotionsordnung sind mir bekannt. Die von mir vorgelegte Dissertation ist von Prof. Dr. Niels Gehring betreut worden.

Köln, den 16. 08. 2018

_____

(Dilyana Filipova)